ARS JOURNAL

A PUBLICATION OF THE AMERICAN ROCKET SOCIETY

FORMERLY JET PROPULSION

June 1959 Volume 29 Number 6

SERGEANT

This missile system with nuclear capability is on the way to becoming a standard Army weapon. To be produced by Sperry-Rand, it is scheduled ultimately to replace the CORPORAL artillery missile system. The Jet Propulsion Laboratory developed SERGEANT is invulnerable to any known enemy electronic counter-measures. And, thanks to a simplified Thiokol solid propellant rocket motor, the missile is extremely mobile — can be transported on military vehicles.

When SERGEANT becomes operational, the Army will possess one of the most maneuverable and accurate artillery weapons in its history.

Engineers, Scientists: perhaps there's a place for you in Thiokol's expanding organization. Our new projects present challenging problems and a chance for greater responsibility.

Thiokol®

CHEMICAL CORPORATION

TRENTON, N. J. • ELKTON, MD.
HUNTSVILLE, ALA. • MARSHALL, TEXAS
MOSS POINT, MISS. • BRIGHAM CITY, UTAH
DENVILLE, N. J. • BRISTOL, PA.

®Registered trademark of the Thiokol Chemical Corporation for its liquid polymers, rocket propellants, plasticizers and other chemical products.

ARS JOURNAL

A PUBLICATION OF THE AMERICAN ROCKET SOCIETY

FORMERLY JET PROPULSION

American Rocket Society

500 Fifth Avenue, New York 36, N. Y.

Founded 1930

Scope of ARS JOURNAL

This Journal is devoted to the advancement of astronautics through the dissemination of original papers disclosing new scientific knowledge and basic applications of such knowledge. The sciences of astronautics are understood here to embrace selected aspects of jet and rocket propulsion, space flight mechanics, high-speed aerodynamics, flight guidance, space communications, atmospheric and outer space physics, materials and structures, human engineering, overall system analysis, and possibly certain other scientific areas. The selection of papers to be printed will be governed by the pertinence of the topic to the field of astronautics, by the current or probable future significance of the research, and by the importance of distributing the information to the members of the Society and to the profession at large.

Information for Authors

Manuscripts must be as brief as the proper presentation of the ideas will allow. Exclusion of dispensable material and conciseness of expression will influence the Editors' acceptance of a manuscript. In terms of standard-size double-spaced typed pages, a typical maximum length is 22 pages of text (including equations), 1 page of references, 1 page of abstract and 12 illustrations. Fewer illustrations permit more text, and vice versa. Greater length will be acceptable only in exceptional cases.

Short manuscripts, not more than one quarter of the maximum length stated for full articles, may qualify for publication as Technical Notes or Technical Comments. They may be devoted to new developments requiring prompt disclosure or to comments on previously published papers. Such manuscripts are usually published within two months of the date of receipt.

Sponsored manuscripts are published occasionally as an ARS service to the industry. A manuscript that does not qualify for publication, according to the above-stated requirements as to subject, scope or length, but which nevertheless deserves widespread distribution among jet propulsion engineers, may be printed as an extra part of the Journal or as a special supplement, if the author or his sponsor will reimburse the Society for actual publication costs. Estimates are available on request. Acknowledgment of such financial sponsorship appears as a footnote on the first page of the article. Publication is prompt since such papers are not in the ordinary backlog.

Manuscripts must be double spaced on one side of paper only with wide margins to allow for instructions to printer. Include a 100 to 200 word abstract. State the authors' positions and affiliations in a footnote on the first page. Equations and symbols may be handwritten or typewritten; clarity for the printer is essential. Greek letters and unusual symbols should be identified in the margin. If handwritten, distinguish between capital and lower case letters, and indicate subscripts and superscripts. References are to be grouped at the end of the manuscript and are to be given as follows: For journal articles: authors first, then title, journal, volume, year, page numbers for books: authors first, then title, publisher, city, edition and page or chapter numbers. Line drawings must be clear and sharp to make clear engravings. Use black ink on white paper or tracing cloth. Lettering should be large enough to be legible after reduction. Photographs should be glossy prints, not matte or semi-matte. Each illustration must have a legend; legends should be listed in order on a separate sheet.

Manuscripts must be accompanied by written assurance as to security clearance in the event the subject matter lies in a classified area or if the paper originates under government sponsorship. Full responsibility rests with the author.

Submit manuscripts in duplicate (original plus first carbon, with two sets of illustrations) to the Editor, Martin Summerfield, Professor of Aeronautical Engineering, Princeton University, Princeton, N. J. Preprints of papers presented at ARS national meetings are automatically considered for publication.

ARS JOURNAL is published monthly by the American Rocket Society, Inc. and the American Interplanetary Society at 20th & Northampton Sts., Easton, Pa., U. S. A. Editorial offices: 500 Fifth Ave., New York 36, N. Y. Price: $12.50 per year, $2.00 per single copy. Second-class mail privileges authorized at Easton, Pa. This Publication is authorized to be mailed at the special rates of postage prescribed by Section 132.122. Notice of change of address should be sent to the Secretary, ARS, at least 30 days prior to publication. Opinions expressed herein are the authors and do not necessarily reflect the views of the Editors or of the Society.

W. P. Knight

Bill Knight is a rocket chemist. His field of interest is research on advanced solid and liquid propellants to meet the stringent requirements of today's military programs (and tomorrow's).

The continued success of the American missile program depends on men like Bill Knight.

But creation takes talent. The kind of talent that top-notch scientists and engineers can use to the utmost on Aerojet's rapidly expanding programs in chemistry and other fields.

There are *many* projects at Aerojet that intrigue the scientific and engineering investigator. Your resume is invited. The address: AEROJET-GENERAL CORP., P. O. Box 296D, Azusa, California or P.O. Box 1947D, Sacramento, California. Attention: Director of Scientific and Engineering Personnel.

AEROJET-GENERAL CORP.

THE GENERAL TIRE

AZUSA AND NEAR SACRAMENTO, CALIFORNIA • A SUBSIDIARY OF THE GENERAL TIRE & RUBBER COMPANY

Magnetohydrodynamic Effects in Aerodynamic Flows[1]

W. R. SEARS

Cornell University
Ithaca, N. Y.

The author became first Director of Cornell University's Graduate School of Aeronautical Engineering in 1946, a position which he currently holds. He received a B.Aero.E. from the University of Minnesota in 1934, did graduate work at California Institute of Technology and was appointed Instructor in Aeronautics in 1937 and Assistant Professor in 1940. He received his Ph.D. in 1938. As Chief of Aerodynamics and Flight Tests at Northrop Aircraft, Inc., he was responsible for the aerodynamic design of several military aircraft. Dr. Sears was one of the original members of the Air Force Scientific Advisory Group, served on the U.S. Naval Technical Mission in Germany in 1945 and later on Scientific Advisory Board, Naval Research Advisory Committee and various NACA subcommittees. Since 1955 he has been Editor of *Journal of Aero/Space Sciences*.

THE name "magnetohydrodynamics" has been given to the branch of fluid mechanics that deals with motion of electrically conducting fluids in the presence of magnetic or electrical fields.

The name is in some ways a poor one, for one is usually not concerned with water but with gases—typically, with gases moving at supersonic or hypersonic speeds. Thus, my colleague Professor Resler and I have suggested the names "magneto-aerodynamics" (1)[2] and "magneto-gasdynamics" (3). But the name magnetohydrodynamics, sometimes abbreviated as MHD, seems to be more popular, and perhaps should be accepted, since "hydrodynamics" is, after all, a synonym for "fluid dynamics" in a broad sense.

This field is not the same as particle physics, although the two have much in common. It is distinguished by the fact that the medium in motion is relatively dense, so that the differential equations of fluid mechanics describe the flow, with new terms being added to them to account for electromagnetic effects. The Maxwell equations of electrodynamics also enter, but they must be solved together with the fluid mechanical equations. From the microscopic point of view, one may say that the word magnetohydrodynamics applies to cases in which there are many and frequent collisions between the constituent particles. The equations that are solved, like the usual fluid mechanical equations, are statements about properly averaged quantities.

Let us now review, from the macroscopic point of view, the new phenomena that appear in fluid motions if the fluid is a conductor and there are electric and/or magnetic fields present.

The first and perhaps the most interesting of these phenomena is a *body force* equal to $\boldsymbol{j} \times \boldsymbol{H}$ per unit volume, where $\boldsymbol{j}$ denotes the current density vector and $\boldsymbol{H}$ the magnetic field vector. We shall consider briefly the origin of this force later, but now let us simply recognize this as a familiar effect, namely the force on any conductor carrying a current in a magnetic field—the force that makes an electric motor operate. Engineers working in fluid mechanics are particularly interested in this body force, for, except for gravity, they do not usually have such forces to work with, and even more rarely do they have a body force that may be controlled.

The second electrical phenomenon is the *induced electromotive force* $\boldsymbol{q} \times \boldsymbol{H}$, where $\boldsymbol{q}$ is the fluid velocity vector. We shall postpone detailed discussion of this effect; again it is familiar in electrical work, the emf induced by moving any conductor across a magnetic field—the phenomenon that makes a generator function. In our work it means that electrical potentials will be set up, in general, when conducting fluids flow in the presence of magnetic fields; thus currents will flow, and the body force will be present.

The third effect to be considered is also familiar in electricity, namely *Joule heating*. It is given by j^2/σ in energy units per unit time per unit volume if σ is the conductivity of the fluid. σ is a material property, the reciprocal of the resistance of a unit cube of the fluid medium; thus its units are (for example) mhos per cm. We shall discuss this fluid property later and try to give some idea of its magnitude in aeronautical situations. At this point let us simply remark that it is the increase of σ from extremely small values for common gases at room temperature and pressure to appreciable values under flight conditions that makes a science of magneto-aerodynamics possible. Everyone knows that atmospheric air is a very good insulator under ordinary conditions. On the other hand, an electric arc is a pretty good conductor, because the air in it is hot enough to be ionized. We are told that the temperatures reached in some problems of hypersonic aerodynamic heating approach those of electric arcs; therefore we recognize the possibility that regions of appreciable electrical conductivity may exist in the vicinity of flying objects.

Equations of Motion

The discussion above permits us to write down the equations of magnetohydrodynamics; they are:

Continuity

$$\partial\rho/\partial t + \operatorname{div}(\rho \boldsymbol{q}) = 0 \qquad [1]$$

Momentum

$$\frac{D\boldsymbol{q}}{Dt} + \frac{1}{\rho}\operatorname{grad} p = \frac{1}{\rho}(\boldsymbol{j} \times \boldsymbol{H}) + (\text{viscous terms}) \qquad [2]$$

Energy

$$c_v \frac{DT}{Dt} + p\frac{D\rho^{-1}}{Dt} = \frac{1}{\rho}\frac{j^2}{\sigma} + Q \qquad [3]$$

Presented at the ARS 13th Annual Meeting, New York, Nov. 17–21, 1958.

[1] This research was supported jointly by the U. S. Air Force through the Office of Scientific Research of ARDC and the Mechanics Branch of the Office of Naval Research. Reproduction in whole or in part is permitted for any purpose of the United States Government.

[2] Numbers in parentheses indicate References at end of paper.

Here D/Dt is the familiar convective derivative, so that Equation [3] is a statement of the heat energy added to an element of the fluid as it flows. Q denotes all forms of heat added to the element, such as by viscous dissipation, heat transfer, combustion or radiation, exclusive of Joule heating. Thus a simplifying assumption has been made in this equation, namely that there is no other transfer of energy from electromagnetic to thermodynamic forms. Although this is not correct for fluids whose magnetic permeability is affected by temperature or field strength, for example, it is a good approximation for our purposes. The viscous terms in Equations [2 and 3] have not been written out because they are somewhat lengthy and are not actually used in this paper.

In the absence of the magnetohydrodynamic terms, this set of equations is rendered determinate by inclusion of an equation of state. Here we employ the equation appropriate for perfect gases

$$p = \mathfrak{R}\rho T \qquad [4]$$

We shall assume that $\mathfrak{R}$ is constant, i.e., that the number of particles per unit mass does not vary. There are flight conditions (where dissociation and ionization of air occur) where, to be more precise, $\mathfrak{R}$ must be considered a variable.

We also have a generalized Ohm's Law, which describes macroscopically the flux of electrical charges under the influence of an electric field E and the induced emf mentioned above

$$\boldsymbol{j} = \sigma(\boldsymbol{E} + \boldsymbol{q} \times \boldsymbol{H}) \qquad [5]$$

This formula will be discussed later but also requires some explanation at this point. It is a correct approximation only for conductors that are electrically neutral; it is a very good approximation for ionized gases (as well as for metallic conductors), because the electrons and positive ions are never separated by more than an extremely small distance. The vector $\boldsymbol{E}$ includes the contribution due to this separation of charges, and this contribution is not necessarily small even though the separation distance is minute. One may interpret Equation [5] as follows: At any point in the fluid there is applied to a small element an emf equal to $\boldsymbol{q} \times \boldsymbol{H}$ plus that part of $\boldsymbol{E}$ that is due to effects exterior to that element, i.e., voltage applied by neighboring elements and external electrodes. This total, local emf is opposed by: (a) the local "IR drop" $\boldsymbol{j}/\sigma$ minus (b) the part of $\boldsymbol{E}$ that is due to charge separation. The fact that we admit charge separation while we describe the fluid as everywhere neutral in charge means that we neglect the charge separation distance and consider the charges as forming doublets. The fluid may be said to be "polarized."

It might also be remarked that $\boldsymbol{E}$ is not invariant to translation of coordinates, and must be measured in the same frame of reference as the velocity $\boldsymbol{q}$.

At this point our set of equations is still indeterminate, but we have not used the so-called Maxwell equations. In the forms suitable for our problems these are (in electromagnetic units and for fluids whose permeability is equal to that of empty space):

$$\text{Ampère's Law} \qquad 4\pi\boldsymbol{j} = \text{curl } \boldsymbol{H} \qquad [6]$$

$$\text{Faraday's Law} \qquad \text{curl } \boldsymbol{E} = -\partial\boldsymbol{H}/\partial t \qquad [7]$$

"Displacement currents" have been neglected in Equation [6]. Two effects are usually included under this name (see (2)), and both of these are negligible in most magnetohydrodynamic problems, as we have pointed out in (3).

Dimensionless Parameters

Although the set of equations [1 to 7] is now determinate, it is indeed formidable and usually requires some simplification in order to provide solutions, except in cases of particularly simple geometry. To make such simplifications, one resorts to the familiar technique of identifying the significant dimensionless parameters and considering the effects of their magnitudes. For example, in (1) we have shown that the typical ratio of the electrical body force to the dynamic or inertial force is given by the parameter

$$N \equiv \sigma H_\infty^2 L/(1/2)\rho_\infty V \qquad [8]$$

Moreover, we evaluated this number for typical high-speed aeronautical cases and concluded that the ratio is large enough to produce important effects.[3]

The typical ratio of body force to viscous forces is the product of this number N and the Reynolds number, which is twice the square of the Hartmann number (5). Thus we concluded that at high Reynolds numbers it is reasonable to neglect viscosity, except in boundary layers and wakes, as in ordinary fluid mechanics. We shall therefore omit the viscous terms in Equations [2 and 3] for the purposes of this discussion. There are, in contrast, some important investigations of boundary layer flow (6 to 8) and channel flow (9 to 11) with magnetohydrodynamic effects.

Perhaps the most important dimensionless parameter is the so-called "magnetic Reynolds number"

$$R_m \equiv \sigma V L \qquad [9]$$

As we have pointed out (1), this can be interpreted as the ratio of the motion-induced magnetic field strength to the applied magnetic field strength. When R_m is large, the applied field may often be neglected, and one is led to the concept of the ideal conductor or fluid of infinite conductivity, as we shall see. On the other hand, for small R_m, one may consider the magnetic field to consist of the applied field only slightly perturbed. This case will also be treated later.

Still another dimensionless parameter is found useful, namely

$$m \equiv \sqrt{4\pi\rho_\infty}\,(V/H_\infty) \qquad [10]$$

This is the ratio of the flow speed V to the speed

$$\alpha \equiv H_\infty/\sqrt{4\pi\rho_\infty} \qquad [11]$$

which is the speed of propagation of certain magnetohydrodynamic waves—the Alfvén waves. Thus m is analogous to a Mach number, i.e., it is the ratio of a characteristic flow speed V to a propagation speed of wavelike disturbances. It might well be called the "Alfvén number" or the "magnetic Mach number."

As usual, additional dimensionless parameters can be formed by combining those already mentioned. Moreover, it is interesting to note that the number N defined in Equation [8] is a combination of R_m and m

$$N = 8\pi R_m m^{-2} \qquad [12]$$

so that the Hartmann number is proportional to the square root of $ReR_m m^{-2}$, etc.

Another interesting combination is the ratio of the magnetic Reynolds number to the Reynolds number, which is, of course, equal to the product $\sigma\nu$, where ν is the kinematic viscosity. As we have shown in (15), $4\pi R_m$ plays the same part in defining certain "magnetohydrodynamic boundary layers" as does Re in defining the viscous boundary layer. Thus the dimensionless number $4\pi\sigma\nu$ is an indication of the relative thicknesses of these two kinds of layers; actually it is the square of the ratio of viscous to magnetohydrodynamic boundary layer thicknesses. This is particularly interesting because $4\pi\sigma\nu$ is a material property; for example, it has a value of about 10^{-7} for mercury at room temperature. This

[3] Unfortunately we erred in plotting Fig. 2 of (1) where the values given are 100 times too small. Thus our conclusion regarding the possibility of appreciable body forces might have been considerably more emphatic. See (4).

parameter might be called the "magnetohydrodynamic Prandtl number."

Magneto-Gasdynamic Channel Flow

In (1 and 3) we considered a problem of particular interest in aeronautics: Quasi-one-dimensional flow of a gas in a channel in the presence of magnetic and electrical fields. We neglected viscosity and assumed all the pertinent parameters, such as cross-section area and applied field strengths, to vary only slowly with the distance along the channel x. The equations for this type of flow are (where primes denote differentiation with respect to x)

$$\rho u A = \text{constant} \qquad [13]$$

$$\rho u u' + p' = \sigma(E - uH)H \qquad [14]$$

$$\rho u c_p T' + u^2 u' = \sigma(E - uH)E + Q \qquad [15]$$

together with Equation [4].

These equations cannot be integrated in general, but only for special geometries $A(x)$. We can calculate the acceleration u', however, in terms of the conditions at any given station x; the result is

$$u' = \frac{1}{M^2 - 1}\left[\frac{A'}{A}u - \frac{\sigma H^2}{\rho}(u - u_3)(u - u_1) - \frac{\gamma - 1}{\gamma}\frac{Q}{p}\right] \qquad [16]$$

where

$$u_1 \equiv \frac{\gamma - 1}{\gamma}\frac{E}{H} \qquad u_3 \equiv \frac{E}{H} \qquad [17]$$

The first and third right-hand terms in Equation [16] are familiar in gasdynamics. The first term describes the effects of convergence or divergence of the channel, which are opposite for subsonic and supersonic flows. The third term likewise describes the opposite effects of heat addition at subsonic and supersonic flows, namely that heat addition tends to accelerate subsonic flow but decelerates supersonic flow.

The remaining right-hand term in Equation [16] is the magnetohydrodynamic effect, a combination of the effects of body force and Joule heating. For supersonic streams the net magnetohydrodynamic effect is acceleration only if u lies between the two significant speeds u_1 and u_3 defined in Equation [17]. This is understandable, for when $u > u_3$ the body force has changed sign and tends to decelerate the flow, as does the Joule heating. u_1 is the speed at which the acceleration due to body force is canceled by the deceleration due to Joule heating, as can easily be confirmed by means of Equations [13 to 15]. The situation at subsonic speeds is somewhat anomalous, for the interval $u_1 < u < u_3$ is the range of deceleration, although both the body force and the Joule heating would seem to be accelerating the flow. In contrast, there is acceleration for $u > u_3$, although here the body force has changed sign.

The importance of the Mach number, as well as the fact of the singularity at $M = 1$, leads us to calculate also the derivative M'; it may be important, in a magnetohydrodynamic channel designed to accelerate (or decelerate) a fluid flow, to avoid the sonic regime, because the singularity there clearly suggests the phenomenon of "choking." The result is

$$M' = \frac{1}{M^2 - 1}\left[\left(1 + \frac{\gamma - 1}{2}M^2\right)M\frac{A'}{A} - \left(1 + \frac{\gamma - 1}{2}M^2\right)\frac{\sigma H^2}{a\rho}(u - u_3)(u - u_2) - \frac{\gamma - 1}{\gamma}\frac{1 + \gamma M^2}{2}\frac{Q}{a\rho}\right] \qquad [18]$$

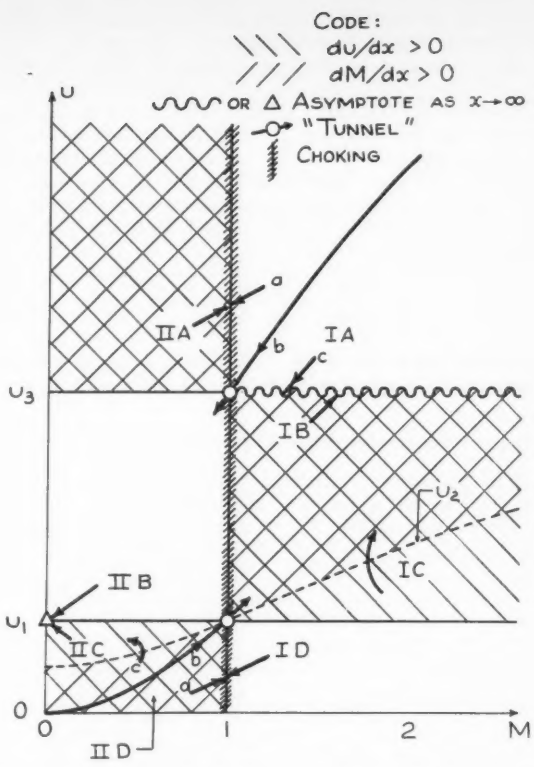

Fig. 1 Magneto-gasdynamic acceleration of one-dimensional flow in a constant-area channel. Regimes of positive acceleration and increasing Mach number are designated by cross-hatching as shown. Arrows denote typical behaviors of flows in the various regimes; arrowheads show direction of increasing x (downstream)

where a denotes $\sqrt{\gamma \mathcal{R} T}$ and

$$u_2 \equiv \frac{1 + \gamma M^2}{2 + (\gamma - 1)M^2}u_1 \qquad [19]$$

Since $0 < u_2 < u_1$ at subsonic speeds, and $u_1 < u_2 < u_3$ at supersonic speeds, it is clear that there are regimes where u and M have opposite tendencies as the result of magnetohydrodynamic effects.

These tendencies can conveniently be summarized in a u, M diagram as shown in Fig. 1. In order to isolate magnetohydrodynamic effects, this diagram is drawn for a constant-area channel without heat addition. Such a diagram contains much useful information, such as the various asymptotic behaviors indicated. The asymptotic approach to the point $(u_1, 0)$ from subsonic speeds means that the temperature increases without limit, as a result of Joule heating. The asymptotic approach to u_3 from supersonic speeds, however, is due to the gradual disappearance of the electric current as u_3 is approached. The value u_3 can be made as large as desired.

Of particular interest in Fig. 1 are the two "tunnels" through the choking barrier at $M = 1$, one for increasing speeds at $(u_1, 1)$, the other for decreasing speeds at $(u_3, 1)$. These are cases for which the numerators as well as the denominators in Equations [16 and 18] (for $A' = 0 = Q$) vanish. Thus these are constant-area magnetohydrodynamic analogs of the Laval nozzle and its reverse (diffuser), respectively. Their stability has not been investigated.

Equations [13 to 15] with constant σ, E and H have been

integrated for constant-area and also for a constant-temperature duct by Rosa at Cornell University (13), and for a constant-density duct by Resler and Sears (3). The constant-density case is of course only one of many incompressible-flow solutions of Equations [13 and 14], but it is the particular one that has gasdynamic significance, since it satisfies Equation [15] as well. In (1) we also used the results of Equations [16 and 18] to design a constant-area duct for maximum acceleration of a supersonic stream, again assuming constant σ; this is one along which E/H is adjusted to maintain the equality

$$\frac{E}{H} = \frac{2\gamma - 1}{2(\gamma - 1)} u \qquad [20]$$

(We neglected to point out in (1) that this value produces maximum deceleration of the fluid at subsonic speeds.)

Magnetohydrodynamic Containment

It has already been remarked that air is a poor conductor at the temperature of common structural materials, and only becomes a good conductor if considerably higher temperatures can be attained. This will pose serious difficulties in the design of magnetohydrodynamic channels. There is a possibility, however, of using a magnetohydrodynamic phenomenon to "contain" the fluid, and thereby to keep it away from duct walls. This is the famous "pinch effect," which occurs in electric arcs and there confines the ionized gas at high temperature and pressure. The phenomenon is sketched in Fig. 2. It is a straightforward result of the body force $\boldsymbol{j} \times \boldsymbol{H}$, as indicated, and has been analyzed in various places, e.g., (14).

The simplified model analyzed is one in which the conducting gas is entirely confined within a cylinder of radius r_1, i.e., the conductivity for $r > r_1$ is zero. Assuming steady axisymmetric flow without viscosity, Equations [2 and 6] state, for $r < r_1$

$$\frac{dp}{dr} = -j_z H_\theta \qquad [21]$$

$$4\pi j_z = \frac{1}{r}\left(\frac{d}{dr} rH_\theta\right) \qquad [22]$$

where j_z is the current-density component in the axial direction and H_θ the tangential magnetic field component. Ohm's Law (Eq. [5]) tells us that j_z is equal to σE_z and is therefore a constant proportional to the voltage difference between the ends of the cylinder. It is easily verified that the solution is

$$j_z = \text{constant} = j_0 \qquad [23]$$

$$p = p_0 - \pi r^2 j_0^2 \qquad [24]$$

$$H_\theta = 2\pi r j_0 \qquad [25]$$

where p_0 denotes the pressure at the axis of the cylinder.

For $r > r_1$

$$p = \text{constant} = p_0 - \pi r_1^2 j_0^2 \qquad [26]$$

$$H_\theta = 2\pi r_1^2 j_0 / r \qquad [27]$$

To be "confined" by the magnetic field, then, the pressure $\pi r_1^2 j_0^2$ must be of the same order of magnitude as the centerline pressure p_0. This result establishes the magnitude of the axial current component for given p_0 and required r_1.

Effects of Varying Magnetic Reynolds Number

It has already been mentioned that the parameter R_m is one of the most important of the dimensionless magnitudes that determine the character of magnetohydrodynamic flows. To illustrate some of its effects, we shall consider in this section a particularly simple class of flows and see how their character changes with changing values of R_m.

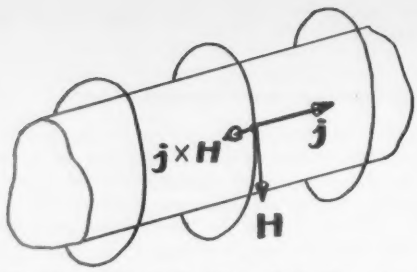

Fig. 2 Sketch of "pinch effect" on fluid filament carrying a current

Before doing so, it will be useful to simplify our equations. Equations [1 to 7], by eliminating both $\boldsymbol{j}$ and $\boldsymbol{E}$. This is done by means of Equations [6 and 7]. Neglecting viscous terms, Equation [2] becomes

$$\frac{D\boldsymbol{q}}{Dt} + \frac{1}{\rho}\,\text{grad}\left(p + \frac{H^2}{8\pi}\right) = \frac{1}{4\pi\rho}\boldsymbol{H}\cdot\nabla\boldsymbol{H} \qquad [28]$$

and Equation [3] becomes

$$c_v \frac{DT}{Dt} + p\frac{D\rho^{-1}}{Dt} = \frac{1}{\rho\sigma}\left(\frac{1}{4\pi}\,\text{curl}\,\boldsymbol{H}\right)^2 \qquad [29]$$

By taking the curl of both sides of Equation [5], Ohm's Law, and using Equations [6 and 7], one has (noting that div $\boldsymbol{H}=0$)

$$-\nabla^2\boldsymbol{H} = 4\pi\sigma\,[-(\partial\boldsymbol{H}/\partial t) + \boldsymbol{H}\cdot\nabla\boldsymbol{q} - \boldsymbol{q}\cdot\nabla\boldsymbol{H} - \boldsymbol{H}\,\text{div}\,\boldsymbol{q}] \qquad [30]$$

Thus, our unknown functions are now $\boldsymbol{q}$, p, ρ, T and $\boldsymbol{H}$, and the set of equations to be solved consists of Equations [1, 4, 28, 29 and 30].

Small-Perturbation Plane Incompressible Flow: Crossed Fields

Consider now a class of flow problems that constitutes a certain extension of the familiar small-perturbation flows of classical aerodynamics; namely, suppose that a uniform stream is perturbed by a thin cylinder in the presence of a magnetic field which, in the undisturbed flow, is also uniform but is directed *normal* to the fluid stream. Thus

$$\boldsymbol{q} = (V + u', v', 0) \qquad [31]$$

and

$$\boldsymbol{H} = (h_x, H_\infty + h_y, 0) \qquad [32]$$

where u' and v' are small compared to V, and h_x and h_y are small compared to H_∞. We assume, and can confirm, that h_x/H_∞ and h_y/H_∞ are at most of the same order of magnitude as u'/V and v'/V. We consider, in particular, steady incompressible flow. If we introduce dimensionless variables, where velocity components are divided by V, the pressure by ρV^2, magnetic field components by H_∞, and coordinate distances by a characteristic length L, we have upon linearization

$$\frac{\partial\bar{q}}{\partial\bar{x}} + \bar{\nabla}\,\bar{p} = m^{-2}\left(\frac{\partial\bar{H}}{\partial\bar{y}} - \bar{\nabla}\bar{h}_y\right) \qquad [33]$$

and

$$-\bar{\nabla}^2\bar{H} = 4\pi R_m\left(\frac{\partial\bar{q}}{\partial\bar{y}} - \frac{\partial\bar{H}}{\partial\bar{x}}\right) \qquad [34]$$

where m and R_m are the quantities defined in Equations [10 and 9].

These are put into an interesting form by operating with the curl operator. Let Ω denote curl $\boldsymbol{q}$, and let ξ denote curl H (or $4\pi\bar{j}$). Both of these vectors are perpendicular to the xy plane. Let the corresponding dimensionless quantities $\bar{\Omega}$ and $\bar{\xi}$ (or $4\pi\bar{j}$) be defined as $(L/V)\Omega$ and $(L/H_\infty)\xi$, respectively. The results are

$$\frac{\partial\bar{\Omega}}{\partial\bar{x}} = m^{-2}\frac{\partial\bar{\xi}}{\partial\bar{y}} \qquad [35]$$

and

$$-\bar{\nabla}^2\bar{\xi} = 4\pi R_m\left(\frac{\partial\bar{\Omega}}{\partial\bar{y}} - \frac{\partial\bar{\xi}}{\partial\bar{x}}\right) \qquad [36]$$

Combining these by cross differentiation, we have

$$\frac{\partial^2\bar{\Omega}}{\partial\bar{x}^2} - m^{-2}\frac{\partial^2\bar{\Omega}}{\partial\bar{y}^2} = \frac{m^{-2}}{4\pi R_m}\bar{\nabla}^2\frac{\partial\bar{\xi}}{\partial\bar{y}} \qquad [37]$$

and

$$\frac{\partial^2\bar{\xi}}{\partial\bar{x}^2} - m^{-2}\frac{\partial^2\bar{\xi}}{\partial\bar{y}^2} = \frac{1}{4\pi R_m}\bar{\nabla}^2\frac{\partial\bar{\xi}}{\partial\bar{x}} \qquad [38]$$

We have treated these equations under various assumptions regarding the magnitude of R_m. First consider the case $R_m = \infty$, i.e., the case of an ideal conductor. According to Equations [37 and 38], both the vorticity Ω and the current density $\xi/4\pi$ satisfy the two-dimensional wave equation. Thus, if the flow is undisturbed at $y = \pm\infty$ these quantities are constant along lines having the inclination $dy/dx = m^{-1}$. The analogy between this geometry and that of familiar (Ackeret) small-perturbation two-dimensional supersonic flow is striking. On the other hand, the velocity components themselves do not satisfy the wave equation, but rather are made up of rotational parts distributed in this way and irrotational parts distributed according to Laplace's equation. All of these components, as well as the corresponding magnetic field components, are finally determined by the boundary conditions and continuity conditions at the solid cylinder.

The wavelike disturbances running outward and downstream from the wall are recognized as Alfvén's electromagnetic waves (12). It is seen that the disturbance pattern consists of irrotational components together with these waves, which propagate outward with the speed mentioned in Equation [11] and are carried downstream.

One of the cases treated in detail in (15) is that of an infinite, sinusoidal, wavy wall constructed of an insulating substance. The calculated pressures at the wall are presented in Fig. 3 in the form of a "vector diagram." This diagram gives the amplitude of the pressure fluctuation and its phase relationship to the wall geometry for various values of m. The particular curve being discussed here is the one marked $R_m = \infty$.

For large but finite values of R_m, the solution just discussed can be corrected by the same technique that is used for sound waves propagating in a medium of small viscosity. We proceed by assuming that the solutions of Equations [37 and 38] are now damped sinusoids; for example

$$\xi = \text{constant} \times e^{i\lambda(x-my)}e^{-\mu y} \qquad [39]$$

It is then found without difficulty that $\mu = O(R_m^{-1})$, where in this case R_m is based on the wave length $2\pi/\lambda$. Neglecting higher order terms, one finds

$$\mu = (1/4)m(1 + m^2)\lambda R_m^{-1} \qquad [40]$$

Thus, one effect of introducing small electrical resistance in the fluid is to cause attenuation of the Alfvén waves that propagate outward from the wall. This is worked out in (15), and in (16) McCune has calculated the corresponding effect on the wall surface pressure. His result for the sinusoidal wall is shown in Fig. 3 for $R_m = 5$. In (15 and 16) these methods were also applied to small-perturbation flows around slender cylinders (airfoils).

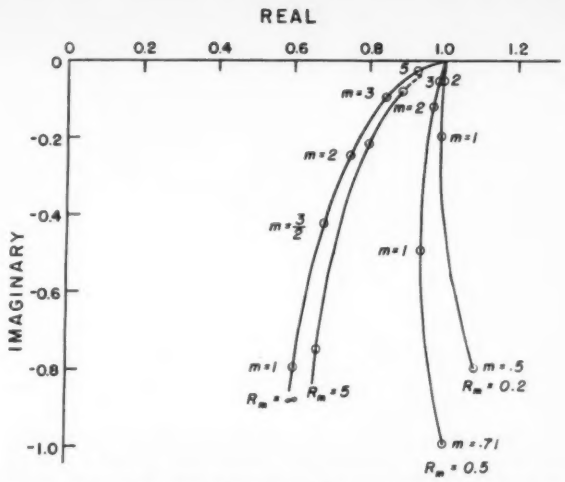

Fig. 3 Vector diagram showing relative magnitude and phase of pressure on sinusoidal wall for various R_m and m. Crossed fields. Results for infinite R_m in comparison with McCune's approximate results for large and small R_m, respectively. R_m is based on wall wave length

Let us now consider, by way of contrast, approximate solutions appropriate for *small* values of R_m. In this case we express all the perturbation quantities in power series in R_m; i.e.

$$f = f_0 + R_m f_1 + R_m^2 f_2 + \ldots \qquad [41]$$

where f denotes any one of the perturbation quantities and terms carrying the subscript 0 are the values for conventional flow without magnetohydrodynamic effects.

Upon introducing such power series expressions into Equa- [34], one quickly finds that $\bar{\xi}_1 = 4\pi\bar{v}_0$, or, in dimensional form, to the first order in R_m

$$j = (H_\infty/VL)R_m u_0 = \sigma H_\infty u_0 \qquad [42]$$

Equation [33] or Equation [2] is then used to construct further details of the first-order flow field. Thus the first-order result corresponds to neglecting the perturbation of the magnetic field in calculating the current density. This is clearly consistent with the interpretation given of R_m earlier in this paper.

This theory has also been worked out by McCune, but is unpublished as yet.[4] He finds that the successive terms can be calculated by a process of iteration, and moreover that the differential equations to be solved at each step of the procedure are all linear. His results for the pressure on an infinite sinusoidal wall, using both the linear and quadratic terms in R_m are again plotted in Fig. 3, for the particular cases $R_m = \frac{1}{5}$ and $\frac{1}{2}$.

It may be of interest to point out that Alfvén waves are completely absent from flows with small R_m.

Finally, for the particular case of the infinite wavy wall, Resler and McCune have succeeded, in an investigation still unpublished,[4] in solving the equations for arbitrary R_m. Thus, for this case we have results free from any assumptions about the size of R_m, with which the approximate results for small R_m and large R_m can be compared. For example, in Fig. 4 we have plotted the drag per wave length against R_m. For the classical case $R_m = 0$, of course, the pressure perturbation is in phase with the wall height, and there is no drag. The terms proportional to R_m contribute to the drag, how-

[4] These results will be included in "The Proceedings of the Third Lockheed Symposium on Magnetohydrodynamics," D. Bershader, Ed., Stanford University Press, 1959.

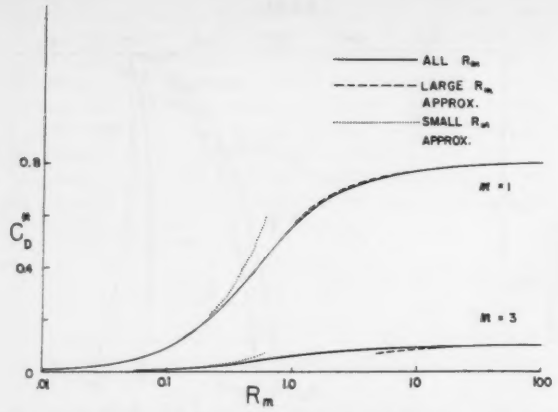

Fig. 4 Coefficient of drag per wave length of sinusoidal wall with crossed fields. Resler-McCune theory (solid curve) compared with approximate results for small and large R_m, respectively. The drag coefficient is defined as (drag per wave length) ÷ $(2\pi^2 \times \rho V^2 \epsilon^2 L^{-1})$ where the wall shape is given by $\epsilon \cos (2\pi x/L)$

ever, while those proportional to R_m^2 do not. It is of particular interest to note that, at least in this problem, the asymptotic value for $R_m = \infty$ is nearly reached at $R_m = 5$. Tentatively we shall take this to be an indication of what is meant by "large" R_m. If this indication is correct, a flow of mercury, for example, at large Reynolds number could be a case of large magnetic Reynolds number as well, in spite of the very small value of the "magnetic Prandtl number" $4\pi\sigma\nu$ mentioned earlier in this paper.

Small-Perturbation Plane Incompressible Flow: Parallel Fields

In (15) we have applied analogous methods to still another class of two-dimensional small-perturbation flows, namely those in which the undisturbed magnetic field is uniform and *parallel* to the stream. In this case

$$\boldsymbol{q} = (V + u', v', 0) \qquad [43]$$

$$\boldsymbol{H} = (H_\infty + h_x, h_y, 0) \qquad [44]$$

The equations analogous to Equations [33 and 34] are now, for incompressible flow

$$\frac{\partial \bar{q}}{\partial \bar{x}} + \bar{\nabla}\bar{p} = m^{-2}\left(\frac{\partial \bar{H}}{\partial \bar{x}} - \bar{\nabla}\bar{h}_x\right) \qquad [45]$$

and

$$-\bar{\nabla}^2\bar{H} = 4\pi R_m\left(\frac{\partial \bar{q}}{\partial \bar{x}} - \frac{\partial \bar{H}}{\partial \bar{x}}\right) \qquad [46]$$

The equation for x-components in Equation [45] leads immediately to the result, familiar in conventional incompressible small-perturbation cases

$$p = \text{constant} - \rho V u' \qquad [47]$$

Again let us begin with a discussion of the case $R_m = \infty$. Equation [46] then leads to

$$\bar{q} = \bar{H} \qquad [48]$$

which means that the velocity and magnetic perturbations are proportional vectors, and the streamlines and magnetic field lines are everywhere parallel to one another. This is an example of a result often stated, that magnetic lines of force are convected with the fluid in flows of infinite conductivity. Actually this result is not always correct; the general situation for $\sigma = \infty$ for both compressible and incompressible flows is seen in Equation [30], namely that the expression within brackets in Equation [30] must vanish. Hayes (17) shows that this leads to the conclusion

$$\frac{D}{Dt}\int_S \boldsymbol{H}\cdot\boldsymbol{n}\, ds = 0 \qquad [49]$$

i.e., that the number of lines passing through any area being convected with the fluid is constant. (This is, of course, consistent with the Law of Induction, for any change of the number of lines intercepted would induce an emf in a circuit enclosing the area, and this in turn would lead to infinite current flow in an ideal conductor.) We have seen in the examples above cases where Equation [49] is satisfied but the field lines are not convected with the fluid.

In view of Equation [48], one may take the curl of both sides of Equation [45] and conclude immediately that, provided $m \neq 1$

$$\Omega = 0 = \xi \qquad [51]$$

Thus, for infinite R_m the flow is irrotational and current-free. The streamline pattern is unaffected by magnetohydrodynamic effects. But the boundary conditions on the magnetic field are not satisfied, in general, by the resulting configuration without introduction of *current sheets* at solid boundaries. These are sheets of infinite current density, and of course they contribute to the force on the boundary. Thus, although the streamline pattern and the pressure in the flow are not affected by magnetohydrodynamics, the force on a solid body is affected.

In this case the introduction of small resistance (large but finite R_m) leads not to the wave equation and wavelike solutions but to an equation of boundary layer character. This equation is Equation [46] (or more generally Eq. [30]), where it is seen that the derivative $\partial^2\bar{H}/\partial\bar{y}^2$ appears only with the small factor R_m^{-1}. It can be proved that there is therefore a layer of thickness $O(R_m^{-1/2})$ in which the current density is large and outside of which it becomes negligible. It is clear that this magnetic boundary layer replaces the current sheet of the infinite-R_m solution. The situation is analogous to boundary layer theory for fluids of small viscosity. The ideal fluid approximation can be thought of as requiring vortex sheets along all solid boundaries in order to satisfy the boundary conditions of viscous flow. The boundary layer then constitutes the next approximation, in which the vortex sheet is replaced by a large but finite vorticity, of thickness $O(Re^{-1/2})$.

In general our small-perturbation equations are not adequate for this boundary layer type of calculation, because the boundary conditions on H often require large perturbations. Equation [30] must then be used to provide the boundary layer equation, and it is, of course, nonlinear. The infinite, insulating, sinusoidal wall again provides a particularly simple example, in which the linearized Equation [46] is sufficient; this case was worked out in (15).

For *small* R_m, on the other hand, the same type of power-series solution (Eq. [41]) can be used as for the case of crossed fields described above. Once again the appropriate form of Ohm's Law, namely Equation [46], leads immediately to the first-order result $\bar{\xi}_1 = -4\pi\bar{v}_0$, or

$$j = -\sigma H_\infty v_0 \qquad [52]$$

to first order in R_m. McCune has studied the infinite wavy wall under this approximation and finds that positive drag appears. Again the first-power terms contribute to drag whereas the quadratic terms do not. His results are plotted in Fig. 5 in comparison with the value (zero) obtained for both large and infinite R_m in (15). Also plotted here are results obtained by Resler and McCune for arbitrary R_m.

It appears that the theory for "large" R_m in this case is not a good approximation for values of R_m less than several thousand. The contrast with the results (Fig. 4) for crossed fields is striking. We propose, as a conjecture, that the difference

is related to the absence of the Alfvén mechanism in the present problem, i.e., that flows producing Alfvénlike waves will generally exhibit greater magnetohydrodynamic effects than flows, like the present one, in which the boundary layer character prevails and magnetohydrodynamic effects are carried into the flow by diffusion.

Small-Perturbation Compressible Plane Flow: Parallel Fields

The analysis of (15) has been extended in still another direction by Professor Resler, namely, to plane, steady compressible flows of an ideal conductor with parallel undisturbed velocity and magnetic fields. The extension is relatively straightforward and can be sketched here; it is as yet unpublished.

The equation of momentum, Equation [28], is unchanged, becomes Equation [45] upon linearization (where now m^2 denotes $4\pi\rho_\infty V^2/H_\infty^2$), and leads once again to a result analogous to Equation [47]

$$p = p_\infty - \rho_\infty V u' \qquad [53]$$

By taking the curl of Equation [45] one again finds a linear relation between Ω and ξ but cannot conclude that either vanishes

$$\bar{\Omega} = m^{-2}\bar{\xi} \qquad \text{or} \qquad \Omega = (H_\infty/4\pi\rho_\infty V)\xi \qquad [54]$$

Similarly, Equation [30] still reads, for $R_m = \infty$

$$\text{curl}\,(\boldsymbol{q} \times \boldsymbol{H}) = 0 \qquad [55]$$

which requires $\boldsymbol{q} \times \boldsymbol{H}$ to be constant for plane flow, and in particular, to be equal to zero in this case. The linearized form of Equation [55] is

$$V h_y = H_\infty v' \qquad [56]$$

Since there is no Joule heating in the ideal conductor, the flow is isentropic. The linearized form of the x-component of Equation [30] is

$$V\frac{\partial h_x}{\partial x} - H_\infty \frac{\partial u'}{\partial x} + H_\infty \,\text{div}\,\boldsymbol{q} = 0$$

or, with the linearized equation of continuity

$$\begin{aligned} V\frac{\partial h_x}{\partial x} - H_\infty \frac{\partial u'}{\partial x} &= H_\infty \frac{V}{\rho_\infty}\frac{\partial \rho}{\partial x} \\ &= \frac{H_\infty}{a_\infty^2}\frac{V}{\rho_\infty}\frac{\partial p}{\partial x} \\ &= -\frac{H_\infty}{a_\infty^2} V^2 \frac{\partial u'}{\partial x} \\ &= -H_\infty M_\infty^2 \frac{\partial u'}{\partial x} \end{aligned} \qquad [57]$$

by virtue of Equation [53]. After integration of Equation [57], the following interesting result appears

$$V h_x = (1 - M_\infty^2) H_\infty u' \qquad [58]$$

The results given in Equations [56 and 58] constitute the generalization of Equation [48] for the case of compressible flow.

Resler has proceeded to introduce the stream function as is sometimes done for small perturbation flow (see (18), for example)

$$-\frac{\partial \psi}{\partial y} = (1 - M_\infty^2)u' \qquad \frac{\partial \psi}{\partial x} = v' \qquad [59]$$

and has worked out the differential equation for ψ. He finds

$$\frac{(1 - M_\infty^2)(m^2 - 1)}{M_\infty^2 + m^2 - 1}\frac{\partial^2 \psi}{\partial x^2} + \frac{\partial^2 \psi}{\partial y^2} = 0 \qquad [60]$$

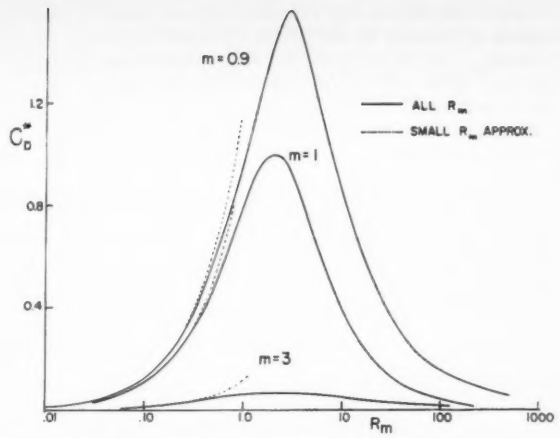

Fig. 5 Coefficient of drag per wave length of sinusoidal wall with parallel fields. Resler-McCune theory (solid curve) compared with approximate results for small R_m. (Large-R_m approximation gives zero drag.) The drag coefficient is defined as in Fig. 4.

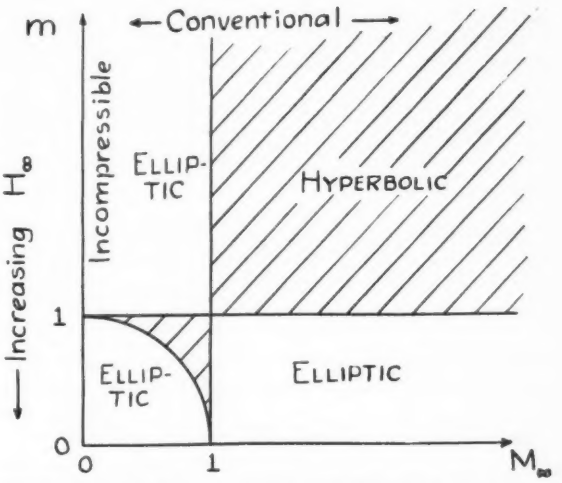

Fig. 6 Diagram showing elliptic and hyperbolic regions for Resler's equation of small-perturbation compressible flow with parallel fields

In Fig. 6 are shown the regions of an m, M_∞ diagram in which Resler's equation is elliptic and hyperbolic, respectively. The physical meanings of "elliptic" and "hyperbolic" are related to the existence of finite propagation speeds. Thus Equation [60] can be used to determine the disturbance-propagation speed; it is V/K where $1 - K^2$ is the coefficient of the first term in Equation [60]; i.e., it is

$$[a_\infty^2 + \alpha^2 - (\alpha^2 a_\infty^2/V^2)]^{1/2} \qquad [61]$$

where α is the Alfvén speed defined in Equation [11]. This is in agreement with an analysis of the speeds of propagation of plane magnetohydrodynamic waves. Thus K rather than M_∞ is the ratio of the stream speed to the true sound speed, given by Equation [61]. When Equation [60] is hyperbolic ($K > 1$), the wave angle of disturbances is $\sin^{-1}(1/K)$.

It is interesting to note that there is a hyperbolic region at subsonic flow speeds (see Fig. 6). In this region the waves (characteristics) involved are forward-facing; i.e., they slant upstream from the point of disturbance. This follows from the fact that the wave angle increases with flow speed V.

In the elliptic regions, Equation [60] is transformed into Laplace's equation by an affine ("Prandtl-Glauert") transformation. Thus the rotational compressible magnetohydrodynamic flows are related to certain irrotational incompressible flows.

Solutions of Equation [60] for hyperbolic regions can be written immediately

$$\psi = f(x - \sqrt{K^2 - 1}\, y) + g(x + \sqrt{K^2 - 1}\, y) \quad [62]$$

where f and g are arbitrary functions. This form can easily be applied to determine the flow pattern and pressure distribution in two-dimensional flows. For a flat plate at angle of attack ϵ, for example, at both the upper and lower surfaces

$$v' = -V\epsilon \quad [63]$$

and

$$u' = \pm \frac{\sqrt{K^2 - 1}}{M_\infty^2 - 1} V\epsilon \text{ on } \begin{matrix}\text{upper} \\ \text{lower}\end{matrix} \text{ surface} \quad [64]$$

Thus, according to Equation [53], the pressure difference between lower and upper surfaces is

$$\Delta p = 2\rho_\infty V^2 \left[\sqrt{K^2 - 1}/(M_\infty^2 - 1)\right] \epsilon \quad [65]$$

Just as in the incompressible case treated in (15), this solution, together with Equations [56 and 58], involves a surface current at the plate. Its value J_s is given by $-1/4\pi$ times the difference in value of h_x between top and bottom surfaces

$$J_s = -\frac{1}{4\pi}(1 - M_\infty^2)\frac{H_\infty}{V} 2\frac{\sqrt{K^2 - 1}}{M_\infty^2 - 1} V\epsilon$$
$$= \frac{1}{2\pi} H_\infty \sqrt{K^2 - 1}\, \epsilon \quad [66]$$

An upward force equal to $H_\infty J_s$ is exerted on the plate by virtue of this current. Thus the total upward load per unit area of the plate is

$$2\rho_\infty V^2 \epsilon (1/\sqrt{K^2 - 1})(1 - m^{-2}) \quad [67]$$

In the incompressible limit, $K^2 - 1$ becomes 1, and the result given in Equation [67] is reduced to that obtained in (15).

Applications to Aeronautics

Some of the examples treated in the preceding sections suggest aeronautical applications of magnetohydrodynamics. There appear to be possibilities of using the phenomena to affect the lift and drag of flying bodies, to inhibit the transfer of heat from hot gas streams to adjacent bodies, and to produce or augment thrust. It is also clear that the magnetohydrodynamic accelerator, with electric potential reversed, becomes a generator of electric power; thus there appears to be a possibility of using these effects to extract electric power directly from a flowing, conducting fluid.

Although it is still too early to predict which, if any, of these possibilities will be found after engineering research and development to be practical and economical, some of the engineering problems that will require solution to make magnetoaerodynamics a reality are easily recognized. The most obvious are those related to the great weights of electrical power components. It will be necessary to provide both electric and magnetic fields at much less cost in weight than in conventional devices.

It appears that the aerodynamicist will also be faced, for some time at least, with problems of producing and maintaining electrical conductivity in gases. In (1) we presented some typical data on the conductivities of pure air and of air "seeded" with a trace of an easily ionized substance, namely potassium. Although those data were based on the best available information at the time, recent shock tube measurements by Lin (19) show considerably greater values of

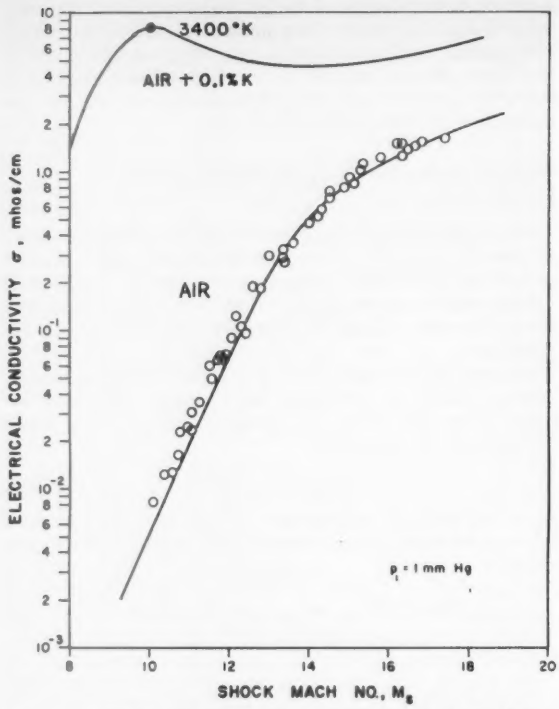

Fig. 7 Electrical conductivity of air measured in shock tube at initial pressure 1 mm Hg (ref. 19), and calculated conductivity of air seeded with 0.1 per cent potassium

σ. A new graph based on Lin's measurements in air and a corresponding calculation for seeded air is shown in Fig. 7. As pointed out in (1), these values of σ do not make air a very good conductor of electricity, in comparison with metals, for example.

There are, moreover, some phenomena related to the conduction of electricity in gases which cause serious loss of conductivity at low densities. Fundamentally, the conductivity arises from the forces that act on charged particles in an electric field. Such forces act in opposite directions on electrons and ions; the electrons, being more mobile, account for most of the conductivity. In a dense gas they experience collisions with atoms and ions, but an electron drift is set up which constitutes a current.

In empty space, however, a charged particle under the influence of simultaneous electric and magnetic fields does not travel in the direction of the electric field but tends to circle about the magnetic lines of force (14), since it experiences a force proportional to the vector product of its velocity and the local magnetic vector.

The electrons and ions of an ionized gas would perform this same circling motion if it were not for their collisions with other particles. It is, in fact, the anisotropic nature of this motion, that, through collisions, gives rise to the body force $\boldsymbol{j} \times \boldsymbol{H}$ introduced in Equation [2] and mentioned frequently in this paper. Now, in a rarefied gas the circling motion becomes more important because of the greater time between collisions, and the drift of electrons in the direction of the electric field is thereby inhibited. If the electrons can flow in the direction perpendicular to both fields, they do so, and they produce the *Hall current*. The theory of this situation is worked out in (14) and elsewhere. The results show how the electrical conductivity is affected by density and magnetic field strength; for the strong fields involved in magnetohydrodynamics, the conductivity would effectively disappear at altitudes of about 200,000 ft.

Fortunately, the conductivity is partially restored if no Hall current can flow; instead, a *Hall potential* is set up, and the electrons again drift in the direction of the original field. Thus, there are possibilities of maintaining conductivity at high altitudes, but their successful realization must depend on details of the geometry. The resulting boundary value problems would seem to be very complicated in practical cases. Thus the kind of magnetohydrodynamic calculations described in the present paper may really be greatly oversimplified in comparison with the practical problems that will occur in connection with the design of vehicles for flight at very high altitudes.

In conclusion, it can be reported that the field of magnetohydrodynamics in the United States is attracting the attention of a growing number of engineers who specialize in fluid mechanics. Both theoretical and experimental studies are being undertaken, although there is little indication of how or when this intriguing new branch of fluid mechanics will contribute to practical engineering. Successful applications may have to wait for new developments in other fields, such as lightweight fission or fusion power sources. It seems more profitable to continue with basic studies of the field, so that a store of knowledge and experience will be built up for future use. The history of science seems to show that new phenomena ultimately find practical applications, and this should apply to the phenomena of conductivity and electrical body force in high-speed aerodynamics.

Nomenclature

a	$= \sqrt{\gamma \mathcal{R} T}$
A	= cross-section area of duct
c_p	= specific heat, constant pressure
c_v	= specific heat, constant volume
$\boldsymbol{E}$	= electric field vector (magnitude E)
f	= perturbation quantity (Eq. [41])
f, g	= arbitrary functions (Eq. [62])
h_x, h_y	= perturbation components of magnetic field vector
$\boldsymbol{H}$	= magnetic field vector (magnitude H)
H_θ	= tangential component of $\boldsymbol{H}$
j	= current-density vector (magnitude j)
j_x, j_y	= components of j
j_0	= see Equation [23]
J_s	= surface current (current per unit length)
K	= ratio of V to speed of propagation of disturbances, Equation [61]
L	= typical length
m	$= V/a$
M	$= V/a$
N	= dimensionless quantity defined in Equation [8]
p	= pressure
$\boldsymbol{q}$	= fluid velocity vector (magnitude q)
Q	= heat added in addition to Joule heating
r	= radial coordinate (cylindrical)
r_1	= value of r at outside edge of conducting cylindrical stream
$\mathcal{R}$	= gas constant
Re	= Reynolds number VL/ν
R_m	= magnetic Reynolds number $VL\sigma$
t	= time
u, v, w	= components of $\boldsymbol{q}$
u', v'	= perturbation velocity components
u_1, u_2, u_3	= significant speeds defined in Equations [17 and 19]
V	= typical speed, e.g., stream speed
x, y, z	= Cartesian coordinates
α	= speed of Alfvén waves (Eq. [11])
γ	$= c_p/c_v$
ϵ	= angle of attack
λ	$= 2\pi \times$ (wave length of sinusoidal wall)$^{-1}$
μ	= damping coefficient of waves
ν	= kinematic viscosity
ξ	= curl $\boldsymbol{H}$ (magnitude ξ)
ρ	= density of fluid
σ	= electrical conductivity of fluid
ψ	= stream function
Ω	= vorticity (magnitude Ω)

Subscripts

∞	= undisturbed, free-stream, or typical value
0, 1, 2, . . .	= successive approximations as defined in Equation [41], except as otherwise noted above

Bar indicates dimensionless quantities, and $\bar{\nabla}$ is the operator involving derivatives with respect to $\bar{x}$, $\bar{y}$ and $\bar{z}$.

References

1 Resler, E. L., Jr. and Sears, W. R., "The Prospects for Magneto-Aerodynamics," *J. Aeron. Sci.*, vol. 25, April 1958, pp. 235–245, 258.

2 Joos, G., "Theoretical Physics," G. E. Stechert & Co., New York, 1934.

3 Resler, E. L., Jr. and Sears, W. R., "Magneto-Gasdynamic Channel Flow," *J. Appl. Math. and Phys.* (*ZAMP*), vol. 9b, 1958 Jakob Ackeret Festschrift, pp. 509–518.

4 Resler, E. L., Jr. and Sears, W. R., "The Prospects for Magneto-Aerodynamics—Correction and Addition," Readers' Forum, *J. Aeron. Sci.*, vol. 26, May 1959, p. 318.

5 Cowling, T. G., "Magnetohydrodynamics," Interscience Publishers, Inc., New York, 1957, p. 10.

6 Rossow, V. J., "On Flow of Electrically Conducting Fluids over a Flat Plate in the Presence of a Transverse Magnetic Field," NACA TN 3971, 1957; *see also* "On Magneto-Aerodynamic Boundary Layers," *J. Appl. Math. and Phys.* (*ZAMP*), vol. 9b, 1958, Jakob Ackeret Festschrift, pp. 519–527; "Magnetohydrodynamic Analysis of Heat Transfer Near a Stagnation Point," *J. Aeron. Sci.*, vol. 25, May 1958, p. 334.

7 Neuringer, J. L. and McIlroy, W., "Incompressible Two-Dimensional Stagnation-Point Flow of an Electrically Conducting Viscous Fluid in the Presence of a Magnetic Field," *J. Aeron. Sci.*, vol. 25, 1958, pp. 194–198; *see also* "Hydromagnetic Effects on Stagnation-Point Heat Transfer," *J. Aeron. Sci.*, vol. 25, May 1958, pp. 332–334.

8 Meyer, Rudolph C., "On Reducing Aerodynamic Heat-Transfer Rates by Magnetohydrodynamic Techniques," *J. Aeron. Sci.*, vol. 25, Sept. 1958, pp. 561–566.

9 Hartmann, J., "Hg-Dynamics I, Theory of the Laminar Flow of an Electrically Conductive Liquid in a Homogeneous Magnetic Field," *Kgl. Danske Videnskabernes Selskab, Math-fys. Meddelelser* XV, 6, Copenhagen, 1937.

10 Shercliffe, J. A., "Steady Motion of Conducting Fluids in Pipes under Transverse Magnetic Fields," *Proc. Cambridge Phil. Soc.*, vol. 49, 1953, pp. 166–168; *see also* "The Flow of Conducting Fluids in Circular Pipes under Transverse Magnetic Fields," *J. Fluid Mech.*, vol. 1, 1956, pp. 644–666.

11 Pai, Shih-I, "Laminar Flow of an Electrically Conducting Incompressible Fluid in a Circular Pipe," *J. Appl. Phys.*, vol. 25, no. 9, Sept 1954, pp. 1205–1207.

12 Alfvén, H., "On the Existence of Electromagnetic-hydrodynamic Waves," *Arkiv för Matematik Astronomi och Fysik*, vol. 29B, no. 2, 1943; *see also Nature*, vol. 150, 1942, pp. 405-406.

13 Rosa, R. J., "Engineering Magneto-Hydrodynamics," Ph. D. Thesis, Cornell University, June 1956.

14 Spitzer, L., Jr., "Physics of Fully Ionized Gases," Interscience Publishers, Inc., New York, 1956.

15 Sears, W. R. and Resler, E. L., Jr., "Theory of Thin Airfoils in Fluids of High Electrical Conductivity," *J. Fluid Mech.*, vol. 5, Feb. 1959, pp. 257–273.

16 McCune, J. E., "On the Motion of Thin Airfoils in Fluids of Large but Finite Electrical Conductivity," to be published in *J. Fluid Mech.*

17 Hayes, W. D., "An Alternate Proof of the Constancy of Circulation," *Quart. Appl. Math.*, vol. 7, 1949, pp. 235–236.

18 Sears, W. R., "Small Perturbation Theory," section C, vol. VI, in "Princeton Series on High Speed Aerodynamics and Jet Propulsion," 1954, pp. 61–120.

19 Lin, S. C., "Electrical Conductivity of Thermally Ionized Air Produced in a Shock Tube," Avco Research Note 26, Feb., 1957.

General

"A Discussion of Magneto-Hydrodynamics," 12 papers, *Proc. Roy. Soc.*, vol. A 233, 1955, pp. 289–406.

Landshof, R. K. M., Ed., "Magnetohydrodynamics, A Symposium," Stanford University Press, 1957.

Landshof, R. K. M., Ed., "The Plasma in a Magnetic Field, A Symposium," Stanford University Press, 1958.

Bershader, D., Ed., *Proc. 1958 Symposium*, to be published by Stanford University Press in 1959.

Lundquist, S., "On the Stability of Magneto-Hydrostatic Fields," *Phys. Rev.*, vol. 83, 1951, pp. 307–311; *also Arkiv Fysik*, vol. 5, no. 15, 1952.

Astrophysical Applications

Alfvén, H., "Cosmical Electrodynamics," Oxford University Press, 1950.

Batchelor, G. K., "Spontaneous Magnetic Field in a Conducting Fluid," *Proc. Roy. Soc., London*, Series A, vol. 201, 1950, p. 405.

Chandrasekhar, S., "Hydromagnetic Turbulence," *Proc. Roy. Soc., London*, Series A, no. 1194, vol. 233, Dec. 29, 1955, pp. 322–349.

Van de Hulst, H. C., "Interstellar Polarization and Magneto-hydrodynamic Waves," Problems of Cosmical Electrodynamics, Central Air Documents Office no. AD-1103347, 1949.

Elsasser, W. M., "Hydromagnetic Dynamo Theory," *Rev. Modern Phys.*, vol. 28, April, 1956, pp. 135–163.

Physics of Conducting Gases

Chapman, S. and Cowling, T. G., "The Mathematical Theory of Non-Uniform Gases," Cambridge University Press, 1939.

Cowling, T. G., "Electrical Conductivity of an Ionized Gas in a Magnetic Field," *Proc. Roy. Soc. of London*, Series A, vol. 183, 1945, pp. 453–478.

Kantrowitz, A., Resler, E. L. and Lin, S. C., "Electrical Conductivity of Highly Ionized Argon Produced by Shock Waves," *J. Appl. Phys.*, vol. 26, Jan. 1955, pp. 95–109.

Lamb, L. and Lin, S C., "Electrical Conductivity of Thermally Ionized Air Produced in a Shock Tube," *J. Appl. Phys.*, vol. 28, no. 7 July 1957, pp. 754–759.

Maecker, H. and Peters, T., "Messung der Plasmaleitfähigkeit im Hochleistungsbogen," *Zeitschrift für Physikalische Chemie*, vol. 198, no. 5/6, 1951, pp. 319–328.

Schlüter, A., "Dynamik des Plasmas I. Grundgleichungen, Plasma in gekreuzten Feldern," *Zeitschrift für Naturforschung*, vol. 5A, 1950, pp. 72–78.

Schlüter, A., "Dynamik des Plasmas II. Plasma mit Neutralgas," *Zeitschrift für Naturforschung*, vol. 6A, 1951, pp. 73–78.

Wave Propagation

Lüst, R., "Magneto-hydrodynamische Stosswellen in einem Plasma unendlicher Leitfähigkeit," *Zeitschrift für Naturforschung*, vol. 8A, no. 5, 1953, pp. 8277–284.

Herlofsen, N., "Magneto-Hydrodynamic Waves in a Compressible Fluid Conductor," *Nature*, vol. 165, 1950, p. 1020.

Friedrichs, K. O. and Kranzer, H., "Notes on Magneto-Hydrodynamics VIII. Nonlinear Wave Motion," NYO-6486, Inst. Math. Sci., N.Y.U. July 1958.

Sen, Hari K., "Structure of a Magneto-hydrodynamic Shock Wave in a Plasma of Infinite Conductivity," *Phys. Rev.*, vol. 102, no. 1, April 1956, pp. 5–11.

Teller, E. and de Hoffman, F., "Rankine-Hugoniot Equations for Shock Waves in an Infinitely Conducting Fluid with Superposed Magnetic Field," *Phys. Rev.*, vol. 80, 1950, p. 692.

Grad, H., "Propagation of Magnetohydrodynamic Waves Without Radial Attenuation," NYO-2537, Inst. Math. Sci., N.Y.U., Jan. 15, 1959.

Cole, J. D., "Magnetohydrodynamic Waves," OSR Tech. Note 59-13, Guggenheim Aero. Lab., Calif. Inst. Tech., Jan. 1959.

Mitchner, M., "Magnetohydrodynamic Flow in a Shock Tube," *Phys. Fluids*, vol. 2, no. 1, 1959, pp. 62–71.

Engineering Applications

Elsasser, W. M., "Dimensional Relations in Magneto-Hydrodynamics," *Phys. Rev.*, vol. 95, no. 1, July 1950, pp. 1–5.

Hartmann, J. and Lazarus, F., "Experimental Investigations on the Flow of Mercury in a Homogeneous Magnetic Field," *Kgl. Danske Videnskabernes Selskab, Math.-fys. Meddelelser* XV, 7, Copenhagen, 1937.

Lock, R. C., "Stability of the Flow of Electrically Conducting Fluid Between Parallel Planes Under a Transverse Magnetic Field," *Proc. Roy Soc., London*, Series A, vol. 233, no. 1192, Dec. 6, 1955, pp. 105–125.

Pai, S. I., "Energy Equation of Magneto-Gas-Dynamics," *Phys. Rev.*, vol. 105, no. 5, March 1, 1957, pp. 1424–1426.

Patrick, R. M., "Magneto-Hydrodynamics of Compressible Fluids," Cornell University Ph.D. Thesis, June 1956.

Covert, E. E., "On Some Fundamentals in Magneto-Fluid-Mechanics," MIT Naval Supersonic Laboratory, Technical Rep. 247, March 1958.

Pai, S. I., "Magnetohydrodynamics and Magnetogasdynamics," Institute for Fluid Dynamics and Applied Mathematics, University of Maryland, Tech. Note BN-59, Sept. 1955.

Pai, S. I., "On Exact Solutions of One-Dimensional Flow Equations of Magneto-Gasdynamics," Institute for Fluid Dynamics and Applied Mathematics, University of Maryland, Tech. Note BN-82, Sept. 1956.

Rocket Thrust Termination Transients

HOWARD C. RODEAN[1]

Chance Vought Aircraft, Inc.
Dallas, Texas

Rocket thrust termination transients are of importance in the range control of ballistic missiles and in the separation of boosters or different missile stages. Items of interest include the nature of the thrust decay, the impulse increment of the thrust termination transient and the time constant of the transient. Equations are developed for these items for idealized cases with reasonable simplifying assumptions, and the results plotted in generalized form. This analysis is considered to be a good approximation for liquid propellant rockets with instantaneous propellant shutoff and "sliverless" burnout of solid propellant rockets.

Assumptions

IN A ROCKET combustion chamber, the rate of burned gas generation is equal to the sum of the gas flow rate out of the combustion chamber through the nozzle plus the rate at which gas accumulates in the combustion chamber

$$\dot{m}_b = \dot{m}_t + (d/dt)\,(m_c) \qquad [1]$$

The following assumptions are made:

1 The transient is initiated by instantaneously stopping burned gas generation.

2 The gas properties are uniform throughout the combustion chamber at every instant of time.

3 The gas flow through the nozzle may be considered as a quasi-steady flow process.

4 The nozzle is choked throughout the transient. This is true for expansion into a vacuum, and is true for the most significant part of the transient for finite values of ambient pressure.

5 The gas processes in the combustion chamber and nozzle are isentropic during the transient.

6 The perfect gas law applies.

Received Sept. 10, 1958.

[1] Senior Specialist, Advanced Weapons Engineering. Project SLAM. Member ARS.

Gas Flow Through the Nozzle During the Transient

The gas flow rate through a choked nozzle during a thrust termination transient may be expressed by the following equation

$$\dot{m}_t = A_t \sqrt{\frac{k}{g\,R\,T_{c_1}} \left(\frac{2}{k+1}\right)^{(k+1)/(k-1)} p_{c_1}{}^{(k-1)/k}\, p_c{}^{(k+1)/k}} \qquad [2]$$

The mass of gas in the combustion chamber at any instant is

$$m_c = \frac{L^* A_t}{g\,R\,T_{c_1}}\, p_{c_1}{}^{(k-1)/k}\, p_c{}^{(1/k)} \qquad [3]$$

Differentiating Equation [3] with respect to time and substituting the result and Equation [2] into Equation [1] for the case when $\dot{m}_b = 0$

$$dt = \frac{-L^*}{k\sqrt{k\,g\,R\,T_{c_1}}} \sqrt{\left(\frac{k+1}{2}\right)^{(k+1)/(k-1)} p_{c_1}{}^{(k-1)/k}\, p_c{}^{-(3k-1)/k}}\, dp_c \qquad [4]$$

The above equation relates time and the combustion chamber

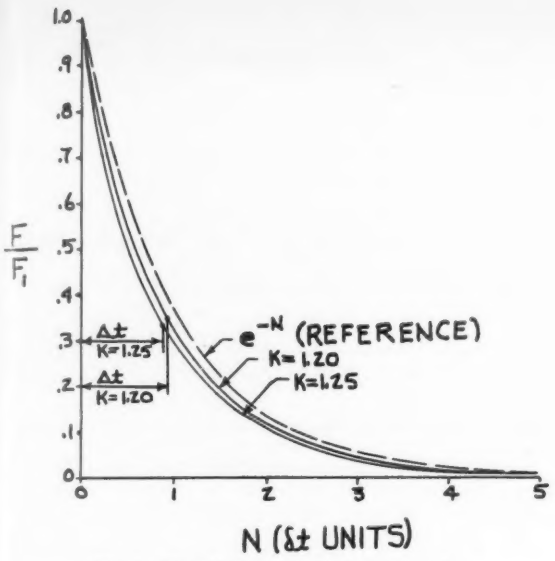

Fig. 1 Thrust decay transient for Case 1

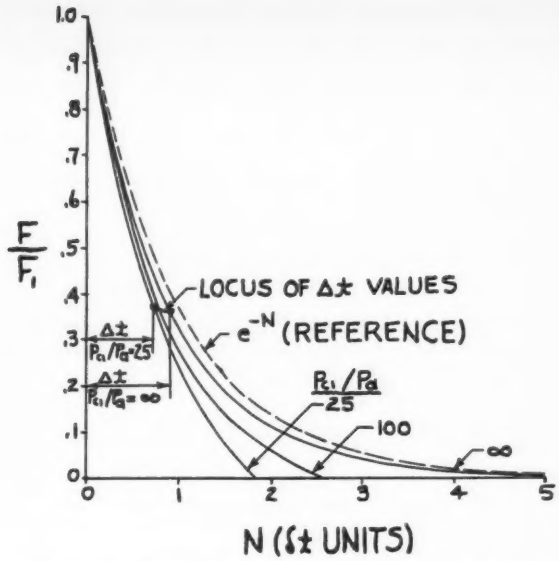

Fig. 2 Thrust decay transient for Case 2 and $k = 1.20$

pressure during the transient. Integrating Equation [4] between the limits t_1 and t, and p_{c1} and p_c

$$t - t_1 = \frac{L^*}{\sqrt{k\,g\,R\,T_{c1}}}\left(\frac{2}{k-1}\right)\sqrt{\left(\frac{k+1}{2}\right)^{(k+1)/(k-1)}} \times \left[\sqrt{\left(\frac{p_{c1}}{p_c}\right)^{(k-1)/k} - 1}\right] \quad [5]$$

Thrust Decay During Thrust Termination

Case 1 Fixed Nozzle Area Ratio and Zero Ambient Pressure

This case is the more practical of those considered because most rocket nozzles have fixed geometry, and the ambient pressure is very small for the altitudes at which thrust termination is initiated for range control and missile stage separation. The rocket thrust equation is (1)[2]

$$F = p_c A_t C_F \quad [6]$$

It may be shown that C_F is constant during the transient under the assumed conditions.

The ratio of thrust at any time ($N\delta t$) after initiation of thrust termination to the initial thrust may be determined by combining Equations [5, 6 and A-1] for the time ($N\delta t$) set equal to ($t - t_1$)

$$\left(\frac{F}{F_1}\right)_{N\delta t} = \left(1 + \frac{k-1}{2}N\right)^{-2k/(k-1)} \quad [7]$$

This equation is plotted in Fig. 1 for $k = 1.20$ and $k = 1.25$

Case 2 Variable Nozzle Area Ratio and Finite Ambient Pressure

This is an idealized case in which the nozzle area ratio is assumed to be continuously variable during the thrust transient so as always to provide complete expansion to ambient pressure. The nozzle throat area remains constant. The thrust equation for this case is (2)

$$F = p_c A_t \sqrt{\left(\frac{2k^2}{k-1}\right)\left(\frac{2}{k+1}\right)^{(k+1)/(k-1)}\left[1 - \left(\frac{p_a}{p_c}\right)^{(k-1)/k}\right]} \quad [8]$$

[2] Numbers in parentheses indicate References at end of paper.

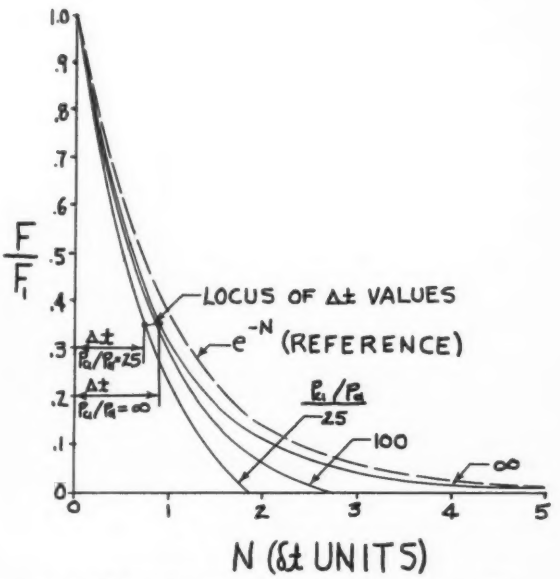

Fig. 3 Thrust decay transient for Case 2 and $k = 1.25$

The ratio of thrust at any time ($N\delta t$) after initiation of thrust termination to the initial thrust may be determined in the same manner as for Equation [7]

$$\left(\frac{F}{F_1}\right)_{N\delta t} = \left(1 + \frac{k-1}{2}N\right)^{-2k/(k-1)} \times \sqrt{1 - \frac{(k-1)N + [(k-1)/2]^2N^2}{\left(\frac{p_{c1}}{p_a}\right)^{(k-1)/k} - 1}} \quad [9]$$

For zero ambient pressure, Equation [9] reduces to Equation [7]. Equation [9] is plotted in Figs. 2 and 3 for $k = 1.20$ and $k = 1.25$, respectively.

Impulse Increment During Thrust Termination

Case 1 Fixed Nozzle Area Ratio and Zero Ambient Pressure

The impulse during the thrust termination transient is

$$\Delta I = \int_{t_1}^{\infty} F\, dt \qquad [10]$$

Substituting Equations [4 and 6] into Equation [10] and integrating

$$\Delta I = \frac{p_{c_1} L^* A_t C_F}{\sqrt{k\, g\, R\, T_{c_1}}} \left(\frac{2}{k+1}\right) \sqrt{\left(\frac{k+1}{2}\right)^{(k+1)/(k-1)}} \qquad [11]$$

A reference impulse increment for this case may be obtained from Equations [6, A-2 and A-3]. Combining the result with Equation [11]

$$\frac{\Delta I}{\delta I} = \frac{2}{k+1} \qquad [12]$$

The above ratio may be regarded as the efficiency of the impulse-producing process during the transient relative to that during steady state operation with the same quantity of gas as discussed in Appendix 1.

Case 2 Variable Nozzle Area Ratio and Finite Ambient Pressure

The impulse during the thrust termination transient in this case is the following when written in terms of a and x from Equations [4 and 8]

$$\Delta I = \frac{p_{c_1} L^* A_t}{\sqrt{k\, g\, R\, T_{c_1}}} \left(\frac{k}{k-1}\right) \sqrt{\frac{2}{k-1}} \sqrt{\frac{1}{2a}} \times \int_1^{2a} \frac{\sqrt{2ax - x^2}}{(x)^{(2k-1)/(k-1)}}\, dx \qquad [13]$$

If the exponent $(2k-1)/(k-1)$ in the above equation is an integer, the integral can be integrated by means of Equation [224] of (3). This exponent is an integer for both $k = 1.20$ and $k = 1.25$, which are reasonable values for rocket exhaust gases

$$(\Delta I)_{k=1.20} = 6\sqrt{10} \left(\frac{p_{c_1} L^* A_t}{\sqrt{1.20\, g\, R\, T_{c_1}}}\right) \sqrt{\frac{1}{2a}}\, (2a-1)^{3/2} \times \left[\frac{1}{11a} + \frac{4}{99a^2} + \frac{4}{231a^3} + \frac{8}{1155a^4} + \frac{8}{3465a^5}\right] \qquad [14a]$$

$$(\Delta I)_{k=1.25} = 10\sqrt{2} \left(\frac{p_{c_1} L^* A_t}{\sqrt{1.25\, g\, R\, T_{c_1}}}\right) \sqrt{\frac{1}{2a}}\, (2a-1)^{3/2} \times \left[\frac{1}{9a} + \frac{1}{21a^2} + \frac{2}{105a^3} + \frac{2}{315a^4}\right] \qquad [14b]$$

The reference impulse increment for this case is obtained in the same manner as for Equation [12]. Then equations analagous to Equation [12] may be obtained

$$\left(\frac{\Delta I}{\delta I}\right)_{k=1.20} = 5(2a-1) \times \left[\frac{1}{11a} + \frac{4}{99a^2} + \frac{4}{231a^3} + \frac{8}{1155a^4} + \frac{8}{3465a^5}\right] \qquad [15a]$$

$$\left(\frac{\Delta I}{\delta I}\right)_{k=1.25} = 4(2a-1)\left[\frac{1}{9a} + \frac{1}{21a^2} + \frac{2}{105a^3} + \frac{2}{315a^4}\right] \qquad [15b]$$

For complete expansion into a vacuum, Equations [15a and 15b] reduce to Equation [12] for $k = 1.20$ and $k = 1.25$, respectively. Equations [15a and 15b] are plotted in Fig. 4 for various values of initial pressure ratio.

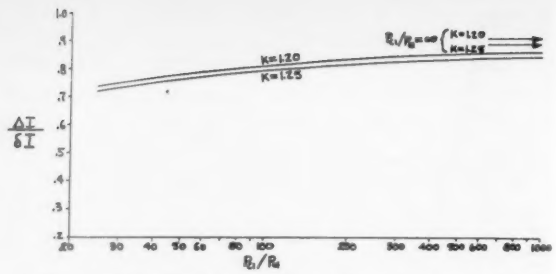

Fig. 4 Thrust termination impulse increment for Case 2

Time Constant of Thrust Termination Transient

The following approximation for the time constant of the thrust termination transient may be made based on the suggestion in Appendix 2 and Equation [B-2]

$$\Delta t = \Delta I / F_1 \qquad [16]$$

The points for Δt indicated on Figs. 1, 2 and 3 show that Δt is a good approximation to the time constant for the thrust termination transient. An exponential curve corresponding to Equation [B-1] is also plotted for reference, indicating that the thrust decay curves for the higher initial pressure ratios do not differ appreciably from an exponential function.

Appendix 1
Reference Time and Impulse Increments

The selected reference time may be defined as the average "dwell time" of the gases in the combustion chamber during steady-state rocket operation as defined by Equation [1] when $(d/dt)\ (m_c) = 0$. The following equation may be written for this "dwell time"

$$\delta t = m_c / \dot{m}_t \qquad [A\text{-}1]$$

Substituting Equations [2 and 3] modified for steady-state operation into Equation [A-1]

$$\delta t = \frac{L^*}{\sqrt{k\, g\, R\, T_{c_1}}} \sqrt{\left(\frac{k+1}{2}\right)^{(k+1)/(k-1)}} \qquad [A\text{-}2]$$

By definition, the mass of the total gas flow through the nozzle during the time δt is equal to the mass of the gas contained within the combustion chamber at any instant during steady-state conditions. This is also equal to the mass of the gas contained in the combustion chamber at the beginning of the thrust transient.

The reference impulse increment is defined as

$$\delta I = F_1 \delta t \qquad [A\text{-}3]$$

where F_1 is the steady-state thrust which is equal to the thrust at the beginning of the transient.

Appendix 2 Response to a Step Input

In a system which has an exponential output described by the function

$$\phi(t) = b\, e^{-ct} \qquad [B\text{-}1]$$

in response to a negative step input, the time constant is defined as that time at which the output has decreased to the fraction $(1/e)$ or 0.368 of the initial value and occurs when $t = 1/c$ (4).

The area under the above exponential curve may be obtained by integrating Equation [B-1]. This is equal to the

area of a rectangle with the height equal to the initial function value (b) and the width equal to the response time ($1/c$). This suggests the following means of defining the time constant for this application

$$\Delta t = \frac{\int_0^\infty \phi(t)\, dt}{\phi(0)} \qquad [B\text{-}2]$$

Nomenclature

A = area
a = $(\frac{1}{2})\,(p_{c1}/p_a)^{(k-1)/k}$
b = constant
C_F = thrust coefficient
c = constant
e = base of natural logarithms
F = thrust
g = standard acceleration of gravity
ΔI = thrust termination impulse increment
δI = reference impulse increment
k = ratio of specific heats
L^* = combustion chamber characteristic length
m = mass
$\dot{m}$ = mass rate with time
N = number of reference time increments
p = pressure
R = gas constant
T = temperature
t = time
Δt = time constant
δt = reference time increment
x = $(p_{c1}/p_c)^{(k-1)/k}$
ϕ = function

Subscripts

a = ambient
b = burned gas
c = combustion chamber
t = nozzle throat
1 = initial conditions

References

1 Crocco, L., "One-Dimensional Treatment of Gas Dynamics," Part B of "Fundamentals of Gas Dynamics," Emmons, H. W., Ed., Princeton Univ. Press., 1958, p. 164,

2 Shapiro, A. H., "The Dynamics and Thermodynamics of Compressible Flow," Ronald, New York, 1953, p. 102.

3 Peirce, B. O. and Foster, R. M., "A Short Table of Integrals," Ginn, Boston, fourth ed., 1956, p. 33.

4 Chestnut, H. and Mayer, R. W., "Servomechanisms and Regulating System Design," vol. 1, John Wiley and Sons, Inc., New York, 1951, p. 39.

Effect of Dissociation on the Performance of Working Fluids for Nuclear Propulsion[1]

J. G. LOGAN[2] and
E. L. COLICHMAN[3]

Space Technology Laboratories, Inc.
Los Angeles, Calif.

Recent developments indicate a growing interest in nuclear propulsion. In this paper, general enthalpy relations are derived for an idealized diatomic gas to investigate the effect of molecular weight, dissociation energy and pressure on the performance of diatomic working fluids. It is shown that maximum performance for a given molecular weight should be obtainable from molecules with bond energies in the range 1.5 to 2.5 ev. The influence of pressure on dissociation is also indicated. The results of the study for the diatomic system also indicate desirable ranges of molecular weight and bond energy for more complex molecular systems.

ANALYSES of chemical rocket systems have shown that performance limitations, aside from material temperature limitations, result from molecular characteristics, such as bond energies, molecular weight and molecular dissociation energy.

Received Sept. 8, 1958.

[1] The investigation upon which this research is based was sponsored by the Air Force Ballistic Missile Division.

[2] Manager, Propulsion Research Dept.

[3] Technical Staff Assistant, Propulsion Research Dept.

With increasing interest in nuclear propulsion, it is desirable to obtain corresponding limits in performance for storable fluids which could be employed for nuclear engines. It would be expected that the same factors limiting performance in chemical systems would also limit performance in nuclear systems, namely: Bond energy, molecular weight and molecular dissociation energy.

In a nuclear propulsion system, there is essentially a constant-temperature, infinite energy source. Consequently, working fluids should be selected which will absorb the maxi-

mum energy. Such systems could include complex polyatomic molecular fluids with large numbers of degrees of freedom which are not excited at low temperatures, and systems with low values of dissociation energies and bond energies. At the temperatures considered for practical heat transfer processes, the effects of ionization may be neglected since relatively little contribution to enthalpy can be expected.

A second requirement is that the excitation process be reversible in the sense that stable, excited or dissociated (free radical) states exist in thermodynamic equilibrium at the heat transfer temperature in order that this energy can be returned to the system by recombination during the expansion process.

Complex molecules with large numbers of degrees of freedom would tend to have large molecular weight values and, hence, small enthalpy per unit mass values. The most promising storable fluids for nuclear applications would, therefore, appear to be those with low molecular weights, low bond energies and low dissociation energies.

In this paper, a general analysis is undertaken of the relationship between dissociation energy, molecular weight and total enthalpy. Enthalpy values are determined for a typical homonuclear diatomic fluid based upon the characteristics possessed by several common diatomic liquids with low vaporization temperatures. The enthalpy values are computed in the molecular weight range 2 to 80 and the dissociation energy range 1 to 5 ev.

The results of this study are generalized for more complicated molecular systems. Detailed calculations for polyatomic systems will be presented in a subsequent paper.

Assumptions and Approximations

In the enthalpy calculations, a temperature of 6200 R was assumed as a characteristic maximum operating temperature for heat transfer applications. Calculations were carried out for the molecular process

$$A_2 \rightleftharpoons A + A \qquad [1]$$

in the molecular weight range 2 to 80 and the dissociation energy range 1 to 5 ev.

The equilibrium constant and enthalpy of the individual constituents are dependent upon the molecular and atomic parameters for the ground and excited states. At a temperature of 6200 R, only the ground state of the atomic species will contribute significantly to the enthalpy. A general atomic state ^2P was assumed in Table 1.

The enthalpy contributions of individual atomic and molecular components are independent of the statistical weight. Statistical weight factors will only effect the equilibrium constant, and even this effect is not significant for large values of the equilibrium constant ($K \gg 1$).

At a temperature of 6200 R, the summation over energy states

$$\sum g_i e^{-E_i/kT}$$

may be approximated by

$$\sum g_i e^{-E_i/kT} \simeq g_1 \simeq 6$$

The molecular state was approximated by the state $^1\Sigma$ with a statistical weight factor of 1. Calculations indicated that a good approximation to the molecular enthalpy contribution would be given by

$$\sum g_1 f_1 e^{-E_1/kT} \simeq f_1 \frac{1}{\sigma_1(1 - e^{-u_1})}$$

with

$$\sigma_1 = 2.6 \times 10^{-4}$$

$$u_1 = 0.24$$

These values were based upon averages for the molecular parameters of typical diatomic molecules.

The molecular parameters will significantly affect the calculation of the degree of dissociation only when the equilibrium constant is of the order of 1. In this paper, primary interest is centered on systems which are almost completely dissociated. Consequently, the molecular mole fraction will be approximately zero, and the molecular contribution to total enthalpy will be small.

Table 1 Atomic statistical weight factors

Atom	State	Statistical weight
Cl	^2P	6
H	^2S	2
F	^2P	6
Br	^2P	6
I	^2P	6

Enthalpy Relations

For thermodynamic equilibrium, the enthalpy per mole is given by (1,2)[4]

$$\frac{H}{RT} = \frac{M_0 T}{M}\left(X_A \frac{1}{f_A}\frac{df_A}{dT} + X_{A_2}\frac{1}{f_{A_2}}\frac{df_{A_2}}{dT} + \frac{1}{T}\right)$$

where X_i is the mole fraction and

$$\frac{1}{f_i}\frac{df_i}{dT}$$

is the dimensionless enthalpy contribution of the species i. f_i is the partition function. Using the molecular and atomic approximations, the enthalpy per unit mass becomes

$$H = \frac{RT^2}{M}\left[X_A\left(\frac{D_{A_2}}{2kT} + \frac{3}{2}\right) + 3.40\,X_{A_2} + 1\right] \qquad [2]$$

The equilibrium constant may be written in the form

$$K_A = 2.11 \times 10^3\, \rho_0/\rho M_A^{3/2} e^{-3.37 D_{A_2}(\mathrm{ev})} T^{3/2} \qquad [3]$$

Mole fractions can be calculated from the relations

$$X_A = \frac{1}{(3/4) + (1/4)\sqrt{1 + 16/K_A}} \qquad [4]$$

$$X_{A_2} = 1 - X_A \qquad [5]$$

Ionization contributions were neglected. Although the ionization process will contribute to the enthalpy in the form

$$X_A{}^+\left(\frac{I}{kT} + \frac{D}{2kT} + \frac{3}{2}\right)$$

the mole fraction, $X_A{}^+$, will be extremely small. For example, using an ionization potential of 4 ev, the equilibrium constant becomes

$$\rho/\rho_0 K = 1.913 \times 10^{-5}$$

Typical ionization values are shown in Table 2.

Typical dissociation energy values are shown in Table 3.

Results

As shown in Fig. 1, the degree of dissociation for the diatomic system is strongly dependent upon the dissociation energy of the molecule as well as the density or pressure.

[4] Numbers in parentheses indicate References at end of paper.

Table 2 Atomic ionization potentials

Element	Ionization potential I
Cs	3.893
Rb	4.176
K	4.339
C	11.264
H	13.595
O	13.614
N	14.540

Table 3 Molecular dissociation energies (D_0)

Molecule	D_0(ev)	Mol. wt.
Li_2	1.03	14
ICl	2.152	162
BeH	2.2	10
Cl_2	2.475	70
LiH	2.5	8
ClF	2.616	54
B_2	3.6	22
HBr	3.75	80
H_2	4.476	2

At high densities or pressures (for density ratios greater than 1, $P/P_0 > 10$) practically no dissociation will occur for dissociation energies greater than 4 ev unless the molecular weight approaches 100.

As shown in Equation [2], the enthalpy per unit mass varies directly with dissociation energy. The variation of the square root of enthalpy with dissociation energy for pressures of 0.1, 10 and 100 atm is shown in Fig. 2. The square root values plotted permit a direct comparison of relative specific impulse values.

Peak enthalpy values, at pressures of $\frac{1}{10}$ atm, occur at about 3 ev for any given molecular weight. Above pressures of 10 atm, peak enthalpy values occur at dissociation energy values between 1 and 2.5 ev.

At pressures between 10 and 100 atm, diatomic molecules with a molecular weight of 6 and a dissociation energy of 2 ev approach the enthalpy of hydrogen molecules with a molecular weight of 2 and a dissociation energy of 4.5 ev.

The calculations for a molecular weight of 2 are in reasonably good agreement with the actual enthalpy values for hydrogen at high pressures. At lower pressure values when the equilibrium constant and fraction of dissociation are more dependent upon molecular parameters, poorer agreement is obtained as a result of the use of average molecular parameters typical of heavier molecules.

Fig. 3 indicates the effect of different heat transfer temperatures on enthalpy for a gas of molecular weight 10 and pressures of 1, 10 and 100 atm.

The square root of enthalpy values shown in Figs. 2 and 3 furnish a direct indication of the relative merits of various diatomic gases for propulsion applications.

The specific effect of pressure on the degree of dissociation enters only through the mole fraction and molecular weight terms. In enthalpy calculations, the enthalpy contribution of the individual species is independent of pressure. When no dissociation occurs, therefore, the enthalpy is pressure independent. Specific pressure dependence of the enthalpy and specific impulse can be demonstrated for small values of

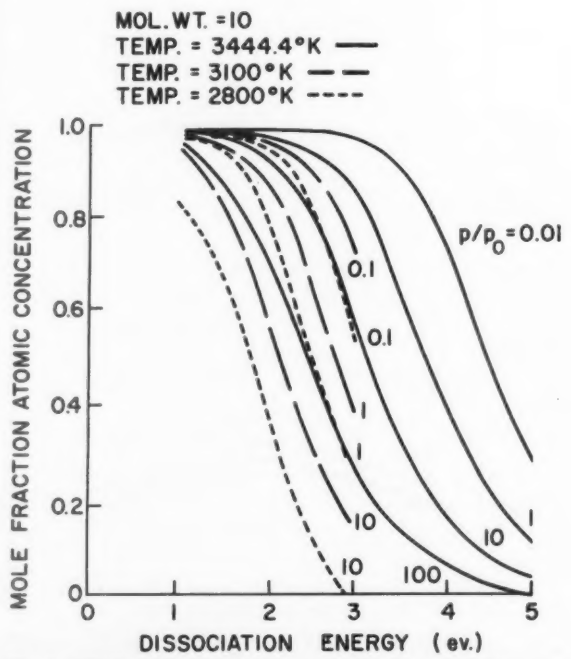

Fig. 1 Effect of dissociation energy and density on the degree of dissociation for diatomic molecules. $A_2 \rightleftarrows 2A$

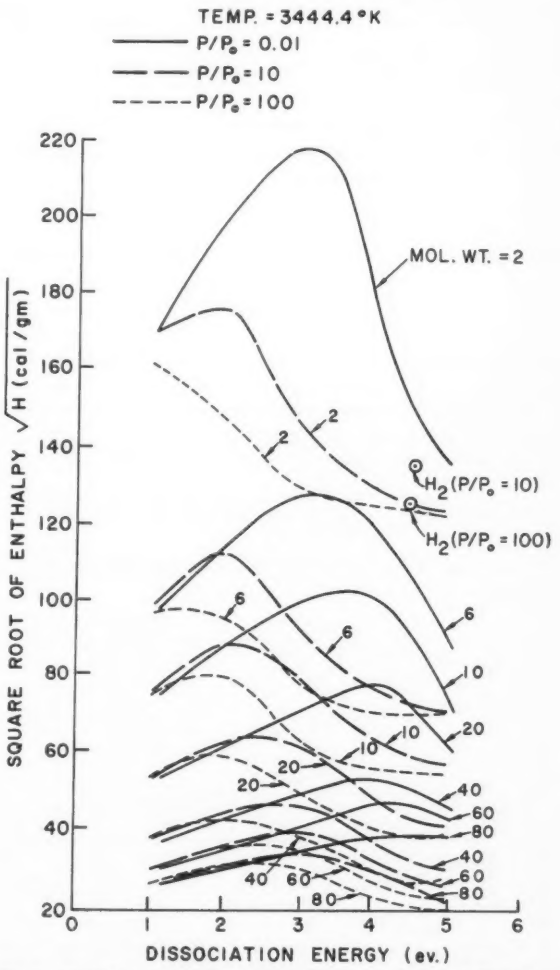

Fig. 2 Variation of enthalpy with molecular weight and dissociation energy for diatomic molecules. $A_2 \rightleftarrows 2A$

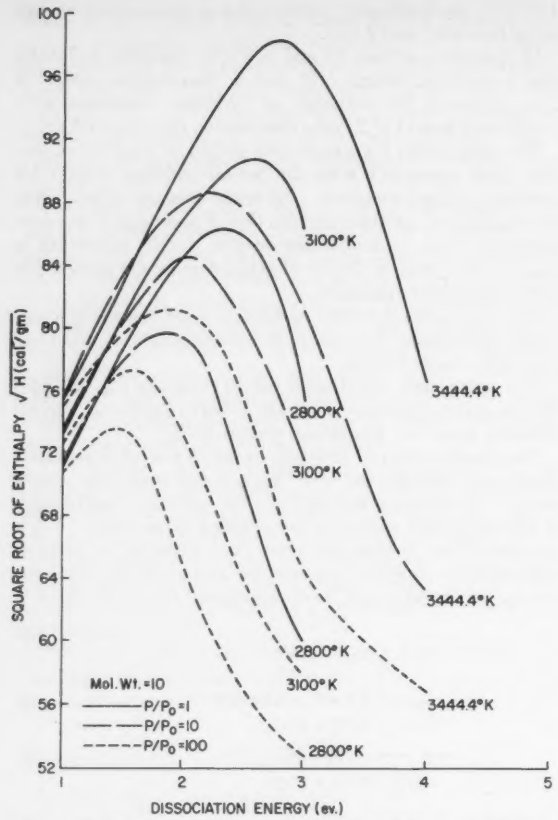

Fig. 3 Variation of enthalpy with dissociation energy and temperature. $A_2 \rightleftarrows 2A$

dissociation. The enthalpy may be written in the form

$$H \frac{\text{cal}}{\text{gm}} \sim C_1(T) + \frac{C_2(T)}{\sqrt{P}}$$

where the first term contains the enthalpy contribution of the molecules, and the second term the contribution of the atoms.

In expansion through a nozzle, the change in enthalpy between the inlet and exit temperatures (i and f) can be written approximately as

$$\Delta H \sim \frac{C_2(T_i)}{\sqrt{P}} + C_1(T_i) - C_1(T_f)$$

and consequently, the impulse in a dissociating system will vary as

$$I_{sp} \sim \sqrt{\Delta H} \sim \left[\frac{C_2(T_i)}{P^{1/2}} + C_1(T_i) - C_1(T_f)\right]^{1/2}$$

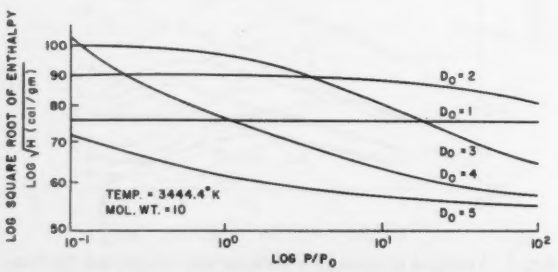

Fig. 4 Variation of enthalpy with pressure

The dissociation contribution to enthalpy can be much larger than the molecular contribution. It can be expected that as dissociation occurs, the specific impulse will demonstrate a strong dependence on pressure of the form

$$I_{sp} \sim P^{-1/4}$$

in regions where dissociation occurs. In regions of no dissociation or almost complete dissociation, enthalpy and impulse are pressure independent (Fig. 4). As shown in Fig. 5, at high pressures specific impulse values between 800 and 1000 sec should be achievable for diatomic systems having molecular weights between 6 and 10 and dissociation energies of above 2 ev.

The relative effects of dissociation energy, pressure and heat transfer temperature on peak specific impulse values are shown in Fig. 6 for a molecular weight of 10.

The results of these analyses can be generalized for more complicated molecular systems which possess bond energies in the range 1.5 to 2.5 ev and whose diatomic constituents also possess dissociation energies in this range. For these values, the molecular system upon breakdown will be composed essentially of free radicals which are stable at the high temperatures. The degree of free radical formation will determine to a large extent the advantages or disadvantages of storable propellants for high pressure applications. Detailed calculations for complex molecular systems will be presented in a subsequent paper.

Summary

This analysis is applicable only to the dissociation of diatomic systems wherein essentially free radicals are formed as a result of the molecular breakdown. It would, therefore, apply to any solid or liquid substance with a low dissociation

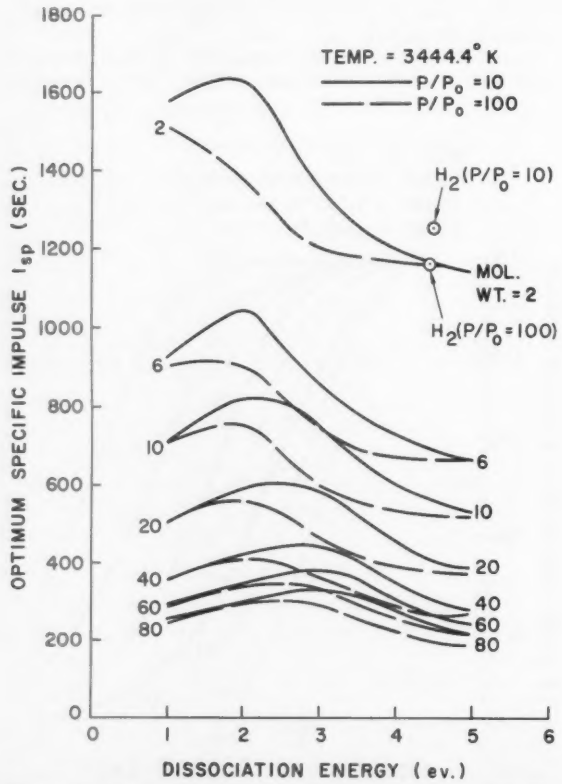

Fig. 5 Variation of optimum specific impulse values with dissociation energy for diatomic molecules. $A_2 \rightleftarrows 2A$

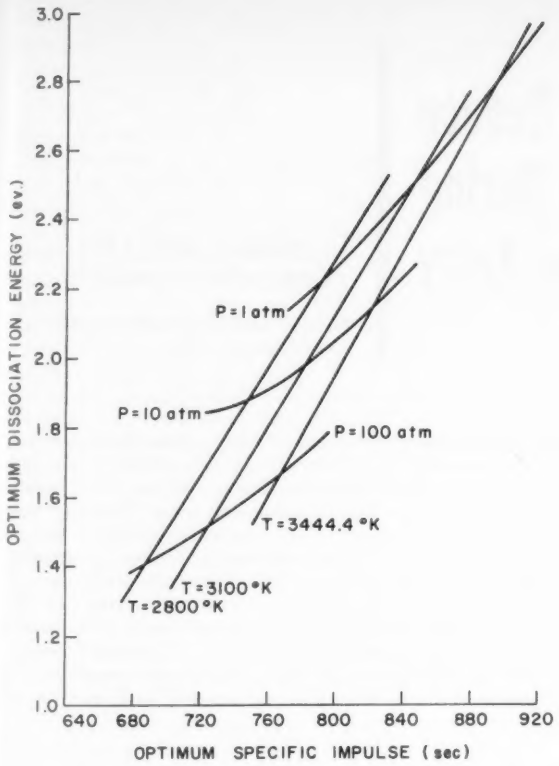

Fig. 6 Dissociation energy values for optimum specific impulse as a function of temperature and pressure. $A_2 \rightleftarrows 2A$

energy. The general calculation may be extended to more complicated molecular systems provided that in the process of molecular breakdown, fragments are formed which are stable in the high temperature region. The energy of dissociation which will increase the enthalpy at a given temperature will then be returned to the system upon expansion.

If, in the breakdown of the complicated molecular system, stable molecular products are formed at the high temperature which will persist in the expansion process at low temperatures, performance gains may not be achievable. However, it is expected that in the general breakdown of molecular systems free radicals will be formed. The extent of the free radical formation will determine to a large extent the advantages or disadvantages of working fluids at high pressure levels.

Probably the most interesting conclusion from these investigations is that it may be possible to achieve a storable working fluid in the pressure range 10 to 1000 psi which will closely approach the performance of hydrogen at high pressure levels. Such systems would be composed of the lightweight atoms, such as carbon, hydrogen, oxygen, lithium, boron and beryllium.

Acknowledgment

The authors wish to thank Mr. H. R. Lawrence for originally suggesting the problem and Miss H. J. Olson for carrying out the numerical calculations.

References

1 Logan, J. G., "The Calculation of the Thermodynamic Properties of Air at High Temperatures," Cornell Aeronautical Laboratory Rep. no. 1052-A-1, May 1956.

2 Treanor, C. E. and Logan, J. G., "Thermodynamic Properties of Oxygen From 2000°K to 5000°K," Cornell Aeronautical Laboratory Rep. no. BE-1007-A-4, Jan. 1957.

Use of Drag Modulation to Reduce Deceleration Loads During Atmospheric Entry

RICHARD L. PHILLIPS[1] and CLARENCE B. COHEN[2]

Space Technology Laboratories, Inc.
Los Angeles, Calif.

The design of a space vehicle which must be capable of entering the Earth's atmosphere involves, among other things, the consideration of the accuracy with which its landing point can be predicted, the maximum deceleration loads which the vehicle will experience, and the aerodynamic heating to which the vehicle is exposed. Since minimization of the landing point dispersion may require the use of entry angles sufficiently large to cause subsequent excessive deceleration loads to the vehicle and its occupants, a scheme is examined whereby these loads may be reduced to a tolerable level. This is accomplished by variation of the drag of the vehicle (either discretely or continuously) in a properly programmed fashion. It is found that the use of continuous drag modulation can reduce the deceleration loads by as much as 50 per cent, without significantly affecting the total aerodynamic heating of the vehicle. Particular numerical solutions of the complete equations of motion are also included. These substantiate the results of the approximate analysis. In addition, several specific applications of drag modulation have been considered, such as to a vehicle returning from the moon.

AMONG the problems of recovering a vehicle from a geocentric orbit are: Minimization of the total heat input to the body, which in turn minimizes the weight of the heat shield necessary to protect the payload; increasing the accuracy with which the landing point can be predicted; and control of the vehicle trajectory in such a way that the peak deceleration load experienced by the vehicle is held to a tolerable maximum. Although these and other factors are not independent in their effect on the design of the vehicle or its trajectory, the latter subject is herein treated in detail as a necessary step in a system analysis.

A method is suggested whereby the largest deceleration load occurring during entry into the atmosphere can be held to a selected value tolerable by human beings or other delicate payloads. Essentially, this method involves a variation of the vehicle parameter W/C_DA in such a way that, for a given dynamic pressure, there results a reduction in the deceleration load. In order to achieve this result, W/C_DA must be increased during that portion of the trajectory where peak dynamic pressure has not yet been realized, and decreased when the peak has been passed. The physical counterpart of W/C_DA variation may involve a shape or flow-field variation which produces a change in the drag coefficient (C_D) or a change of the frontal area (A) of the vehicle. Jettisoning of depleted components which diminishes the weight (W) may, of course, also need to be considered. The modulation may occur in a stepwise manner (such as dropping a flared skirt at a predetermined point in the trajectory) or may occur continuously, such as by programmed flap deflection. The conditions which prevail when the vehicle enters the sensible atmosphere will dictate which method of W/C_DA variation is required. In addition to treating the deceleration problem, the associated aerodynamic heating and landing point prediction problems will be considered briefly.

Received July 3, 1958.

[1] Member of Technical Staff, Astrosciences Laboratory. Member ARS.

[2] Associate Manager, Aerodynamics Dept. Member ARS.

Equations of Motion

The problem at hand will be analyzed by using the two-dimensional equations of motion of a point mass being acted upon by gravity, inertia and aerodynamic forces. These equations are derived in (1)[3] which assumes a round, non-rotating Earth, a variable gravitational acceleration g, and that the drag force acts in a direction parallel and opposite to the inertial velocity vector.[4]

These equations are

$$\frac{V}{g}\frac{d\theta}{dt} = -\left(\frac{L}{D}\right)\frac{\rho V^2}{2\Delta} + \cos\theta\left[1 - \frac{V^2}{g(R+h)}\right] \qquad [1]$$

$$\frac{1}{g}\frac{dV}{dt} = -\frac{\rho V^2}{2\Delta} + \sin\theta \qquad [2]$$

$$\frac{dh}{dt} = -V\sin\theta \qquad [3]$$

where L/D is the lift-drag ratio, and the remaining notation used is illustrated in Fig. 1. Since it is not clear that Equations [1, 2 and 3] can be solved analytically unless some simplifying assumptions are made, one may begin by defining an area of interest in any given trajectory as follows: Each trajectory will be examined only to the point where the deceleration loads have become small enough to be of no concern to the vehicle designer (or the pilot of the vehicle if it be manned). Subsequent to this point, the continued decelera-

[3] Numbers in parentheses indicate References at end of paper.

[4] In the analysis that follows, it has been implicitly assumed that the dynamic oscillations of the vehicle in no way affect the motion of its center of gravity. For a discussion of the effects of drag modulation on the entry dynamics of a rigid body see (2).

tion will relegate the problem of successful recovery of the vehicle to the area of responsibility of the parachute and landing-system designer. With this philosophy in mind, one may examine more closely the equations of motion, particularly the second term in the right member of Equation [1]. Notice first that this term will be identically zero at satellite velocities for which $V^2 = g(R + h)$. The maximum satellite velocity (corresponding to minimum altitude satellites) is about 26,000 ft per sec. For velocities well above and below this value, the term $[1 - V^2/g(R + h)]$ is different from zero and must be retained in Equation [1] if accurate solutions are to be expected. However, for $V_E \approx 26{,}000$ ft per sec, the inaccuracies introduced by neglecting this term do not prove important, because the salient features of the trajectory under analysis will have already been determined during the high speed portion of the trajectory, that is, before the errors become significant. On the other hand, if one is dealing with entry velocities of 30,000 to 35,000 ft per sec, to neglect the aforementioned term in an approximate analysis would yield unreliable results. This conclusion is clearly demonstrated in Fig. 2 which shows the results of "exact" machine solutions[6] of Equations [1, 2 and 3]. The peak g's encountered during entry for a constant W/C_DA trajectory are plotted as a function of entry velocity. Also indicated by dashed curves are the approximate solutions of the present analysis for the regions in which agreement with the exact solutions to within 10 per cent or better is achieved. It is apparent that as the entry angle is decreased the area of agreement is diminished. A fact not discernible from this figure but which is significant to the present analysis (and which has been demonstrated by the exact calculations) is that the *relative* performance of different trajectories with the same entry conditions is much more accurately predicted by the approximate treatment than are the *absolute* values of the performance, particularly for low entry angles. This will be further illustrated subsequently.

With the above limitations in mind, the assumption is made that

$$\left[1 - \frac{V^2}{g(R + h)}\right] \cong 0$$

Then, since this analysis is concerned with nonlifting trajectories for which $L/D = 0$, Equation [1] reduces to

$$\frac{d\theta}{dt} = 0$$

Under these circumstances, the flight path angle θ remains essentially constant (and equal to its value at entry) during the portion of the trajectory which commands one's interest. The utility of this approach was first demonstrated by Allen and Eggers (3). For entry velocities reasonably near 26,000 ft per sec, the machine solutions of the complete equations of motion have shown θ to be constant within 5 per cent for the significant portions of the trajectories.

An additional simplification is introduced by the assumption that $\sin \theta$ in Equation [2] is sufficiently small compared with the remaining terms so that it may be neglected. This means that the component of the weight of the craft along the flight path is small compared with the deceleration loads the craft will experience; this is a good approximation, especially for small entry angles. Finally, the variation of gravitational acceleration with altitude is neglected. The foregoing assumptions and simplifications leave the following set of equations to be solved

$$\frac{dh}{dt} = -V \sin \theta_E \qquad [3]$$

$$-\frac{1}{g}\frac{dV}{dt} = \frac{\rho V^2}{2\Delta} \qquad [4]$$

[6] The computer programming for these solutions was performed by J. Bundsen, whose assistance is gratefully acknowledged.

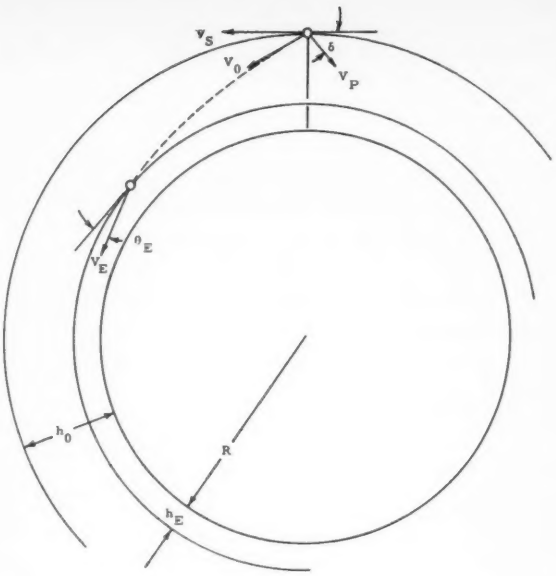

V_S - Satellite Velocity
V_P - Retrorocket Velocity Increment
V_0 - Resultant Vehicle Velocity

Fig. 1 Illustration of notation

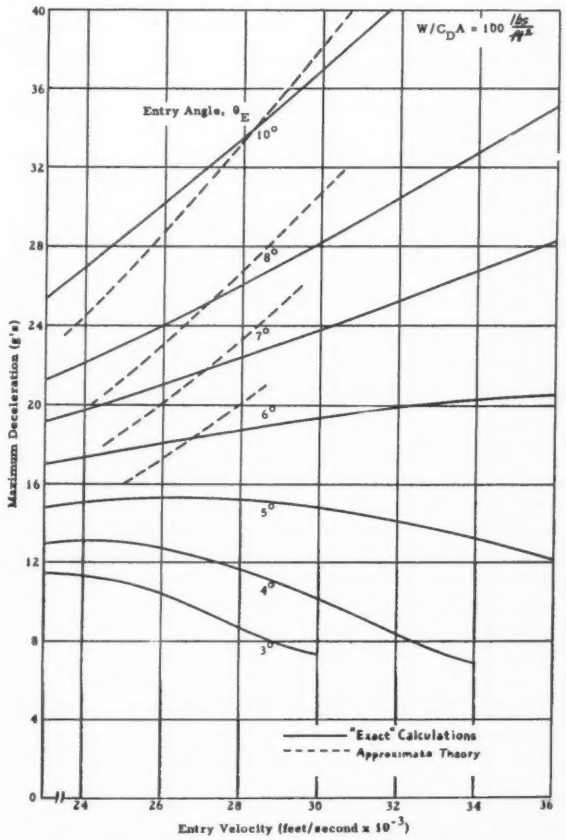

Fig. 2 Maximum deceleration during a pure ballistic trajectory as a function of entry velocity. Entry angle arbitrarily selected at 300,000-ft altitude

In effecting the solution of the above equations, it is mathematically convenient to change the independent variable from time (t) to the density ratio ρ/ρ_0 or σ, and to introduce the parameter n, the deceleration expressed in terms of g. Equation [4] can then be expressed as

$$n = \frac{\rho_0 \sigma V^2}{2\Delta} \qquad [4a]$$

For the range of interest to the present analysis, the atmospheric density variation is well approximated by

$$\sigma = \frac{\rho}{\rho_0} = e^{-\beta h} \qquad [5]$$

If the constants are evaluated from the data of (4), the resulting values are

$$\rho_0 = 2.6 \times 10^{-3}\ (\text{slug/ft}^3) \qquad \beta = 1/23{,}350\ (\text{ft}^{-1})$$

The deceleration can also be expressed as

$$n \equiv -\frac{1}{g}\frac{dV}{dt} = -\frac{1}{g}\frac{dV}{d\sigma}\frac{d\sigma}{dt}$$

But since

$$\frac{d\sigma}{dt} = -\beta e^{-\beta h}\frac{dh}{dt} = \beta \sigma V \sin\theta_E$$

Equation [4a] becomes

$$\frac{dV}{d\sigma} = -\frac{\rho_0 g}{2\beta}\frac{V}{\Delta \sin\theta_E}$$

For constant Δ this expression may be integrated to yield

$$\frac{V}{V_E} = \exp\left[-\frac{\rho_0 g}{2\beta}\frac{(\sigma - \sigma_E)}{\Delta \sin\theta_E}\right]$$

Defining

$$\frac{\rho_0 g}{2\beta} = \alpha \qquad [6]$$

and assuming $\sigma_E = 0$, one obtains the following expression for the velocity (V) as a function of σ when Δ is constant

$$V = V_E \exp\left[-\frac{\alpha\sigma}{\Delta \sin\theta_E}\right] \qquad [7]$$

Discrete Variation of W/C_DA (Single-Step Modulation)

The simplest application of drag modulation to a typical entry trajectory will be considered first, that being a single stepwise change of W/C_DA. Given an initial value of W/C_DA, V_E and θ_E, it is desired to find the point in the trajectory at which to increase instantaneously W/C_DA to a new value such that the maximum deceleration during the entire flight will be the smallest of all possible values. One begins by considering a pure ballistic trajectory wherein no drag variation is introduced; i.e., W/C_DA is considered to be constant at a value of Δ_0 during the entire flight, as was done by Eggers and Allen (3). Then Equation [4a] is

$$n' \equiv \left(-\frac{1}{g}\frac{dV}{dt}\right)' = \frac{\rho_0 \sigma}{2\Delta_0} V^2$$

The deceleration n' will be a maximum when

$$\frac{d}{d\sigma}(\sigma V^2) = 0 = V^2 + 2\sigma V\frac{dV}{d\sigma}$$

Using Equation [7] for the velocity, one obtains for the values of σ and V at maximum deceleration

$$\sigma = \sigma_m = \frac{\Delta_0 \sin\theta_E}{2\alpha} \qquad [8]$$

$$V = V_m = V_E e^{-1/2} \qquad [9]$$

The maximum deceleration is

$$n'_{\max} = \frac{\rho_0 V_E^2 \sin\theta_E}{4\alpha e} \qquad [10]$$

Some of the inadequacies of this result, which are related to the simplification of the equations of motion, were discussed earlier with the aid of Fig. 2. In addition one may note that Equation [10] indicates that the maximum deceleration which occurs during a constant drag trajectory is independent of W/C_DA. Although this is true for a large range of values of W/C_DA, θ_E and V_E pertinent to long range ballistic missiles, the complete machine solutions previously referred to have shown $n'_{\max}$ to depend upon W/C_DA to the extent that absolute values may be in error by 2 to 5 g for extreme variations in W/C_DA. Since the machine computations utilized the "real" variation of density as given in the ARDC model atmosphere (4), rather than the simple exponential variation (Eq. [5]) used in the approximate analysis, this may partially account for the trends just described.

Proceeding, one may ask in what way the deceleration history of a vehicle will be altered if at some point in the trajectory W/C_DA is changed from Δ_0 to some higher value, Δ_1 in a stepwise fashion (single step). The density ratio $\sigma = \sigma^*$ will characterize the point in the trajectory where W/C_DA is to be modulated. Prior to this point, Equation [7] applies. To find an expression for the velocity when $\sigma > \sigma^*$, one must return to Equation [4]

$$\frac{dV}{V} = \frac{\alpha d\sigma}{\Delta_1 \sin\theta_E}$$

Integrating, there results

$$V = V^* \exp\left[-\frac{\alpha(\sigma - \sigma^*)}{\Delta_1 \sin\theta_E}\right] \qquad [11]$$

Now, one wishes to determine the maximum value of

$$-\frac{1}{g}\frac{dV}{dt}$$

which the vehicle will experience subsequent to the point of drag modulation.

Defining

$$n_1 = \left(-\frac{1}{g}\frac{dV}{dt}\right)_1 = \left(\frac{\rho_0}{2\Delta_1}\right)\sigma V^2$$

one proceeds as before. (The subscript 1 denotes values after modulation, and the subscript 0 denotes values before.) Then, the density ratio and velocity at peak deceleration are

$$\sigma_{m,1} = \frac{\Delta_1 \sin\theta_E}{2\alpha}$$

$$V_{m,1} = V^* \exp\left[-\frac{\alpha(\sigma_1 - \sigma^*)}{\Delta_1 \sin\theta_E}\right]$$

where the peak deceleration is given by

$$n_{1\max} = \frac{\rho_0 V^{*2} \sin\theta_E}{4\alpha e}\exp\left[\frac{2\alpha\sigma^*}{\Delta_1 \sin\theta_E}\right] \qquad [12]$$

Sketch A indicates the deceleration histories of a pure ballistic trajectory and of two drag-modulated trajectories with arbitrary choices of density ratio, σ_a^*, σ_b^* at the modulation point.

One may note from Equation [12] and with the aid of the sketch that, as σ^* is increased (thereby decreasing V^*), $n_{1\max}$ is decreased. This occurs because an increase in σ^* results in a sufficiently larger decrease in V^* (which value is in turn squared), so that the net result is a decrease in $n_{1\max}$. Upon examination of Equations [10 and 12] and Sketch A, it becomes clear that the optimum location for σ^* is the one

which satisfies the equality

$$n_0^* = n_{1_{max}} \qquad [13]$$

That is, with given values of Δ_0 and Δ_1, the capability to reduce the maximum deceleration is used to best advantage when W/C_DA is increased from Δ_0 to Δ_1 at the point in the trajectory such that the peak deceleration subsequently realized has exactly the same value as that which was experienced at the last instant before W/C_DA was modulated. Evaluating Equation [4a] at that instant yields

$$n_0^* = \frac{\rho_0 \sigma^*}{2\Delta_0} V^{*2}$$

Combining this expression with Equations [12 and 13] one obtains

$$\frac{\sigma^*}{2\Delta_0} = \frac{\sin \theta_E}{4\alpha e} \exp\left[\frac{2\alpha\sigma^*}{\Delta_1 \sin \theta_E}\right]$$

Further, if one defines

$$\lambda_1 = \frac{2\alpha\sigma^*}{\Delta_1 \sin \theta_E} \qquad [14]$$

there results

$$\left(\frac{\Delta_1}{\Delta_0}\right) = \frac{e^{(\lambda_1 - 1)}}{\lambda_1} \qquad [15]$$

Equation [15] may be solved for a range of (Δ_1/Δ_0), thereby determining the optimum σ^* for a given set of entry conditions. Having determined the optimum value of σ^*, one can now proceed to find the reduction in maximum deceleration which can be realized if W/C_DA is modulated at this σ^*. One may define the reduction in peak g's as being characterized by the fraction n_0^*/n'_{max}, where n'_{max} is the peak deceleration load that would have been experienced had one chosen not to modulate W/C_DA but to keep it constant at Δ_0 for the entire duration of the trajectory.

Then from Equations [10 and 4a]

$$\frac{n_0^*}{n'_{max}} = \frac{\rho_0 \sigma^*}{2\Delta_0} V^{*2} \frac{4\alpha e}{\rho_0 \sin \theta_E V_E^2}$$

But recall

$$\frac{V^{*2}}{V_E^2} = \exp\left[-\frac{2\alpha\sigma^*}{\Delta_0 \sin \theta_E}\right]$$

Therefore

$$\frac{n_0^*}{n'_{max}} = \frac{2\alpha\sigma^*}{\Delta_0 \sin \theta_E} \exp\left[1 - \frac{2\alpha\sigma^*}{\Delta_0 \sin \theta_E}\right]$$

However, by virtue of the definition of λ_1 and Equation [15], this may be arranged to yield

$$\frac{n_0^*}{n'_{max}} = \exp\left[\lambda_1\left(1 - \frac{\Delta_1}{\Delta_0}\right)\right] \qquad [16]$$

where the relation between λ_1 and Δ_1/Δ_0 (Eq. [15]) is implied. Thus, as one might have expected, the maximum realizable reduction in peak g's is a function solely of Δ_1/Δ_0. These optimum solutions of λ_1 and n_0^*/n'_{max} as functions of (Δ_1/Δ_0) have been plotted in Fig. 3. Here it should be noted that Equation [15] has two solutions for each Δ_1/Δ_0. However, the applicable solution can be selected simply by noting that the optimum σ^* must be less than σ_m. That is, the modulation must take place before n'_{max} is reached, or there will be no reduction in peak g's whatsoever.

Once the correct σ^* has been selected, it can be seen from Fig. 3 that there is a rather easily discernible point of diminishing returns after which an increase in the W/C_DA ratio is not very profitable. It can further be seen that since n_0^*/n'_{max} reaches a minimum value of only about 0.70, the application of single step drag modulation as a g-reduction scheme is limited to cases where peak deceleration loads need only to be reduced by 20 to 30 per cent. However, as will be seen in the next section, the use of continuous drag modulation can result in peak g reductions of as much as 50 per cent for reasonable values of (Δ_1/Δ_0).

Continuous Variation of W/C_DA

The opposite extreme of single-step drag modulation is the case which corresponds to an infinite number of infinitesimal steps in W/C_DA, that is, a continuous variation. These two extremes define an envelope which encloses all other possible ways of modulating W/C_DA so as to reduce maximum deceleration loads. The trajectory which results from the use of continuous drag modulation can be divided into three phases. Phase 1 will be the same as in the first part of single-step modulation, namely, a portion of a constant W/C_DA (pure ballistic) trajectory. In Phase 1 the velocity is given by Equation [7]. Phase 2 will begin at a point in the trajectory to be subsequently determined and at which $\sigma = \sigma^*$. At this point, the deceleration will have reached a value which is to be maintained constant thereafter by properly varying W/C_DA, specifically in direct proportion to the variation of the dynamic pressure, $\frac{1}{2}\rho V^2$. The aforementioned value of deceleration load will be designated by n_0^* since the maximum g force which will be experienced during the entire flight is the same as that value at which the modulation started. Finally, a point in the trajectory will be reached such that if one stops modulating W/C_DA the deceleration load will drop off from that same value (n_0^*). This point will initiate Phase 3 wherein W/C_DA is again held at a constant value, and, as in Phase 1, Equation [11] with V^* and σ^* replaced by V_1 and σ_1 describes

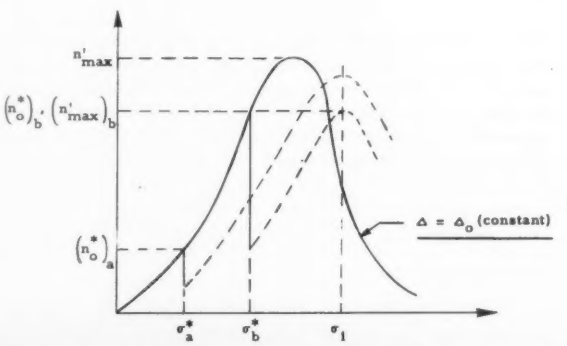

Sketch A Deceleration history as a function of density ratio

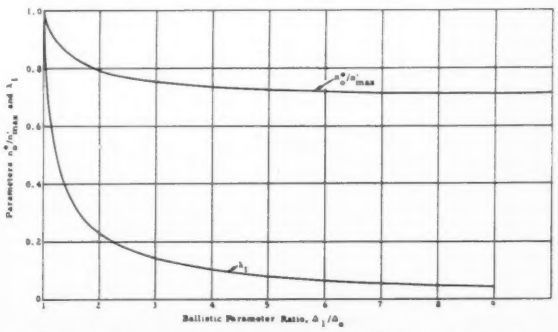

Fig. 3 Parameters for discrete modulation (single step)

the motion of the vehicle

$$\frac{V}{V_1} = \exp\left[-\frac{\alpha(\sigma - \sigma_1)}{\Delta_1 \sin\theta_E}\right] \qquad [17]$$

During Phase 2 it has been specified that

$$\left(-\frac{1}{g}\frac{dV}{dt}\right) = n_0^*$$

therefore

$$\frac{dV}{dt} = -gn_0^* = \frac{dV}{d\sigma}\frac{d\sigma}{dt} = \frac{dV}{d\sigma}(\beta\sigma V \sin\theta_E)$$

or

$$VdV = \left(-\frac{gn_0^*}{\beta \sin\theta_E}\right)\frac{d\sigma}{\sigma}$$

Integration results in an expression for the velocity during Phase 2

$$V^2 - V^{*2} = -\frac{2gn_0^*}{\beta \sin\theta_E}\log_e\frac{\sigma}{\sigma^*}$$

or eliminating V^{*2} by means of Equation [4a]

$$V^2 = \frac{2n_0^*\Delta_0}{\rho_0\sigma^*}\left(1 - \frac{2\alpha\sigma^*}{\Delta_0 \sin\theta_E}\log_e\frac{\sigma}{\sigma^*}\right) \qquad [18]$$

The trajectory during Phase 2 must also satisfy the regular equation of motion [4a], which may be written

$$V^2 = \frac{2n_0^*}{\rho_0}\left(\frac{\Delta}{\sigma}\right)$$

where Δ is no longer considered to be a constant but is a function of σ. Eliminating V^2 between this expression and Equation [18] yields

$$\frac{\Delta}{\sigma} = \frac{\Delta_0}{\sigma^*} - \frac{2\alpha}{\sin\theta_E}\log_e\frac{\sigma}{\sigma^*} \qquad [19]$$

This equation describes the required variation of the ballistic parameter Δ with density ratio σ during Phase 2.

Next it is necessary to determine the limits of Phase 2. It is desired to find the point in the trajectory, characterized by σ_1, V_1 and Δ_1 where, if cessation of W/C_DA modulation occurs, the maximum deceleration subsequently experienced by the vehicle during Phase 3 of the trajectory will equal the value which was maintained during Phase 2, namely n_0^*.

The maximum value of deceleration that would occur after termination of modulation at any arbitrary density ratio σ_1 is found by the same procedure as was used in the analysis of the single-step variation. Corresponding to Equation [8], one finds that the density ratio at that maximum deceleration is given by

$$\sigma_{m,1} = \frac{\Delta_1 \sin\theta_E}{2\alpha} \qquad [20]$$

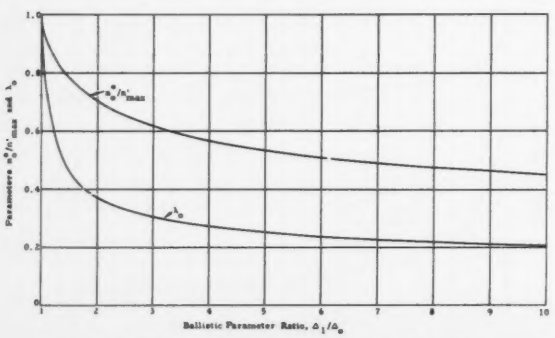

Fig. 4 Parameters for continuous modulation

Substituting this expression into Equation [17] determines the velocity at this value of σ

$$V_{m,1} = V_1 \exp\left(\frac{\alpha\sigma_1}{\Delta_1 \sin\theta_E} - \frac{1}{2}\right)$$

One is now in a position to determine from Equation [4a] the value of that maximum deceleration as

$$n_{1_{max}} = \frac{\rho_0 V_1^2 \sin\theta_E}{4\alpha}\exp\left[\frac{2\alpha}{\sin\theta_E}\left(\frac{\sigma_1}{\Delta_1}\right) - 1\right] \qquad [21]$$

The above requirement that $n_{1_{max}} = n_0^*$ can be used in conjunction with Equations [20 and 21] to evaluate σ_1 and V_1. It can be shown that if the deceleration initially decreases at the end of modulation it will continue to do so. Since this is the only accepted deceleration pattern consistent with the above requirement, it follows that $\sigma_{m,1} = \sigma_1$, so that Equation [20] yields

$$\frac{\sigma_1}{\Delta_1} = \frac{\sin\theta_E}{2\alpha} \qquad [22]$$

Substituting Equation [22] into Equation [21] then determines the velocity at the termination of Phase 2

$$V_1^2 = \frac{4\alpha n_0^*}{\rho_0 \sin\theta_E} \qquad [23]$$

Having determined the limits of Phase 2 for specified trajectory and vehicle parameters, it is now possible to determine what values of n_0^* may be realized or, more important, what values of n_0^*/n'_{max} may be achieved: Define

$$\lambda_0 = \frac{2\alpha\sigma^*}{\Delta_0 \sin\theta_E} \qquad [24]$$

Then, at the end of Phase 1, the equation immediately preceding Equation [16] still applies, and substitution of Equation [24] therein yields

$$\frac{n_0^*}{n'_{max}} = \lambda_0 \exp(1 - \lambda_0) \qquad [25]$$

Now Equation [19], describing the variation of (Δ/σ), must be consistent with Equation [22] which defines this ratio at the termination of Phase 2. Equating these expressions yields

$$1 - \lambda_0 \log_e\frac{\sigma_1}{\sigma^*} = \lambda_0 \qquad [26]$$

Furthermore, Equations [22 and 24] may be combined to give

$$\frac{\sigma_1}{\sigma^*} = \frac{1}{\lambda_0}\left(\frac{\Delta_1}{\Delta_0}\right) \qquad [27]$$

so that Equations [26 and 27] yield

$$\frac{\Delta_1}{\Delta_0} = \lambda_0 \exp\left(\frac{1}{\lambda_0} - 1\right) \qquad [28]$$

From Equations [25 and 28] it is seen that λ_0 is a parameter which allows one to determine n_0^*/n'_{max} in terms of Δ_1/Δ_0 exclusively. Furthermore, the density ratio at the start of drag modulation is given in terms of λ_0 and the known values of α, Δ_0 and θ_E by Equation [24]. The values of n_0^*/n'_{max} and λ_0 are shown as functions of (Δ_1/Δ_0) in Fig. 4.

Discussion

Drag Modulation

The most significant results of the preceding analysis are presented in Figs. 3 and 4. Indicated therein is the magnitude of the possible reduction in maximum deceleration load which

Table 1 **Comparison of discrete and continuous modulation, V_E = 26,000 ft per sec, θ_E = 0.1 radian, Δ_0 = 50 lb per ft², Δ_1 = 200 lb per ft²**

	λ	n_0^*/n'_{max}	σ^*	h^*, ft	V^*, ft per sec	σ_1	h_1, ft	V_1, ft per sec	n_0^*	n'_{max}
Discrete modulation	0.101	0.736	1.036×10^{-3}	160,000	21,200	Not applicable to discrete modulation case			12.2	16.6
Continuous modulation	0.270	0.560	0.692×10^{-3}	170,000	22,700	1.026×10^{-3}	107,000	11,800	9.3	16.6

a vehicle must experience, compared with that it would undergo in a pure ballistic (W/C_DA constant) trajectory, if the vehicle possessed the capability of varying its ballistic parameter W/C_DA between the limits Δ_0 and Δ_1. The reduction depends on the ratio Δ_1/Δ_0 and the program of modulation of W/C_DA. As stated earlier, the two cases which have been considered (single-step and continuous drag modulation) constitute the boundaries of an envelope which encloses all other possible manners of modulating W/C_DA to reduce peak g's.

In order to more fully illustrate the potentialities of drag control as a g-reduction device, two representative examples have been calculated. For an entry velocity of 26,000 ft per sec and an entry angle of 0.100 radian at an altitude of 300,000 ft, a ratio (Δ_1/Δ_0) of 4 and a value of Δ_0 = 50 lb per ft² has been selected to show what values of peak deceleration may be expected when:

1 W/C_DA is increased in a stepwise fashion (single step).

2 W/C_DA is continuously increased to its maximum value.

The velocities and altitudes which characterize the critical points in the trajectories, i.e., the points at which modulation begins and ends, are shown in Table 1.

Finally, for the case of continuous modulation, Fig. 5 shows the various values of V_E and θ_E which, when combined, will result in trajectories all of which have the same percentage reduction in peak deceleration. That is, for a given value of Δ_1/Δ_0 there is a corresponding value of n_0^*/n'_{max} and hence λ_0. Thus, for each constant value of n'_{max} ($V_E^2 \sin \theta_E$ = constant) the value n_0^* will also be the same.

The dashed portions of the curves in Fig. 5 indicate the regions in which the present analysis is unreliable, the limit of reliability being the same as that defined previously, i.e., maximum g's predictable to within 10 per cent of the exact values shown in Fig. 2.

As was mentioned earlier, the use of discrete drag modulation must be restricted to somewhat limited applications, since the reduction in peak g's which can be effected is appreciably less than that associated with continuous modulation. However, an attractive feature of the discrete modulation scheme is the probable simplicity of construction of such a device and subsequent adaptation to a given vehicle. One may visualize such a device as being a lightweight flare which would be fitted to the after portion of the vehicle and discarded by explosive bolts at the appropriate point in the trajectory.

On the other hand, the use of continuous drag modulation may require a somewhat more complex mechanism to vary W/C_DA in the necessary manner. This additional complexity, however, allows atmospheric entry under conditions which high g would otherwise make untenable. Continuous drag modulation could find application to manned vehicles returning from any satellite orbit, or even (as exact machine solutions of the complete equations of motion have shown) could allow a manned vehicle to safely enter the Earth's atmosphere at velocities as great as 35,000 ft per sec and entry angles as large as 8 deg. Since the escape velocity of the Earth is roughly 35,000 ft per sec, there would probably be few instances in which it would be necessary to enter the sensible atmosphere at velocities in excess of this figure.

Of the many possible schemes which have been suggested for varying drag continuously, three are illustrated in Fig. 6. The first scheme, (a), is simply a cruciform arrangement of flared panels which move in the indicated path. They might be actuated by a semipassive servo system which has a de-

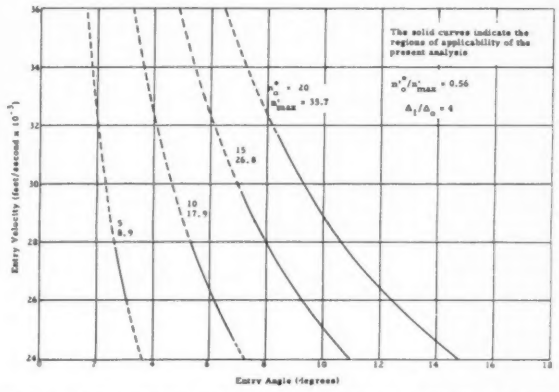

Fig. 5 **Entry velocity and entry angle ranges for constant values of n_0^***

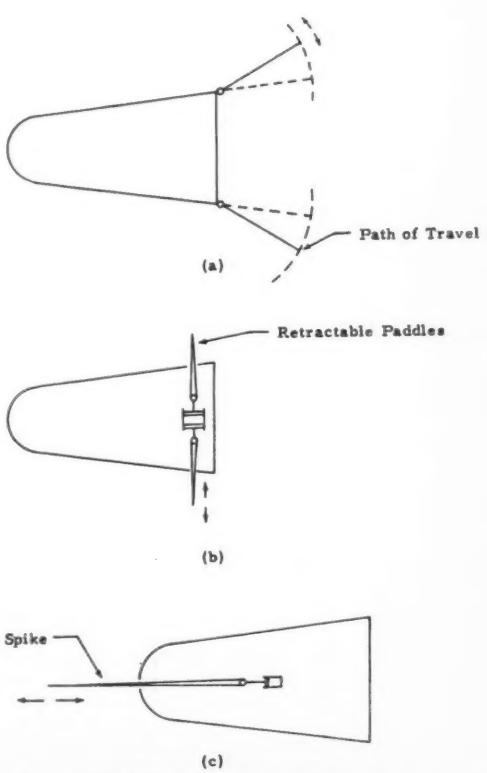

Fig. 6 **Possible methods for varying drag**

celeration-initiated, predetermined time variation of W/C_DA programmed into it; or it could be operated by a closed loop system having an "on-off" micro-switch which controls the position of the flaps so as to maintain a constant value of deceleration. The second arrangement, (b), replaces the flares with paddles which retract into the interior of the vehicle, and which may be actuated by the same methods suggested above. Finally, (c) illustrates the use of a retractable spike which it might be possible to position so as to alternately increase or decrease the hypersonic drag coefficient in the proper manner, thereby achieving a variation in W/C_DA. The success of such a scheme would depend on a sufficient knowledge of the flow separation induced by the spike at hypersonic speeds. The best method for modulating drag, of course, could only be determined from a system study with the point of view of minimizing the weight of the vehicle while retaining a maximum capacity of varying drag over a wide range.

Here it should be observed that if a vehicle has the capability of increasing W/C_DA continuously from a low Δ_0 to a higher value Δ_1, then it obviously possesses the capability of subsequently decreasing W/C_DA from Δ_1 to Δ_0. In view of this fact, it should be evident that Phase 2 of a trajectory, wherein the vehicle drag is being continuously modulated, can be extended. This can be accomplished simply by continuously decreasing W/C_DA in the proper manner, beginning this "reverse" modulation at the point in the trajectory characterized by σ_1, V_1, etc. This point is where peak dynamic pressure occurs. One possible advantage in extending Phase 2 of the trajectory would be to decrease further the vehicle velocity (at the prevailing high rate) an amount sufficient to lessen the demands on the recovery system.

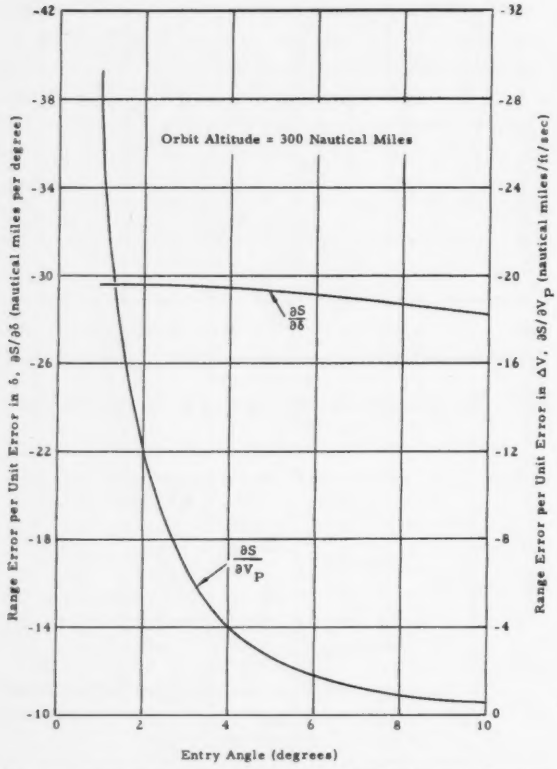

Fig. 7 Range errors due to errors in magnitude and direction of retrorocket velocity increment

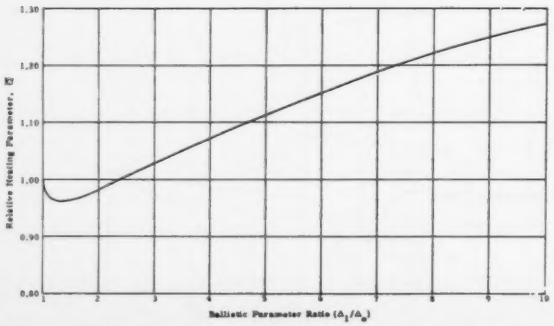

Fig. 8 Relative heating due to continuous drag modulation

Dispersion and Heating

The discussion of any hypervelocity entry problem would, of course, not be complete without including some mention of the attendant but no less important dispersion and heating problems. The studies of (5) show that when a vehicle leaves a satellite orbit by means of a retro-thrust, thereby establishing a transfer trajectory leading to the Earth's surface, the greatest contributions to the dispersion of the landing point result from errors in the orientation and magnitude of the retrorocket velocity increment during the "deboost" period. Fig. 7 shows these errors in range S per unit error in retrorocket orientation angle δ and deboost velocity magnitude ΔV as a function of the entry angle θ_E for an orbit at an altitude of 300 nautical miles. From these curves it is evident that from the point of view of minimizing dispersion, it is desirable to have as large an entry angle as possible.[6] However, Equation [10] has indicated that the maximum deceleration loads expected of a ballistic type of entry increase as the sine of the entry angle. Consequently, the reduction of dispersion to an acceptable value may require unacceptable g-loads, unless the vehicle is provided with a deceleration control mechanism. Equipping the vehicle with such a device would permit it to enter the atmosphere at a relatively high angle, thereby keeping the dispersion low and at the same time holding the peak g's to a tolerable value.

Still within the systems frame of view, one must examine the effects of entry angle and W/C_DA on the total aerodynamic heating to which the vehicle is exposed. Several investigators have shown (see (3)) that the laminar heating rate at the stagnation point of a blunt body of revolution is proportional to the square root of the free stream density and the cube of the free stream velocity thus

$$\dot{q} \sim \sqrt{\rho}\, V^3 \qquad [29]$$

An expression for the ratio of the total heating during a drag modulated flight to the heat pulse which a vehicle would experience during a constant W/C_DA trajectory with the same peak deceleration has been derived in (6). The result is

$$\bar{Q} = \left(\frac{n_0^*}{n'_{max}}\right)^{1/2}\left\{\text{erf}\,(\lambda_0^{1/2}) + 0.42\left(\frac{n_0^*}{n'_{max}}\right)\times\left[3.38\left(\frac{\Delta_1}{\Delta_0}\right)^{1/2} - \lambda_0^{1/2}\left(\frac{1}{\lambda_0}+2\right)\right]\right\} \qquad [30]$$

This expression for $\bar{Q}$ has been evaluated and is shown in Fig. 8. It is seen that for modest g-reduction, the heating actually is reduced slightly (4 per cent for 18 per cent g-reduction), although for appreciable modulation some increase in heating occurs (16½ per cent for a 50 per cent g-reduction).

[6] This effect is magnified as the orbit altitude is increased. For a 500-nautical mile orbit, $\partial S/\partial\delta$ decreases from 2460 nautical miles per deg at $\theta_E = 1$ deg to -25.8 nautical miles per degree at 6 deg.

Concluding Remarks

A scheme has been examined for limiting to a selected value the maximum deceleration load experienced by a returning space vehicle entering the atmosphere at a given flight path angle. Although in some cases reduction of the entry angle might be acceptable, in general, rather large entry angles (5 deg and higher) are necessary if the landing point dispersion of these vehicles is to be held within reasonable limits. Therefore, drag modulation schemes may provide a solution to the problem of limiting the g-loads to values tolerable by a human being. The aerodynamic heating is not significantly affected.

An interesting application of drag modulation which has been considered is that of a returning moon vehicle entering the Earth's atmosphere at about 35,000 ft per sec. As previously pointed out, the limitations of the present analysis, when dealing with low entry angles, preclude accurate predictions for the case of entry from the moon when absolute results are desired. However, reliable values of n_0^*/n'_{max} can be obtained by the methods of this paper. This is evidenced by the comparison of analytic and machine results in Table 2.

The results of machine computations for the case of entry from the moon are shown in Fig. 9 where the absolute values of peak g's during entry are plotted as a function of θ_E. If the vehicle attempts to enter at angles less than about 4 deg it will not remain in the atmosphere but will "pierce" it and either return to the moon, assume a geocentric orbit, or perform a series of skipping maneuvers before finally descending to the Earth's surface. For values of θ_E greater than about 6 deg, the deceleration loads experienced on a pure ballistic trajectory will be intolerable to a human passenger.[7] As shown in Fig. 9, the use of drag modulation on such a vehicle might extend the "safe" range of entry angles from 5 ± 1 deg to 6 ± 2 deg. It will be appreciated that the protection afforded by widening this tolerance could easily make the difference between a successful and unsuccessful recovery of a manned space vehicle.

Table 2 Comparison of exact and analytical results

Δ_1/Δ_0	(n_0^*/n'_{max}) exact	(n_0^*/n'_{max}) approx.	$\bar{Q}$ exact	$\bar{Q}$ approx.
4.89	0.579	0.536	1.12	1.11
8.01	0.513	0.475	...	1.22
9.65	0.489	0.455	1.19	1.26

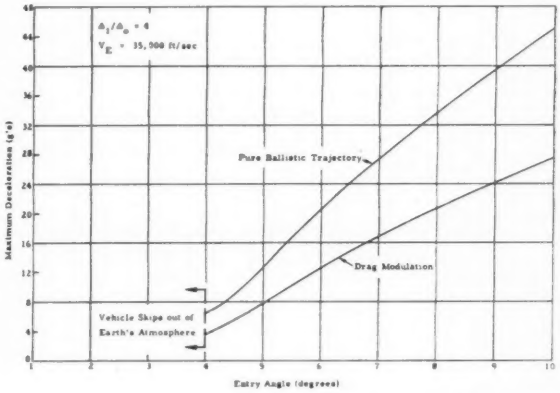

Fig. 9 Maximum deceleration experienced by a vehicle returning from the moon

Nomenclature

- A = frontal or drag reference area of the vehicle, ft²
- C_D = drag coefficient of the vehicle, dimensionless
- D = drag force, lb
- e = base of the natural logarithm, 2.718...
- g = acceleration due to gravity, 32.2 ft per sec² at the Earth's surface
- h = altitude above the Earth's surface, ft
- L = lift force, lb
- n = defined as the quotient of the deceleration of the vehicle and the acceleration due to gravity g. Also referred to as g's, dimensionless
- Q_T = total aerodynamic heat pulse per unit area, Btu/ft²
- $\bar{Q}$ = ratio of the Q_T for a drag modulated trajectory to the Q_T for a constant W/C_DA trajectory, dimensionless
- $\dot{q}$ = rate of aerodynamic heating to a vehicle, Btu/ft²-sec
- R = mean radius of the Earth, 2.09×10^7 ft
- S = distance traveled by the vehicle along the surface of a nonrotating Earth during the time elapsed from entry to impact—referred to as range, nautical miles
- $\partial S/\partial\delta$ = error coefficient or the error in range S per unit error in δ, nautical miles/deg
- t = time of flight of the vehicle, usually taken as zero at entry, sec
- V_P = retrorocket velocity increment, ft per sec
- V = inertial velocity of the vehicle, ft per sec
- V_0 = resultant inertial velocity of the vehicle immediately after firing retrorocket, ft per sec
- V_S = inertial velocity of the vehicle in a satellite orbit ft per sec
- (W/C_DA) = vehicle ballistic parameter; weight divided by the drag coefficient times the drag reference area, lb per ft²
- W = weight of the vehicle, lb
- Z = parameter defined to facilitate the solution of Equation [21]
- α = atmospheric constant defined in Equation [6] as $\rho_0 g/2\beta$, lb per ft²
- β = constant used in Equation [5], ft⁻¹
- Δ = mathematical symbol for the vehicle parameter W/C_DA, lb per ft²
- δ = angle, measured from the orbital flight path direction, at which the retrorocket velocity increment is applied, deg
- θ = flight path angle of the vehicle (see Fig. 1), radian or deg
- λ_0 = defined in Equation [27]
- λ_1 = defined in Equation [14]
- ρ = free stream or atmospheric density, a function of altitude, slug per ft³
- ρ_0 = reference density used in Equation [5], slug per ft³
- σ = density ratio, ρ/ρ_0, dimensionless

Subscripts

- E = refers to conditions at entry (arbitrarily selected at $h = 300{,}000$ ft) into the Earth's atmosphere
- 0 = refers to conditions in a drag modulated trajectory when $\Delta = \Delta_0$, the lower limit value of W/C_DA. Also accompanies parameters which contain Δ_0 in their definitions, e.g., λ_0. An exception occurs in the case of ρ_0, defined above.

[7] A tolerable upper limit on the maximum deceleration load has been arbitrarily selected as 20 g.

1 = refers to conditions in a drag modulated trajectory when $\Delta = \Delta_1$, the upper limit value of $W/C_D A$. Also accompanies parameters which contain Δ_1 in their definitions, e.g., λ_1.

m = refers to a parameter evaluated at the point where maximum g's occur

Superscripts

* = refers to conditions in a drag modulated trajectory at which drag variation begins

′ = refers to conditions in a trajectory wherein the drag is held constant at Δ_0 (pure ballistic trajectory)

References

1 Ferri, A., Feldman, L. and Daskin, W., "The Use of Lift for Re-Entry From Satellite Trajectories," JET PROPULSION, vol. 27, Nov. 1957, pp. 1184–1191.

2 Leon, H. I., "Angle of Attack Convergence of a Uniformly Decelerating Missile," unpublished, Space Technology Laboratories.

3 Allen, H. J. and Eggers, A. J., "A Study of the Motion and Aerodynamic Heating of Missiles Entering the Earth's Atmosphere at High Supersonic Speeds," NACA TN 4047, Oct. 1957.

4 Minzner, R. A. and Ripley, W. S., "The ARDC Model Atmosphere, 1956," Air Force Surveys in Geophysics, No. 86, Geophysics Research Directorate, AFCRC, ARDC, Dec. 1956.

5 Phillips, R. L., "Descent Trajectories for Manned Space Vehicles," GM-TR-0165-00416, Space Technology Laboratories, Inc., June 20, 1958.

6 Phillips, R. L. and Cohen, C. B., "The Use of Drag Modulation to Reduce Deceleration Loads During Atmospheric Entry," Space Technology Laboratories, Report GM-TR-0165-00352, April 9, 1958.

Interplanetary Travel by Solar Sail

T. C. TSU[1]

Westinghouse Research Laboratories
Pittsburgh, Pa.

Although the existence of radiation pressure has long been known, its application to spaceship propulsion has not been explored thoroughly. A solar sailing ship has a mass ratio of unity, needs no fuel or propellant, has no powerplant aboard ship and no waste-heat disposal problem. The propulsive force, although small, can be applied continuously in a controlled direction. The ship has an infinite "propellant" reserve to correct errors of navigation, or to return it to Earth at any time. A sailing project can be realized relatively soon. In this paper, the characteristics of a solar sail are examined in some detail, the equations of motion solved, the sail tilt angle optimized, the time of travel computed, and the performance compared with that of chemical-rocket and ionic propulsion systems.

ALTHOUGH the existence of radiation pressure has been known for many years, its application to spaceship propulsion has been mentioned only infrequently. A solar sail derives its propulsive force from the pressure due to the sun's light falling on a sail, which may be a thin sheet of aluminum foil, or a thin plastic sheet silvered or aluminized on the sunny side to reflect the light. Some obvious advantages of the solar sail are: Mass ratio of unity (mass of ship remaining constant), availability of sail force throughout ship's entire journey, no need of fuel or propellant, no propulsive powerplant aboard ship and its associated waste-heat disposal problem. Although the available force is small compared to that of chemical rockets, it can be applied for as long as it is needed. A trip to Mars or Venus can perhaps be made in less time by solar sail than by chemical rocket. A solar sail is equivalent to a rocket of mass ratio unity with an infinite propellant reserve. As far as propulsion is concerned, the ship can always return to Earth or make in-flight navigational corrections. Also, since the ship moves at a nonuniform speed under a noncentral force system, the ship's contents are not absolutely weightless, although the weight of any object would be much less than that at Earth's surface. In a recent paper (1),[2] Garwin states that the solar sail is of negligible cost, and is perhaps more powerful and less difficult than many often-cited competing schemes. We might add that a sailing project can be realized fairly soon without extensive research and development. In this paper the solar sail will be examined in some detail; the equations of motion will be solved; the time of travel will be computed, and the performance will be compared with that of chemical-rocket and ionic propulsion systems. Problems regarding departure from one planet and arrival at another will not be dealt with.

Received Oct. 7, 1958.

[1] Advisory Engineer, Mechanics Department.

[2] Numbers in parentheses indicate References at end of paper.

The Sail

Perhaps the most important requirement of the sail is that it must have a low mass per unit area. The presence of holes, tears and other defects is unimportant. The radiation pressure on the sail can be calculated from Maxwell's electromagnetic theory of light or the quantum theory. On a normally oriented reflecting surface at Earth's orbit, the pressure is

$$p_0 = 2S_0/c \qquad [1]$$

If the sail is at distance r from the sun and oriented at an angle of incidence θ, the pressure is (2)

$$p = p_0 \cos^2 \theta (r_0/r)^2 \qquad [2]$$

The numerical value of S_0 is 1.94 cal/(cm²) (min) or 1.35 × 10^6 erg/(cm²) (sec); c is 3 × 10^{10} cm/sec; so that p_0 = 0.9 × 10^{-4} dyne/cm².

It is of some importance to compare the magnitude of radiation pressure with that of space drag, the latter being proportional to material density in interplanetary space. Space density is not known with certainty. There may be local variations. However, Alfvén states that (3) gas density in interplanetary space is probably intermediate between the density in interstellar space (1 atom/cm³) and that in the outer corona (10^6 atoms/cm³), and that a fair guess would be 10^2 or 10^3 atoms/cm³. If we assume a mean density of 10^3 hydrogen atoms/cm³, and a ship speed of 3 × 10^6 cm/sec, then space drag is on the order of 10^{-8} dyne/cm². Since Alfvén's estimate appears to be a reasonable one, we can say with some confidence that space drag is negligibly small compared to solar radiation pressure.

There is a possibility that while the ship is in motion its sail may be punctured by meteoroids. Small punctures are inconsequential and need to cause no concern. Large punctures may need repair during the voyage.

From the definitions given under Nomenclature, and remembering that α is the acceleration due to radiation pressure p_0 alone, we see that

$$\frac{m_0}{A} = \frac{p_0}{\alpha} - \rho \qquad [3]$$

Equation [3] is plotted in Fig. 1. The top line represents the hypothetical, limiting case where the sail material has no mass. The bottom line corresponds approximately to existing technology, e.g., a sail material 0.1-mil thick with a specific gravity of 1.18. As an example, if a value of 0.2 cm/sec² is desired for α, and ρ = 2 × 10^{-4} gm/cm², then m_0/A = 2.5 × 10^{-4} gm/cm². If m_0 = 500 kg, the required sail area A is 2 × 10^9 cm², which is equivalent to a circle 500 m (1650 ft) in diameter. With ρ = 3 × 10^{-4} gm/cm², the maximum attainable value for α is 0.3 cm/sec². This value increases to 0.45 cm/sec² for ρ = 2 × 10^{-4} gm/cm², and to 0.9 cm/sec² for ρ = 10^{-4} gm/cm². It is clearly important that the sail should have low mass per unit area.

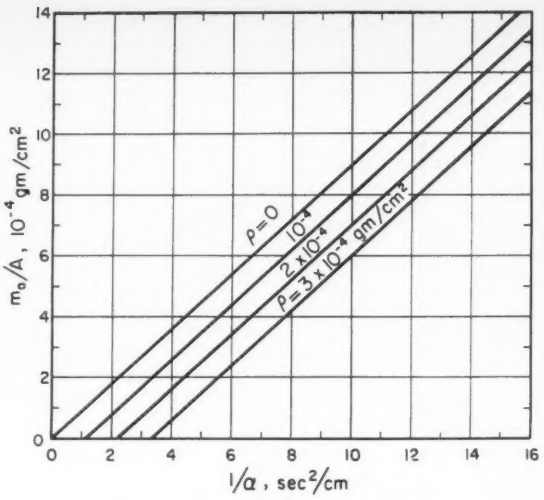

Fig. 1 Characteristics of solar sail

Equations of Motion

Let us now consider a ship propelled by solar sail in interplanetary space. The forces acting on it are shown in Fig. 2. F_g is the sun's gravitational force. F_s is the force due to radiation pressure on the sail and is equal to pA. Space drag, being negligibly small, is not considered. We also neglect gravitational forces due to Earth and other planets. The equations to follow, therefore, are inaccurate when the ship is very close to a planet (say, within a million miles). The problems connected with departure from one planet and arrival at another are not treated in this paper. However, these problems are no more difficult with solar sail than with other means of propulsion. Under the specified conditions, the equations of motion are

$$\frac{-F_g + F_s \cos\theta}{m} = \ddot{u} - \frac{v^2}{r} \qquad [4]$$

$$\frac{-F_s \sin\theta}{m} = \dot{v} + \frac{uv}{r} \qquad [5]$$

By using Equation [2], the quantity F_s/m can be expressed

$$\frac{F_s}{m} = \frac{pA}{m} = \frac{p_0 A}{m} \cdot \cos^2\theta \left(\frac{r_0}{r}\right)^2 = \alpha \cos^2\theta \left(\frac{r_0}{r}\right)^2 \qquad [6]$$

The quantity F_g/m can be written

$$\frac{F_g}{m} = \frac{F_{g0}}{m}\left(\frac{r_0}{r}\right)^2 = a_0 \left(\frac{r_0}{r}\right)^2 \qquad [7]$$

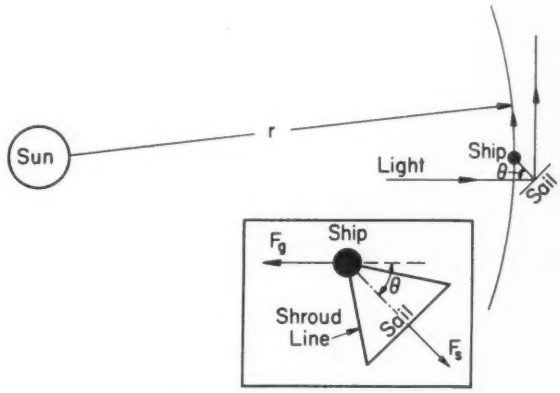

Fig. 2 Forces acting on spaceship

where a_0 is the sun's gravitational acceleration at Earth's orbit. It has the numerical value 0.592 cm/sec². Substituting Equations [6 and 7] into [4 and 5], we obtain, respectively

$$(-a_0 + \alpha \cos^3\theta)\left(\frac{r_0}{r}\right)^2 = \ddot{u} - \frac{v^2}{r} \qquad [8]$$

$$-\alpha \sin\theta \cos^2\theta \left(\frac{r_0}{r}\right)^2 = \dot{v} + \frac{uv}{r} \qquad [9]$$

These equations are not difficult to solve in detail. For our purpose here, however, we shall make one simplification by neglecting the term $\ddot{u}$ in Equation [8]. We shall show later that this approximation is a reasonable one for the type of motion here considered. The simplified equation reads

$$(a_0 - \alpha \cos^3\theta)\left(\frac{r_0}{r}\right)^2 = \frac{v^2}{r} \qquad [8a]$$

which can be solved directly to give

$$v = r^{-1/2} r_0 (a_0 - \alpha \cos^3\theta)^{1/2} \qquad [10]$$

Eliminating v between Equations [9 and 10] and solving the resultant equation for u, we obtain

$$u = \dot{r} = -r^{-1/2} r_0 \frac{2\alpha \sin\theta \cos^2\theta}{(a_0 - \alpha \cos^3\theta)^{1/2}} \qquad [11]$$

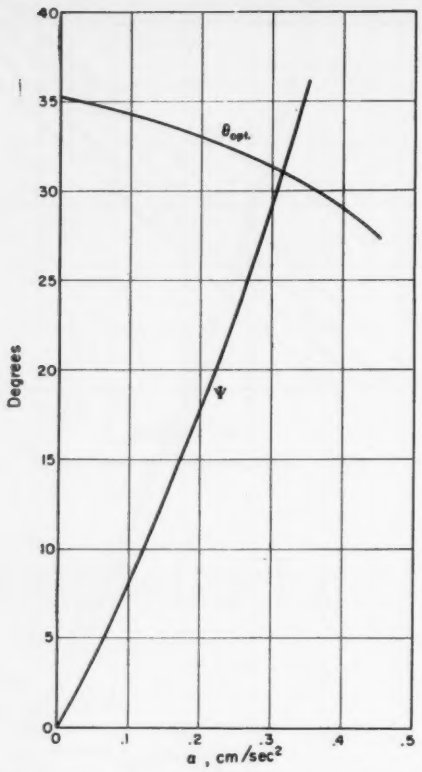

Fig. 3 Optimum sail setting and spiral angle of ship's path

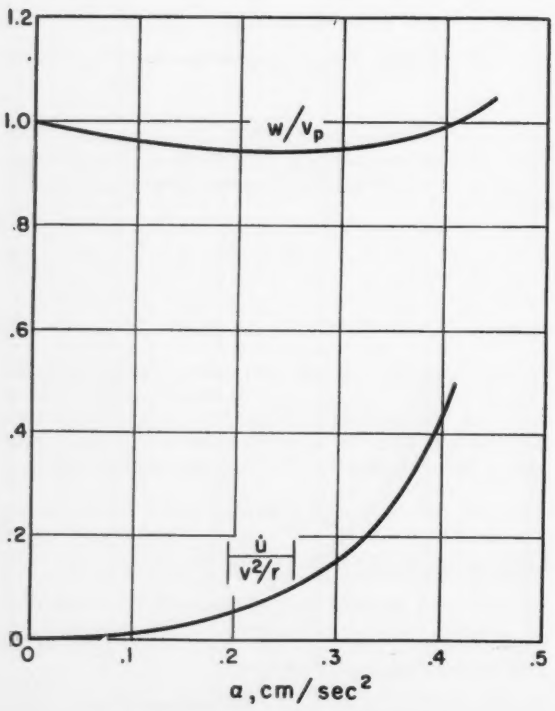

Fig. 4 w/v_p and $\dot{u}/(v^2/r)$ at optimum θ

Equation [11] can be integrated directly to give the time of travel between radii r_0 and r

$$t = \frac{1}{3} \cdot \frac{r_0^{3/2} - r^{3/2}}{r_0 \alpha^{1/2}} \cdot \frac{(a_0/\alpha - \cos^3\theta)^{1/2}}{\sin\theta \cos^2\theta} \qquad [12]$$

From Equations [10 and 11], it is seen that

$$\left|\frac{u}{v}\right| = \frac{2 \sin\theta \cos^2\theta}{a_0/\alpha - \cos^3\theta} = \tan\psi \qquad [13]$$

The path of the ship is therefore a logarithmic spiral; the spiral angle $\psi = \tan^{-1} u/v$ depends only on the acceleration ratio a_0/α and the sail setting θ.

Suppose a planet is in orbit at a distance r from the sun. If the orbit is assumed to be circular, the orbital speed v_p of that planet is given by

$$\frac{v_p^2}{r} = a_0 \left(\frac{r_0}{r}\right)^2 \qquad [14a]$$

or

$$v_p = r^{-1/2} r_0 a_0^{1/2} \qquad [14b]$$

Combining Equations [10, 11 and 14], we find

$$\frac{w}{v_p} = \frac{(u^2 + v^2)^{1/2}}{v_p} = \left[\left(1 - \frac{\alpha}{a_0}\cos^3\theta\right) + \frac{4(\alpha/a_0)^2 \sin^2\theta \cos^4\theta}{1 - (\alpha/a_0)\cos^3\theta}\right]^{1/2} \qquad [15]$$

The ratio w/v_p is independent of r. It depends only on α/a_0 and θ. For a given sail design and sail tilt, the ratio of ship speed to planet speed, when the ship arrives at that planet's orbit, is the same for all planets in the solar system.

The power applied to the ship by the sail is

$$P = (\text{tangential component of sail force}) \cdot v + (\text{radial component of sail force}) \cdot u$$

which can be readily shown to be

$$P = -m\alpha \sin\theta \cos^2\theta \frac{a_0 + \alpha\cos^3\theta}{(a_0 - \alpha\cos^3\theta)^{1/2}} \cdot \frac{r_0^3}{r^{5/2}} \qquad [16]$$

It follows that the work done by the sail in going from r_0 to r is

$$W = \int P dl = \frac{m r_0^2 (a_0 + \alpha\cos^3\theta)}{2}\left(\frac{1}{r_0} - \frac{1}{r}\right) \qquad [17]$$

Optimum Sail Setting

In order to go from r_0 to r in the shortest time, Equation [12] shows that we must minimize the quantity

$$\frac{(a_0/\alpha - \cos^3\theta)^{1/2}}{\sin\theta \cos^2\theta}$$

This has been done. The result is shown in Fig. 3, which also shows the spiral angle ψ computed from Equation [13] as a function of α for optimum sail settings.

By differentiating Equation [11] we obtain $\dot{u}$, which, when combined with Equation [8a], enables us to compute

$$\frac{\dot{u}}{v^2/r} = -\frac{2\alpha^2 \sin^2\theta \cdot \cos^4\theta}{(a_0 - \alpha\cos^3\theta)^2} \qquad [18]$$

Equation [18] is plotted in Fig. 4 for optimum sail settings. It is seen that for α up to 0.25 cm/sec^2, $\dot{u}$ is numerically less than 10 per cent of v^2/r. Hence our original approximation of neglecting $\dot{u}$ in Equation [8] is a reasonable one. If very accurate results are desired, the term $\dot{u}$ should be retained, and the equations of motion solved more exactly.

Fig. 4 also shows the ratio w/v_p plotted from Equation [15], the sail setting θ being the optimum value corresponding to the value of α used. It is seen that for α up to 0.25 cm/sec^2,

the difference between ship speed and planet speed is less than 6 per cent, the ship being slightly slower than the planet.

Trip to Venus

As an example, let us consider a trip from Earth to Venus. The sail setting is shown in Fig. 5. The angle θ is taken to be positive when the setting is as shown in Fig. 2 or Fig. 5. By differentiating Equation [10] and using [11], we obtain

$$\dot{v} = (r_0/r)^2 \alpha \sin\theta \cos^2\theta \qquad [19]$$

which is positive when θ is positive. Equation [11] shows that, for positive θ, $u = \dot{r}$ is negative, meaning that the ship will move toward the sun. Equation [17] shows that in moving from r_0 to a smaller radius r, the work done by the sail, W, is negative, meaning that energy is removed from the ship. Therefore, as the ship moves in toward Venus, it gains speed and loses energy. It may be recalled that to bring an object from a larger orbit to a smaller one, it is necessary to increase the object's speed and decrease its energy. The solar sail does this naturally.

Substituting the numerical values $r_0 = 1.495 \times 10^{13}$ cm, $r = r_1 = 1.081 \times 10^{13}$ cm, $a_0 = 0.592$ cm/sec^2, in Equation [12], and by using the optimum value of θ for each value of α (Fig. 3), the time of travel t can be calculated as a function of α. The results are shown in Fig. 6. A value for α in the neighborhood of 0.2 cm/sec^2 should be attainable in the reasonable future. Based on that value for α, the trip from Earth to Venus takes 52 days.

Fig. 7 shows trip time t as a function of α and θ. The curves are calculated from Equation [12]. When α is small, the angle of sail setting is rather critical.

It should be mentioned that the Venus orbit is inclined to the ecliptic at an angle of 3.394 deg. Therefore, unless the ship arrives at Venus' orbit just when the planet is at one of its nodes (where the orbital planes intersect), the two will not meet, although the ship is at the correct radial distance. To insure contact, we must have at our command a force normal in direction to the ecliptic. We will not go into detailed calculations of such a force or the motion it causes. It suffices to say that such a force is readily obtained by properly orienting the main sail or perhaps by using a smaller, auxiliary sail. Should the ship by miscalculation miss Venus on the first try, the sail will always provide the necessary propulsive force to turn it back for another try or return it to Earth. Since the ship is endowed with infinite "propellant" reserve, this advantage is not easily matched by other propulsion schemes.

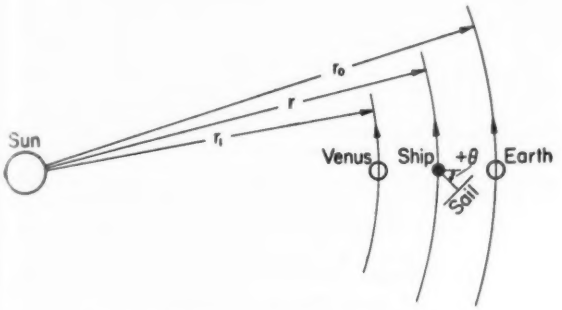

Fig. 5 Sail setting for Earth to Venus trip

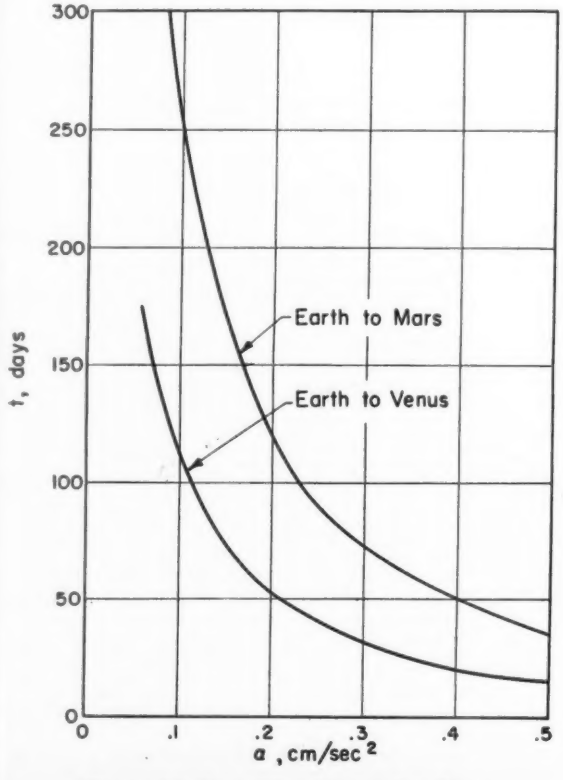

Fig. 6 Trip time with optimum sail setting

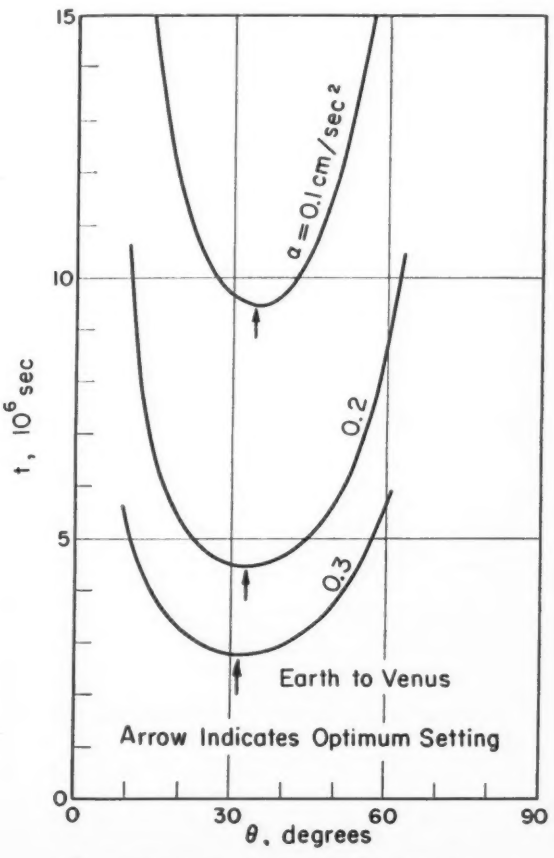

Fig. 7 Time of travel as a function of θ and α

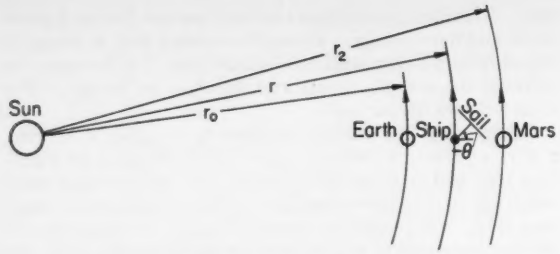

Fig. 8 Sail setting for Earth to Mars trip

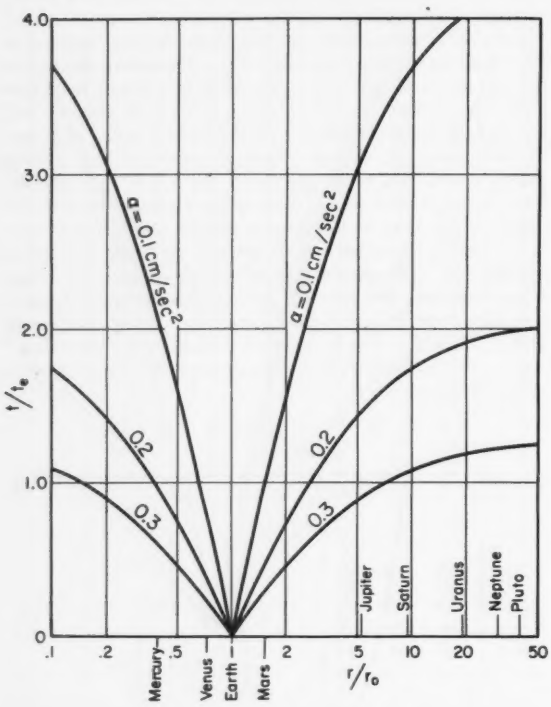

Fig. 9 Trip time along logarithmic spiral (t) compared with that along transfer ellipse (t_e)

Table 1 Comparison of chemical rocket and solar sail for trip to Mars

	Solar sail	Chemical rocket
mass of ship leaving circum-tellurian orbit/mass of ship entering circum-Martian orbit	1	9
mass of ship leaving circum-tellurian orbit/mass of ship re-entering circum-tellurian orbit	1	73
mass of ship leaving circum-tellurian orbit/mass of useful load	1.8	9 (one way) 73 (round trip)
one-way voyaging time, days	118	260
time to escape Earth	several weeks	negligible
time to adapt to circum-Martian orbit	several weeks	negligible

Trip to Mars

For a trip from Earth to Mars, the sail setting is shown in Fig. 8. Here θ is negative. Hence, according to Equation [11], $\dot{r}$ is positive, meaning that the ship will move away from the sun. Equation [19] shows that $\dot{v}$ is negative. Equation [17] indicates that W is positive, meaning that work is done upon the ship to increase its energy. As the ship moves out toward Mars, it loses speed and gains energy, again a desirable combination.

By substituting $r_0 = 1.495 \times 10^{13}$ cm, $r = r_2 = 2.28 \times 10^{13}$ cm, and $a_0 = 0.592$ cm/sec², the optimum trip time can be calculated from Equation [12]. The results are shown in Fig. 6. If we again take a value for α of 0.2 cm/sec², the trip takes 118 days.[3] By using chemical-rocket propulsion, it has been estimated (4) that the trip to Mars would take 260 days. It should be added, however, that the 118-day sailing time does not include the time required by the sail to escape Earth's gravitation. If we assume the ship is first put into an orbit circling the Earth at a height of, say, 1000 miles, it may take several weeks to escape from Earth.

The Martian orbit is inclined to the ecliptic at an angle of 1.850 deg. The remarks made regarding orbital inclination for the Venus trip are equally applicable here.

For the return trip from Mars, the sail should be set in the same manner as for the trip from Earth to Venus (Fig. 5).

Comparison With Chemical-Rocket Propulsion

It has been shown that a solar sailing ship describes a logarithmic spiral. The time of travel between radii r_0 and r is given by Equation [12]. Another method of space propulsion is to apply large thrust to the ship for short durations. By executing suitable thrust maneuvers (4), it is possible to make the ship follow a transfer ellipse whose major axis extends from the Earth's orbit (mean radius = r_0) to the destination planet's orbit (mean radius = r). The ellipse contains the sun at one of its foci. If t_e is the time required for a one-way journey along this ellipse, then, according to Kepler's third law

$$t_e = \pi q^{3/2}/r_0 a_0^{1/2} \qquad [20]$$

where q is the semi-major axis of the ellipse. Since $q = (1/2)(r_0 + r)$, Equation [20] can be written as

$$t_e = \frac{\pi}{(2)^{3/2}} \left(\frac{r_0}{a_0}\right)^{1/2} \left(1 + \frac{r}{r_0}\right)^{3/2} \qquad [21]$$

Combining Equations [12 and 21], and simplifying, we obtain

$$\frac{t}{t_e} = \frac{(2)^{3/2}}{3\pi} \cdot \frac{\{(a_0/\alpha)\,[(a_0/\alpha) - \cos^3\theta]\}^{1/2}}{\sin\theta\cos^2\theta} \cdot \frac{1 - (r/r_0)^{3/2}}{(1 + r/r_0)^{3/2}} \qquad [22]$$

This is the ratio of time of travel along logarithmic spiral (i.e., by solar sail) to that along transfer ellipse. Equation [22] is plotted in Fig. 9, the optimum value of θ being used for each value of α. To travel to very distant planets (Saturn and beyond), the solar sail would take longer, especially when α is small. This is because the sail would have to spiral around the sun several times in order to reach a distant planet. To go to nearby planets, however, sailing is perhaps the faster mode of transportation. The sailing ship appears attractive for a trip to Mars or Venus.

A comparison of mass ratios brings out another important advantage of the sailing ship. Table 1 compares a trip to Mars by solar sail and by chemical rocket.

A few words of explanation of Table 1 may be in order. The figures under chemical rocket are taken from (4). The term "useful load" means payload plus the necessary structures and equipment to protect and preserve the payload.

[3] This is travel time to mean Martian orbital distance (2.28×10^{13} cm). Travel time to perihelion distance (2.06×10^{13} cm) is 83 days.

It is essentially the ship less the propulsion system. The ratio "mass of ship leaving circum-tellurian orbit to mass of useful load" has the value 1.8 for the solar sail. This is based on the assumptions that α is 0.2 cm/sec² and the sail material has a value for ρ of 2×10^{-4} gm/cm². For these conditions, Fig. 1 gives $m_0/A = 2.5 \times 10^{-4}$ gm/cm². Hence

$$\frac{m}{m_0} = 1 + \frac{\rho A}{m_0} = 1 + \frac{2 \times 10^{-4}}{2.5 \times 10^{-4}} = 1.8$$

The author has not computed the time required by the sail to escape Earth, or that required to change the ship's course from a spiral around the sun to an orbit circling Mars. A rough estimate is several weeks for each maneuver. When the time required for these maneuvers is included, it still appears possible that sailing might make better time to Mars. There is also a possibility that by using a combined solar sail and solar rocket, these maneuvers could be speeded considerably with relatively little increase of mass.

The implications of the first three items in the table are clear. To send a 1-ton useful load to Mars and return it to Earth, we would, if we chose chemical propulsion, have to ferry a 73-ton mass to a space station circling Earth. If we chose to sail, the mass to be ferried would be only 1.8 tons. If the 1-ton load were abandoned to circle Mars forever, the ferried mass for chemical propulsion would be reduced to 9 tons, which is still five times the 1.8-ton mass required for sailing.

Comparison With Ionic Propulsion

One scheme of spaceship propulsion that has received considerable attention is the ionic rocket. In this scheme an easily ionized material, such as cesium or rubidium, is first ionized and then electrically ejected behind the ship to create a thrust. The thrust is small but can be maintained for a relatively long period of time. This propulsion method has been studied by Stuhlinger (5, 6) and others. An example given in (5) shows that a ship with an initial acceleration of 0.0657 cm/sec² requires 124.5 days to escape Earth, 222.5 days for the main journey from Earth to Mars, 54.3 days for approach maneuvers when arriving at Mars, or a total of 401.3 days for a one-way trip. Thrust is applied during 390 of these 401 days. In (6), a performance chart is given for an ionic rocket with a propulsion time of 347 days. Using that chart, and for an initial acceleration of 0.0657 cm/sec², we estimate that the take-off mass is 2.5 times that of the useful load.

If we chose to sail, the corresponding ratio would be 1.8; and the main journey would require only 118 days, as compared to 222 days by ionic propulsion.

The comparison is a bit sharper for an Earth-Mars-Earth round trip. Excluding the time required for waiting and for escape and approach maneuvers, the main journey takes 427 days by ionic propulsion vs. 236 days by sailing. The (take-off mass)/(useful load) ratio is 4.86 for the ionic rocket (5) vs. 1.8 for the sailing ship.

These comparisons should be regarded as indicative but not conclusive, since they are based on examples which, although not unrealistic, are taken somewhat off-handedly. Nevertheless, it seems clear that the solar sail possesses performance characteristics at least on a par with the ionic rocket. It should also be remembered that the ionic engine is not a simple one. Its major components include: Nuclear reactor, shielding, heat exchanger (boiler), turbine, electric generator, radiative cooler, and ionization and thrust chambers. It has to carry a propellant, which is exhaustible. Surely, the solar sail also needs development work: Material and fabrication of the sail, its packaging, handling and control. But these appear to be relatively less difficult compared to what is required for the ionic engine. The author believes that a sailing ship is easier, less costly, and can be made operational sooner than an ionic rocket.

Concluding Remarks

The solar sail seems to have important performance advantages over either chemical or ionic propulsion for trips to Mars or Venus. It should be easier, cheaper and quicker to develop than an ionic engine. Some serious consideration toward the development of a sailing vehicle for interplanetary travel would be warranted.

Nomenclature

- A = area of sail
- a_0 = sun's gravitational acceleration at Earth's orbit; $a_0 = F_{g0}/m$
- c = velocity of light
- F_g = sun's gravitational force on ship at radius r
- F_{g0} = sun's gravitational force on ship at radius r_0
- F_s = force on sail due to radiation pressure
- m = total mass of spaceship (including sail)
- m_0 = mass of spaceship proper (excluding sail)
- P = power applied to ship by sail
- p = solar radiation pressure
- p_0 = solar radiation pressure on a normally oriented reflecting surface at Earth's orbit
- q = semi-major axis of transfer ellipse
- r = plane polar coordinate; radial distance from sun
- $\dot{r}$ = time derivative of r
- r_0 = mean distance of Earth from sun
- r_1 = mean distance of Venus from sun
- r_2 = mean distance of Mars from sun
- S_0 = solar constant at Earth's orbit (normally incident energy flux outside Earth's atmosphere)
- t = time; travel time by solar sail
- t_e = travel time by transfer ellipse
- u = radial velocity = $\dot{r}$
- $\dot{u}$ = time derivative of u
- v = tangential velocity = $r\dot{\phi}$
- $\dot{v}$ = time derivative of v
- v_p = orbital speed of planet at distance r from sun
- W = work done by sail
- w = speed of ship = $(u^2 + v^2)^{1/2}$
- α = acceleration of ship due to radiation pressure p_0 acting on sail area A; $\alpha = p_0 A/m$
- θ = angle of incidence
- ρ = mass per unit area of sail
- ϕ = plane polar coordinate
- $\dot{\phi}$ = time derivative of ϕ
- ψ = spiral angle = $\tan^{-1}(u/v)$

References

1 Garwin, R. L., "Solar Sailing—A Practical Method of Propulsion Within the Solar System," JET PROPULSION, vol. 28, no. 3, March 1958, pp. 188–190.

2 Richtmyer, F. K., Kennard, E. H. and Lauritsen, T., "Introduction to Modern Physics," McGraw-Hill, 5th Ed., 1955, p. 108.

3 Alfvén, H., "On the Origin of the Solar System," Oxford University Press, 1954, p. 3; *see also* U. S. National Committee for the IGY, "Research in Outer Space," *Science*, vol. 127, no. 3302, April 11, 1958, p. 795.

4 von Braun, W., "The Mars Project," University of Illinois Press, Urbana, Ill., 1953.

5 Stuhlinger, E., "The Flight Path of an Electrically Propelled Space Ship," JET PROPULSION, vol. 27, no. 4, April 1957, pp. 410–414, 397.

6 Stuhlinger, E., "Design and Performance Data of Space Ships with Ionic Propulsion Systems," Proc. 8th International Astronautical Congress, Barcelona, 1957, pp. 403–412.

Prediction Theory of Missile and Satellite Orbits

W. J. BERGER[1] and J. R. RICUPITO[2]

Convair-Astronautics
San Diego, Calif.

This paper presents a minimal set of equations applicable to radio detection of an ICBM or reconnaissance satellite and preliminary prediction of its path and impact point (if any). The input data, obtainable by modern radio tracking instrumentation systems, are assumed to consist of the position and velocity vectors of a "flying object" relative to a geodetic station. A necessary and sufficient condition is derived for deciding whether or not the object is moving in a gravitational orbit. Equations are then given for each case; for a satellite, the elements of the orbit and the time of visibility are found; for a missile, the geodetic coordinates of the impact point and the time of impact are computed; for an aircraft, geodetic coordinates of position are found. The method may serve as the basis of a real-time computing system for identifying flying objects and predicting their paths.

SINCE observations of an artificial Earth satellite or ballistic missile obtained by modern radio tracking systems differ in character from those of classical astronomy, it appears likely that the direct vectorial method (4)[3] leads to somewhat simpler determination of the orbit. The classical methods (5), e.g., those of Laplace and Gauss, are based on observation of angular positions relative to "fixed stars," but most radio tracking systems give directly the position vector of the vehicle and its rate of change relative to the observing site.

We shall present a minimal set of equations applicable to detection of an ICBM or reconnaissance satellite and determination of its path and impact point (if any). The equations, based on central-force theory, are "minimal" in that they suffice to determine a preliminary orbit or an impact point, but they are not intended for very accurate long-time predictions.

General Theory

Let the (U, V, W) orthogonal Cartesian axes have constant directions relative to the fixed stars, with origin at the centroid O of the Earth, and the W-axis positive toward the geographic north pole. The Earth rotates with constant angular velocity Ω about the W-axis. (Effects of precession are negligible in our problem.) The observing station S on the Earth has coordinates (U, V, W), which, as functions of time t, are

$$\begin{bmatrix} U \\ V \\ W \end{bmatrix} = \begin{bmatrix} \rho \cos \Omega t \\ \rho \sin \Omega t \\ S_w \end{bmatrix} \qquad [1]$$

where ρ and S_w are constants determined by the figure of the Earth.

At station S there is an orthogonal coordinate system (S_1, S_2, S_3) with the S_3-axis positive upward along the normal to the Earth, and the S_1- and S_2-axes directed east and north, respectively. It is in this (S_1, S_2, S_3) system that the radio instrumentation system measures the position vector $\bar{P}$ of the vehicle M and its velocity $\dot{\bar{P}}$.

If $\bar{S}_3$ is the unit vector along the S_3-axis, we assume that M is observed by the instrumentation system during a set of time values (t_i) which satisfy the "visibility" condition (1)

$$\bar{P} \cdot \bar{S}_3 \geq 0 \qquad [2]$$

Within an approximation sufficient for our purpose, we assume that the gravitational field of the Earth is spherically symmetrical, in which case the path of M is a fixed plane curve (conic section), relative to the (U, V, W) system. Let $\bar{R}$ and $\dot{\bar{R}}$ be the position and the velocity vectors, respectively, of M relative to the centroid O of the Earth in the (U, V, W) system.

According to Milne (4), the orbital motion of a particle in a central gravitational field is described by the vector equations

$$\bar{H} = \bar{R} \otimes \dot{\bar{R}} \qquad [3]$$

$$\bar{B} = \bar{H} \otimes \dot{\bar{R}} + \mu \frac{\bar{R}}{|\bar{R}|} \qquad [4]$$

where $\bar{H}$ and $\bar{B}$ denote vector constants of integration, and

$$\mu = 1.407735 \times 10^{16} \text{ ft}^3/\text{sec}^2$$

denotes a constant of the central field. Generally, $\mu = G(M_0 + m)$, G = universal gravitational constant, M_0 = mass of central body, m = the (negligible) mass of satellite. Physically, $\bar{H}$ represents the angular momentum (3) per unit mass.

The orbital curve is a conic section with one focus at the centroid O of the Earth. The vector $\bar{B}$ points from O along the major axis of the conic in a direction away from the nearer vertex (perigee) of the conic. The semi-latus rectum l and the eccentricity e are given by

$$l = H^2/\mu \qquad [5]$$

$$e = |\bar{B}|/\mu \qquad [6]$$

Furthermore, the conic is an ellipse or a hyperbola when $e < 1$ or $e > 1$, respectively, and the length a of the semi-major axis is

$$a = |l/(1 - e^2)| \qquad [7]$$

Evaluation of $\bar{B}$

Substituting Equation [3] in Equation [4] and expanding the vector triple product, we find

$$\bar{B} = [(\mu/|\bar{R}|) - \dot{R}^2]\bar{R} + (\bar{R} \cdot \dot{\bar{R}})\dot{\bar{R}} \qquad [8]$$

Received Sept. 23, 1958.

[1] Senior Research Engineer. Presently Scientist-Associate, Research, Lockheed Missiles and Space Division, Palo Alto, Calif.

[2] Senior Research Engineer. Present address: Lockheed Missiles and Space Division, Palo Alto, Calif.

[3] Numbers in parentheses indicate References at end of paper.

Since $$\bar{R} = \bar{P} + \bar{S} \qquad [9]$$

it follows that in order to compute $\bar{B}$ by Equations [8 and 9], we should express $\bar{P}$ and $\bar{S}$ in the (U, V, W) system. Then by differentiating Equation [9], we find $\dot{\bar{R}}$ in the (U, V, W) system as

$$\dot{\bar{R}} = \dot{\bar{P}} + \dot{\bar{S}} \qquad [10]$$

so that by substituting Equations [9 and 10] in Equation [8] we can compute $\bar{B}$ in terms of known quantities. We now consider the necessary transformation.

Coordinate Transformation

An orthogonal transformation exists between coordinates in the (S_1, S_2, S_3) system and those in the (U, V, W) system.

Let

$\bar{S}$ = position vector of station S relative to O
Ω = angular velocity of Earth rotation
ρ = distance from W-axis to station S
S_w = distance from the (U, V) plane to S
ϕ = geodetic latitude (2) of station S
t_0 = initial time of observation
λ_0 = longitude of station S at time t_0

measured in the (U, V) plane clockwise from the U-axis. Let $(\bar{S}_1, \bar{S}_2, \bar{S}_3)$ and $(\bar{U}, \bar{V}, \bar{W})$ be unit vectors along the respective axes. Then the angle η between $\bar{U}$ and the projection of $\bar{S}$ in the $(\bar{U}, \bar{V})$ plane, measured counterclockwise from $\bar{U}$, is given at time t by

$$\eta = \Omega(t - t_0) - \lambda_0 \qquad [11]$$

Hence

$$\bar{S} = (\rho \cos \eta)\bar{U} + (\rho \sin \eta)\bar{V} + S_w\bar{W} \qquad [12]$$

and

$$\begin{bmatrix} \bar{S}_1 \\ \bar{S}_2 \\ \bar{S}_3 \end{bmatrix} = \begin{bmatrix} -\sin \eta & \cos \eta & 0 \\ -\sin \phi \cos \eta & -\sin \phi \sin \eta & \cos \phi \\ \cos \phi \cos \eta & \cos \phi \sin \eta & \sin \phi \end{bmatrix} \begin{bmatrix} \bar{U} \\ \bar{V} \\ \bar{W} \end{bmatrix} \qquad [13]$$

Since the observed data consists of

$$\bar{P} = P_1\bar{S}_1 + P_2\bar{S}_2 + P_3\bar{S}_3 \qquad [14]$$

and

$$\dot{\bar{P}} = \dot{P}_1\bar{S}_1 + \dot{P}_2\bar{S}_2 + \dot{P}_3\bar{S}_3 \qquad [15]$$

we can now express $\bar{P}$ and $\dot{\bar{P}}$ in the $(\bar{U}, \bar{V}, \bar{W})$ system by Equations [13, 14 and 15].

Hence by Equations [9, 12, 13, 14 and 15] we find

$$\bar{R} = R_u\bar{U} + R_v\bar{V} + R_w\bar{W} \qquad [16]$$

where

$$\begin{aligned} R_u &= -P_1 \sin \eta - P_2 \sin \phi \cos \eta + P_3 \cos \phi \cos \eta + \rho \cos \eta \\ R_v &= P_1 \cos \eta - P_2 \sin \phi \sin \eta + P_3 \cos \phi \sin \eta + \rho \sin \eta \\ R_w &= P_2 \cos \phi + P_3 \sin \phi + S_w \end{aligned} \qquad [17]$$

Differentiating Equations [16 and 17] we find

$$\dot{\bar{R}} = \dot{R}_u\bar{U} + \dot{R}_v\bar{V} + \dot{R}_w\bar{W} \qquad [18]$$

where

$$\begin{aligned} \dot{R}_u &= [-\dot{P}_1 + \Omega(P_2 \sin \phi - P_3 \cos \phi - \rho)] \sin \eta + \\ &\qquad [-P_1\Omega - \dot{P}_2 \sin \phi + \dot{P}_3 \cos \phi] \cos \eta \\ \dot{R}_v &= [-\Omega P_1 - \dot{P}_2 \sin \phi + \dot{P}_3 \cos \phi] \sin \eta + \\ &\qquad [\dot{P}_1 - \Omega(P_2 \sin \phi - P_3 \cos \phi - \rho)] \cos \eta \\ \dot{R}_w &= \dot{P}_2 \cos \phi + \dot{P}_3 \sin \phi \end{aligned} \qquad [19]$$

For each observation $(\bar{P}_k, \dot{\bar{P}}_k)$ and corresponding time t_k where, depending upon the computing facilities available, k may or may not include all points covered by the index i occurring in the "General Theory," we evaluate $\bar{R}$ and $\dot{\bar{R}}$ by Equations [16 to 19], and then compute $\bar{H}$ and $\bar{B}$ by Equations [3 and 4].

Test for Orbit

By the method just given, we thus generate a set of values $(\bar{H}_k, \bar{B}_k, t_k)$. To decide whether or not the observations $(\bar{P}_k, \dot{\bar{P}}_k)$ are descriptive of a gravitational orbit, we may compute the derivative of a vector $\bar{Z}_k(t_k)$ by a finite-difference formula, e.g., if the t_k's are equi-spaced at interval Δt, then

$$\dot{Z} = \frac{d}{dt}(\bar{Z}_k)\,|_{n=0} = \frac{3\sum_{\alpha=-n}^{\alpha=+n} \alpha Z_\alpha}{(\Delta t)n(n+1)(2n+1)} \qquad [20]$$

Let $\bar{B}_I$ and $\bar{R}_I$ denote unit vectors along $\bar{B}$ and $\bar{R}$, resepectively, and let $\dot{\bar{B}}_I$ and $\dot{\bar{R}}_I$ be their respective time derivatives, as computed by Equation [20]. From Equation [8] we derive a necessary and sufficient condition for existence of a gravitational orbit, namely, that the position and velocity vectors must satisfy the inequality

$$|\dot{\bar{B}}_I| < |\dot{\bar{R}}_I| \qquad [21]$$

To see that condition [21] is necessary, we note that if the gravitational field of the Earth were spherically symmetric, then the position $\bar{R}$ and velocity $\dot{\bar{R}}$ of an orbiting vehicle must be such that $\bar{B}$, by Equation [8], remains constant, and since $\dot{\bar{R}}$ is never zero in the orbit, then evidently inequality [21] holds. The actual gravitational field of the Earth is not spherically symmetric, but even in this case we note that $|\dot{\bar{B}}_I|$ and $|\dot{\bar{R}}_I|$ represent the angular rate of rotation of $\bar{B}$ and $\bar{R}$, respectively. The nonspherical part of the gravitational field causes $|\dot{\bar{B}}_I|$ to differ from zero, i.e., the line of apsides, or $\bar{B}$, rotates slowly with time, but from the theory of perturbations ((5) pp. 333–334) we know that the change in $\bar{B}$ is quite small per revolution of the orbiting body, and so again inequality [21] holds.

To see that inequality [21] is sufficient, we consider a vehicle in nonorbital motion, say an aircraft or spaceship moving at constant speed and altitude along any great-circle route, and we use the position and velocity vectors $\bar{R}$ and $\dot{\bar{R}}$ of the vehicle to compute a vector $\bar{B}$ by Equation [8]. Since $\bar{R} \cdot \dot{\bar{R}} = 0$, and since the vehicular speed differs from that of an orbiting body at the same altitude, Equation [8] shows that $\bar{B}$ is not zero and that $\bar{B}$ rotates at the same absolute angular rate as $\bar{R}$, i.e., $|\dot{\bar{B}}_I| = |\ddot{\bar{R}}_I|$. If now the vehicle deviates from its course (as by starting to dive, climb or turn), then $\bar{B}$ will start to rotate faster than $\bar{R}$, because Equation [8] shows that, in this case, $\dot{\bar{B}}$ has nonzero components along both $\bar{R}$ and $\ddot{\bar{R}}$. The nonspherical part of the gravitational field will not sensibly alter the preceding statement. Thus, when a vehicle is in nonorbital motion in the vicinity of the Earth, the vehicular position $\bar{R}$ and velocity $\dot{\bar{R}}$ satisfy the condition

$$|\ddot{\bar{B}}_I| \geq |\dot{\bar{R}}_I| \qquad [22]$$

Hence, a vehicle is in orbital motion about the Earth if, and only if, the vehicular position and velocity vectors satisfy inequality [21].

Determination of Orbit

After deciding that a gravitational orbit exists, we are naturally interested in computing the elements of the orbit.

From the previously computed set $(\bar{H}_k, \bar{B}_k, t_k)$, we estimate $\bar{H}$ and $\bar{B}$ by

$$\bar{H} = \frac{1}{k} \sum_{\alpha=1}^{k} \bar{H}_\alpha$$

$$\bar{B} = \frac{1}{k} \sum_{\alpha=1}^{k} \bar{B}_\alpha$$

..... [23]

Then using Equations [23] in Equations [5, 6 and 7], we find the semi-latus rectum l, the eccentricity e and the length a of the semi-major axis. Then an equation of the orbit is

$$l = |\bar{R}| \, (1 - e \cos \theta) \qquad [24]$$

where

$$\cos \theta = \frac{\bar{B} \cdot \bar{R}}{|\bar{B}| \, |\bar{R}|} \qquad [25]$$

As a check on the calculation, we have

$$|\dot{\bar{R}}|^2 = \mu \left(\frac{2}{|\bar{R}|} \mp \frac{1}{a} \right) \qquad [26]$$

using the minus or the plus sign when $e < 1$ or $e > 1$, respectively.

Angular Orientation of Orbit (7)

Although the vectors $\bar{H}$ and $\bar{B}$ in Equations [23] suffice to orient the orbit, usually the orientation is specified by three angular coordinates (I, L, Q) defined as follows:

I = inclination of the orbit. We take I positive when measured from the equatorial plane toward the orbital plane on the descending side of the orbit.

L = longitude of a node (ascending or descending). In Fig. 1 we show L as positive measured westward in the equatorial plane from the U-axis to the line OF which points to the descending node F.

Q = angle between the major axis of the orbit and a nodal line. We take Q positive when measured from minor axis of the orbit to the line OF of the descending node F.

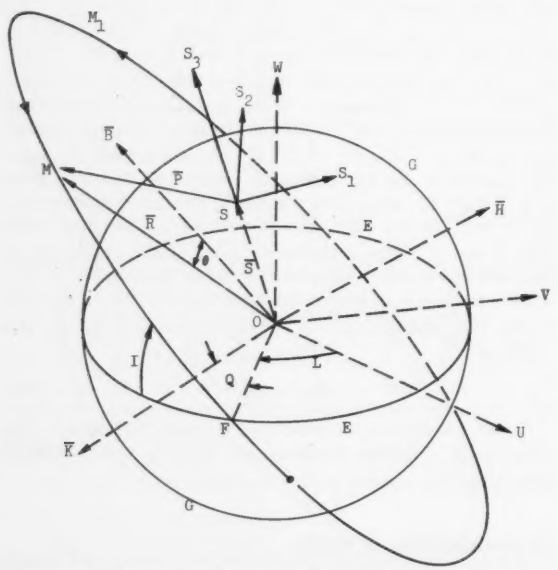

Fig. 1 Curve GG, surface of the Earth. Curve EE, equator. Curve M_1M, track of vehicle. Point S, observation station

From the definition of I and $\bar{H}$, it follows that

$$I = \arccos \frac{\bar{H} \cdot W}{|\bar{H}| \, |\bar{W}|} \qquad [27]$$

A vector $\bar{K}$ pointing along the minor axis of the orbit is given by the vector product

$$\bar{K} = \bar{H} \otimes \bar{B}$$

and a vector $\bar{J}$ pointing along the line of intersection of the orbital and equatorial planes is given by

$$\bar{J} = \bar{H} \otimes \bar{W}$$

Hence, since Q is the angle between vectors $\bar{K}$ and $\bar{J}$, it is given by

$$Q = \arccos \frac{\bar{K} \cdot \bar{J}}{|\bar{K}| \, |\bar{J}|} \qquad [28]$$

and since L is the angle between vectors $\bar{J}$ and $\bar{U}$, it is given by

$$L = \arccos \frac{\bar{J} \cdot \bar{U}}{|\bar{J}| \, |\bar{U}|} \qquad [29]$$

Test for Impact

If it has been determined that the vehicle is moving in a gravitational orbit, we must decide whether or not this orbit intersects the Earth. Since the eccentricity e and the semi-major axis a of the orbit have been found by Equations [6 and 7], the distance d from the center of the Earth to the perigee point of the orbit is given by

$$d = |a(1 - e)| \qquad [30]$$

Let r_0 be the equatorial radius of the Earth. Then if $e < 1$, the orbit is elliptical, and the vehicle will collide with the Earth if

$$d < r_0 \qquad [31]$$

whereas if

$$d \geq r_0 \qquad [32]$$

the vehicle moves in a satellite orbit about the Earth.

Otherwise, if $e > 1$, the orbit is hyperbolic, and if the inequality [31] holds, then the vehicle will collide with the Earth or recede into outer space according as $|\bar{R}|$ decreases or increases in time, respectively. If $e > 1$ and the inequality [32] holds, the vehicle recedes indefinitely.

If impact conditions prevail, we determine the time and location of the impact. Otherwise, we find the time of perigee passage.

Time of Perigee (5)

At any time t of observation, we know the polar angle θ by Equation [25], the eccentricity e by Equation [6], and the semi-major axis by Equation [7]. If $e < 1$ (elliptic case), we compute

$$E = 2 \arctan \left[\left(\frac{1 - e}{1 + e} \right)^{1/2} \tan \frac{\theta}{2} \right] \qquad [33]$$

and the period of the orbit is

$$T = 2\pi a^{3/2} / \sqrt{\mu} \qquad [34]$$

Then the time τ_0 of perigee passage is found from Kepler's equation as

$$\tau_0 = t - (T/2\pi) \, (E - e \sin E) \qquad [35]$$

If $e > 1$ (hyperbolic case), we compute

$$F = 2 \operatorname{arc\,tanh} \left[\left(\frac{e - 1}{e + 1} \right)^{1/2} \tan \frac{\theta}{2} \right] \qquad [36]$$

$$\tau_0 = t + (a^{3/2} / \sqrt{\mu}) \, (F - e \sinh F) \qquad [37]$$

Visibility of Orbital Points

After evaluation of τ_0, all six elements (a, e, τ_0, I, L, Q) of the orbit are known; i.e., the orbit is determined. Then the values of the times at which the vehicle is visible from any observing site may be computed as in (1).

Prediction of Impact

Assuming that impact conditions prevail, we may find the impact point by constructing a vector equation for orbital points and then imposing the condition that such a point also coincide with a point on the spheroid representing the Earth.

By Equations [3 and 4], we have already evaluated the two vectors $\bar{H}$ and $\bar{B}$ which determine the orientation of the orbit. Another vector $\bar{K}$, lying in the orbital plane, is conveniently given by the vector product

$$\bar{K} = \bar{H} \otimes \bar{B} \qquad [38]$$

Let $\bar{B}_0$ and $\bar{K}_0$ denote unit vectors along $\bar{B}$ and $\bar{K}$, respectively. Then the position vector $\bar{R}$ of an orbital point may be expressed as

$$\bar{R} = |\bar{R}| \, (\bar{B}_0 \cos\theta + \bar{K}_0 \sin\theta) \qquad [39]$$

where $|\bar{R}|$ can be found from Equations [16 and 17] as

$$|\bar{R}| = |R_u^2 + R_v^2 + R_w^2|^{1/2} \qquad [40]$$

and the angle θ (the "true anomaly") is defined by Equation [25]. Combining Equations [24 and 39] gives

$$\bar{R} = [l/(1 - e\cos\theta)] \, (\bar{B}_0 \cos\theta + \bar{K}_0 \sin\theta) \qquad [41]$$

Since H, $\bar{B}$, $\bar{K}$ are vectors with known numerical components in the (U, V, W) system, we have

$$\bar{B}_0 = b_1\bar{U} + b_2\bar{V} + b_3\bar{W} \qquad \bar{B}_0^2 = 1$$

$$\bar{K}_0 = k_1\bar{U} + k_2\bar{V} + k_3\bar{W} \qquad \bar{K}_0^2 = 1 \qquad [42]$$

where b and k are known numerically. Hence, Equation [41] becomes

$$\bar{R} = R_1\bar{U} + R_2\bar{V} + R_3\bar{W}$$

$$R_j = (b_j \cos\theta + k_j \sin\theta) l/(1 - e\cos\theta) \qquad (j = 1, 2, 3) \qquad [43]$$

If the surface of the Earth is represented by the spheroid

$$\frac{U^2 + V^2}{A^2} + \frac{W^2}{C^2} = 1 \qquad [44]$$

the value of θ corresponding to the impact point is, by Equations [43 and 44], a solution of

$$C^2(R_1^2 + R_2^2) + A^2R_3^2 = A^2C^2 \qquad [45]$$

We find that Equation [45] becomes

$$q_1 \cos^2\theta + q_2 \sin 2\theta + q_3 \cos\theta + q_4 = 0 \qquad [46]$$

where

$$q_1 = b_1^2 + b_2^2 - k_1^2 - k_2^2 + A^2\left(\frac{b_3^2}{C^2} - \frac{e^2}{l^2} - \frac{k_3^2}{C^2}\right)$$

$$q_2 = b_1k_1 + b_2k_2 + \frac{A^2}{C^2} b_3k_3$$

$$q_3 = \frac{2A^2e}{l^2}$$

$$q_4 = k_1^2 + k_2^2 + A^2\left(\frac{k_3^2}{C^2} - \frac{1}{l^2}\right)$$

Although Equation [46] can be rearranged in the form of a fourth degree polynomial equation, in $\cos\theta$, it can probably be more conveniently solved by iteration (e.g., Newton's method) in its present form, especially since we are interested in just one root.

After θ, $\theta = \theta_p$ has been found by Equation [46], the radius vector $\bar{R}_p$ of the impact point is given by Equation [43]. The geocentric latitude ψ_p of the impact point is determined by

$$\sin\psi_p = \frac{\bar{R}_p \cdot \bar{W}}{|\bar{R}_p|} \qquad [47]$$

which, by Equation [43] with $\theta = \theta_p$, becomes

$$\psi_p = \text{arc sin} \frac{R_3}{|(R_1^2 + R_2^2 + R_3^2)|^{1/2}} \qquad [48]$$

Hence the geodetic latitude of the impact point is expressed as

$$\phi_p = \text{arc tan} \, [(A^2/C^2) \tan\psi_p] \qquad [49]$$

where A and C are the semi-major and semi-minor axes of the spheroid [44] representing the surface of the Earth.

In order to find the longitude of the impact point, we must first determine the time t_p of impact, which can be found from Equations [33 to 37].

Thus, knowing the true anomaly θ_p of the impact point, and having already found the time τ_0 of the perigee, we substitute θ_p for θ in either Equation [33] or [36] (according as $e < 1$ or $e > 1$, respectively) and solve either Equation [35] or [37] (as required), to find $t = t_p$, the time of impact.

At the time of impact, the azimuth η_p of the station S in the (U, V) plane is by Equation [11]

$$\eta_p = \Omega(t_p - t_0) - \lambda_0 \qquad [50]$$

Hence, by Equation [43] with $\theta = \theta_p$, the longitude λ_p of the impact point measured westward from S (with S as origin) is

$$\lambda_p = \text{arc tan} \, (R_2/R_1) - \eta_p \qquad [51]$$

Geodetic Coordinates of the Vehicle

Regardless of the type of vehicle, we are naturally interested in the geodetic coordinates (6) of the projection G_M of the vehicular position on the surface of the Earth.

Since the position vector $\bar{R}$ of the vehicle at any time is

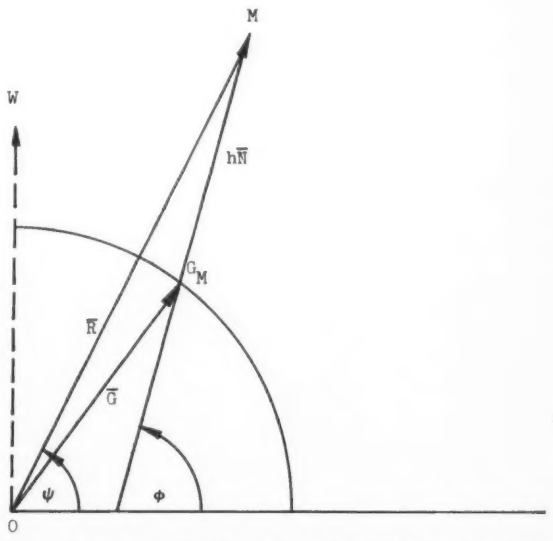

Fig. 2 Vehicle's geocentric and geodetic latitudes projected on the surface

given in the (U, V, W) system by Equations [16 and 17], then the corresponding geodetic position vector is

$$\bar{G} = \bar{R} - h\bar{N} \qquad [52]$$

where the vector $\bar{N}$ is the unit vector normal to the surface of the Earth at point G_M and pointing to the vehicle, and h is the altitude of the vehicle above the Earth.

Let ϕ and ψ be the angles between the equatorial (U, V) plane and the vectors $h\bar{N}$ and $\bar{R}$, respectively. Let A and C be the semi-major and semi-minor axes, respectively, of the spheroid representing the Earth.

The geocentric latitude is given by

$$\psi = \arcsin\left(R_w/|\bar{R}|\right) \qquad [53]$$

The geodetic latitude is given by

$$\phi = \arcsin\{A^2R_w/[C^4|\bar{R}|^2 + (A^4 - C^4)R_w^2]^{1/2}\} \qquad [54]$$

The altitude h of the vehicle is given by

$$h = |\bar{R}|\cos(\phi - \psi) - \sqrt{|\bar{G}|^2 - |\bar{R}|^2\sin^2(\phi - \psi)} \qquad [55]$$

where

$$|\bar{G}|^2 = (A^4\cos^2\phi + C^4\sin^2\phi)/(A^2\cos^2\phi + C^2\sin^2\phi)$$

The longitude λ of the point G_M as measured westward from station S with S as the origin is

$$\lambda = \arctan(R_v/R_u) - \eta \qquad [56]$$

References

1 Berger, W. J. and Ricupito, J. R., "Visibility of Orbital Points," Jet Propulsion, vol. 28, no. 12, Dec. 1958, pp. 825–827.

2 Bomford, B. G., "Geodesy," Oxford University Press, London, 1952, pp. 329–337.

3 MacMillan, W. D., "Statics and the Dynamics of a Particle," McGraw-Hill Book Co., New York, 1927.

4 Milne, E. A., "Vectorial Mechanics," Interscience Publishers, Inc., New York, 1958, pp. 235–241.

5 Moulton, F. R., "An Introduction to Celestial Mechanics," MacMillan Co., New York, 2nd ed., 1914, chap. 6, pp. 140–260.

6 Ricupito, J. R. and Herrick, C. E., "Determination of Geodetic Coordinates," Convair-Astronautics Inter-office Rep., Aug. 6, 1956, unclassified.

7 Smart, W. M., "Spherical Astronomy," Cambridge University Press, England, 1940, chap. V, pp. 98–135.

Effect of Thrust Termination Process Upon Range Dispersion of a Ballistic Missile

ARNOLD J. KELLY[1]

Rocketdyne Division
North American Aviation, Inc.
Canoga Park, Calif.

The contribution to the range dispersion of a ballistic missile caused by the thrust termination characteristics of its powerplant is analyzed and discussed. The range dispersion attributable to the nominal cutoff impulse acting on a variation in missile burnout mass is found to have a marked effect as compared to a variation in cutoff impulse from nominal. These results are based upon reasonable estimates of engine and missile parameters. A generalized graph is presented which permits the estimation of the combined contribution of cutoff impulse deviation and burnout mass variation to range dispersion to be made once the nominal burnout conditions of the missile and engine are known. A numerical example of a hypothetical 500-nautical mile ballistic missile is presented.

IN GENERAL, the ultimate miss distance of a ballistic missile from its intended impact point can be attributed to errors associated with guidance, target mapping or powerplant. These errors are reflected as a variation in the burnout velocity vector or position from the intended nominal. This supposition assumes, as will be the case in the analysis, that the trajectory of the center of mass of the missile is not influenced by any external influence other than gravity after burnout (no terminal guidance and vacuum re-entry). If mapping errors are neglected, the range dispersion of the missile is a function of irregularities in the burnout velocity vector and position caused by the guidance and powerplant.

This study is concerned with the influence of the powerplant's thrust termination characteristics upon the inaccuracies in position and velocity at the end of powered flight on the dispersion of the missile. The relationship between the cutoff characteristics of the engine and the performance of the missile is then of particular importance, for example

1 It permits the calculation (for a given missile) of the thrust termination characteristics of the powerplant for a given contribution to range dispersion.

2 Conversely, the range dispersion for a missile powered by an engine having specified cutoff characteristics can be estimated.

The former is of importance, for the thrust termination characteristics can be specified and the engine designed accordingly during the early stages of the powerplant design.

Discussion

During the thrust termination process of a ballistic missile's

Received Nov. 12, 1958.

[1] Research Engineer, Advanced Design Section. Member ARS.

Liquefied gases from Air Products equipment supply all major U.S. missiles.

HOW THE MILITARY SERVICES use Air Products CAPACITY

Large-scale low-temperature systems, ultra pure gases and liquids, and a broad range of specialized cryogenic "hardware" are supplied by Air Products to the military. When large quantities of liquefied gases were needed for rocket engine development and missile testing, Air Products quickly designed, manufactured and put on stream complete production facilities. Typical facilities paid for themselves in less than a year's time. Air Products also provides a broad line of portable air separators for field and shipboard use . . . and has advanced the development of exotic fuels. And, Air Products produces advanced design liquefied-gas pumps, cryogenic storage and transfer systems, electronic cooling devices and refrigeration and distillation equipment for military uses.

YOU will find here tangible evidence of a growing technology. Applying "Cryogenics" (the science of low temperatures) and engineering broad new routes to low-cost, high-purity industrial gases is the main business of Air Products.

Air Products combines original research knowledge with engineering and manufacturing capabilities and substantial operating experience. These integrated activities have

These companies and many others are the beneficiaries of major facilities provided by Air Products:
Acme Steel • Bethlehem Steel • Brazilian National Steel • Celanese • Dow Chemical • du Pont • Grace Chemical • Great Lakes Steel

Petrochemical plants use Air Products equipment in feedstock preparation and product purification

HOW THE STEEL INDUSTRY uses Air Products CAPACITY

In the blast furnace, the open hearth and the new converter processes — Air Products oxygen efficiently increases steel mill capacity. Annealing nitrogen and other gases are also provided on a low-cost tonnage basis.

Air Products' complete gas supply systems are installed at steel mills without capital investment or operating worries on the part of the users. Continuity and reliability of supply are assured. On-site facilities pioneered by Air Products reduced the cost of oxygen 80% in 12 years — transforming oxygen from a costly chemical to a practical working utility.

Further progress marks on-the-job development work now continuing around the clock at major steelmaking facilities. Entirely new metallurgical techniques . . . and new profits . . . are available through Air Products.

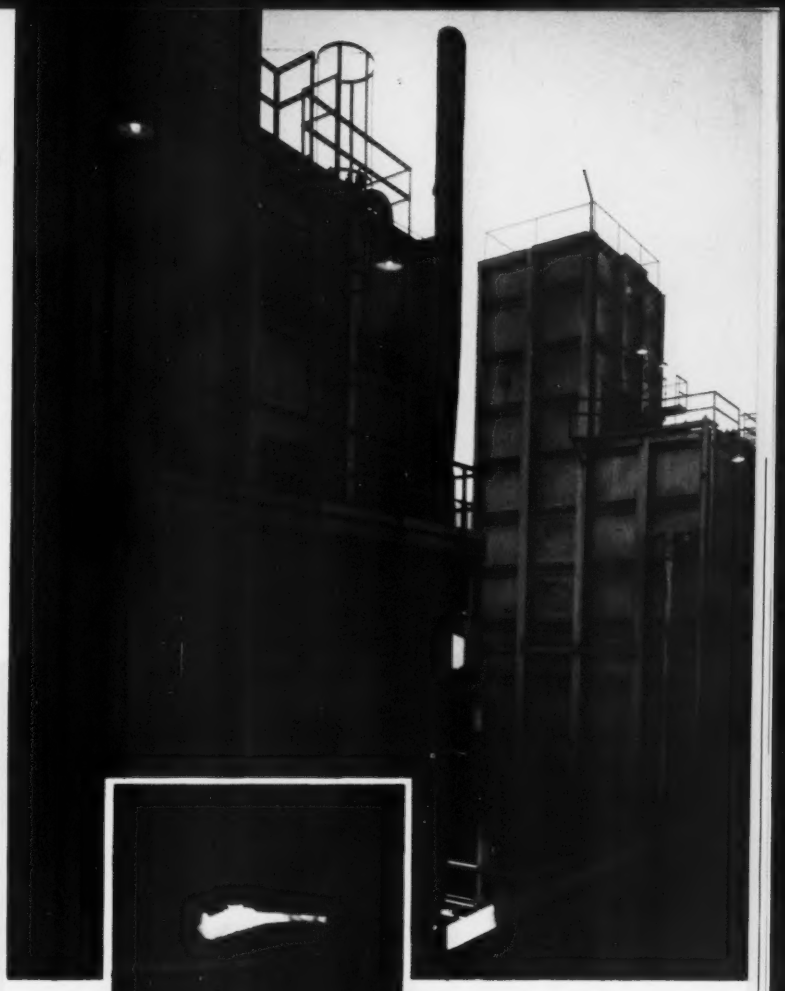

Air Products pipeline oxygen serves the Basic Oxygen Furnace Process.

helped provide many Air Products customers with distinct competitive advantages.

Air Products is the world's leader in APPLIED CRYOGENICS — the practical and profitable use of low-temperature science for industry.

Perhaps this CAPACITY can help solve your problems — in cryogenics, in industrial gas supply systems, or in some new area where "ground rules" are yet to be established.

• Jones & Laughlin Steel • Osaka Oxygen • Spencer Chemical • Sun Oil • U.S. Government—All major research and defense agencies • United States Steel • Venezuelan Ministry of Mines • Weirton Steel

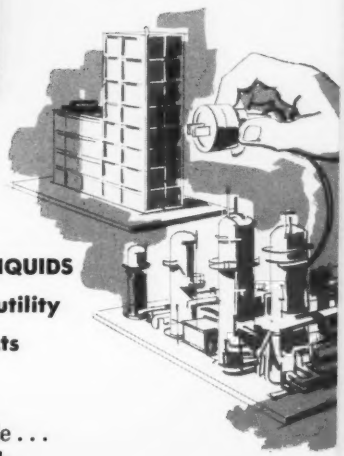

HIGH PURITY GASES AND LIQUIDS —available like any other utility with the help of Air Products CAPACITY

. . . The supply is dependable . . . the price guaranteed . . . with Air Products on the job.

HOW THE CHEMICAL INDUSTRY uses Air Products CAPACITY

Air Products low-temperature systems permit many modern chemical plants to improve operating efficiency and end-product quality — and to develop new processes and products. This results from the ready availability of low-cost tonnage quantities of oxygen, nitrogen, hydrogen, ammonia and methanol syn-gas, carbon monoxide and hydrocarbons such as purified methane, acetylene and ethylene. Low-temperature separations of gaseous mixtures now make it practical to recover valuable components from natural gas, refinery off-gases, coke-oven gas and other "waste" gases. The versatility of cryogenics—as applied by Air Products—works profitably for the chemical industry today . . . offers unparalleled future opportunity in this fast-growing industry.

Air Products
INCORPORATED

powerplant, two distinct phenomena occur which contribute to the range dispersion. These two effects are:

A deviation in the cutoff impulse from nominal.

A variation in the burnout mass from nominal acted on by the total cutoff impulse.

The latter effect is, in reality, attributed to an inadequacy present in virtually all guidance systems which, lacking provision to sense net thrust, cannot compute the instantaneous mass of the missile.

The following analyses will present a method for assessing the change in the velocity vector because of these two effects and will relate this to range dispersion.

Effect of Cutoff Impulse Deviation on Range Dispersion

During the thrust termination process of any rocket engine, liquid or solid, variations in sequencing or actuation cause the engine to exhibit an uncertainty in its thrust decay characteristics. The cross-hatched region in Fig. 1 illustrates this uncertainty. In order to relate this uncertainty to a variation in burnout velocity, consider the following development.

Writing the fundamental rocket equation (1)[2]

$$\Delta U_f = U_e - U_0 = I_{sco}\, g \ln\left(\frac{M_0}{M_e}\right) - g \sin \zeta (t_e - t_c) \quad [1]$$

the change in velocity along the thrust vector during the cutoff process can be determined. Noting that

$$I_{sco} g = \frac{I_{co}}{\Delta M} \quad [2]$$

and $\Delta M \ll M_0$ then

$$\Delta U_f = \frac{I_{co}}{M_0} - g \sin \zeta (t_e - t_0) \quad [3]$$

It should be noted that the time (t_e) when the thrust decays to zero is usually poorly defined, because of asymptotic tail-off characteristics, or oscillations near zero thrust. Therefore, t_e should be defined as the time when some percentage of nominal thrust is reached (say 5 per cent) where the remaining impulse due to tail-off or oscillation would be small.

The change in the velocity increment because of a deviation in cutoff impulse from nominal (ΔI_{co}) will be denoted by $\delta(\Delta U_f)$. It is assumed that $t_c - t_o$ is invariant; i.e., t_c is constant at the nominal value. This assumption is allowable, as the normal variation to be expected in t_c produces a variation in $\delta(\Delta U_f)$ which is, for all practical cases, one order of magnitude smaller than that due to the variation in the first term of Equation [3]. Furthermore, a variation in t_c in essence prolongs or shortens the burning time of the missile and shifts the position of the burnout point in space from its nominal position. This effect is in opposition to the change in velocity because of Δt_c, so that the change in range is negligible. Then

$$\delta(\Delta U_f) = \frac{I_{co} + \Delta I_{co}}{M_0} - \frac{I_{co}}{M_0} = \frac{\Delta I_{co}}{M_0} \quad [4]$$

Defining the parameter $\alpha = \Delta I_{co}/I_{co}$, then Equation [4] reduces to

$$\delta(\Delta U_f) = \alpha I_{co}/M_0 \quad [5]$$

As noted, this change in velocity is in the direction of the thrust vector. It is reflected as a change in range because of two effects: Variation in magnitude, and variation in direction of the velocity vector (U).

In Fig. 2, the change in the magnitude of the velocity vector (U) because of $\delta(\Delta U_f)$ can be derived, to a very close approximation as shown below

$$\delta(U_0) = \delta(\Delta U_f) \cos \xi_0 \quad [6]$$

[2] Numbers in parentheses indicates References at end of paper.

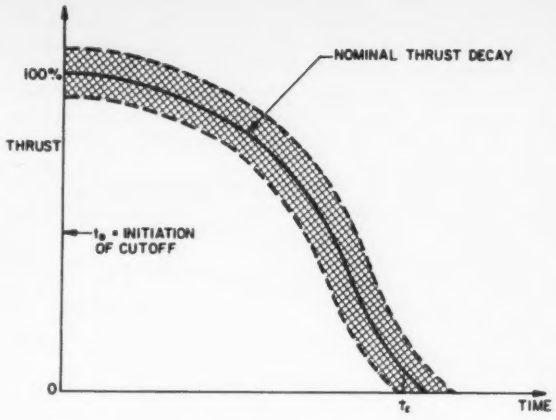

Fig. 1 Typical thrust decay characteristics

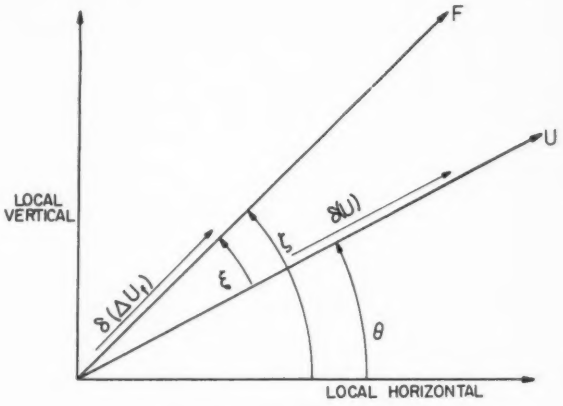

Fig. 2. Velocity vector diagram

$\xi_0 > 0$ for vehicles flying with a constant pitch attitude at burnout.

The range change because of the velocity magnitude variation is then, combining Equations [5 and 6]

$$\delta(U_0) \frac{\partial R}{\partial U_0} = \frac{\alpha I_{co}}{M_e} \left(\frac{\partial R}{\partial U_0}\right) \cos \xi_0 \quad [7]$$

The exchange factor $\partial R/\partial U_0$ is a function of the missile parameters at burnout. The nominal burnout conditions will be used because the variations in these parameters are small. The derivation of this exchange factor is shown later.

Not only the magnitude, but the direction (θ) of the velocity vector changes because of $\delta(\Delta U_f)$. Since $\tan \delta(\theta_0) \doteq \delta(\theta_0)$, and $\delta(U_0) \ll U_0$, then

$$\delta(\theta_c) = \frac{\delta(U_0) \sin \xi_0}{U_0} \quad [8]$$

The range change corresponding to this effect is then

$$\frac{\delta(U_0)}{U_0} \frac{\partial R}{\partial \theta_0} \sin \xi_0 = \frac{\alpha I_{co} \sin \xi_0}{M_0 U_0} \left(\frac{\partial R}{\partial \theta_0}\right) \cos \xi_0 \quad [9]$$

The exchange factor $\partial R/\partial \theta_0$ is evaluated in the same manner

as $\partial R/\partial U_0$. As noted above, because $\delta(U_0) \ll U_0$, the factor $\delta(U_0)/U_0$ would be expected to be exceedingly small. However, because the magnitude of $\partial R/\partial\theta_0$ is unknown, the relative magnitude of the range dispersion caused by the direction change Equation [9] compared with that due to the change in the magnitude Equation [7] will have to be evaluated numerically.

Thus the total range dispersion because of a deviation in the cutoff impulse of the engine denoted as ΔR_1, can be written as follows

$$\Delta R_1 = \frac{\alpha I_{co}}{M_0}\left[\frac{\partial R}{\partial U_0}\cos\xi_0 + \frac{\partial R}{\partial\theta_0}\frac{\sin 2\xi_0}{2U_0}\right] \quad [10]$$

Letting

$$Q = \frac{\partial R}{\partial U_0}\cos\xi_0 + \frac{\partial R}{\partial\theta_0}\frac{\sin 2\xi_0}{2U_0} \quad [11]$$

then

$$\Delta R_1 = \frac{\alpha I_{co}}{M_0}Q \quad [12]$$

Effect of Total Cutoff Impulse on Range Dispersion

The typical radio-inertial or all-inertial guidance system senses acceleration and not net thrust; therefore the instantaneous mass of the missile cannot be calculated. This fact prevents the guidance system from making a correction for variations in the burnout mass. These variations occur because of uncertainties in structure weight and propellant residue. Propellant residue is by far the most significant. For example, if it is possible to have ± 1 per cent of the gross propellant as residue (or sliver), then a missile with a mass ratio of 10 could have approximately ± 9 per cent variation in burnout mass. This variation in the propellant residue can be caused by an engine which is running within specification limits.

It can be seen that an engine having perfectly reproducible cutoff impulse, i.e., $\Delta I_{co} = 0$, can still introduce an error in the cutoff velocity because of the above mentioned variation in the burnout mass.

Considering Equation [12], the nominal range contribution during the cutoff process can be written, for a missile having nominal burnout mass, as

$$I_{co}Q/M_0$$

The change in range from nominal because of a variation in burnout mass will be designated as ΔR_2. Considering that a missile which is heavier than nominal at burnout will fall short of the intended impact point, for a given total cutoff impulse, then

$$\Delta R_2 = \frac{-\beta I_{co}Q}{(1+\beta)M_0} \quad [13]$$

Derivation of the Exchange Factors

In this study for the trajectory after burnout, the following assumptions will be used:

The Earth is spherical.

The Earth is nonrotating.

The effects of the atmosphere are neglected.

These assumptions simplify the derivation of the exchange factors $\partial R/\partial U_0$ and $\partial R/\partial\theta_0$, but the errors introduced by their use should be reasonably small and in keeping with the intended use of this work, i.e., the rapid estimation of the effect of thrust termination characteristics upon range dispersion.

The range equation from which the partial derivatives are taken as exchange factors is Kepler's problem in classical mechanics, which can be written as (2)

$$\Delta\phi = 3\cos^{-1}\left(\frac{-2cZ_h + b}{\sqrt{b^2+4ac}}\right) - \cos^{-1}\left(\frac{-2cZ_R + b}{\sqrt{b^2+4ac}}\right) \quad [14]$$

where

$$\begin{aligned} Z_h &= 1/(r_0 + h_0) \\ Z_R &= 1/r_0 \\ a &= U_0^2 - [2gr_0^2/(r_0 + h_0)] \\ b &= 2gr_0^2 \\ c &= +[(r_0 + h_0)U_0 \sin\theta_0]^2 \end{aligned}$$

The change in angular displacement is related to the range in nautical miles (from the burnout point) by

$$\Delta R = 3438\,\Delta\phi \quad [15]$$

Taking the partial derivative of the range equation with respect to the burnout velocity U_0 yields

$$\frac{\partial R}{\partial U_0} = \frac{6876}{U_0(b^2+4ac)}\left\{\frac{3[Z_h(b^2+2ac-2cU_0^2)+b(a+U_0^2)]}{\sqrt{+(a/c)+(b/c)Z_h - Z_h^2}} - \frac{Z_R(b^2+2ac-2cU_0^2)+b(a+U_0^2)}{\sqrt{+(a/c)+(b/c)Z_R - Z_R^2}}\right\} \quad [16]$$

and the partial with respect to the angle θ_0 at burnout is

$$\frac{\partial R}{\partial\theta_0} = \frac{6876}{\tan\theta_0(b^2+4ac)}\left\{\frac{3[(b^2+2ac)Z_h + ab]}{\sqrt{+(a/c)+(b/c)Z_h - Z_h^2}} - \frac{(b^2+2ac)Z_R + ab}{\sqrt{+(a/c)+(b/c)Z_R - Z_R^2}}\right\} \quad [17]$$

Once the nominal conditions at burnout have been ascertained, it is then possible to calculate the contributions to range dispersion because of the cutoff process (ΔR_1 and ΔR_2). Equations [16 and 17] have been left in the form as shown because they do not simplify when the functions for a, b and c are inserted.

Total Contribution to Range Dispersion Due to the Cutoff Process

The two factors contributing to range dispersion are independent, because they stem in part from two separate aspects of engine operation. The variation in cutoff impulse is a function of the sequencing and actuation times of the cutoff process. The burnout mass variation is largely dependent upon the engine operation (performance) during mainstage, which is totally independent of conditions during cutoff.

These two effects will be assumed to have normal distributions which permit a root mean square (rms) sum to be made to take both into account.

Letting σ denote the rms range dispersion, then

$$\sigma = \sqrt{(\Delta R_1)^2 + (\Delta R_2)^2} = \frac{QI_{co}}{M_0}\sqrt{\alpha^2 + \left(\frac{\beta}{1+\beta}\right)^2} \quad [18]$$

Another parameter λ is designated here to permit the development of the generalized plot shown in Fig. 3, where

$$\lambda = \frac{\sigma M_0}{QI_{co}} = \sqrt{\alpha^2 + \left(\frac{\beta}{1+\beta}\right)^2} \quad [19]$$

An interesting feature of Equation [19], which can be seen in Fig. 3, is that range dispersion is not symmetric in β as it is in α. Range dispersion is the same for positive α or negative α, while it is greater for negative β than for positive β. As mentioned in connection with Equation [13], a missile having a positive β will fall short of the intended impact point. Because of this, the following convention will be used: Positive β will always be associated with negative σ and vice versa.

It should be mentioned that the total cutoff impulse I_{co} refers to altitude conditions as does ΔI_{co}. Because virtually all engine testing is conducted at or near sea level, it is desirable to be able to predict the engine's altitude cutoff characteristics on the basis of these static tests. One method of accomplishing this would be to use the chamber pressure decay

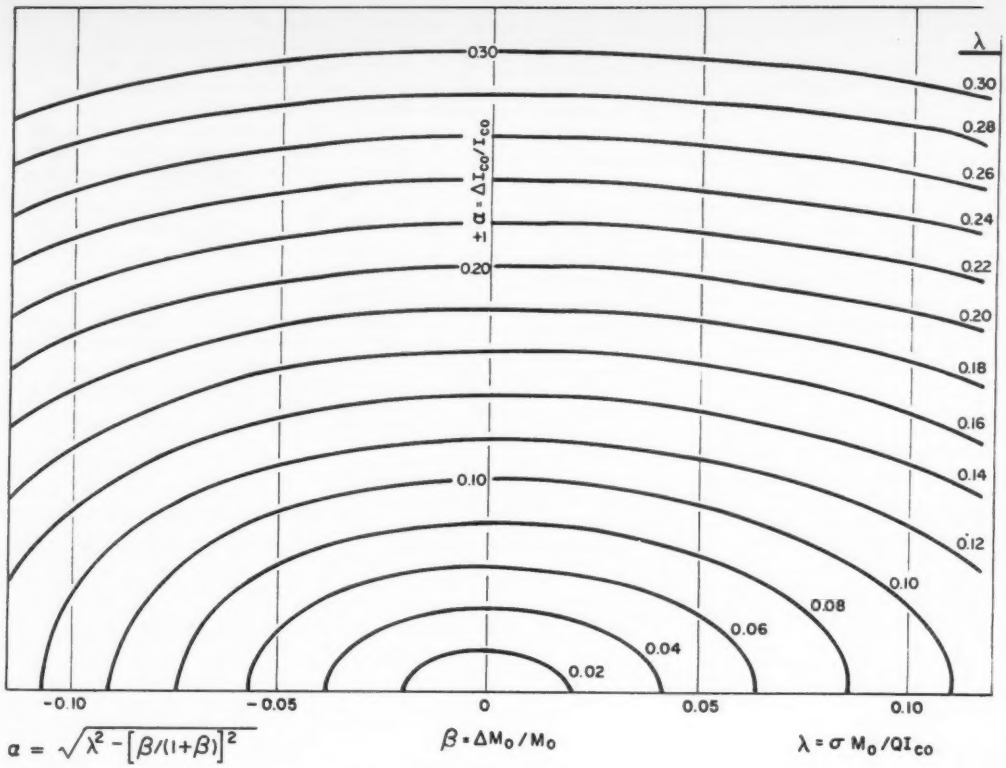

Fig. 3 α **vs.** β **for various** λ

characteristics to estimate the altitude thrust termination characteristics as shown in Equation [20]

$$F = P_c A_t C_f \qquad [20]$$

This method is approximate for two reasons:

1 The chamber pressure decay characteristics under flight conditions may vary from those recorded during static testing because of acceleration, etc.

2 The thrust coefficient during the decay process varies because of fluctuations in the chamber mixture ratio. All tables of C_f are determined for steady-state conditions, whereas the cutoff process represents a transient condition.

However, this method should be adequate for preliminary design purposes.

Sample Problem

Consider a hypothetical missile having the following nominal burnout characteristics:

M_0 = 100 slugs
U_0 = 10,000 fps
θ_0 = 30 deg
ζ_0 = 40 deg
ξ_0 = 10 deg
h_0 = 200,000 ft
I_{co} = 5000 lb-sec
gross propellant wt. = 400 slugs

Determine the maximum allowable cutoff impulse deviation for a range dispersion of $\frac{1}{2}$ nautical mile (n. mi) and a propellant residue variation of ± 1 per cent of the gross propellant.

Substitution of the above characteristics into the range equation indicates that the missile will impact approximately 480 n. mi down range of the burnout point. Then

$\partial R/\partial U_0$ = 0.117 n. mi/fps
$\partial R/\partial \theta_0$ = 57.3 n. mi/rad
Q = 0.116
λ = 0.086

Referring to Fig. 3 using the above parameters

$\beta = \pm 0.04$
$\alpha = \pm 0.0769$ for $\beta = +0.04$
$\alpha = \pm 0.0752$ for $\beta = -0.04$

The minimum value for α (0.0752) which will give the maximum allowable range dispersion must be used. If the other value α were to be used ($+\beta$), the maximum allowable range dispersion would be exceeded. Then $\alpha = 0.0752$, which corresponds to ΔI_{co} = 375 lb-sec.

For this particular case

$$\Delta R_1 = \pm 0.436 \text{ n. mi}$$

and

$$\Delta R_2 = +0.247 - 0.223 \text{ n. mi}$$

The asymmetrical effect of β upon range dispersion can be clearly seen from the above numerical example. Maximum range dispersion corresponds to a negative value of β (the missile is lighter than nominal at burnout).

It is significant to note that even if the cutoff impulse deviation could be reduced to zero ($\alpha = \Delta I_{co} = 0$), the missile's range dispersion would only be approximately halved. The same effect could be secured by simply halving the total cutoff impulse keeping α and β constant at the values given above.

Conclusions

This method of analysis is quite general and can be applied to any ballistic missile. Using Fig. 3, the required thrust termination characteristics of a powerplant can be determined quite rapidly for a given missile and mission with sufficient accuracy to satisfy preliminary design requirements.

The total cutoff impulse (I_{co}) acting on a variable burnout mass (ΔM_0) can have a marked effect upon the range dispersion of a ballistic missile. The most effective manner in which to reduce range dispersion because of the cutoff characteristics of the engine is to reduce the total cutoff impulse rather than attempting a precision cutoff where only ΔI_{co} is reduced. A rapid cutoff process is the most desirable in effectively reducing this contribution to range dispersion.

Nomenclature

A_t = thrust chamber throat area, in.^{2}
C_f = thrust coefficient
F = thrust, lb
g = gravitational constant = 32.2 fps^2
h = height above a spherical Earth, ft
I_{co} = cutoff impulse, lb-sec
I_s = specific impulse, sec
I_{sco} = average specific impulse during cutoff, sec
M = missile mass, slug
P_c = thrust chamber, chamber pressure, psi
Q = defined in Equation [11]
r = distance from the center of a spherical Earth, ft
r_0 = radius of a spherical Earth = 20.903×10^6, ft
R = distance measured along Earth's surface, n. mi
t = time, sec
U = velocity, fps
Z = $(r)^{-1}$
α = $\Delta I_{co}/I_{co}$
β = $\Delta M_0/M_0$
δ = small change
ζ = angle measured between local horizon and thrust vector
θ = angle measured between local horizon and velocity vector
λ = defined by Equation [19]
ξ = angle measured between thrust and velocity vector
σ = rms range dispersion, n. mi
ϕ = angle around Earth from burnout, rad

References

1 Sutton, G. P., "Rocket Propulsion Elements," John Wiley and Sons New York, 1949.
2 Goldstein, H., "Classical Mechanics," Addison-Wesley Publishing Co., Cambridge, 1953.

Technical Notes

Relation of Droplet Consumption Rates to Liquid Strand Consumption Rates[1]

G. A. MEAD[2]

Air Reduction Company, Inc., Central Research Laboratories, Murray Hill, N. J.

Three possible modes of droplet behavior have been examined to find the requirements for consistency with Godsave's equation for liquids burning or decomposing in spherically symmetrical, nonconvective systems with evaporation rate controlling. The empirical diameter-squared rule for small droplets is invalid for surfaces of low curvature, while the constancy of mass consumption rate per unit area observed for flat surfaces is untenable for small droplets. However, the assumption of a constant distance from liquid surface to flame front leads to results which are consistent with both situations. Agreement with some experimental investigators is shown. It is suggested that if the aforementioned assumption is valid over a large enough range, consumption rate data obtained from liquid strand burners can be used to predict droplet behavior.

Received Jan. 23, 1959.
[1] This research was supported by the U. S. Air Force under contract AF 33(616)-5732, monitored by Rocket Fuels Branch, Propulsion Laboratory, Directorate of Laboratories, Wright Air Development Center, Wright-Patterson Air Force Base, Ohio.

[2] Section Head, Combustion and Fuels Technology. Member ARS.

Godsave's Equation and the Diameter-Squared Rule

THE equation derived by Godsave (1)[3] for the evaporation of liquid from a spherical liquid droplet surrounded by a concentric hot surface is

$$\dot{m}_f = \frac{4\pi\lambda r_l \ln\left[1 + \frac{C_p}{\Delta L}(T_c - T_l)\right]}{C_p\left(1 - \frac{r_l}{r_c}\right)} \qquad [1]$$

Equation [1] is rigorously true only for the ideal situation which it is intended to describe. In real systems, complications and deviations must be expected because of convective effects and variations in gas properties caused by the temperature gradient across the gas film. However, it appears to be a good approximation in a number of cases of practical interest. If mass consumption rate per unit area is considered rather than total mass consumption rate, and quantities which are constant or nearly so for a particular combination of liquid and atmosphere are lumped as B, Godsave's equation can be written as

$$\frac{\dot{m}_f}{A} = \frac{B}{r_l[1 - (r_l/r_c)]} \qquad [2]$$

A number of investigators (1,2,3) have found that the behavior of burning or evaporating droplets can be represented empirically by

$$D^2 = D_0^2 - k't \qquad [3]$$

[3] Numbers in parentheses indicate References at end of paper.

EDITOR'S NOTE: The Technical Notes and Technical Comments sections of ARS JOURNAL are open to short manuscripts describing new developments or offering comments on papers previously published. Such manuscripts are published without editorial review, usually within two months of the date of receipt. Requirements as to style are the same as for regular contributions (see masthead page).

which implies that the total mass rate of consumption is proportional to the radius of the droplet (the so-called "first-power law"), or that $\dot{m}_f/A$ is inversely proportional to the droplet radius. Heat transfer considerations indicate that behavior of this sort might be expected, since it seems quite reasonable that either the ratio of hot surface area to liquid surface area will increase, or that gas film thickness will decrease as droplet radius decreases. Conversely, it does not seem reasonable that the distance between the hot surface and the droplet surface should increase as droplet radius decreases, which would be required if $\dot{m}_f/A$ were to remain constant.

If Equation [3] is to be consistent with Godsave's equation, r_c/r_l must remain constant. This behavior does not appear implausible, since it means simply that the system would maintain geometric similarity during combustion. Penner (4) claims some theoretical justification for this. However, it is apparent that Equation [3], with its corollary of constant r_c/r_l, cannot be applied to large droplets or, in the limit, to systems in which the hot surface area is equal to the liquid surface area. It is inconceivable that the distance from the hot surface to the liquid surface would increase indefinitely. Furthermore, since $\dot{m}_f/A$ must be inversely proportional to the radius of the liquid surface, the impossibility of combustion in the limiting type of system is implied. This consequence is contrary to experience, since it is well-established that combustion can take place from flat surfaces, and decomposition can take place in liquid strands (i.e., columns of liquid confined in tubes) where the hot surface area is very nearly equal to, or possibly even smaller than, the liquid surface area. It is known that in systems of this kind, a constant distance from hot surface to liquid surface and a constant $\dot{m}_f/A$ are established. It was shown above, though, that the constancy of $\dot{m}_f/A$ is very unlikely for small droplets.

There might appear to be, therefore, two distinct types of droplet behavior, depending on whether the gas film between the liquid and the hot surface is thick or thin. Further, direct extrapolation from either type of behavior to the other is not satisfactory. The distinction between the two types appears to lie in the mathematical approximations which have been employed rather than in the actual behavior of the droplets. There is undoubtedly a gradual transition between the two types, and it is probable that neither approximation applies very well in this range. (It is also possible, but less likely, that either approximation would be satisfactory in the transition regions.) The transition range is probably important in practice.

Consequences of Constant Distance to Flame Front

A somewhat more consistent model can be developed by using the observed characteristic of burning and decomposition from nearly flat liquid surfaces, that the distance from the hot surface to the droplet surface remains constant. Godsave's equation for total mass consumption rate can be written

$$\dot{m}_f = \frac{4\pi\, Br_l(C + r_l)}{C} \qquad [4]$$

where C is the distance from the hot surface to the liquid surface. Also

$$\dot{m}_f = \rho \frac{dV}{dt} = 4\pi\rho r_l^2 \frac{dr_l}{dt} \qquad [5]$$

Combining Equations [4 and 5] and separating variables

$$\frac{r_l dr_l}{C + r_l} = \frac{B dt}{\rho C} \qquad [6]$$

Integrating, and evaluating the integration constant by letting $t = 0$

$$r_l - C \ln (C + r_l) = \frac{Bt}{\rho C} + r_{l0} - C \ln (C + r_{l0}) \qquad [7]$$

which implies that, when r_l is large compared to C, r_l will be a nearly linear function of t, and $\dot{m}_f/A$ will be nearly constant. In other words, the behavior of liquids evaporating from droplets would become increasingly similar to that of liquids evaporating from flat surfaces as droplet radius is increased, which is a desirable result.

The derivative, Equation [6], can be written in the form

$$\frac{dr_l}{dt} = \frac{B}{\rho}\left(\frac{1}{C} + \frac{1}{r_l}\right) \qquad [8]$$

from which it can be seen that, if $1/C$ can be neglected in comparison with $1/r_l$, an equation having the form of Equation [3] will be obtained upon integration. If this is done, it is found that

$$k' = \frac{-8B}{\rho} \qquad [9]$$

The equations based on the assumption that the distance from the flame front to the liquid surface remains constant have, therefore, the advantage that they are consistent with observed results for the limiting cases of both small droplets and flat surfaces, and may offer some possibility of correlating results for intermediate types of droplet burning or decomposition.

The table summarizes the implications of constant $r_c - r_l$ for the two extreme ranges of liquid radius. Oddly enough, it appears that either the assumption of constant r_c/r_l or the assumption of constant $r_c - r_l$ leads to the result that r_l^2 should be a linear function of time for small droplets.

Table 1 Consequences of constant distance to flame front

Range of r_l	Behavior of liquid diameter with time	Behavior of $\dot{m}_f/A$
$r_l \ll C$	$D^2 = D_0^2 - k't$	$\dot{m}_f/A \propto r_l$
$r_l \gg C$	$D = D_0 - k''t$	$\dot{m}_f/A$ = constant

Comparison With Various Experimental Results

In the investigation of Hall and Diederichsen (3), the times required for complete burning of droplets of varying initial diameter, rather than variation in diameter of single burning droplets, were measured. This method has a decided advantage over the suspended droplet methods because of the wider range of variation in droplet radius which it is possible to study. A somewhat more reliable empirical description of the droplet behavior is to be anticipated for this reason. For example, the data given by Godsave (1), obtained from droplets burning in still air at atmospheric pressure, appear to be almost as linear when the first power of droplet diameter is plotted against time as when the square is plotted. This is because the droplet radii did not vary by a very large ratio. Hall and Diederichsen, by plotting the log of droplet lifetime against the log of initial radius for droplets of widely varying initial radius, came to the conclusion that droplet lifetime was proportional to the 2.05 ± 0.15 power of initial radius, and, therefore, that the droplets were behaving according to Equation [3]. The observation was also made that $r_c - r_l$ was constant. To get some idea of how the data might fit the equations derived from the constant $r_c - r_l$ assumption, the droplet lifetime from Equation [7] is

$$t = \frac{C\rho}{B}\left[r_{l0} - C \ln \frac{(C + r_{l0})}{C}\right] \qquad [10]$$

If values of t calculated from Equation [10] in the range from $C = 0.5\, r_{l0}$ to $C = 5\, r_{l0}$ (very approximately the range indicated by Diederichsen and Hall's measurements of flame front distance at the forward stagnation point) are plotted vs.

r_{l0} on log-log coordinates, the droplet lifetime is found to be proportional to about the 1.8 power of initial radius, which appears to be in fairly good agreement with the experimental value.

On the other hand, the data given by Agoston, Wood and Wise (5) for several materials burning on fairly large (up to 1 cm in diameter) porous spheres do not fit any of the equations based on the constancy of a single parameter (r_c/r_l, $\dot{m}_f/A$, $r_c - r_l$). To quote the authors, "At constant pressure the distance of flame at the forward stagnation point from the surface of a sphere or suspended drop decreases with decreasing diameter, but the ratio of flame diameter to drop or sphere diameter increases."

Conclusions

From this brief study, it appears that the lack of a reliable way to predict the variation of r_c/r_l or $r_c - r_l$ with r_l is a serious obstacle to the development of a completely analytical description of droplet burning. However, if the constancy of $r_c - r_l$ is acceptable as an approximation, droplet consumption rates can be estimated from liquid strand burner data.

Nomenclature

- $\dot{m}_f$ = mass rate of consumption
- λ = average conductivity of gas between the hot surface and the liquid surface
- r = radius
- C_p = average specific heat of gas between the hot surface and the liquid surface
- ΔL = heat of vaporization of the liquid
- T = temperature
- A = liquid surface area
- B = a lumped constant
- D = droplet diameter
- t = time
- k' = evaporation constant
- C = $r_c - r_l$
- V = liquid volume
- ρ = liquid density

Subscripts

- c = hot surface condition
- l = liquid surface condition
- 0 = initial condition

References

1 Godsave, G. A. E., "Studies of the Combustion of Drops in a Fuel Spray—The Burning of Single Drops of Fuel," in "Fourth Symposium (International) on Combustion," Williams & Wilkins, Baltimore, 1953, p. 818.

2 Goldsmith, M. and Penner, S. S., "On the Burning of Single Drops of Fuel in an Oxidizing Atmosphere," Jet Propulsion, vol. 24, no. 4, July-Aug. 1954, p. 245.

3 Hall, A. R. and Diederichsen, J., "An Experimental Study of the Burning of Single Drops of Fuel in Air at Pressures up to Twenty Atmospheres," in "Fourth Symposium (International) on Combustion," Williams & Wilkins, Baltimore, 1953, p. 837.

4 Penner, S. S., "Chemistry Problems in Jet Propulsion," Pergamon Press, New York, 1957, p. 277 ff.

5 Agoston, G. A., Wood, B. J. and Wise, H., "Influence of Pressure on the Combustion of Liquid Spheres," Jet Propulsion, vol. 28, no. 3, March 1958, pp. 181–188.

Chemical Reactions in Supersonic Flow[1]

F. A. WILLIAMS[2]

Harvard University, Cambridge, Mass.

RECENT experimentation first reported by Nicholls (1)[3] has demonstrated that the establishment of a stationary normal shock in a combustible gas stream may initiate a chemical reaction in the flow behind the shock. In this arrangement the pressure and temperature rise across the shock wave are sufficient to ignite the combustible mixture, forming a reaction front which cannot propagate upstream into the supersonic flow. The obvious similarity between this phenomenon and the detonation produced by igniting a reactant gas in a tube has prompted the reasonable definition "steady detonation." In addition to the fact that these new detonations are stationary in the laboratory reference frame, they differ from previously observed detonations in that the final state is not determined by the Chapman-Jouguet condition (Mach number $M = 1$). The observation that these combustion waves are strong detonations ($M < 1$ finally) (2) invalidates previous inconclusive arguments that non-Chapman-Jouguet detonations are unstable (3). The chemical reaction appears to have a relatively small effect upon the shock Mach number (1) which is largely determined by the aerodynamic configuration. Thus, unlike deflagrations, there does not exist a unique detonation velocity. It might therefore be expected that in a suitable arrangement, weak detonations ($M > 1$ finally) may be produced, in which case combustion would occur in supersonic flow. It is the purpose of this note to present tractable governing characteristic equations for chemical reactions in steady supersonic flow and to offer an incomplete hypothetical answer to Gross' challenge to find an application for supersonic combustion (2).

For supersonic flow, it is reasonable to neglect the effects of viscosity, diffusion and thermal conduction in comparison to those of convective transport. It can then be shown that the general equations of mass, momentum and energy conservation, chemical reaction rate, and state can be written, respectively, as (3, 4)

$$\rho \nabla \cdot \vec{v} = -\frac{1}{a^2}\frac{Dp}{Dt} - \frac{\beta}{c_p}\sum_{j=1}^{n} h_j w_j \qquad [1]$$

$$\rho D\vec{v}/Dt = -\nabla p \qquad [2]$$

$$\frac{Ds}{Dt} = -\frac{1}{\rho T}\sum_{j=1}^{n} \mu_j w_j \qquad [3]$$

$$\frac{DY_j}{Dt} = \frac{w_j}{\rho} \qquad (j = 1, \ldots, n) \qquad [4]$$

$$\rho = \rho(p, s, Y_1, \ldots, Y_n) \qquad [5]$$

where

- ρ = density
- $\vec{v}$ = velocity
- p = pressure
- T = temperature
- s = specific entropy
- Y_j = mass fraction of chemical species j of the n-component mixture
- w_j = mass rate of production of component j per unit volume
- μ_j = chemical potential of species j

Here $a^2 = (\partial p/\partial \rho)_{s,Y_j}$, $\beta = \rho[\partial(1/\rho)/\partial T]_{p,Y_j}$, and $c_p = (\partial h/\partial T)_{p,Y_j}$ represent, respectively, the square of the sound velocity, the volumetric thermal expansion coefficient, and the specific heat at constant pressure for the mixture, all evaluated for the chemically frozen system; h is the total enthalpy of the mixture, and $h_j = (\partial h/\partial Y_j)_{\rho,p,Y_{i(i\neq j)}}$ equals the absolute specific enthalpy of species j for the case in which the mixture is an ideal gas.

For steady-state flow, by using thermodynamic relations and the momentum equation, the entropy equation (Eq. [3]) can be replaced by an equation for the enthalpy h which is often more useful in combustion applications. The steady-

Received Feb. 20, 1959.

[1] This research was largely supported by a National Science Foundation Fellowship at the California Institute of Technology.

[2] Member ARS.

[3] Numbers in parentheses indicate References at end of paper.

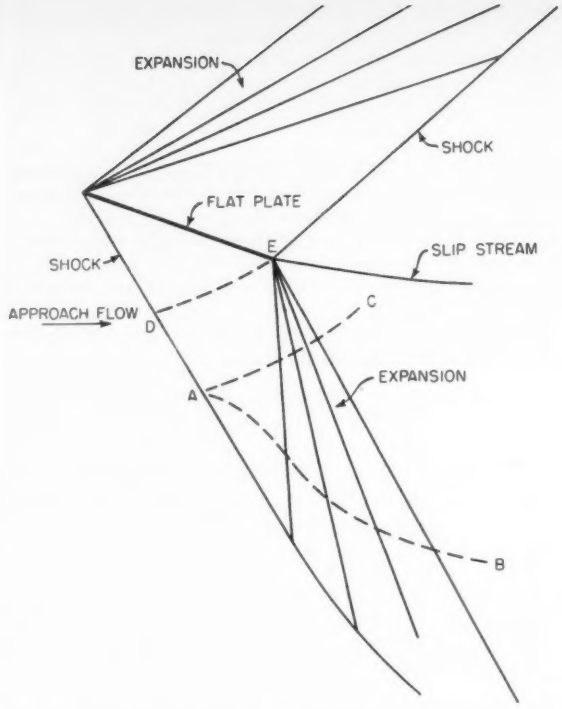

Fig. 1 Supersonic flow with combustion about a flat plate

state forms of Equations [1 through 5] then become

$$\rho\nabla\cdot\vec{v} = -\frac{1}{a^2}\vec{v}\cdot\nabla p - \frac{\beta}{c_p}\sum_{j=1}^{n} h_j w_j \qquad [6]$$

$$\rho\vec{v}\cdot\nabla\vec{v} = -\nabla p \qquad [7]$$

$$\vec{v}\cdot\nabla(h + V^2/2) = 0 \qquad [8]$$

$$\vec{v}\cdot\nabla Y_j = w_j/\rho \qquad (j = 1, \ldots, n) \qquad [9]$$

$$\rho = \rho(p, h, Y_1, \ldots, Y_n) \qquad [10]$$

where $V = |\vec{v}|$.

In the case of plane two-dimensional or axially symmetric flow, this set of equations is easily expressed in finite difference form. If ξ is the distance along a streamline, η is the coordinate normal to ξ, $M = V/a$ represents the Mach number referred to the frozen sound speed, θ is the angle between the local flow direction and the axis of symmetry, and r is the radial distance from the axis of symmetry, then it is found that

$$\frac{(M^2-1)^{1/2}}{\rho V^2}\Delta p \pm \Delta\theta = \frac{\Delta\xi}{(M^2-1)^{1/2}} \times \left[-\frac{\beta}{\rho c_p V}\sum_{j=1}^{n} h_j w_j - N\frac{\sin\theta}{r}\right] \text{for } \Delta\eta = \pm\frac{\Delta\xi}{(M^2-1)^{1/2}} \qquad [11]$$

$$\Delta V = -\Delta p/\rho V \quad \text{for} \quad \Delta\eta = 0 \qquad [12]$$

$$\Delta(h + V^2/2) = 0 \quad \text{for} \quad \Delta\eta = 0 \qquad [13]$$

$$\Delta Y_j = (w_j/\rho V)\Delta\xi (j = 1, \ldots, n) \quad \text{for} \quad \Delta\eta = 0 \qquad [14]$$

$$\rho = \rho(p, h, Y_1, \ldots, Y_n) \qquad [15]$$

where the factor N in Equation [11] is zero for the plane case and unity for axially symmetric flow. These $n + 4$ equations constitute a tractable governing set for chemical reactions in supersonic flow and may be solved by characteristic techniques quite similar to those used for rotational flow. Equation [11] determines the manner in which pressure changes propagate along Mach lines, while Equations [13 and 14] illustrate that the total stagnation enthalpy remains constant along streamlines, and composition changes propagate only along streamlines.

A further simplification arises for flow in the neighborhood of a flat surface, in which case Equations [11 through 15] reduce approximately to the one-dimensional flow relations for a reacting gas. In particular, changes in θ are small, and Equation [11] becomes approximately

$$\Delta p = -\frac{\beta V}{(M^2-1)c_p}\sum_{j=1}^{n} h_j w_j \Delta\xi \qquad [16]$$

which illustrates that exothermic reactions

$$-\sum_{j=1}^{n} h_j w_j > 0$$

in supersonic flow tend to increase the pressure, a well-known result which may conceivably be used for lift or thrust augmentation. In the classical example of supersonic flow about a flat plate, fuel might be injected into the supersonic stream from the leading edge of the plate. The pressure and temperature rise across the oblique shock may ignite the mixture, producing a flow pattern for which typical streamlines and Mach lines are represented by the lines AB and AC, respectively, in Fig. 1. The flow along the flat plate is completely determined by the approach flow crossing the shock between the nose and the end point D of the limiting Mach line DE. If L is the length of the flat plate, p_2 is the pressure above the flat plate, and p_1 is the pressure directly behind the oblique shock, then according to Equation [16], an approximate expression for the fractional increase in the lift coefficient is

$$\frac{\Delta C_L}{C_L} = \frac{\int_0^L\int_0^\xi [V\beta/(M^2-1)c_p]\left(-\sum_{j=1}^{n} h_j w_j\right) d\xi' d\xi}{(p_1 - p_2)L} \qquad [17]$$

References

1 Nicholls, J. A., Dabora, E. K. and Gealer, R. L., "Studies in Stabilized Gaseous Detonations," Seventh International Symposium on Combustion. Butterworth's Sci. Pub., London, 1958, pp. 144–150.

2 Gross, R. A., "Research on Supersonic Combustion," ARS JOURNAL, vol. 29, no. 1, Jan. 1959, pp. 63–64.

3 Hirschfelder, J. O., Curtis, C. F. and Bird, R. B., "Molecular Theory of Gases and Liquids," John Wiley and Sons, New York, 1954.

4 Penner, S. S., "Chemistry Problems in Jet Propulsion," Pergamon Press, New York, 1957.

On Turbulent Supersonic Diabatic Wakes

R. H. PAGE[1]

Stevens Institute of Technology, Hoboken, N. J.

IN THE past, the calculation of a theoretical model for the diabatic base region in transonic and supersonic flow (1)[2] had been somewhat hampered by its numerical complexity. The recent release of excellent charts of auxiliary integrals (2) greatly simplifies the non-isoenergetic jet mixing portion of the calculations. The purpose of this note is to illustrate results which may now be obtained easily through the use of the new generalized jet mixing information (2). Using the new charts, sample calculations of the base pressure ratio for a diabatic

Received March 2, 1959.

[1] Professor of Mechanical Engineering.

[2] Numbers in parentheses indicate References at end of paper.

wake were completed, and typical results are presented in this note. The computations were carried out for the *restricted theory* (i.e., the theory for thin approaching boundary layers) as it applies to supersonic flow past a two-dimensional back-step. Integral methods (2) were used to evaluate the energy addition to the wake from the free stream.

Although tractable, the theory for calculating the base pressure ratio of a back-step is not easily condensed to a single simple explicit equation. Hence, the theoretical result is indicated here functionally

$$\frac{P_b}{P_1} = \frac{P_b}{P_1}\left(M_1,\ k,\ \sigma\mathrm{H},\ \frac{T_{0B}}{T_{0a}},\ \sigma\Lambda\right) \qquad [1]$$

where

M_1 $\geq$ 1.0
k = the ratio of specific heats
H = the dimensionless bleed number (see Eq. [2])

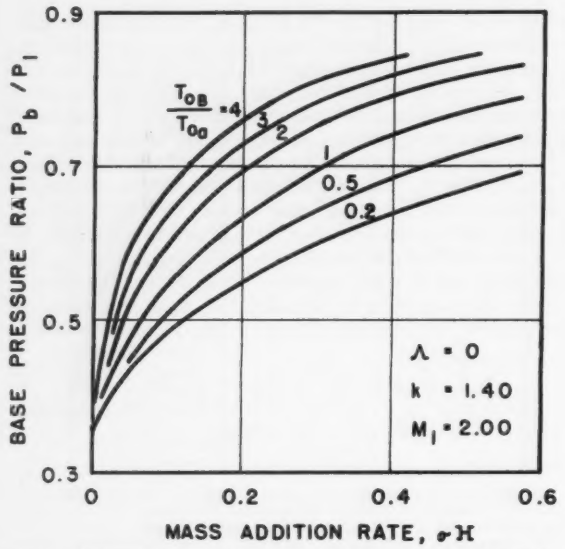

Fig. 1 Influence of bleed gas rate and temperature on a wake

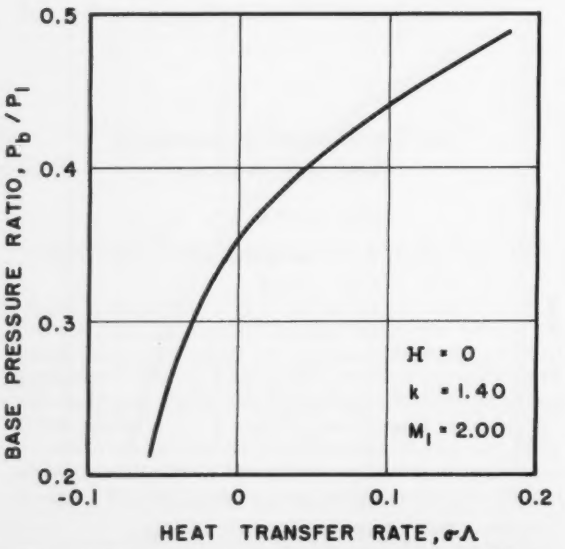

Fig. 2 Influence of heat transfer on a wake with zero bleed

T_{0B}/T_{0a} = the ratio of bleed gas stagnation temperature to free stream temperature
Λ = dimensionless heat transfer number (see Eq. [3])
σ = the similarity parameter for the homogeneous coordinate of the fully developed turbulent mixing profiles

In order to show the flexibility of the theory, two examples are presented, one with no heat transfer from the walls but having mass addition to the wake, and a second with heat transfer from the walls but no mass addition to the wake. Both calculations were performed for an approach Mach number (immediately before the base) of 2.00 and a specific heat ratio of 1.40.

Fig. 1 shows the effect of bleed mass rate and temperature on the base pressure ratio. By definition

$$\mathrm{H} = \frac{G_B\sqrt{T_{0a}}}{HP_{01a}}\left(\frac{R}{kg_c}\right)^{1/2} \qquad [2]$$

where

G_B = the mass bleed rate per unit width at which gas is added externally to the wake
H = the step height
R = the gas constant
g_c = the gravitational constant
T_{0a} = the free stream stagnation temperature
P_{01a} = the stagnation pressure of the free stream before the base

Physical appreciation for the dimensionless bleed number can be obtained by realizing that the quantity

$$\left(\frac{k+1}{2}\right)^{(k+1)/2(k-1)}\mathrm{H}$$

is the actual mass rate per unit width at which gas is added externally to the wake, divided by the maximum mass rate (from free stream initial conditions) per unit width at which gas could be added externally to the base.

Fig. 2 illustrates the effect of heat transfer on a *closed* wake. By definition

$$\Lambda = \frac{Q_b}{Hc_pP_{01a}\sqrt{T_{0a}}}\left(\frac{R}{kg_c}\right)^{1/2}\left(\frac{k+1}{2}\right)^{(k+1)/2(k-1)} \qquad [3]$$

where

c_p = the specific heat at constant pressure
Q_b = the heat transfer rate per unit width from the adjacent walls to the wake

The other symbols are identified above. The dimensionless heat transfer rate may be interpreted as the actual heat transfer rate (per unit width) through the walls adjacent to the wake, divided by the maximum free stream convective energy rate (per unit width), i.e., the energy rate determined from the initial free stream stagnation enthalpy and the maximum mass rate (from free stream initial conditions) at which gas could be added externally to the base.

It is noteworthy that these results are obtained without the use of empirical constants. However, for further application of Figs. 1 and 2, the numerical values of σ must be known. Although complete σ data for supersonic mixing are not available, the temporary relationship

$$\sigma = 12 + 2.758M_{2a} \qquad [4]$$

(based on data with $M_{2a} < 2$) suggested by Korst and Tripp (3) may tentatively be applied until more experimental information on supersonic mixing becomes available. (M_{2a} is the value of the Mach number immediately after the Prandtl-Meyer expansion to the base pressure.)

The theoretical trends indicated in Figs. 1 and 2 are in agree-

ment with those obtained experimentally by heating the forebody and base (4).

References

1 Page, R. H. and Korst, H. H., "Nonisoenergetic Turbulent Compressible Jet Mixing with Consideration of Its Influence on the Base Pressure Problem," Proc. Fourth Midwestern Conf. on Fluid Mech., Purdue Univ., Sept. 1955, pp. 45–68.

2 Korst, H. H. and Chow, W. L., "Compressible Nonisoenergetic Two-Dimensional Turbulent Jet Mixing at Constant Pressure, Auxiliary Integrals, Heat Transfer and Friction Coefficients for Fully Developed Mixing Profiles," Univ. of Illinois, Eng. Exp. Sta., ME-TN-392-4, Jan. 1959.

3 Korst, H. H. and Tripp, W., "The Pressure on a Blunt Trailing Edge Separating Two Supersonic Two-Dimensional Air Streams of Different Mach Numbers and Stagnation Pressures but Identical Stagnation Temperatures," Proc. Fifth Midwestern Conf. on Fluid Mech., Univ. of Michigan, April 1957, pp. 187–199.

4 Kurzweg, H. H., "Inter-Relationship Between Boundary Layer and Base Pressure," *J. Aeron. Sci.*, vol. 18, 1951, pp. 743–748.

Optimum Staging Techniques

LEON WEISBORD[1]

Curtiss-Wright Corp., Wood-Ridge, N. J.

METHODS for the determination of the optimum staging ratios for multistaged rockets were presented by Schurmann (1)[2] and Weisbord (2). Although dealing with similar conditions, there was a basic difference in the variables used. Schurmann minimized the gross missile weight for the case of different structural factors, and final thrust to weight ratios among the stages, but the same specific impulse in every stage. Weisbord handled the problem for the case of different structural factors and specific impulses.

Arens (3) commenting on (2) did not realize this distinction and stated that the solution of (2) is implicitly contained in (1). However, the solution offered in (3) is simply a solution to the problem of (2) through the use of Lagrangian multipliers. Moreover, this solution has already been presented by Vertregt (4) in 1956 (who used slightly different definitions for some of the variables).

Nevertheless, it might be worthwhile to derive solutions for the following more general cases: Different structural factors ϵ, different specific impulses I, and either different final thrust to weight ratios r_f or initial thrust to weight ratios r_0. (The definition of the structural factor ϵ is the ratio of the gross weight less propellant and payload weight of the stage to the gross weight less payload of the stage.)

$$\epsilon_n = \frac{W_{g_n} - W_{p_n} - W_{g_{n+1}}}{W_{g_n} - W_{g_{n+1}}}$$

Case 1 Variable ϵ, I and r_f

Define the payload ratio of the nth stage λ_n as the ratio of the gross weight of the nth stage to the gross weight of the $(n + 1)$ stage

$$\lambda_n = W_{g_n}/W_{g_{n+1}} \qquad [1]$$

The overall payload ratio, $W_{g_1}/\bar{W}$, which is to be minimized, is

$$W_{g_1}/\bar{W} = \lambda_1\lambda_2, \ldots . \lambda_N \qquad [2]$$

where $\bar{W}$ is the payload weight.

The burning time of a stage can be expressed as

$$\Delta t_n = \frac{I_n}{r_{f_n}} \cdot \frac{(\lambda_n - 1)(1 - \epsilon_n)}{1 + \epsilon_n(\lambda_n - 1)} \qquad [3]$$

Received March 11, 1959.

[1] Assistant Project Engineer, Wright Aeronautical Division.

[2] Numbers in parentheses indicate References at end of paper.

The choice of λ is constrained by the velocity equation

$$\varphi = 0 = -\frac{V}{g} + \sum_{n=1}^{N} I_n \ln \frac{\lambda_n}{1 + \epsilon_n(\lambda_n - 1)} - \sum_{n=1}^{N} \frac{I_n \sin \bar{\psi}_n}{r_{f_n}} \left[\frac{(\lambda_n - 1)(1 - \epsilon_n)}{1 + \epsilon_n(\lambda_n - 1)}\right] \qquad [4]$$

where $\bar{\psi}_n$ is the average thrust attitude angle. $\sin\bar{\psi}_n = 1$ in (1).

The use of Lagrangian multipliers offers a convenient method for the solution of the problem. The equations to be solved are

$$\frac{W_{g_1}}{\bar{W}} \cdot \frac{1}{\lambda_1} + \eta \frac{\partial \varphi}{\partial \lambda_1} = 0$$

$$\frac{W_{g_1}}{\bar{W}} \cdot \frac{1}{\lambda_n} + \eta \frac{\partial \varphi}{\partial \lambda_n} = 0 \qquad [5]$$

where η is the Lagrangian multiplier.

The solution to Equations [5] is

$$I_n - \frac{I_n \epsilon_n \lambda_n}{1 + \epsilon_n(\lambda_n - 1)} - \frac{I_n \sin \bar{\psi}_n}{r_{f_n}} \cdot \frac{\lambda_n(1 - \epsilon_n)}{[1 + \epsilon_n(\lambda_n - 1)]^2} = \text{constant} \qquad [6]$$

Equations [6 and 4] must be solved for $\lambda_1, \lambda_2, \ldots \lambda_N$ by an iterative method.

Case 2 Variable ϵ, I and r_0

In many cases, it is more convenient to specify the initial thrust to weight ratio r_0 rather than the final r_f. For this situation, a minimization can be performed if Equation [3] is rewritten in terms of r_0

$$\Delta t_n = \frac{I_n}{r_{0_n}} \cdot \frac{(\lambda_n - 1)(1 - \epsilon_n)}{\lambda_n} \qquad [7]$$

The velocity Equation [4] using [7] becomes

$$\varphi = 0 = -\frac{V}{g} + \sum_{n=1}^{N} I_n \ln \frac{\lambda_n}{1 + \epsilon_n(\lambda_n - 1)} - \sum_{n=1}^{N} \frac{I_n \sin \bar{\psi}_n}{r_{0_n}} \left[\frac{(\lambda_n - 1)(1 - \epsilon_n)}{\lambda_n}\right] \qquad [8]$$

Re-solving Equations [5] using Equation [8] as the new constraining relation, obtain

$$I_n - \frac{I_n \epsilon_n \lambda_n}{1 + \epsilon_n(\lambda_n - 1)} - \frac{I_n \sin \bar{\psi}_n}{r_{0_n}} \cdot \frac{(1 - \epsilon_n)}{\lambda_n} = \text{constant} \qquad [9]$$

For Case 2, a numerical solution can be obtained by an iteration between Equations [9 and 8].

It should be noted that Equations [6 and 9] are general expressions that contain certain more special cases. For instance, if

$$\epsilon_1 = \epsilon_2 = \ldots = \epsilon_N$$

$$I_1 = I_2 = \ldots = I_N$$

and neither r_{0_n} nor r_{f_n} are considered, then

$$\lambda_1 = \lambda_2 = \ldots = \lambda_N \qquad [10]$$

is the criterion for minimization. Equation [10] will be recognized as the optimization criterion of Malina and Summerfield (5).

For the case where r_{0_n} and r_{f_n} are not considered, Equations [6 and 9] can be rewritten as

$$\frac{1}{\lambda_n} = \frac{I_1 \epsilon_n(1 - \epsilon_1)}{(1 - \epsilon_n)(1 - \epsilon_1)(I_n - I_1) + I_n \epsilon_1(1 - \epsilon_n)\lambda_1} \qquad [11]$$

which is equivalent to the optimization criterion of (2).

Lastly, a conversion to the optimization criterion of (1) can be made by using the conversion

$$\tau_n = \frac{(1 - \epsilon_n)(\lambda_n - 1)}{r_{f_n}(1 + \epsilon_n\lambda_n - \epsilon_n)} \qquad [12]$$

and setting $I_1 = I_2 = \ldots = I_N$.

Mention should be made of the excellent articles on optimum staging techniques by Subotowicz (6) and Hall and Zambelli (7). Both of these papers present weight minimization procedures for the case of variable specific impulses and structural factors.

It is hoped that this note will clarify the comment of Arens (3), and will be of some use to persons interested in missile weight minimization.

References

1 Schurmann, E. E. H., "Optimum Staging Technique for Multistaged Rocket Vehicles," JET PROPULSION, vol. 27, Aug. 1957, pp. 863–865.

2 Weisbord, L., "A Generalized Optimization Procedure for N-Staged Missiles," JET PROPULSION, vol. 28, March 1958, pp. 164–167.

3 Arens, M., "On a Generalized Optimization Procedure for N-Staged Missiles," JET PROPULSION, vol. 28, Nov. 1958, p. 766.

4 Vertregt, M., "A Method for Calculating the Mass Ratios of Step Rockets," *J. British Interplanet. Soc.*, vol. 15, March-April 1956, p. 95.

5 Malina, F. J. and Summerfield, M., "The Problem of Escape from the Earth by Rocket," *J. Aeron. Sci.*, vol. 14, Aug. 1947, pp. 471–480.

6 Subotowicz, M., "The Optimization of the N-Step Rocket With Different Construction Parameters and Propellant Specific Impulses in Each Stage," JET PROPULSION, vol. 28, July 1958, pp. 460–463.

7 Hall, H. H. and Zambelli, E. D., "On the Optimization of Multistage Rockets," JET PROPULSION, vol. 28, July 1958, pp. 463–465.

Suppression of Combustion Instability in the Plungerjet Rocket Engine

HERBERT SHIEBER[1]

Hughes Tool Co., Culver City, Calif.

RECENT issues of the ARS JOURNAL have indicated a marked difference of opinion among researchers regarding a mechanism for explaining combustion instability in rocket engines (1 to 5).[2] In the interest of supporting the contention expressed in (5) that "intellectual controversy is a strong stimulus to scientific progress," some combustion instability phenomena experienced during the development of the Hughes Plungerjet XLR107-HT-1 monopropellant rocket engine are reported herein. These experimental phenomena, while unique to the Plungerjet engine geometry, pertain to the subject dispute in such a manner as to suggest possible experiments for resolving the argument, or at least for amplifying the contending combustion instability theories.

In order to appreciate the pertinence of the Plungerjet experimental experience to the controversy, it will be necessary to comprehend the operation of the Plungerjet engine. Fig. 1 is a cutaway view of this engine, showing its essential features. It can be noted that the device employed to pressurize the propellant is a free piston, which also serves as the injector head separating the propellant reservoir from the combustion chamber. This piston, by virtue of the area inequality existing on its liquid and gas sides, provides the pressure differential essential for propellant feed. As the propellant is expended, the combustion chamber volume grows in the manner of an end-burning solid grain.

It is thus seen that the Plungerjet engine traces the effect of chamber length on combustion instability during each firing. This is particularly relevant because much of the subject controversy appears to concern the relative sufficiencies of the contending theories to predict the existence of a maximum chamber length beyond which the fundamental longitudinal mode of oscillation does not occur. Peculiarly enough, the original configuration of the piston assembly (Fig. 2, Configuration A) was such as to inhibit any combustion instability, irrespective of chamber length during operation. The choice of this configuration (piston rod vented into combustion chamber) was due at the time solely to structural considerations, that is, the piston rod weight was minimized by reacting most of the propellant pressure on the piston rod with internal gas pressure.

However, in a later design of the engine, it was considered expedient to use the piston Configuration B shown in Fig. 2, inasmuch as the saving in piston rod weight did not appear to justify the cost of sealing and insulating the interior of the rod. When Configuration B was static fired, however, the engine operation became a striking example of high-frequency instability. Although the length of the Plungerjet piston stroke was evidently not sufficient to demonstrate the aforementioned stability boundary effect of critical maximum chamber length, the exhibited instability otherwise conformed

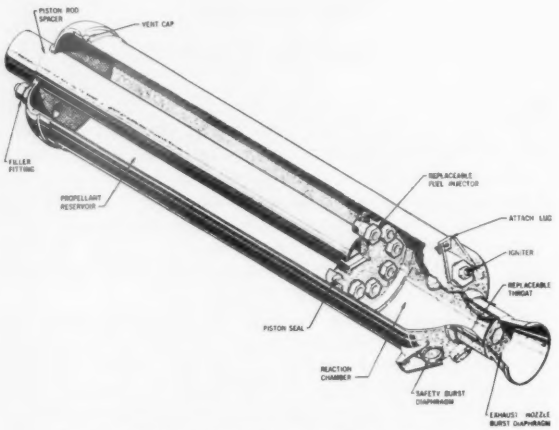

Fig. 1 Cutaway view of Plungerjet rocket engine

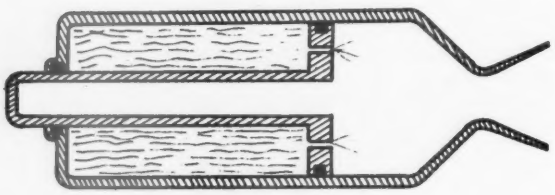

Configuration A
Original and Final Piston Assembly Design

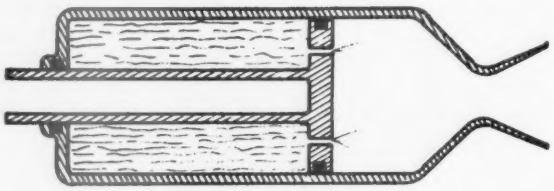

Configuration B
Intermediate Piston Assembly Design

Fig. 2 Plungerjet piston assembly designs

Received April 20, 1959.

[1] Chief Propulsion Development Engineer. Member ARS.

[2] Numbers in parentheses indicate References at end of paper.

very closely to that predicted by the theory and experiments reported in (1 and 2). That is, the frequency of the pressure oscillations showed dependence on instantaneous piston position (chamber length), and the factors affecting the onset and amplitude of the oscillations were likewise typical of longitudinal high-frequency combustion instability.

The onset of instability appeared sooner and the amplitude of the oscillations were greater when the larger of two replaceable exhaust nozzle throats was installed in the engine. With the smaller of the two throats installed, there were practically no pressure oscillations, even at maximum chamber length. However, with the larger throat installed, the engine operation was invariably unstable.

A second factor that had a strong influence on the severity of the instability was the presence of inert matter in the propellant. For considerations that are outside the scope of this Note, the propellant loading procedure included a thorough flushing of the propellant reservoir with Freon 12 gas. This gas is very soluble in the propellant, and on occasions when the engine was defueled and the propellant subsequently reused after another exposure to the Freon flushing procedure, the ensuing instability was appreciably increased.

The magnitude of the chamber pressure (which can be preadjusted in the Plungerjet) also seemed to affect the onset and amplitude of the combustion instability, with the higher chamber pressures appearing to create somewhat more severe pressure oscillations than did the lower chamber pressures. This effect, however, was not so pronounced as the aforementioned effects.

Needless to say, this experience with the destabilizing influence of piston Configuration B prompted a design return to the original piston Configuration A. From a developmental point of view, this engine's combustion instability tendency has now been effectively suppressed. From a more fundamental viewpoint, however, several interesting questions remain, and these questions may have some bearing on the subject controversy concerning combustion instability explanatory mechanisms.

For instance, is the stabilizing influence of the open piston rod (Configuration A) explained by the fact that the cavity represents enough additional chamber length to exceed the critical chamber length? There are objections to this explanation. In the first place, the open piston rod is forward of the injectors and, as such, should provide a different phase relationship between the pressure waves and the local burning rates than would be the case in the conventional combustion model with an equivalent increase in chamber length applied downstream of the injectors. Secondly, the open piston rod represents only a small portion of the cross-sectional area of the chamber, further departing from geometric equivalence.

It would be most interesting if the research teams investigating combustion instability could correlate this cavity effect into their combustion theories. Specifically, is there a correlation between critical combustion chamber length and cavity length? Is the placement of the cavity forward of the injectors significant, or could it be placed at the exhaust nozzle end, or even radially disposed? Is there a cavity length that would reinforce rather than attenuate the pressure oscillations? Answers to these questions would not only illuminate the subject dispute, but might also provide an effective design tool for suppressing combustion instability.

References

1 Zucrow, M. J. and Osborn, J. R., "An Experimental Study of High-Frequency Combustion Pressure Oscillations," JET PROPULSION, vol. 28, no. 10, Oct. 1958, pp. 654–659.

2 Crocco, L., Grey, J. and Harrje, D. T., "On the Importance of the Sensitive Time Lag in Longitudinal High-Frequency Combustion Instability," JET PROPULSION, vol. 28, no. 12, Dec. 1958, pp. 841–843.

3 Crocco, L. "Comments on the Zucrow-Osborn Paper on Combustion Oscillations," JET PROPULSION, vol. 28, no. 12, Dec. 1958, pp. 843–844.

4 Zucrow, M. J. and Osborn, J. R., "Reply to Crocco's Criticism of the Zucrow-Osborn Paper," ARS JOURNAL, vol. 29, no. 3, March 1959, pp. 221–222.

5 Summerfield, M., "And Now the Editor Has His Say," ARS JOURNAL, vol. 29, no. 3, March 1959, p. 222.

Theoretical and Experimental Analysis of a Cowling as a Means of a Drag Reduction for an Axisymmetric Center Body[1]

MARIAN VISICH Jr.[2] and ANTHONY MARTELLUCCI[3]

Polytechnic Institute of Brooklyn, Freeport, N. Y.

INTERFERENCE principles have been employed quite extensively for the reduction of the wave drag of various supersonic configurations. Linearized flow techniques have been the major tool for the analyses conducted. However, in order to contain a sizable volume these techniques represent slender bodies with relatively large fineness ratios.

The present investigation employs nonlinear techniques for the drag reduction of a system that contains a large volume per unit length. The configuration consists of a boat-tailed body of revolution surrounded by a large diameter ring which effectively reduces the wave or thickness drag of the center body. This reduction is accomplished by reflecting the conical shock generated from the apex of the center body on to the boat-tailed rear part. Thus, the static pressure on the rear part of the body is increased, and the pressure drag considerably reduced in comparison to that of the center body alone. This type of drag reduction has been investigated for various configurations of body and ring by both the method of characteristics (1)[4] and by linearized techniques (2). In this report, however, a finite-strength conical shock from both the nose of the center body and the lip of the cowling ring is considered. The result is only verified for a particular configuration at a design point Mach number of 3.09. It should be noted that a vehicle of this type is efficient in a limited range of Mach number close to the design value.

Theoretical Investigation

A theoretical investigation has been conducted in order to determine a ring-body combination that will demonstrate the use of this method as a means of drag reduction. The body was designed for a Mach number of 3.09. A body with a large volume per unit length was desired; thus nonlinear techniques were required in the design. The center body length, leading edge semi-apex angle and maximum diameter were selected somewhat arbitrarily. In addition, a cuspated forebody was selected so that a greater part of the compression would be isentropic. The method of characteristics for axisymmetric irrotational flow was utilized to design the body. The generalized equations employed are given in (3). From the apex to the position of maximum thickness, the body shape was selected in a manner that would insure a gradual isentropic compression and an ensuing expansion which would avoid separation. With the forebody selected, the remaining body shape was established.

The minimum diameter ring and its approximate axial position were then selected so that the area of the annulus, between the center body and ring, would permit supersonic flow to be established. An abbreviated characteristics analysis was then conducted to place the ring axially relative to the center body.

The rear section of the center body was then calculated with the cowling ring in place. This calculation was more complicated due to the intersection of the tip shock with the

Received Feb. 24, 1959.

[1] This research was supported by the U. S. Air Force through the Air Force Office of Scientific Research, Air Research and Development Command, under Contract no. AF 49(638)-217, Project no. 9781, under the supervision of Professor Antonio Ferri.

[2] Assistant Professor of Aeronautical Engineering. Member ARS.

[3] Research Assistant.

[4] Numbers in parentheses indicate References at end of paper.

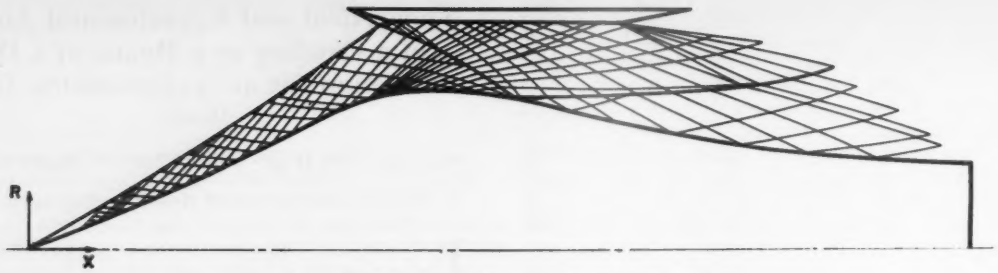

Fig. 1 Characteristics of the center body with the ring

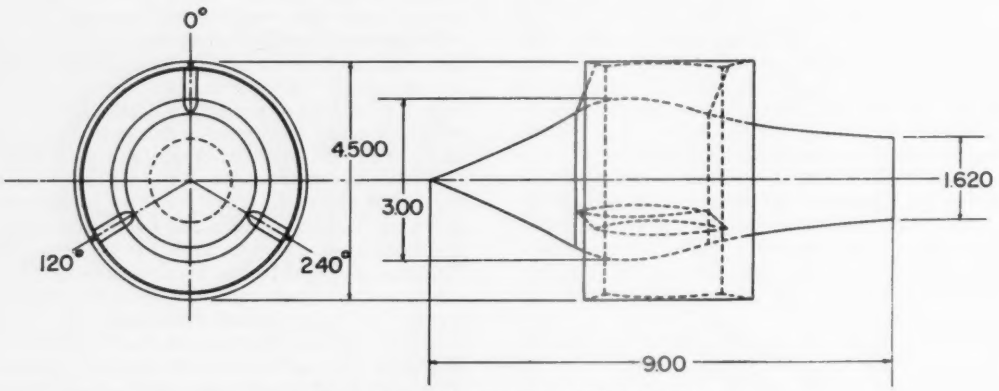

Fig. 2 Assembly drawing of cowling model

shock emanating from the ring. The shape of the reflected shock was determined point-by-point, since conditions upstream were known. From this shock, once again the method of characteristics for irrotational flow was used to determine the body shape. This is permissible, since the variations in entropy are small, and in a first approximation may be neglected while sufficient accuracy is maintained. The characteristic net for the center body with the cowling ring is shown in Fig. 1. An assembly view of the cowling model is shown in Fig. 2.

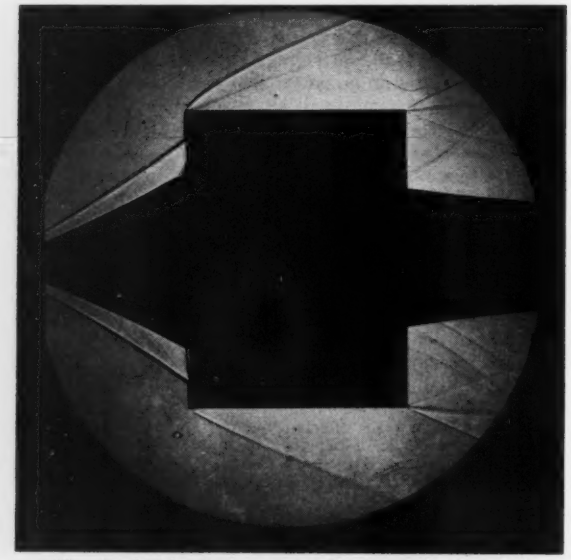

Fig. 3 Spark shadowgraph of the cowling model

Experimental Apparatus and Testing Technique

The experimental investigation of the body of revolution, surrounded by a cowling or ring, was conducted in the 10 × 10-in. supersonic blowdown wind tunnel of the Polytechnic Institute of Brooklyn Aerodynamics Laboratory. Tests were conducted at a stagnation pressure of 200 psia with a corresponding test section Reynolds number per foot of 3.37×10^7. A typical spark shadowgraph of the cowling model is shown in Fig. 3.

The pressure drag was obtained by measuring the pressure distribution over the body and integrating it over the drag surface on which it acts. Tests were made of the center body without a ring and of the center body with the cowling. The experimental C_P distribution for the center body without a ring is shown in Fig. 4. Also shown for comparison is the distribution obtained by the characteristics analysis. The experimental C_P distribution for the ring configuration is shown in Fig. 5.

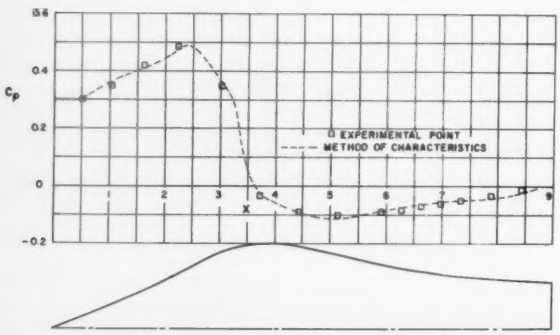

Fig. 4 Comparison of theoretical and experimental pressure coefficient distribution for the center body alone

Table 1 Comparison of drag components for bodies of equal volume and length

Volume = 31.068 Length = 9.000

Body	A_{max}	A_{base}	Wetted area	Pressure drag, D_P/q	Base drag, D_b/q	Total drag, D_T/q	Estimate of skin friction drag, D_f/q
center body	7.07	2.06	55.0	2.573	0.224	2.797	0.194
cowling body	7.07	2.06	172.0	0.702	0.185	0.887	0.605
cone—11.4 deg semi-apex angle	10.36	10.36	52.4	1.075	1.040	2.115	0.184
Haack-Adams	6.73	6.61	58.2	0.697	0.661	1.358	...
TR 1271	6.73	6.61	58.2	0.560	0.661	1.221	...

Method of Data Reduction

The pressure drag of the center body was determined from a numerical integration of the static pressures over the surface, utilizing the experimental values of the recorded pressures. The pressure drag on the ring and struts was obtained by measuring the pressures on the respective surfaces.

The base pressure on the center body was also measured, and the value of the drag coefficient computed. These results are of the same order of magnitude as the values obtained by Chapman (4) and Love (5). Since the pressure distribution along the body was known, using the method outlined in (6), an estimate of the skin friction was made. For this calculation, it was assumed that the boundary layer was entirely turbulent and the wall temperature constant.

Results and Conclusions

For the center body without the ring, the pressure drag coefficient based on the maximum diameter is 0.364, while for the configuration tested, the value for the center body alone is 0.060. This corresponds to a reduction of 83.5 per cent of the pressure drag of the center body. Comparison of the total drag of the cowling configuration (pressure drag of the entire system and skin friction on the ring and struts) to the total drag of the center body without the ring indicates a reduction of 50.0 per cent.

A comparison of the drag of the present cowling system with various linear systems of given length and volume cannot be achieved because of the relatively large volume per unit length. Therefore, the system is compared to various bodies of revolution to further evaluate the reduced drag. Since the bodies considered have different maximum cross-sectional areas, the drag coefficients based on this reference area cannot be compared, but values of the product of the drag coefficient and the body maximum cross-sectional area are considered.

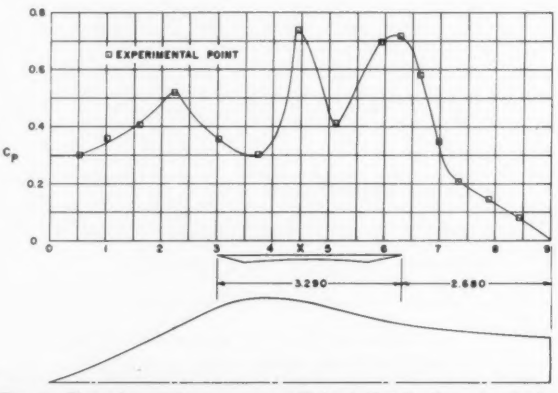

Fig. 5 Experimental pressure coefficient distribution of a body of revolution surrounded by a cowling ring

The results are illustrated in Table 1. Comparison of the cowling system to the optimized Haack-Adams (7) body tends to indicate that the drag reduction is appreciable. One must note that the cowling body is capable of producing a substantial L/D.

Thus the cowling center body presents a useful and practical system for employment as a flight vehicle with a circular wing. In addition, the annulus contains air possessing a high pressure recovery; thus a system of this type could also be used as an auxiliary ramjet engine or as a bypass for a ramjet engine.

References

1 Ferri, A., "Application of the Method of Characteristics to Supersonic Rotational Flow," NACA Technical Rep. no. 841, 1946.

2 Johnson, R. P., "Drag Transformation and Reduction for Bodies of Revolution," Rand Corporation Rep. RM-2107, Aug. 1957.

3 Sears, W. R., "General Theory of High Speed Aerodynamics, Vol. VI," Princeton University Press, Princeton, 1954, p. 659ff.

4 Chapman, D. R., "An Analysis of Base Pressure at Supersonic Velocities and Comparison with Experiment," NACA Technical Rep. no. 1051, 1951.

5 Love, E. S., "Base Pressure at Supersonic Speeds on Two-Dimensional Airfoils and Bodies of Revolution With and Without Fins Having Turbulent Boundary Layer," NACA Technical Note no. 3819, 1957.

6 Bloom, M. H. and Martellucci, A., "A Method for Calculating Turbulent Boundary Layer Characteristics in High Speed Flow," Gruen Applied Science Laboratories, Inc., Rep. 27, March 1957.

7 Harder, K., C. and Rennemann, C., Jr., "On Boattail Bodies of Revolution Having Minimum Wave Drag," NACA Technical Rep. no. 1271, 1956.

An Optimum Transfer Path From an Elliptical Orbit to a Higher Energy Circular Orbit

H. MUNICK[1]

Grumman Aircraft Engineering Corp., Bethpage, N. Y.

THE PROBLEM considered in this paper is an optimum transfer path from the perigee of an elliptic orbit to any point on a higher energy circular orbit. The optimum considered is the minimization of characteristic velocity, or the amount of fuel consumed, using two impulses. The time of transfer is left open. Lawden (1)[2] has treated this problem, and similar more general problems, exceptionally well.

A rigorous mathematical derivation is presented, proving an optimum path to follow is the Hohmann (2) transfer ellipse.

Introduce a hypothetical circular orbit (B) (see Fig. 1) of radius r_p. Such an orbit has a smaller major axis than the

Received March 2, 1959.

[1] Dynamics Group, Research Mathematician.

[2] Numbers in parentheses indicate References at end of paper.

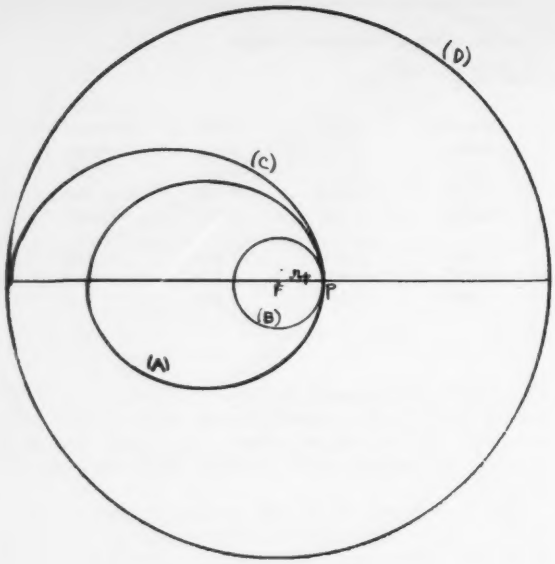

Fig. 1 Orbits in a central force field

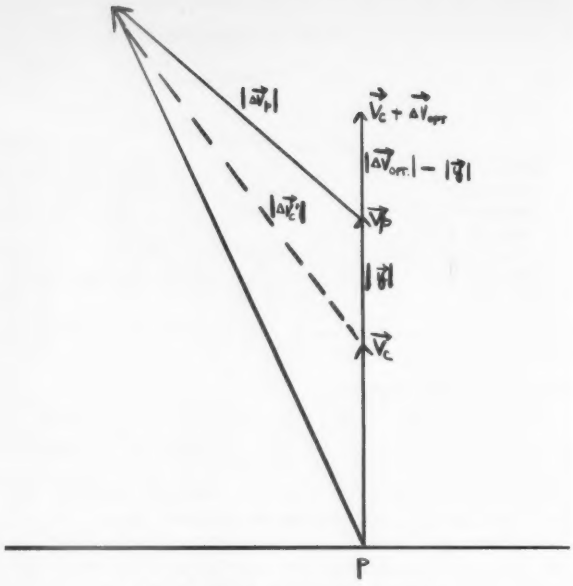

Fig. 2 Diagram of vector velocities

major axis of elliptic orbit (A) and is therefore a lower energy orbit. At the point of tangency P of orbits (A) and (B), a space vehicle in orbit (A) or in orbit (B) would have the same potential energy. Therefore a space vehicle at point P in orbit (B) would have less linear velocity than a space vehicle traveling in orbit (A) at point P.

Consider a space vehicle traveling in elliptic orbit (A). Suddenly an impulse is applied at P, giving rise to a velocity increment, $\overrightarrow{\Delta V_p}$ (see Fig. 2). The magnitude $|\overrightarrow{\Delta V_p}|$ is such that energy is added to orbit (A). Another way to describe this energy addition is

$$|\overrightarrow{V_p} + \overrightarrow{\Delta V_p}| \geq |\overrightarrow{V_p}| \qquad [1]$$

For such a $\overrightarrow{\Delta V_p}$, there exists a $\overrightarrow{\Delta V_c'}$ (see Fig. 2) such that

$$\overrightarrow{V_p} + \overrightarrow{\Delta V_p} = \overrightarrow{V_c} + \overrightarrow{\Delta V_c'} \qquad [2]$$

A comparison is next made between the transfer from orbit (A) to orbit (D), with the transfer from orbit (B) to orbit (D). Consider the following three characteristic velocities:

1 Ellipse-Circle

$$|\overrightarrow{\Delta V_p}| + |\overrightarrow{\Delta F}|$$

2 Circle-Circle

$$|\overrightarrow{\Delta V_c'}| + |\overrightarrow{\Delta F}|$$

3 Hohmann Optimum Circle-Circle

$$|\overrightarrow{\Delta V_{opt}}| + |\overrightarrow{\Delta F_{opt}}|$$

From [2], the final correcting velocities $\overrightarrow{\Delta F}$ appearing in 1 and 2 are the same.

From Fig. 2 we observe

$$|\overrightarrow{\Delta V_c'}| \leq |\overrightarrow{y}| + |\overrightarrow{\Delta V_p}| \qquad [3]$$

Since the Hohmann circle-to-circle transfer ellipse gives an optimum path, we have

$$|\overrightarrow{\Delta V_{opt}}| + |\overrightarrow{\Delta F_{opt}}| \leq |\overrightarrow{\Delta V_c'}| + |\overrightarrow{\Delta F}| \qquad [4]$$

From Equations [3 and 4]

$$|\overrightarrow{\Delta V_{opt}}| + |\overrightarrow{F_{opt}}| \leq |\overrightarrow{V_c'}| + |\overrightarrow{\Delta F}| \leq |\overrightarrow{y}| + |\overrightarrow{\Delta V_p}| + |\overrightarrow{\Delta F}| \qquad [5]$$

From Equation [5]

$$|\overrightarrow{\Delta V_p}| + |\overrightarrow{\Delta F}| \geq |\overrightarrow{\Delta V_{opt}}| + |\overrightarrow{\Delta F_{opt}}| - |\overrightarrow{y}| \qquad [6]$$

The Hohmann characteristic velocity $|\overrightarrow{\Delta V_{opt}}| + |\overrightarrow{\Delta F_{opt}}|$ provides a lower bound for the class of characteristic velocities in the circle-to-circle transfer. Likewise the right-hand side of Equation [6] provides a lower bound for the class of characteristic velocities in the ellipse-to-circle transfer, since the lower bound given by Equation [6] can actually be achieved by taking the Hohmann transfer ellipse. This Hohmann transfer ellipse would be identical to the optimum transfer path taken from circular orbit (B) to circular orbit (D).

Since the greatest lower bound for the class of characteristic velocities can be achieved, it follows

$$\left[|\overrightarrow{\Delta V_p}| + |\overrightarrow{\Delta F}|\right]_{min} = |\overrightarrow{\Delta V_{opt}}| + |\overrightarrow{\Delta F_{opt}}| - |\overrightarrow{y}| \qquad [7]$$

Nomenclature

r_p = distance of perigee from focus

$\overrightarrow{\Delta V_p}$ = velocity increment at perigee P in elliptic orbit (A)

$\overrightarrow{V_p}$ = velocity at perigee in elliptic orbit (A)

$\overrightarrow{\Delta V_c'}$ = velocity increment at P in circular orbit (B)

$\overrightarrow{\Delta F}$ = velocity increment correcting final velocity of transfer path to circular velocity

$\overrightarrow{\Delta V_{opt}}$ = Hohmann optimum velocity increment at P in circular orbit (B)

$\overrightarrow{\Delta F_{opt}}$ = Hohmann optimum, correcting final velocity of transfer path to circular velocity

$\vec{V}_c$ = velocity in circular orbit (B)

$\vec{y}$ = difference between $\vec{V}_p$ and $\vec{V}_c$

Acknowledgment

The author expresses his gratitude to E. Beltrami of the Operations Research Group, for valuable discussions concerning the problem. Also to W. Lindorfer of the Dynamics Research Group, for his excellent mathematical criticisms.

References

1 Lawden, D. F., "Entry into Circular Orbits—I," *J. Brit. Interplanet. Soc.*, vol. 10, no. 1, Jan. 1951, pp. 5–17.

2 Hohmann, W., "Die Erreichbarkeit der Himmelskorper," R. Oldenbourg, Munich, 1925.

Electrically Charged Bodies Moving in the Earth's Magnetic Field

W. W. FAIN[1] and B. J. GREER[2]

Chance Vought Aircraft, Inc., Dallas, Texas

AN INVESTIGATION has been initiated to determine the effect on the path of electrically charged bodies moving in the Earth's magnetic field. The study is applicable to

1 Perturbation in satellite orbits (charging the satellite can be used to afford a small measure of control over the orbit).

2 The effect on the path of a rocket fired from the Earth.

3 The effect on charged particles entering the Earth's magnetic field. (In particular it is hoped that the shape of the radiation belt around the Earth can be deduced from this.)

Received March 2, 1959.

[1] Engineering Specialist, Aircraft Systems Analysis Group.

[2] Associate Aerodynamics Design Engineer.

So far, the two-dimensional model has been programmed. In this, it is assumed that the magnetic and rotational equators are the same. The effect on charged satellites of various masses and charge have been investigated for an initially circular orbit. A charge-discharge procedure has also been studied to determine the feasibility of using this to control and change the orbit.

At present the general three-dimensional equations are being programmed. These include the angle between the rotational and magnetic axes, the Earth's rotation, and a charged body moving with any initial velocity.

Two-Dimensional Equations of Motion for a Charged Body in the Magnetic and Gravitational Field

If the rotational and magnetic equator are taken to be the same, then for a charged body moving in the equatorial plane of the Earth and subject to a magnetic dipole field, the equations governing its motion are

$$\frac{-GM_sM_E + hQ\dot{\theta}}{r^2} = (\ddot{r} - r\dot{\theta}^2)M_s$$

$$-\frac{hQ\dot{r}}{r^3} = (2\dot{r}\dot{\theta} + r\ddot{\theta})M_s$$

where

r = distance from the Earth's center to the center of the charged body
M_s = mass of the charged body
M_E = mass of the Earth
h = strength of the dipole
Q = charge on the body
θ = angular distance measured from an arbitrary reference
G = gravitational constant

Results for Two-Dimensional Model

The body was given sufficient angular velocity for a circular orbit at a distance 6.5×10^3 km from the center of the model Earth, and the charge was "turned on." In Fig. 1 the difference in the new orbit and the old orbit $R - R_0$ is plotted as a function of the angular distance from the "turn-on"

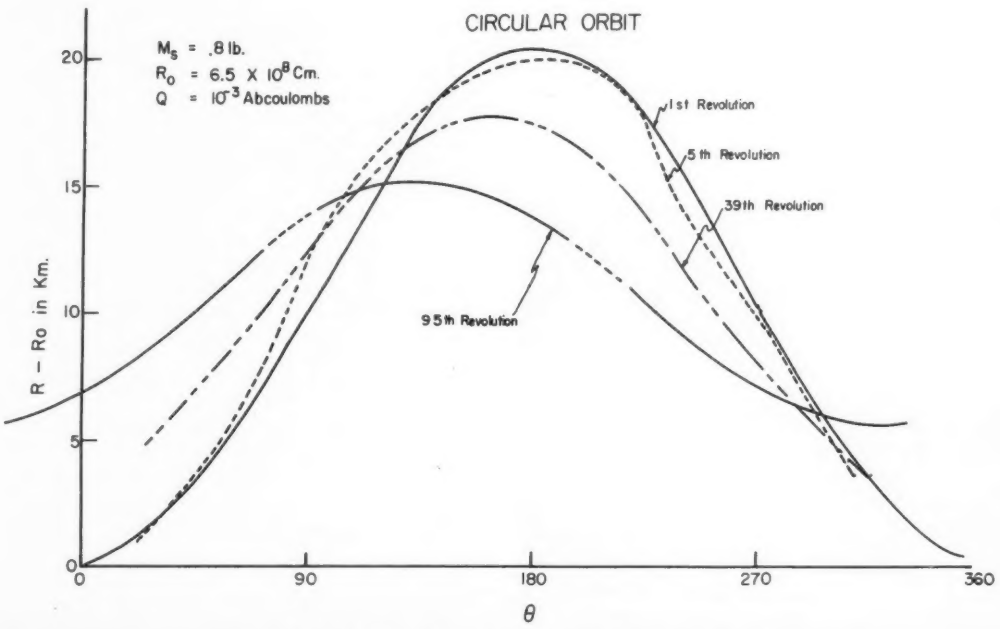

Fig. 1 Variations from initially circular orbit as function of angle

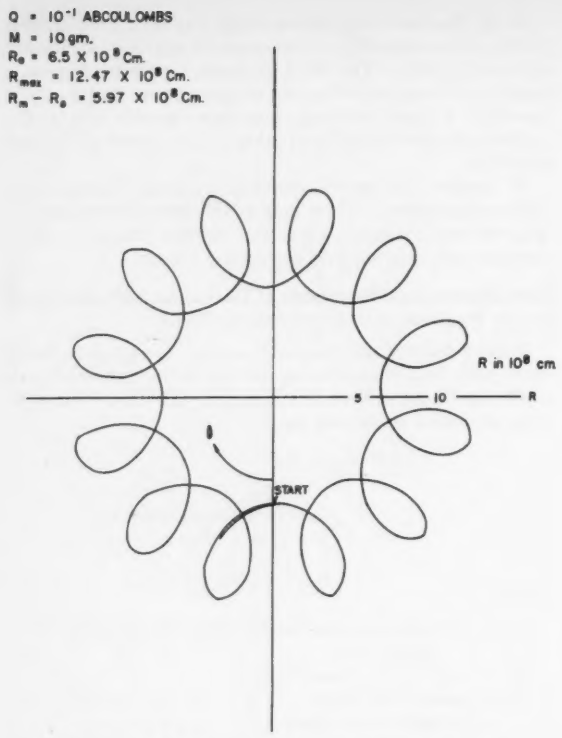

Fig. 2 Example of path followed by small mass with large charge

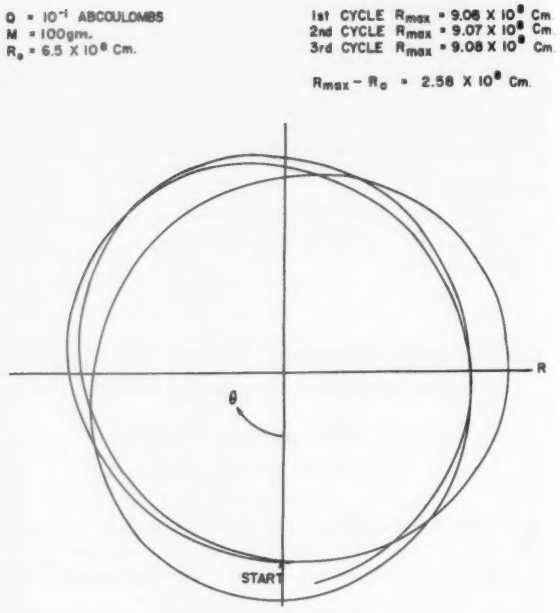

Fig. 3 Example of path followed by satellite with mass 10 times that in Fig. 2

point. It can be seen that the maximum variation in distance from the initial orbit is approximately 20 km for a body of this mass and charge. With continued revolution of the satellite the peak distance shifts away from its original position, and the peak reduces in amplitude. At the same time, the average distance from the Earth's center is increasing, and the indications are that a new circular orbit is approached asymptotically.

In Fig. 2, an example is shown in which the acceleration afforded by the magnetic field on the moving charged body is large compared to the gravitational acceleration. The looping is not surprising, since a charged body originally in straight

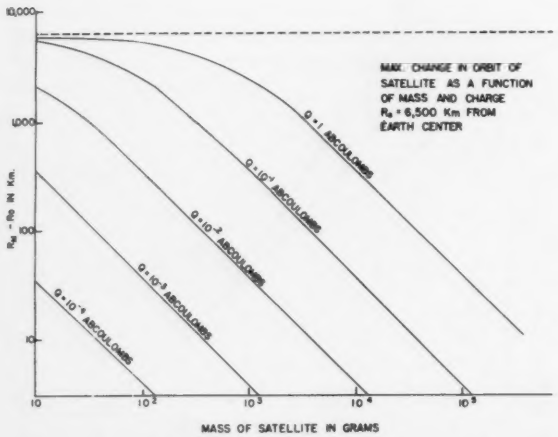

Fig. 4 Maximum variation in orbit for the first revolution as a function of mass and charge

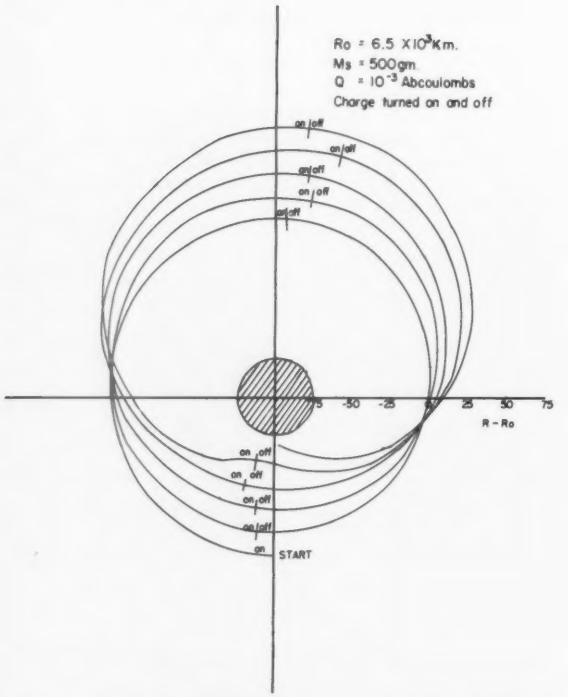

Fig. 5 Effect of charge-discharge procedure on the orbit

line motion takes up a circular path in a magnetic field (cyclotron, for example). It will be noticed that the maximum distance approaches twice the radius of the original orbit. Twice the distance is the upper limit, since at this distance all of the kinetic energy is converted to potential energy. It will be noted that the orbit does not necessarily repeat itself upon subsequent revolution.

In Fig. 3 the orbit is shown for a satellite of 10 times the mass of the satellite in Fig. 2. It does not loop, and the maximum variation in orbit from the original circular orbit is 2580 km.

In Fig. 4 the maximum variation in orbit (for the first revolution) is plotted as a function of mass of the satellite and the charge in abcoulombs. The dotted line at the top is the upper limit at twice the initial orbit distance.

In Fig. 5 the charge was repeatedly turned on at the minimum distance from the original circular orbit and turned off close to the maximum distance. This tends to "walk" the satellite away from its original orbit. (It should be noted that the scale is considerably distorted since zero is at 6500 km from Earth center—the shaded area is actually very large compared to the variation.)

Application

The practical use for this method of satellite control is probably very limited, since for a realizable charge (10^{-3} to 10^{-2} abcoulomb is probably optimistic for reasonable radii) only small masses can be moved significant distances. It is possible that it could be useful for fine control (several km) and possibly for transfer of small masses from one orbit to another (possibly small missiles).

The three-dimensional case will give further information, particularly as concerns rotating the plane of the orbit.

On the Use of Side-Jets as Control Devices

H. P. LIEPMAN[1]

University of Michigan, Ann Arbor, Mich.

Wind tunnel experiments with side-jets, issuing laterally near the base of slender bodies in a supersonic stream, have suggested the existence of a sizable and usable interaction. With this interaction force, the use of jet reaction controls may be as attractive for flight within the atmosphere as it obviously is for flight outside the atmosphere. This note indicates the altitude regime of interest and the order of magnitude of the interaction bonus for a lateral control jet located near the base of a body of revolution.

EVER since flight beyond the Earth's atmosphere has been under consideration, the value of jet reactions for control of attitude and flight path has been obvious. Furthermore, jet reactions may also provide useful control forces during atmospheric flight. In this case, the interaction of the gas jet or its component with the external flow field must be taken into account.

A modest and exploratory study[2] of such interaction effects has been under way at the Aeronautical Engineering Laboratories of the University of Michigan since 1950 (1 to 3).[3] A typical Schlieren picture from this program is shown in Fig. 1 showing an air jet from a sonic orifice issuing into a Mach 3.9 stream. Other test parameters are $(d/D) = 0.08$ and $(p_{0_j}/p) = 414$.

Recent results (2, 3) of tests with side-jets near the base of a missile indicate that considerable advantage may be gained by utilizing the interaction effect between a side-jet and supersonic main stream as an additional control force contribution. This note summarizes the magnitude of the interaction effect and the altitude regime over which it may be useful.

Interaction Effect

Experimental data and theoretical studies (2, 3) show that the interaction of a lateral jet near the base of a body of revolution with supersonic flow leads to a significant normal force increment (N_I) which is additive to the normal jet reaction (N_v) experienced in a vacuum where aerodynamic interactions do not exist. Side-jets located forward of the base, such as near the nose or the midpoint, do not produce significant additive interaction forces (1, 2).

A simple theoretical model (3) of the interaction effects of a two-dimensional side-jet indicates that the ratio of interaction force to vacuum-jet reaction (N_I/N_v) depends on the jet stagnation to ambient pressure ratio (p_{0_j}/p), and on the specific heat ratio of the jet gas. Furthermore, theory as well as experiments to date have shown no significant dependence of the interaction force on the type of boundary layer, i.e., laminar or turbulent; hence, Reynolds number effects seem negligible.

It has been found convenient (2) to express the experimental and theoretical results in terms of a normal force magnification factor $K = 1 + (N_I/N_v)$ which is simply the ratio of the vacuum-plus-interaction normal force to the normal force in a vacuum. Test results, using room temperature air exhausting through a sonic orifice at three free stream Mach numbers, are given in Fig. 2 in terms of the normal force magnification parameter $K/(M + 1)$ vs. the pressure ratio (p_{0_j}/p). The denominator $(M + 1)$ was chosen in an attempt to eliminate the Mach number effects from this discussion. It is seen in Fig. 2 that this Mach number correlation is only fair, but useful for the subsequent discussion, and probably acceptable for Mach numbers from 2 to 5.

From the curve of Fig. 2, some impressive values for the magnification of the vacuum normal force due to interaction effects can be predicted. Representative normal force magnification factors K are

(p_{0_j}/p)	50	100	500
M			
3	1.50	1.35	1.10
5	2.25	2.02	1.66

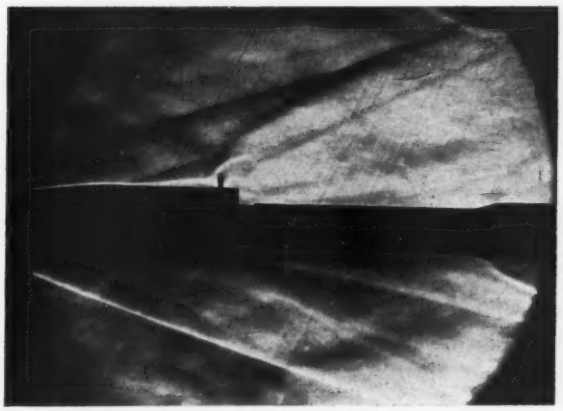

Fig. 1 Schlieren picture of sonic side-jet issuing from ogive-cylinder model into $M = 3.9$ stream. $(p_{0_j}/p) = 414$, $(d/D) = 0.08$, exposure time $\frac{1}{50}$ sec

Received March 17, 1959.

[1] Associate Professor of Aeronautical Engineering. Member ARS.

[2] Past and present support of this research by the following sponsors is gratefully acknowledged: NACA, Contract NAw-6466, and BuOrd, Contract NOrd 16595 under the technical direction of the Applied Physics Laboratory, The Johns Hopkins University.

[3] Numbers in parentheses indicate References at end of paper.

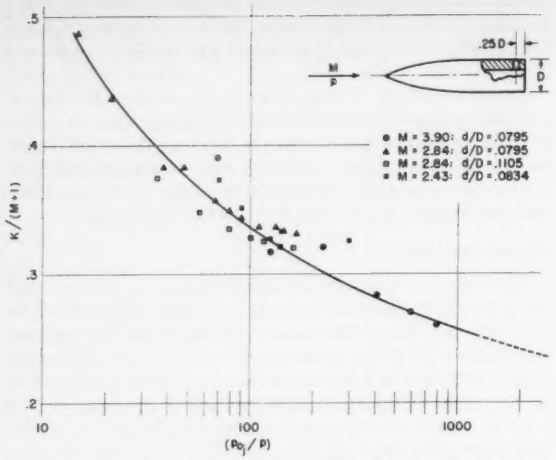

Fig. 2 Normal force magnification parameter vs. jet stagnation pressure ratio

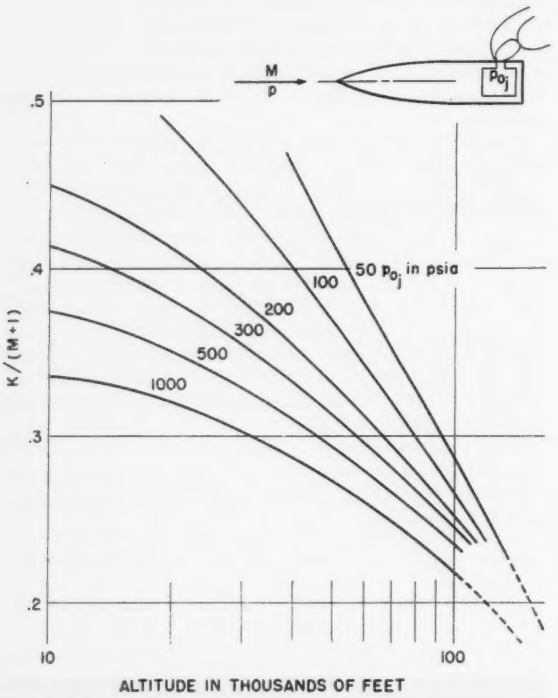

Fig. 3 Normal force magnification parameter vs. altitude and jet stagnation pressure

Side-Jet Control Effectiveness

It is clear that magnifications of jet reactions due to interaction effects can be used to advantage either to increase the effectiveness of reaction controls or to decrease the amount of control thrust needed. For convenience in predicting side-jet effectiveness, the normal force magnification parameter of Fig. 2 has been plotted against altitude for various jet stagnation pressures in Fig. 3. The ICAO atmosphere was used to relate altitude and ambient pressure. It is seen that the interaction magnification is most pronounced at low altitudes. However, at high Mach numbers, say 5, the magnification is still quite significant at altitudes as high as 150,000 ft.

Fig. 4 has been prepared to show the resultant control force of a nominal 100-lb control jet with a stagnation pressure of 500 psia as a function of altitude at flight Mach numbers of 3, 4 and 5. It is obvious that the interaction bonus can be traded for a sizable reduction in fuel, or size and weight of the control jet. In specific applications, the use of control jets within the atmosphere may be entirely competitive with aerodynamic control devices.

Conclusions

Some results of a continuing investigation into the interactions between a side-jet and the supersonic flow field of a slender vehicle show that there exists a helpful interaction force which considerably magnifies the vacuum reaction of a control jet near the base. The magnification decreases with decreasing free stream Mach number and with increasing ratio of jet stagnation to ambient static pressure.

For practical applications, the helpful interaction force is most significant at altitudes up to about 100,000 ft depending on Mach number and jet stagnation pressure. Since reaction controls are needed for flight beyond the atmosphere, their practical use within the atmosphere may, therefore, be quite competitive with conventional aerodynamic means of control.

Nomenclature

d = jet exit diameter
D = body diameter
K = normal force magnification factor = $1 + (N_I/N_v)$
M = free stream Mach number
p = ambient pressure
p_{0_j} = jet stagnation pressure
N_I = interaction normal force
N_v = normal force due to jet exhausting into vacuum

References

1 Morkovin, M. V., Pierce, C. A., Jr. and Draven, C. E., "Interaction of a Side-Jet with a Supersonic Main Stream," University of Michigan, Engng. Res. Bulletin no. 35, Sept. 1952.

2 Amick, J. L., Carvalho, G. F. and Liepman, H. P., "Interaction Experiments of Lateral Jets with Supersonic Streams," Minutes of the 39th regular meeting of the Bumblebee Aerodynamics Panel on Sept. 30 and Oct. 1, 1958, at the University of Texas, Austin. APL/JHU TG-14-36 (unclassified paper).

3 Vinson, P. W., Amick, J. L. and Liepman, H. P., "Interaction Effects Produced by Jet Exhausting Laterally Near Base of Ogive-Cylinder Model in Supersonic Main Stream," NASA Memo 12-5-58W, Feb. 1959.

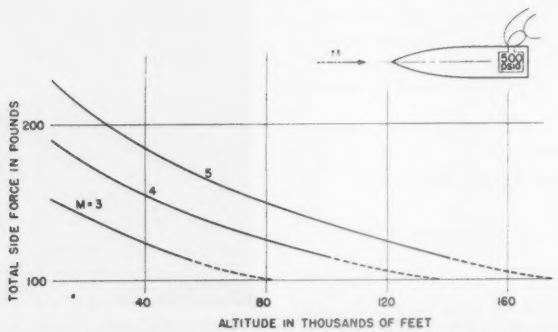

Fig. 4 Resultant side force of a nominal 100-lb side-jet as a function of altitude and flight Mach number

Technical Comments

Remark on Thermodynamics of Al_2O_3

JOHN S. GORDON[1]

Thiokol Chemical Corp., Denville, N. J.

THE IDEALIZED treatment of inert liquid Al_2O_3 recommended at temperatures below 3000 K in a recent contribution (1)[2] will, in most cases of current interest, lead to approximate and optimistic specific impulse values.

The work of Brewer and Searcy (2) has indicated that the significant gaseous species occurring in the volatilization of Al_2O_3 are Al, O_2, O, AlO, Al_2O and possibly Al_2O_2, but not Al_2O_3. Al_2 and Al_2O_2 are usually omitted from propellant performance calculations since no molecular constant data have been deduced for them. It is important, however, to allow for the interaction of aluminum-oxide vapors and halogens, since the Al—Cl bond energy is about 105 kcal, as compared to 119 kcal for Al = 0 (3). Nor must AlN be ruled out as a possible combustion product, since its heat of formation in the crystalline state is −57.7 kcal/mole (4). Theoretical performance calculations have shown large amounts of AlCl, $AlCl_2$ and $AlCl_3$ gases at temperatures of 2500 to 3500 K, usually exceeding the amounts of AlO, Al_2O, Al and AlH present. Unfortunately, nothing whatever is presently known about OAlCl gas which may be the most important species of all.

We have recently recomputed the thermodynamic functions of AlO and AlCl gases, as well as many other molecules, from Herzberg's data (5). These data are necessary in propellant performance calculations, and are shown in Tables 1 and 2. Data have also been compiled for $AlCl_2$ and $AlCl_3$.

More recent values for H°_{f298} and S°_{298} of Al_2O_3 are available (6, 7).

Received March 31, 1959.

[1] Unit Supervisor, Propellants Liaison and Theoretical Chemistry, Reaction Motors Div. Member ARS.

[2] Numbers in parentheses indicate References at end of paper.

Table 1 Thermodynamic functions of AlO, cal/mole, K

T, K	$-(F - E_0)/T$	$H - E_0/T$	S°	C_p°	$H^T_{298.16}$, kcal/mole
400	47.213	7.182	54.395	7.767	0.77186
800	52.365	7.715	60.081	8.568	4.0714
1200	55.563	8.050	63.613	8.829	7.5589
1600	57.910	8.261	66.172	8.951	11.117
2000	59.770	8.407	68.178	9.028	14.714
2400	61.313	8.516	69.829	9.086	18.337
2800	62.632	8.601	71.234	9.138	21.982
3200	63.786	8.671	72.458	9.191	25.648
3600	64.811	8.732	73.544	9.250	29.336
4000	65.734	8.787	74.522	9.317	33.049
4400	66.574	8.839	75.413	9.394	36.792
4800	67.345	8.889	76.234	9.479	40.566
5200	68.059	8.938	76.997	9.571	44.376
5600	68.723	8.986	77.710	9.668	48.224
6000	69.344	9.035	78.380	9.767	52.112

Table 2 Thermodynamic functions of AlCl, cal/mole, K

T, K	$-(F - E_0)/T$	$H - E_0/T$	S°	C_p°	$H^T_{298.16}$, kcal/mole
400	49 221	7 718	56.940	8.560	0.85917
800	54.764	8.252	63.016	8.917	4.3734
1200	58.161	8.494	66.655	9.029	7.9654
1600	60.625	8.637	69.263	9.100	11.592
2000	62.564	8.736	71.300	9.159	15.244
2400	64.164	8.811	72.975	9.212	18.918
2800	65.527	8.872	74.399	9.263	22.614
3200	66.715	8.924	75.639	9.313	26.329
3600	67.769	8.970	76.739	9.362	30.064
4000	68.716	9.011	77.728	9.411	33.819
4400	69.577	9.050	78.627	9.460	37.593
4800	70.366	9.086	79.453	9.512	41.388
5200	71.095	9.121	80.216	9.565	45.203
5600	71.772	9.155	80.927	9.622	49.041
6000	72.405	9.188	81.593	59.684	52.902

References

1 Farber, M., "Thermodynamics of Al_2O_3," JET PROPULSION, vol. 28, 1958, p. 760.

2 Brewer, L. and Searcy, A., "The Gaseous Species of the Al-Al_2O_3 System," *J. Amer. Chem. Soc.*, vol. 73, 1951, p. 5308.

3 Brewer, L., "Dissociation Energies of Gaseous Oxides," Univ. Calif. Radiation Lab. Communication 8356, 1958.

4 Rossini, F. et al., "Selected Values of Chemical Thermodynamic Properties," Nat. Bur. Standards Circular 500, 1952, p. 323.

5 Herzberg, G., "Molecular Spectra and Molecular Structure—I. Spectra of Diatomic Molecules," Van Nostrand Co., New York, 1950, p. 504.

6 Mah, A., "Heats of Formation of Alumina, Molybdenum Trioxide and Molybdenum Dioxide," *J. Phys. Chem.*, vol. 61, 1957, p. 1572.

7 Furukawa, G. et al., "Thermal Properties of Aluminum Oxide from 0° to 1200° K.," *J. Res. Nat. Bur. Standards*, vol. 57, 1956, p. 67.

Comment on "Performance Calculations for Hybrid Nuclear-Chemical Rocket Propulsion Systems"

JOHN S. GORDON[1]

Thiokol Chemical Corp., Denville, N. J.

THE PERFORMANCE estimates by Green and Carter (1)[2] for metal-H_2O systems are subject to revision when more reliable data on light-metal combustion products become available. Thermodynamic functions for Li_2O, LiOH, LiO and other lithium species were generated by the author during January 1957 and have been made available to Aerojet-General Corp. personnel on two separate occasions; there is no evidence in the paper by Green and Carter that these data were considered. The thermodynamic functions for Li_2O (g) are included here (Table 1), since this appears to be the only Li species considered in their paper.

The sublimation of Li_2O has been studied by Brewer and Margrave(2) and Blue, Margrave, Berkowitz and Chupka (3). It has been demonstrated that Li_2O vaporizes mainly to the elements, with minor amounts of Li_2O and LiO, and that

$$Li_2O\ (s) \rightarrow Li_2O\ (g) + 104 \pm 5\ \text{kcal/mole}$$

Received March 31, 1959.

[1] Unit Supervisor, Propellants Liaison and Theoretical Chemistry, Reaction Motors Div. Member ARS.

[2] Numbers in parentheses indicate References at end of paper.

Table 1 Thermodynamic functions of Li_2O (gas)

T, K	$H^T_{298.16}$ Kcal/mole	$-(F - E_o)/T$	$(H - E_o)/T$	S°	C_p°, cal/mole, K
298.16	...	45.81	8.123	53.93	8.764
400	0.9363	48.23	8.396	56.63	9.633
800	5.345	54.46	9.709	64.17	12.05
1200	10.37	58.59	10.66	69.26	12.96
1600	15.65	61.75	11.29	73.05	13.35
2000	21.03	64.32	11.72	76.05	13.54
2400	26.47	66.49	12.04	78.53	13.65
2800	31.95	68.37	12.27	80.64	13.71
3200	37.44	70.02	12.45	82.48	13.76
3600	42.96	71.49	12.60	84.10	13.79
4000	48.48	72.83	12.72	85.55	13.81
4400	54.01	74.05	12.82	86.87	13.83
4800	59.54	75.17	12.91	88.08	13.84
5200	65.08	76.20	12.98	89.18	13.85
5600	70.63	77.17	13.04	90.21	13.86
6000	76.17	78.07	13.09	91.17	13.86

and that

$$LiO\ (g) \rightarrow Li\ (g) + 0\ (g) + 83\ kcal/mole$$

These data partially invalidate Green and Carter's results

References

1 Green, L., Jr. and Carter, J. M., "Performance Calculations for Hybrid Nuclear-Chemical Rocket Propulsion Systems," ARS JOURNAL, vol. 29, no. 3, 1959, pp. 180–186.

2 Brewer, L. and Margrave, J., "The Vapor Pressures of Lithium and Sodium Oxides," *J. Phys. Chem.*, vol. 59, 1955, p. 421.

3 Blue, G., Margrave, J., Berkowitz, J. and Chupka, W., *J. Amer. Chem. Soc.*, in publication.

Comments on "Exhaust Nozzle Contour for Maximum Thrust"

R. W. FANSELAU[1]

North American Aviation, Inc., Downey, Calif.

IN A RECENT article[2] Rao maximizes exhaust nozzle exit momentum by formulating an extremal problem involving two constraints: Nozzle length and propellant mass flow. The extremal problem is formulated with a noncharacteristic line as the control surface. An investigation of the extremal problem together with the assumptions adhered to in its formulation indicate that the last left-running characteristic line is assumed for the control surface. Subsequent verification of this assumption is treated therein as an independent result which emerges from the first variation and exclusively characterizes the solution sought. Even though the control surface of the maximum solution is recognized by Rao as the last left-running characteristic line, there appears to be an error in the suggested use of the Euler-Lagrange constants to obtain solutions for any nozzle length. It is, therefore, predicted that for a given ambient pressure, the nozzle contours obtained therein yield integrated exit momentum values other than the maximum. Comments concerning the foregoing extremal problem and its solution are given in the following paragraphs.

The extremal problem is formulated for a given pressure ratio. Thus, the formulation can represent an investigation for either a singly or a doubly infinite family of nozzle contours. The exit momentum J, the propellant mass flow M and the nozzle length L are originally expressed by the following line integrals along some control surface

$$J = \int_C^E g_1(P, \rho, W, \theta, \phi, y)dy \qquad [1a]$$

$$M = \int_C^E g_2(\rho, W, \theta, \phi, y)dy = C_2 \qquad [2a]$$

$$L = \int_C^E g_3(\phi)dy = C_3 \qquad [3a]$$

Equations [1a, 2a and 3a] represent the formulation for a doubly infinite family of nozzles; both isentropic and nonisentropic nozzles are investigated. The control surfaces admissible in the extremal problem are left-running characteristic lines of two types

$$\frac{d\theta}{dy} - \frac{dM(M^2 - 1)^{1/2}}{dyM\{1 + [(\gamma - 1)/2]M^2\}} + \frac{\sin\theta \sin\alpha}{y \sin\phi} = 0 \qquad [4]$$

and

$$\frac{d\theta}{dy} - \frac{dM(M^2 - 1)^{1/2}}{dyM\{1 + [(\gamma - 1)/2]M^2\}} + \frac{\sin\theta \sin\alpha}{y \sin\phi} - \frac{ds \sin^2\alpha \cos\alpha}{dn\ \gamma R \sin\phi} = 0 \qquad [5]$$

Thus far, the formulation is quite general. However, a considerable loss of generality results by introducing the isentropic relations

$$P = P_0\left[1 + \left(\frac{\gamma - 1}{2}\right)M^2\right]^{-\gamma/(\gamma - 1)} \quad \text{(isentropic perfect)}$$

$$\rho = \rho_0\left[1 + \left(\frac{\gamma - 1}{2}\right)M^2\right]^{-1/(\gamma - 1)} \quad \text{(isentropic perfect)}$$

$$T = T_0\left[1 + \left(\frac{\gamma - 1}{2}\right)M^2\right]^{-1} \quad \text{(adiabatic perfect)}$$

Through the preceding relations, only the control surfaces satisfying Equation [4] are admissible. For this reason, Equation [4] need not be entered as an additional constraint. Rao introduces the preceding isentropic relations into Equations [1a, 2a and 3a] to obtain for J, M and L, respectively

$$J = \int_C^E f_1(M, \theta, \phi, y)dy \qquad [1b]$$

$$M = \int_C^E f_2(M, \theta, \phi, y)dy = C_2 \qquad [2b]$$

$$L = \int_C^E f_3(\phi)dy = C_3 \qquad [3b]$$

Thus, the doubly infinite family of nozzles is reduced to a

Received April 20, 1959.

[1] Research Engineer, Missile Division.

[2] Rao, G. V. R., "Exhaust Nozzle Contour for Maximum Thrust," JET PROPULSION, vol. 28, no. 6, June 1958, pp. 377–382.

singly infinite family of isentropic types. Fortunately, this loss of generality does not invalidate the solutions of the extremal problem, as the condition for a maximum is satisfied by nozzles from this isentropic family. The Lagrange constants are

$$-\lambda_2 = W \frac{\cos(2\theta - \phi)}{\cos(\phi - \theta)} \qquad [6]$$

and

$$-\lambda_3 = y\rho W^2 \sin^2\theta \tan(\phi - \theta) \qquad [7]$$

Also, from the first variation

$$\frac{\partial f_1}{\partial M}\frac{\partial f_2}{\partial \theta} = \frac{\partial f_1}{\partial \theta}\frac{\partial f_2}{\partial M} \qquad [8]$$

Letting

$$G = \frac{\partial f_1}{\partial M}\frac{\partial f_2}{\partial \theta} - \frac{\partial f_1}{\partial \theta}\frac{\partial f_2}{\partial M} = 0$$

$$F_2 = \lambda_2$$

$$F_3 = \lambda_3$$

the sufficiency condition is satisfied everywhere along the isentropic left-running characteristic line by the Jacobian

$$\begin{vmatrix} \frac{\partial G}{\partial M} & \frac{\partial G}{\partial \theta} & \frac{\partial G}{\partial \phi} \\ \frac{\partial F_2}{\partial M} & \frac{\partial F_2}{\partial \theta} & \frac{\partial F_2}{\partial \phi} \\ \frac{\partial F_3}{\partial M} & \frac{\partial F_3}{\partial \theta} & \frac{\partial F_3}{\partial \phi} \end{vmatrix} \neq 0 \qquad [9]$$

where

$$G = G(y, M, \theta, \phi)$$
$$F_2 = F_2(y, M, \theta, \phi)$$
$$F_3 = F_3(y, M, \theta, \phi)$$

Solutions of the foregoing extremal problem are obtained in the following manner. For a particular ambient pressure P_a, one chooses the Mach number M_E at the nozzle exit. The flow angle θ_E at the nozzle exit is then obtained from

$$\sin 2\theta_E = \frac{2(P_E - P_a)}{\rho_E W_E^2} \cot \alpha_E \qquad [10]$$

The flow parameters M and θ along the last left-running characteristic line are obtained by solving Equation [4] together with

$$\theta + \alpha = \phi \qquad [11]$$

for values of M and θ, using Y/YE as a parameter. Rao obtains the flow parameters M and θ along the same control surface directly from Equations [6 and 7]. Solutions of the extremal problem obtained in this way will satisfy the Euler equation, but do not necessarily satisfy the sufficiency condition given by Equation [9]. To insure the sufficiency condition, the solutions of the foregoing extremal problem must also satisfy Equation [4], which can be derived by differentiating the Lagrange constants with respect to the independent variable. The location of the nozzle kernel design point and the construction of the nozzle contour follow as discussed therein.

Transmitting performance data from missiles and test vehicles, direct to ground stations, Lockheed-developed TV camera-transmitter and PAM-FM telemetry systems are acknowledged to be the world's smallest, world's best.

Revolutionary "fuel cell," under development at Lockheed, converts chemical energy directly into electrical power—for auxiliary power requirements of miniaturized spacecraft instrumentation and space communications systems.

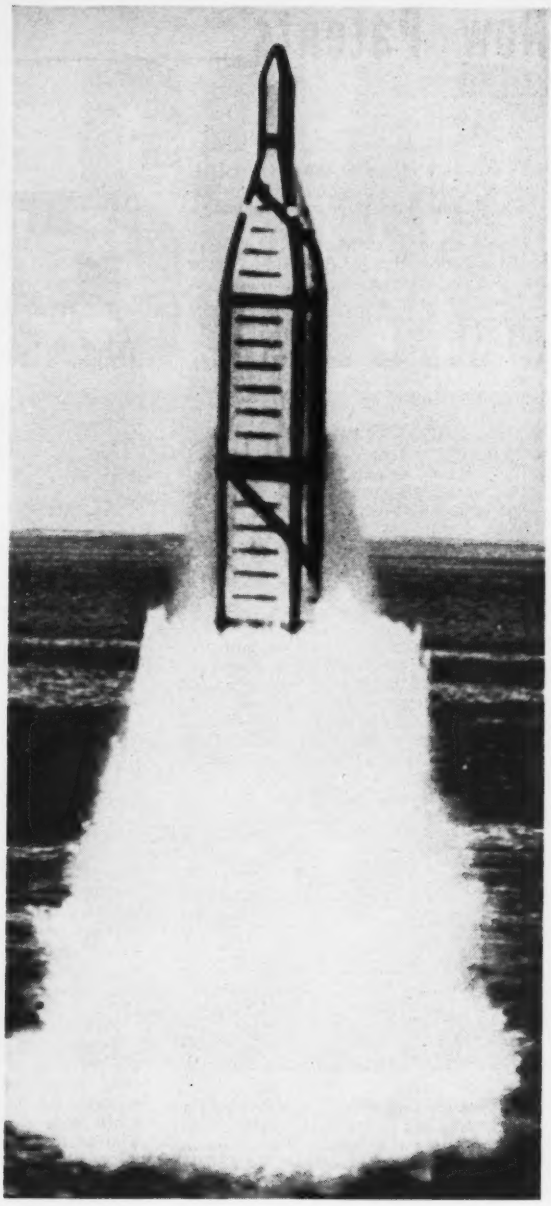

Erupting from beneath the sea, a full-scale POLARIS test vehicle demonstrates how operational missile will be launched from submerged U.S. Navy subs. Ultimate range of the POLARIS will be 1500 nautical miles.

LOCKHEED

JET TRANSPORTS • JET FIGHTERS • JET TRAINERS • COMMERCIAL & MILITARY PROP-JET TRANSPORTS • ROCKETRY
BALLISTIC MISSILE RESEARCH & DEVELOPMENT • WEAPON SYSTEM MANAGEMENT • ANTI-SUBMARINE PATROL AIRCRAFT
NUCLEAR-POWERED FLIGHT • ADVANCED ELECTRONICS • AIRBORNE EARLY-WARNING AIRCRAFT • AIRPORT MANAGEMENT
NUCLEAR REACTOR DESIGN & DEVELOPMENT • GROUND SUPPORT EQUIPMENT • WORLD-WIDE AIRCRAFT MAINTENANCE

New Patents

George F. McLaughlin, *Contributor*

Two-axis rate gyros (2,868,023). C. R. Bonnell, Columbia Heights, Minn., assignor to Minneapolis-Honeywell Regulator Co.

Liquid disposed within an enclosure so that the unfloated mass attached to either side of a flexible diaphragm is equal, permitting displacement of a hollow sealed housing about two axes at right angles to each other.

Anti-backlash gear train (2,868,028). J. C. Ziegler, Maywood, N. J., assignor to Bendix Aviation Corp.

Gear arranged to drives in either direction through a clutch and two associated gear units. A friction member associated with one unit applies a relatively low torque to the other unit, and a torque less than the torque to the first unit, through the driven gear.

Rocket motor (2,868,127). H. M. Fox, Bartlesville, Okla., assignor to Phillips Petroleum Co.

Piston disposed within a fuel tank to form a movable wall. The piston head within an oxidizer tank forms a movable wall of the tank and combustion chamber. A pressure sensitive means seals a hypergolic fuel within the hollow piston shaft. A resilient member ruptures the sealing means, moving the piston into the oxidizer tank and into the fuel tank when released by a starting means.

Propulsion of vehicles (2,869,479). P. Hutchinson, Ruislip, Middlesex, England.

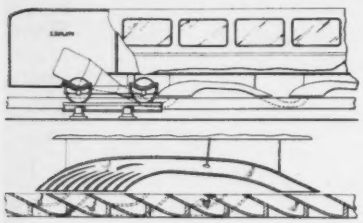

System for propelling a vehicle along a track, using gas in jet form directed into ducts, fixed to the track. Vehicle ducts register with successive track duct inlets and receive jet flow from track duct outlets as the vehicle travels along the track.

Convertiplane with tiltable cylindrical wing (2,868,476). E. W. Schlieben, Concord, Mass.

Means for propelling a wing comprising a circular body of toric section. A fuselage is mounted in the wing in hinged relationship.

Rocket control (2,868,478). T. McCloughy, Morris Plains, N. J.

Steering device comprising a tubular housing in which a lining of refractory material is rotatably mounted. The housing extends in a space-surrounding relation to the jet stream. Pivoting the housing causes part of the housing to engage the perimeter of the jet stream.

EDITOR'S NOTE: Patents listed above were selected from the Official Gazette of the U.S. Patent Office. Printed copies of patents may be obtained from the Commissioner of Patents, Washington 25, D. C., at a cost of 25 cents each; design patents, 10 cents.

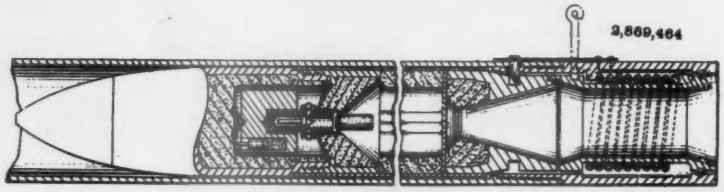

Friction type fuse (2,869,464). J. G. Villepigue and E. Schmued, Los Angeles, Calif., assignors to Northrop Aircraft, Inc.

Rocket with centrifically releasable restraining means holding a firing pin in cocked position to fire a percussion element when the rocket is spun prior to launching. A longitudinally movable cylinder is mounted to rotate on the spin axis in accordance with forces produced when the rocket is decelerated after launching. A friction member and friction surface generate heat to fire the explosive charge when the member is rotated around the surface.

Control of air flow over an aircraft wing (2,868,479). M. Kadosch, J. LeFoll, F. M. L. Maunoury and J. Bertin, Nevilly-sur-Seine, France, assignors to SNECMA.

Nozzles extending spanwise of a high camber wing and positioned at a distance above the upper surface, ahead of the trailing edge. Fluid pressure applied to the nozzles forms jets crosswise of the air flow, preventing separation of the flow from the wing surface.

High lift supercirculation system using supersonic blowing (2,868,480). J. S. Attinello, Falls Church, Va.

Method of increasing circulation while maintaining constant attack angle when the airfoil behaves in accordance with the Kutta-Joukowsky law. A stream of expanding and accelerating fluid is injected into the flow field above the airfoil at a velocity of at least Mach 1 to attract the flow in proximity to the injected stream.

Ceramic bodies (2,868,658). W. W. Coffean, Westfield, N. J., assignor to Metal & Thermit Corp.

Body having low electrical conductance consisting of 0.03 per cent (by weight) to 0.3 per cent of at least one metal oxide (iron, nickel, zinc, cobalt, manganese or copper), 0.5 per cent to 50 per cent bismuth oxide, and the remainder tin oxide. The analysis of the metal content is expressed in corresponding metal oxides.

Impact accelerometer (2,868,611). H. Carleton, Silver Spring, Md.

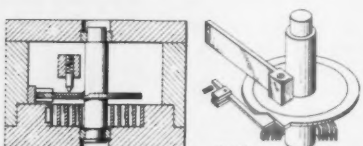

Measuring device containing a magnet which locks a shaft and disk in place against the forces of a wound spring. A predetermined amount of acceleration causes the spring to rotate the disk while a stylus moves to mark a record in a soft metal indicating washer.

Control system for dirigible craft (2,869,063). J. J. Hess Jr., Garden City, N. Y., assignor to Sperry Rand Corp.

Servomotor system for maintaining a craft at a predetermined reference attitude about an axis. A reversible servomotor modifies the normal reference provided by the system, providing a signal in accordance with the output of the servomotor. A bandpass filter receiver detects malfunction of the system, and means are provided for comparing the signals and controlling the craft.

Hypergolic fuel for developing thrust (2,869,320). J. M. Burton, Waco, Texas, assignor to Phillips Petroleum Co.

Bipropellant components injected separately and simultaneously in contact with each other in the combustion chamber of a reaction motor to produce spontaneous combustion. Component consists of between 70 and 80 per cent (by volume) of pyrrole, and between 30 and 20 per cent of pyridine.

Rocket fuse (2,869,465). J. G. Villepigue, Inglewood, Calif., assignor to Northrop Aircraft, Inc.

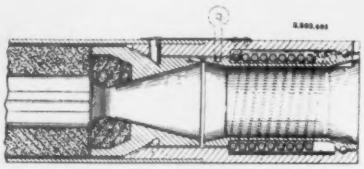

Impact switch connected with an energy source, an acceleration operable switch and thermally actuated means operative over a predetermined period after launching a rocket. The impact switch is positioned to close and detonate the charge after an additional time interval has elapsed.

Apparatus for nondestructive tests of initiators (2,869,364). I. Kabik and J. N. Ayres, Washington, D. C., assignors to the U. S. Navy.

Potentiometer connected across a source of electrical energy, and a condenser in the circuit chargeable to a level below that required for firing. Means spatially displaced relative to the connected initiator for indicating the magnitude of the energy radiated by the conductive path.

Vortex frequency airspeed indicator (2,869,366). A. Nitikman, Inglewood, Calif., assignor to Northrop Aircraft, Inc.

Airfoil shaped member mounted near its leading edge to swing into the direction of the airstream. The streamlined leading edge separates the airstream and generates vortices. Sound produced by the vortices is transmitted to a microphone on the member.

DYNA-SOAR

Dyna-Soar (for dynamic soaring) is a joint project between the Air Force and the NASA, and is an attempt to solve the technical problems of manned flight in the sub-orbital regions. Advance knowledge on the project indicates how a boost-glide vehicle can operate from the outer fringes of the atmosphere where it can maneuver and be recovered undamaged. Studies show that by varying the original rocket boost, and thus the velocity, and with the control available to the pilot, the Dyna-Soar aircraft can circumnavigate the earth, followed by a normal and controlled landing. Boeing Airplane Company, one of the competing companies for the development contract for the complete boost-glide system, has delegated to RCA the responsibility for the development of important electronic components of Dyna-Soar.

RCA Tmk(s) ®

RADIO CORPORATION of AMERICA

DEFENSE ELECTRONIC PRODUCTS

CAMDEN, N. J.

Force-ratio-responsive system (2,869,367). D. W. Moore, Pacific Palisades, Calif., assignor to Servomechanisms, Inc.

Synchro with a pair of electrically spaced exciting windings and a rotor winding. First and second signals developed vary with the forces, and are applied to the windings. A servo responsive to the signals produced adjusts the rotor to reduce the signal to zero, the position of the rotor winding being representative of the ratio between two forces as indicated on a Mach number scale.

Optical pyrometer (2,869,369). S. N. Howell, Huntington, N. Y., assignor to Servo Corp. of America.

Electrically responsive radiation pyrometer containing a heat sensitive element and collecting optics. The reading of an indicator is optically displayed when looking into the sight.

Balancing machine (2,869,372). K. E. Sihronen, Detroit, Mich., assignor to General Motors Corp.

Means for measuring unbalance in a rotating workpiece. A pivoted reflector, directing a band of parallel light rays on a remote screen, moves in response to vibrations in the workpiece to produce a light pattern having a size proportional to the magnitude of unbalance.

Means for detecting and suppressing explosions (2,869,647). A. Mathisen, London, England, assignor of one-half to Graviner Mfg. Co. Ltd. and The Wilkinson Sword Co. Ltd.

Photo-multiplier adapted to produce an electrical signal when exposed to the illumination from an incipient explosion. Amplified current from the signal shatters a container of a liquid suppressant, projecting the liquid at an initial velocity of 150 fps.

Vehicles (2,869,803). J. D. McGee, Ealing, London, England, assignor to Electrical & Musical Industries, Ltd.

Remotely controlled space vehicle containing a television camera for transmitting signals indicating the position of a target relative to the course of the craft. Gyro controls maintain the craft on the course established from a remote control station.

Apparatus for measuring accelerations and inclinations (2,869,851). H. B. Sedgfield, M. L. Jofeh and R. Albrecht, London, England, assignors to The Sperry Gyroscope Co. Ltd.

Inertia element mounted in a casing for relative movement along the axis of an axial member. Signal generating means produce a signal dependent upon the displacement of the element from a null position along the axis exerting an electromagnetic force restoring the member to its null position.

Book Reviews

Ali Bulent Cambel, Northwestern University, *Associate Editor*

Celestial Mechanics, edited by E. Finlay-Freundlich, Pergamon Press, New York, 1959, 150 pp. $7.50.

Reviewed by S. F. SINGER
University of Maryland

It is interesting to see the renewed appreciation of celestial mechanics which has been brought about by the rapid development of astronautics. That in itself would be sufficient reason to write new books on the subject. The present volume, however, was written for quite a different reason. The author, a distinguished astrophysicist and astronomer, wants to stress the importance of celestial mechanics to astrophysical problems, such as the motion of close binary systems, and includes also revisions brought about by the theory of relativity.

The result is a book which is very concise but, unfortunately, addressed primarily to the astronomer, or at least to someone who has had a considerable background in classical mechanics. The reader who is looking for guidance either for planning of space orbits or for reduction of orbit observations will be disappointed. On the other hand, if he is looking for an elegant advanced presentation of the principles of celestial mechanics, the book can be heartily recommended.

The Atom and the Energy Revolution, by Norman Lansdell, Philosophical Library, New York, 1958, 200 pp. $6.00.

Reviewed by DONALD H. LOUGHRIDGE
General Motors Corporation

This work is addressed to the businessman who faces the necessity of accommodating himself and his industry to the new factors introduced into commerce by the energy of the atom, to the citizen who must assist in making intelligent democratic decisions with respect to the social and political changes being wrought by the new source of energy, and to the general, nontechnical reader who desires to understand the implications in these revolutionary scientific developments now worldwide in their effects.

The author has succeeded remarkably well in condensing within the short space of 200 pages a coverage—in many fields quite superficial—of the world energy resources of all types. The ever-increasing energy demands of industrialized countries are discussed in regard to future requirements; the various potential sources beyond those of the heat forms of atomic energy, the various known methods of releasing atomic energy, are all discussed in a clear, completely nontechnical way.

After treating many means of potential utilization of this form of energy, such as electric power generation, space heating, marine power, locomotives, airplane, road transport and medical applications, the author discusses the other side of the coin, namely, the risks involved in airborne contamination, isotope selective concentrations, waste disposal problems and third party insurance liabilities inherent in such applications, and also the legal and sociological steps which must be taken if the maximum good is to be expected from such applications.

Finally, a short but illuminating discussion of the world impacts of the new military, industrial and world trade effects being brought about by the atom and the alterations in state and private industry's relationship, provide impact which should prove most thought-provoking to the serious reader.

If a negative criticism were to be mentioned, it would be the discouraging effect on the average reader of so many tables and statistical data in the first few chapters. These should have been relegated to an appendix, with references thereto for smoother reading.

An Introduction to Rocket Missile Propulsion, by the Rocketdyne Training Department, published by Rocketdyne, Canoga Park, Calif., 1958, 130 pp.

Reviewed by WILLIAM T. SNYDER
North Carolina State College

This book is written for those who do not have a background in rocket propulsion theory or in rocket engine operation. The book does a very fine job of presenting the fundamental principles of rocket propulsion with sufficient clarity to be useful to a nontechnically trained reader. The scope of the book is illustrated by the chapter headings as follows: 1 and 2 Rocket Fundamentals, 3 Rocket Missile Flight, 4 Liquid Propellants, 5 Liquid Propellant Feed Systems, 6 Thrust Chamber Assembly, 7 Rocket Engine Controls, 8 Solid Propellant Rockets.

Each chapter includes a series of review questions at the end, and numerous example problems are included in the book. The terminology and vocabulary of missile technology are introduced and defined in simple terms. Well-drawn illustrations add to the overall clarity of the presentation. The appendix contains a complete list of symbols and units used, a summary of the more important formulas used in the text, a condensed table of properties of the atmosphere, a rather detailed flow diagram of the V-2 engine including an engine operation sequence, and a flow diagram of the NAA 50–4.5 rocket-sled engine. The book does not contain an extensive bibliography.

The general level of the book, from a technical point of view, is quite low, but this statement is intended as one of evaluation rather than criticism. No mathematics more sophisticated than elementary algebra is employed, and it is the broad, qualitative description of missile propulsion which gives the book significance. With one evening of rather rapid

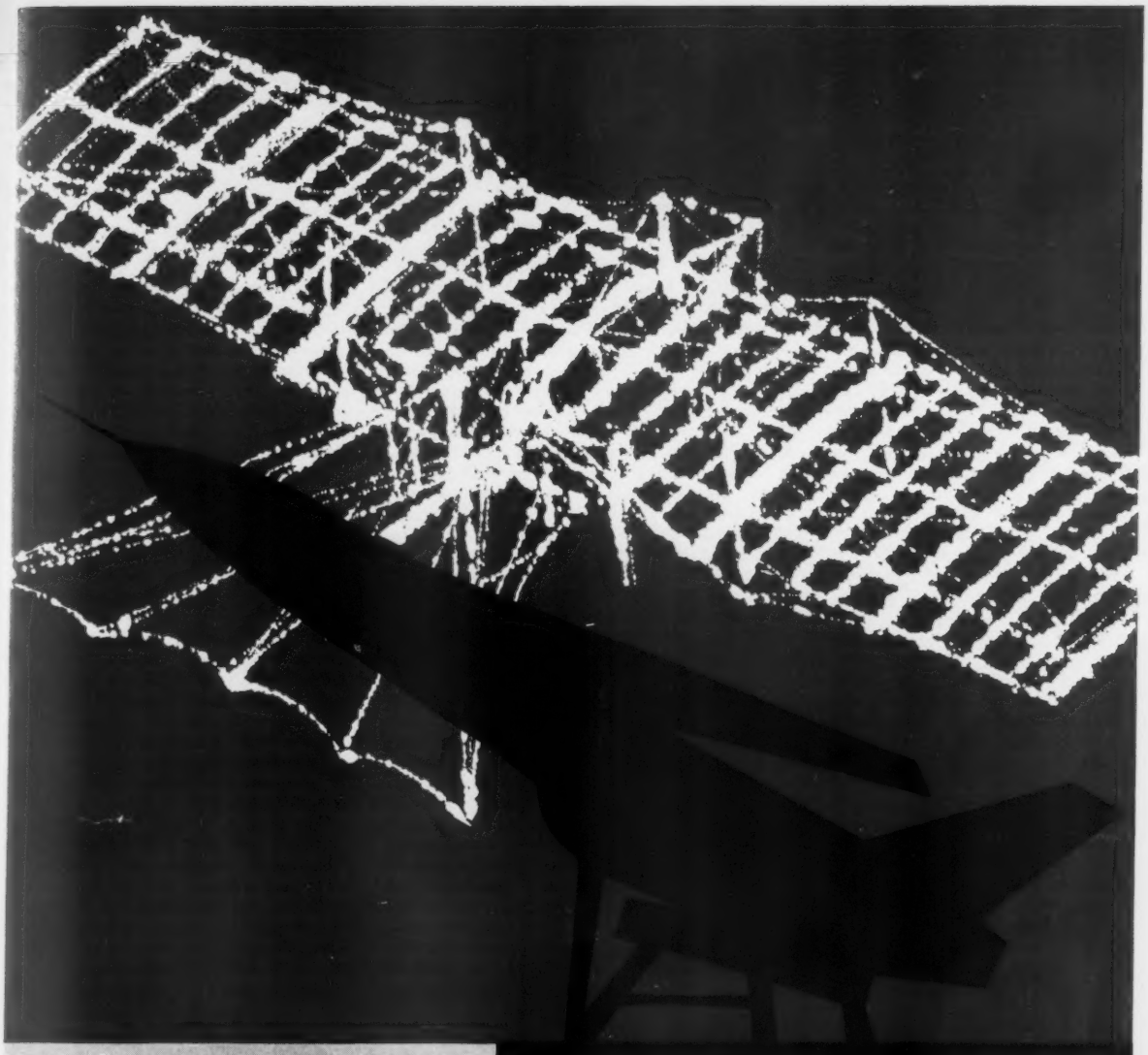

REVOLUTION IN DESIGN

As revolutionary in design and engineering as the technological transition from flying machine to space vehicle... Achieved a quarter of a century ago, the only regulators which could be used for the first missile experiments in the Navy Experimental Station at Annapolis ... still today the standard for the critical control of high pressure fluids... Now on the threshold of space, Grove is uniquely prepared—through advance research and development—to meet the challenge of even higher pressures ahead.

GROVE POWREACTOR DOME REGULATOR MODEL GH-408–50-6000 PSI INLET...5-3000 PSI REDUCED PRESSURE

GROVE VALVE and REGULATOR COMPANY

6529 Hollis St., Oakland 8, California • 2559 W. Olympic Blvd., Los Angeles 6, California

Offices in other principal cities

Subsidiary of Walworth

reading, a reader can cover the book and acquire a useful degree of understanding of rocket propulsion theory and the hardware components of rocket engines.

The Gas Turbine Power Plant, The Turboprop, Turbojet, Ramjet, and Rocket Engines, vol. II of **Aircraft and Missile Propulsion,** by M. J. Zucrow, John Wiley and Sons, Inc., New York, 1958, 636 + xiv pp. $13.00.

Reviewed by ALLEN E. FUHS
Northwestern University

The title of volume II is a succinct book review in itself and is indicative of the thoroughness with which the topics have been covered. Gas turbines which are designed primarily to provide shaft horsepower are discussed in the first tenth of the book. This includes gas turbines for locomotives, electrical power generation and marine propulsion. It seems rather strange to find such a discussion in a book on aircraft and missile propulsion; however, an understanding of these gas turbines is helpful for a mastery of the turboprop. All the cycles which can be obtained by the permutations and combination of regenerative, nonregenerative, reheat, nonreheat, intercooling, noncooling, open, semiclosed and closed cycles are analyzed for the ideal gas turbine. In the following chapter, the turboprop and stationary turbines are examined component-by-component, from the compressor, combustion chamber and turbine to the exhaust nozzle. Combining the performance of each component, the design performance of the complete gas turbine is discussed, along with the effects of changes in ambient conditions. The enthalpy of the products of combustion is tabulated to assist in numerical calculations. The designer of a turboprop has the choice of how much of the available power to proportion to the propeller and how much to the exhaust gases. The best way to make this choice is not discussed in detail.

Almost a half of the book is devoted to the turbojet. After presenting the thrust equation and the definitions of numerous turboject performance parameters, static and in-flight performance at the design point is considered. In many books the discussion of similarity and its application to corrected mass flows, engine speeds, etc., is dismissed with a statement "It can be shown that . . . ." Not so in this book; there is an excellent section which deals with similarity starting with the fundamental concepts. Off-design performance, variable area nozzles and thrust augmentation conclude the turbojet chapter. The dual-spool turbojet is not discussed; Prof. Zucrow probably saves that as a final exam problem for his students!

A comparison of the turbojet and ramjet leads off the brief chapter on ramjets. As in the previous chapters, only the component performance and not the design details is presented. A consideration of component design is deferred to volume III. The chapter includes sections on efficiencies, definition of performance parameters, the ideal ramjet, the deviations from ideal and a ramjet with variable geometry.

From the front cover to the rear cover there is a spectrum of jet propulsion engines; the final chapter is concerned with the missile mainstay, the rocket motor. The aspects of rocket propulsion common to both liquid and solid propellant rockets are considered first; this includes thrust equation, performance parameters and nozzle flow. Solid propellants and the internal ballistics of the solid propellant rocket are discussed. A familiarity with combustion and thermochemical equilibrium is essential background for understanding frozen or equilibrium expansion. A section on these subjects is inserted between the solid and liquid propellant rocket discussions. Exterior ballistics of rocket propelled vehicles conclude volume II.

In summary, each chapter has nearly identical format: An introductory section which gives the history and perspective, a section defining the pertinent parameters, and a discussion of component performance. With this background the ideal device is presented, followed by the consideration of real effects. Many figures and graphs enhance the value of the book, as do the numerous numerical examples solved in the text.

Formulas for thrust, specific fuel consumption, thrust coefficients are not developed as explicit functions of known quantities, i.e., Mach number, heat addition and ambient conditions. Rather a stepwise calculation procedure is followed. For example, the nozzle exit velocity appears in the thrust equation; several supplementary calculations are required to obtain this velocity. Of course, it can be argued that explicit functions become unwieldy and obscure rather than clarifying. In this book the conversion factors J and g are carried along through algebraic manipulations. By suitable choice of units, the need for J and g is eliminated easing the manipulation test—for example, using ft-lb instead of Btu for enthalpy dispenses with J. Ducted fans, turborockets and similar jet propulsion engines might profitably have been included.

The book is written for the senior or first-year graduate engineering student. The reader, whether he is a student or practicing engineer, will find here a book of continuing usefulness. As a textbook, it provides an understanding of the fundamentals and a store of information. As a reference, it provides numerous tables and graphs of important formulas.

Technical Literature Digest

M. H. Smith, *Associate Editor,* **and M. H. Fisher,** *Contributor*
The James Forrestal Research Center, Princeton University

Aerodynamics of Jet Propelled Missiles

Hypersonic Flow About a Thin Body of Revolution, by R. Timman, *NATO, Advisory Group Aeron. Res. and Dev., Rep.* no. 141, July 1957, 10 pp.

Effects of Nose Angle and Mach Number on Transition on Cones at Supersonic Speeds, by K. R. Czarnecki and Mary W. Jackson, *NACA TN* no. 4388, Sept. 1958, 17 pp.

EDITOR'S NOTE: Contributions from Professors E. R. G. Eckert, J. P. Hartnett, T. F. Irvine Jr. and P. J. Schneider of the Heat Transfer Laboratory, University of Minnesota, are gratefully acknowledged.

Solution of the Three Dimensional Laminar Boundary Layer Over the Surface of a Rotating Cone, by Ching-Sheng Wu, *Princeton Univ., Dept. Aeron. Engng. Rep.* no. 415 (*AFOSR TN* 58-301; *ASTIA AD* 154, 211), April 1958, 7 pp.

Hypersonic Viscous Flow over Slender Cones, by Lawrence Talbot, Toyoki Koga and Pauline M. Sherman, *NACA TN* 4327, Sept. 1958, 34 pp.

Inviscid Flow around a Blunt Body of a Reacting Mixture of Gases, Part A: General Analysis, by W. Lick, *Rensselaer Polytech. Inst., Dept. Aeron. Engng., Tech. Rep.* AE 5810 (*AFOSR TN* 58-522; *ASTIA AD* 158335), May 1958, 52 pp.

Inviscid Hypersonic Flow Around Spheres and Circular Cylinders, by E. Dale Martin, *Rensselaer Polytech. Inst., Dept. Aeron. Engng., Tech. Rep.* AE 5807 (*AFSOR TN* 58-448; *ASTIA AD* 158254), April 1958, 70 pp.

Preliminary Heat-transfer Studies on Two Bodies of Revolution at Angle of Attack at a Mach Number of 3.12, by Norman Sands and John R. Jack, *NACA TN* 4378, Sept. 1958, 29 pp.

An Investigation of Supersonic Turbulent Boundary Layers on Slender Bodies of Revolution in Free Flight by Use of a Mach-Zehnder Interferometer and Shadowgraphs, by Alvin Seiff and Barbara J. Short, *NACA TN* 4364, Sept. 1958, 57 pp.

Simultaneous Effects of Pressure Gradient and Transverse Curvature on the Boundary Layer along Slender Bodies of Revolution, by Michiru Yasuhara, *Univ.*

Tokyo, Aeron. Res. Inst., Rep. 335, Aug. 1958, 169 pp.

The Effects of Blunt Leading Edges on Delta Wings at Mach 5.8, by Kenneth F. Nicholson, *Calif. Inst. Tech., Guggenheim Aeron. Lab., Hypersonic Res. Proj., Mem.* 45, June 1958, 67 pp.

The Boundary-layer Equation for Axially Symmetric Flow Past a Body of Revolution—Motion of a Sphere, by David Meksyn, *J. Aero/Space Sci.*, vol. 25, Oct. 1958, pp. 631–634, 664.

Heat Transfer and Fluid Flow

Similar Solutions for the Compressible Boundary Layer on a Yawed Cylinder with Transpiration Cooling, by Ivan E. Beckwith, *NACA TN* no. 4345, Sept. 1958, 72 pp.

On the Mechanism of Thermal Ionization Behind Strong Shock Waves, by H. D. Weymann, *Univ. Maryland, Inst. Fluid Dynamics Appl. Math., TN* no. BN-144 (*AFOSR TN* no. 58-788; *ASTIA AD* 2-3113,) July 1958, 36 pp.

Small Perturbations in Hydromagnetics, Free Oscillations in a Rectangular Box, and the Perfectly Conducting Gas, by G. S. S. Ludford, *Univ. Maryland, Inst. Fluid Dynamics Appl. Math., TR* no. BN-143 (*AFOSR TN* no. 58-700; *ASTIA AD* 162, 234), July 1958, 24 pp.

Theory and Experiments on Supersonic Air-to-Air Ejectors, by J. Fabri and J. Paulon, *NACA Tech. Mem.* no. 1410, Sept. 1958, 30 pp. (Translated from *France ONERA NT* no. 36, 1956.)

Determination of High Gas Temperatures at High Speeds, by E. Neher, *Archiv Tech. Messen* no. 270, July 1958, pp. 133–136. (In German.)

Evaporation into a Boundary Layer, by Ernest Bauer and Martin Zlotnick, *Phys. Fluids*, vol. 1, July-Aug. 1958, pp. 355–356.

Heat Transfer to a Sphere at the Transition from Free Molecule Flow, by P. Hammerling and B. Kivel, *Phys. Fluids*, vol. 1, July-Aug. 1958, pp. 357–358.

Higher Order Interactions in Homogeneous Turbulence Theory, by Robert H. Kraichnan, *Phys. Fluids*, vol. 1, July-Aug. 1958, p. 358.

Heat Transfer by Laminar Free Convection in Enclosed Plane Gas Layers, by G. Poots, *Quart. J. Mech. Appl. Math.*, vol. 11, Aug. 1958, pp. 257–273.

Three-dimensional Steady, Radial Flow of Viscous, Heat-conducting Compressible Fluid, by Akira Sakurai, *Quart. J. Mech. Appl. Math.*, vol. 11, Aug. 1958, pp. 274–289.

Improved Method of Gamma-ray Calorimetry, by I. T. Myers, *Rev. Sci. Inst.* vol. 29, Sept. 1958, pp. 758–761.

Calculation of the Laminar Boundary Layer on an Insulated Flat Plate by the Klunker-McLean Method, by Leslie M. Mack, *Calif. Inst. Tech., Jet Propulsion Lab., Prog. Rep.* no. 20-352, July 1952, 120 pp.

A Theoretical Study of Stagnation-point Ablation, by Leonard Roberts, *NACA TN* no. 4392, Sept. 1958, 29 pp.

Aerodynamic Heating Characteristics of a Nose Cone at Angle of Attack, by William M. van Camp, *McDonnell Aircraft Corp., Res. Dept., Rep.* no. 5978, May 1958, 175 pp.

Interaction of a Shock Wave with a Turbulent Boundary Layer at M-3.85, by

I. E. Vas and S. M. Bogdonoff, *Princeton Univ., Dept. Aeron. Engng., Rep.* no. 294 (*AFOSR TN* 55-199), April 1955, 9 pp.

The Performance of a Small Helical Tube Heat Exchanger, by J. C. Breeze, *Atomic Energy Comm.*, CF-57-9-33, Dec. 1957, 16 pp.

Free Convection Heat Transfer to Horizontal Cylinders from an Ordinary Fluid Containing a Volume Heat Source, by Jose Pineda de Guzman, *Atomic Energy Comm.*, AECU-3579, Jan. 1958, 95 pp. (M.S. Chem. Engng.).

Axisymmetric Stagnant Flow of a Viscous and Electrically Conducting Fluid Near the Blunt Nose of a Spinning Body with Presence of Magnetic Field Part I. Exact Solution of Incompressible and Constant Properties Model, by Ching-Sheng Wu and Wallace D. Hayes, *Princeton Univ., Dept. Aeron. Engng., Rep.* no. 431 (*AFOSR TN* 58-405; *ASTIA AD* 158208), April 1958, 44 pp.

Steam Slip and Burnout in Bulk Boiling Systems, by A. E. Galson, *Atomic Energy Comm.*, GEAP-1076, June 1957, 21 pp.

Effect of Magnetic Field on Forced-convection Heat Transfer, by R. Siegel, *J. Appl. Mech.*, vol. 25, Sept. 1958, pp. 415–416.

High-temperature Heat Conductivity of Some Metal Oxides, by John C. Jamieson and A. W. Lawson, *J. Appl. Phys.*, vol. 28, Sept. 1958, pp. 1313–1314.

On Reducing Aerodynamic Heat-transfer Rates by Magnetohydrodynamic Techniques, by Rudolph C. Meyer, *J. Aero/-Space Sci.*, vol. 25, Sept. 1958, pp. 561–572.

The Effect of Extreme Cooling and Local Conditions on Boundary-layer Transition, by John R. Jack and Richard J. Wisniewski, *J. Aero/Space Sci.*, vol. 25, Sept. 1958, p. 592.

An Experimental Investigation of the Stability of the Hypersonic Laminar Boundary Layer, by A. Demetriades, *J. Aero/Space Sci.*, vol. 25, Sept. 1958, pp. 599–600.

Simple Test Method for Determining the Drop Size Distribution of a Hollow Cone Spray, by Hikmet Binark and W. E. Ranz, *Project Squid TR* no. PSU-2-P (*ASTIA AD* 200822), Aug. 1958, 13 pp. (Available only on microcards.)

Film Coefficients for Heat Transfer to Liquid Drops, by E. R. Elzinga Jr. and J. T. Banchero, *AIChE Preprint* no. 3, Aug. 1958, 49 pp.

Graphs of Reduced Variables for Computing Histories of Vaporizing Fuel Drops, and Drop Histories Under Pressure, by G. L. Borman, M. M. El Wakil, O. A. Uyehara and P. S. Myers, *NACA TN* no. 4338, Sept. 1958, 55 pp.

Void Volumes in Subcooled Boiling Systems, by P. Griffith, J. A. Clark and W. M. Rohsenow, *ASME Paper* no. 58-HT-9, Aug. 1958, 20 pp.

Heat Transfer to a Boiling Liquid; Mechanism and Correlations, by K. E. Forster and R. Greif, *ASME Paper* no. 58-HT-11, Aug. 1958, 33 pp.

Bubble Growth Rates in Highly Subcooled Nucleate Boiling, by S. G. Bankhoff and R. D. Mikesell, *AIChE, Preprint* no. 5, Aug. 1958, 12 pp.

A Prediction of Surface Temperature at Incipient Boiling, by S. G. Bankoff, *AIChE Preprint* no. 4, Aug. 1958, 18 pp.

Generalized Correlation of Boiling Heat Transfer, by S. Levy, *ASME Paper* no. 58-HT-8, Aug. 1958, 6 pp.

A Preliminary Study of Boiling Burnout Heat Fluxes for Water in Vortex Flow, by W. R. Gambill and N. D. Greene, *AIChE, Preprint* no. 29, Aug. 1958, 29 pp.

Selected Topics from the Theory of Gas Flow at High Temperatures. V. The Application of Transfer Equations to the Calculation of Diffusion, Heat Conduction, Viscosity and Electric Conductivity, by J. M. Burgers, *Univ. Maryland, Inst. Fluid Dynamics Appl. Math., TN* nos. BN-124a and b (*AFOSR TN* 58-427 and 427a; *ASTIA AD* 158230 and 158230a), May 1958, 125 pp.

The Second Approximation to the Stress Tensor and the Heat Flux Vector in a Gas for Krook's Form of the Collision Equation, by Hsun-Tiao Yang (supplement to "Selected Topics from the Theory of Gas Flow at Temperatures," Chapter IV), *Univ. Maryland, Inst. Fluid Dynamics Appl. Math., TN* no. BN-142 (*AFOSR TN* 58-753; *ASTIA AD* 201612), July 1958, 10 pp.

Investigation of Boiling Burnout and Flow Stability for Water Flowing in Tubes, by Warren H, Lowdermilk, Chester D. Lanzo and Byron L. Siegel, *NACA TN* no. 4382, Sept. 1958, 51 pp.

Analytical and Experimental Investigation of Temperature Recovery Factors for Fully Developed Flow of Air in a Tube, by R. G. Deissler, W. F. Weiland and W. H. Lowdermilk, *NACA TN* no. 4376, Sept. 1958, 35 pp.

A Cooled Gas Pyrometer for Use in High-temperature Gas Streams, by Lloyd N. Krause, Robert C. Johnson and George E. Glawe, *NACA TN* no. 4383, Sept. 1958, 32 pp.

An Experimental Investigation of a Simplified Method for Measuring Heat Transfer at Supersonic Speeds, by Robert M. O'Donnell, *Univ. Texas, Defense Res. Lab.*, CF 2709 (DRL-427), Aug. 1958, 20 pp, 11 figs.

Statistical Distribution of Solid Phase in Two Phase Turbulent Motion, by S. L. Soo and Richard L. Peskin, *Proj. Squid, Tech. Rep.* PR-80-R (*ASTIA AD* 158-714), May 1958, 55 pp. (Available only on microcards.)

Effects of Normal Surface Vibration on Laminar Forced Convective Heat Transfer, by J. A. Scanlan, *Ind. Engng. Chem.*, vol. 50, Oct. 1958, pp. 1565–1568.

Reduced Thermal Conductivity Correlation, Gaseous and Liquid Hydrogen, by C. A. Schaefer and George Thodos, *Ind. Engng. Chem.*, vol. 50, Oct. 1958, pp. 1585–1588.

Electroconvectional Heat Transfer in Gases, by Sigurds Arajs and Sam Legvold, *J. Chem. Phys.*, vol. 29, Sept. 1958, pp. 531–536.

Energy Transfer through a Dissociated Diatomic Gas in Couette Flow, by John F. Clarke, *J. Fluid Mech.*, vol. 4, Sept. 1958, pp. 441–451.

On the Melting of a Semi-infinite Body of Ice Placed in a Hot Stream of Air, by Leonard Roberts, *J. Fluid Mech.*, vol. 4, Sept. 1958, pp. 505–511.

Nucleate Boiling—a Correlation, by Charles H. Gilmour, *AIChE Preprint* 27, Aug. 1958, 12 pp.

Active Sites for Nucleate Boiling, by H. B. Clark, P. S. Strange and J. W. Westwater, *AIChE Preprint* 13, Aug. 1958, 15 pp.

Forced Convection, Local Boiling Heat Transfer in Narrow Annuli, by Louis Bernath and William Begell, *AIChE Preprint* 9, Aug. 1958, 13 pp.

The Effects of Superimposed Forced and Free Convection in Horizontal and Vertical Rectangular Ducts, by M. Altman and F. W. Staub, *AIChE Preprint* 2, Aug. 1958, 39 pp.

Condensing Heat Transfer within Horizontal Tubes, by W. W. Akers, H. A. Deans and O. K. Crosser, *AIChE Preprint* 1, Aug. 1958, 22 pp.

Mass Transfer Cooling Near the Stagnation Point, by Leonard Roberts, *NACA TN* 4391, Sept. 1958, 42 pp.

A Literature Survey on the Applicability of Steady State Heat Transfer Coefficients to Transients in Power or in Flow with Single Phase Flow and with Two Phase Flow, by R. H. Norris, *AEC*, AECU-3611, Nov. 1957, 15 pp.

Mechanically Aided Heat Transfer, by D. Q. Kern and H. J. Karakas, *AIChE Preprint* 17, Aug. 1958, 24 pp.

Internal Energy-Compressibility-Temperature Equation for Air in Dissociative and Ionic Equilibrium, by Perrin Winchell, *J. Chem. Phys.*, vol. 29, Oct. 1958 pp. 687–688.

Statistical Mechanical Theory of Transport Processes in Liquids, by Frank C. Collins and Helen Raffel, *J. Chem. Phys.*, vol. 29, Oct. 1958, pp. 699–710.

Effect of Combustion on Heat and Mass Transfer in a Laminar Boundary Layer, by E. R. G. Eckert and J. P. Hartnett, *ZAMP.*, vol. 9B, March 25, 1958 (Jakob Ackeret anniv. vol.), pp. 259–265. (In German.)

The Dissociation of a Pure Diatomic Gas behind a Strong Normal Shock Wave, by G. Jarre, *ZAMP.*, vol. 9B, March 25, 1958 (Jakob Ackeret anniv. vol.), pp. 389–395.

Magneto-gasdynamic Channel Flow, by E. L. Resler Jr. and W. R. Sears, *ZAMP*, vol. 9B, March 25, 1958 (Jakob Ackeret anniv. vol.), pp. 509–516.

On Magneto-aerodynamic Boundary Layers, by V. J. Rossow, *ZAMP*, vol. 9B, March 25, 1958 (Jakob Ackeret anniv. vol.), pp. 519–527.

Boundary Layer Stability Diagrams for Electrically Conducting Fluids in the Presence of a Magnetic Field, by Vernon J. Rossow, *NACA TN* 4282, Aug. 1958, 32 pp., diagrs., tabs.

Interaction of a Turbulent Boundary Layer with a Step at M = 3.85, by I. E. Vas and S. M. Bogdonoff, *Princeton Univ., Dept. Aeron. Engng., Rep.* 295, April 1955, 25 pp. (*Air Force, Office of Scientific Res. TN* 55-200.)

Influence of Solid-body Rotation on Screen-produced Turbulence, by Stephen C. Traugott, Johns Hopkins Univ., *NACA TN* 4135, Aug. 1958, 100 pp., diagrs., photos.

Report on Boiling Heat Transfer (Russian Work), by Novak Zuber, *AEC*, AECU-3569, Sept. 1957, 5 pp., 27 refs.

A Study of Burnout Heat Fluxes Associated with Forced-convection, Subcooled and Bulk Nucleate Boiling of Water in Source-vortex Flow, by W. R. Gambill and N. D. Greene, *AEC* CF[57–10–118, Oct. 29, 1957, 15 pp.

Cryogenic Data Book, by Dudley B. Chelton and Douglas B. Mann, *AEC* UCRL-3421, May 15, 1956, 116 pp.

On the Spectrum of Turbulence, by Donat G. Wentzel, *Phys. Fluids*, vol. 1, May-June 1958, pp. 213–214.

Shock-front-thickness Measurements by an Electron Beam Technique, by H. N. Ballard and Douglas Venable, *Phys. Fluids*, vol. 1, May-June 1958, pp. 225–229.

Relaxation Time for Reactions Behind Shock Waves and Shock Wave Profiles, by Russel E. Duff, *Phys. Fluids*, vol. 1, May–June 1958, pp. 242–244.

Variational Approach to Magnetohydrodynamics, by Philip Rosen, *Phys. Fluids,* vol. 1, May–June 1958, p. 251.

Magneto Hydrodynamic Distortion of a Magnetic Field Due to a Uniform Flow, by David S. Falk, *AVCO Res. Lab., Res. Rep.* 29, April 30, 1958, 5 pp.

Ionization Phenomena of Shock Waves in Oxygen-nitrogen Mixtures, by S. C. Lin, *AVCO Res. Lab., Res. Rep.* 33. June 1958, 23 pp., 15 refs.

Measurements in a Shock Tube of Heat-transfer Rates at the Stagnation Point of a 1.0-inch-diameter Sphere for Real-gas Temperatures up to 7,900°F, by Alexander P. Sabol, *NACA TN* 4354, Aug. 1958, 15 pp.

Turbulence and Temperature Fluctuations Behind a Heated Grid, by R. R. Mills Jr., A. L. Kistler, V. O'Brien and S. Corrsin, *NACA TN* 4288, Aug. 1958, 67 pp.

Temperature and Thermal-stress Distributions in Some Structural Elements Heated at a Constant Rate, by William A. Brooks Jr., *NACA TN* 4306, Aug. 1958, 77 pp.

Approximate Formulas for the Viscosity and Thermal Conductivity of Gas Mixtures, by Richard S. Brokaw, *J. Chem. Phys.*, vol. 29, Aug. 1958, pp. 391–397.

Turbulent Convection in a Pipe in the Case of a Fluid of High Prandtl Number, by G. Ribaud, (Aerothermodynamics Seminar of the Paris Faculty of Science, 1956–1957), *France, Ministere de l'Air, Publications Sci. et Tech., Note Tech.*, 73, 1958, 192 pp. (In French.)

Effects of External Stream Flow and Afterbody Variations on the Performance of a Plug Nozzle at High Subsonic Speeds by R. J. Salmi and E. M. Cortright Jr., *NACA Res. Mem.* E56F11a, Oct. 1956, 19 pp., diagrs. (Declassified from Confidential by authority of *NACA Res. Abstr.* 128, 7/28/58.)

Internal Characteristics and Performance of an Aerodynamically Controlled Variable-discharge Convergent Nozzle, by Jack G. McArdle, *NACA TN* 4315, July 1958, 33 pp., diagrs., photo., tabs.

An Example of Unsteady Laminar Boundary Layer Flow, by Itiro Tani, *Univ. of Tokyo, Aeron. Res. Inst., Rep.* 331, (vol. 24, no. 2), June 1958, 42 pp.

Extended Applications of Hot Wire Anemometry to High Speed Turbulent Boundary Layers, by Mark V. Morkovin and Ralph E. Phinney, *Johns Hopkins Univ., Dept. Aeron.*, (*AFOSR-TN-58–469*; *ASTIA AD* 158279), June 1958.

An Unsteady Turbulent Boundary Layer, by Sture K. F. Karlsson, *Johns Hopkins Univ., Dept. Aeron.*, 1958, 59 pp., 20 figs.

Boundaries of Supersonic Axisymmetric Free Jets, by Eugene S. Love, Mildred J. Woodling and Louise P. Lee, *NACA Res. Mem.* L56G18, Oct. 1956, 98 pp., diagrs. (Declassified from Confidential by authority of *NACA Res. Abstr.* 125, 2/26/58.)

A Review of the Thermodynamic, Transport, and Chemical Reaction Rate Properties of High-temperature Air, by C. Frederick Hansen and Steve P. Heims, *NACA TN* 4359, July 1958, 33 pp., diagrs.

Tables of Thermodynamic Properties of Argon Free Air to 15000°K, by Joseph Hilsenrath and Charles W. Beckett, *Arnold Engng. Dev. Center, TN* 56–12, (*ASTIA AD* 98974), Sept. 1956, 45 pp.

Spreading of Exhaust Jet from 16-inch Ram Jet at Mach Number 2.0, by Fred Wilcox and Donald Pennington, *NACA Res. Mem.* E52F25, Aug. 1952, 14 pp., diagrs., photo., tab. (Declassified from

Confidential by authority of *NACA Res. Abstr.* 128, 7/28/58.)

Cylindrical Shock Waves from Exploding Wires, by Frederick D. Bennett, *Aberdeen Proving Ground, Ballistic Res. Labs., Rep.* 1035, April. 1958, 19 pp.

An Experimental Investigation of Viscous Effects on Static and Impact Pressure Probes in Hypersonic Flow, by Malcolm L. Matthews, *Calif. Inst. Tech., Guggenheim Aeron. Lab., Hypersonic Res. Proj., Mem.* 44, June 1958, 38 pp.

Free Field Measurements of Sound Radiated by Subsonic Air Jets, by Robert Lee, *David Taylor Model Basin Rep.* 868, Dec. 1953, 13 pp.

Mass Transfer Cooling in a Laminar Boundary Layer in Steady Two Dimensional Stagnation Flow, by A. A. Hayday, *Minn. Univ., Mech. Engng. Dept., Heat Transfer Lab., TN* 19, (*AFOSR-TN*-58-337; *ASTIA AD* 154241), April 1958, 17 pp., 19 figs.

Bodies in an Expanded Electromagnetic High Frequency Field, by H. Stolz, *Annalen Physik,* vol. 1, June 1958, pp. 334–343. (In German.)

Schumann-Runge Oxygen Absorption in Shock-heated Air, by W. H. Wurster, C. E. Treanor and H. S. Glick, *J. Chem. Phys.*, vol. 29, July 1958, pp. 250–256.

Finite Amplitude Cellular Convection, by W. V. R. Malkus and G. Veronis, *J. Fluid Mech.*, vol. 4, July 1958, pp. 225–232.

Characteristics of the Equations of Motion of a Reacting Gas, by L. J. F. Broer, *J. Fluid Mech.*, vol. 4, July 1958, pp. 276–283.

The Thermal Boundary Layer on a Non-isothermal Surface with Non-uniform Free Stream Velocity, by E. M. Sparrow, *J. Fluid Mech.*, vol. 4, July 1958, pp. 321–328.

Detached Shock Waves Ahead of Gas-sampling Probes, by Robert Friedman and Donald R. Boldman, *J. Aero/Space Sci.*, vol. 25, Aug. 1958, p. 526.

On the Performance of a Double-diaphragm Shock Tube Using the Reflected-shock Method and a Light-gas Buffer, by Charles J. Schexnayder Jr., *J. Aero/-Space Sci.*, vol. 25, Aug. 1958, pp. 527–528.

A New Function in the Theory of Fluids and an Equation of State for Liquids and Gases, by A. G. McLellan, *Phil. Mag.*, vol. 3, July 1958, pp. 707–715.

Classical Theory of Transport Phenomena in Dilute Poly-atomic Gases, by N. Taxman, *Physical Rev.*, vol. 110, June 15, 1958, pp. 1235–1238.

Magnetic Field Effects on Bow Shock Stand-off Distance, by Richard W. Ziemer and William B. Bush, *Physical Rev. Letters*, vol. 1, no. 2, July 15, 1958, p. 58.

Development of the Calorimeter Heat Transfer Gauge for Use in Shock Tubes, by Peter H. Rose, *Rev. Sci. Instr.*, vol. 29, July 1958, pp. 557–560.

Combustion, Fuels and Propellants

Burning Velocities of Hydrocarbon Flames—Fuel Lean Mixtures, by S. A. Weil, J. R. Hasenberg and R. T. Ellington, *Inst. of Gas Tech.*, June 1958, 83 pp.

The Hyperscopicity of Lithium and Ammonium Nitrates and Perchlorates, by R. F. Muraca and L. L. Taylor, *Calif. Inst. Tech., Jet Prop. Lab., Progr. Rep.* 20–347, Jan. 1958, 4 pp.

Effect of High Temperature Storage upon the Ballistic Stability of Small Arms Ammunition, by M. E. Levy, *Frankford Arsenal, Pitman Dunn Labs. Group, Rep.* R1433, Jan. 1958, 58 pp.

Preparation and Physical Properties of Di- and Trinitrotoluene Isomers, by Cornelius Conklin and Frank Pristera, *Picatinny Arsenal, Tech. Rep.* 2525, July 1958, 24 pp.

The Underwater Shock-wave Initiation of Cast Pentolite, by C. H. Winning, *Proc. Roy. Soc., London,* vol. A 246, July 29, 1958, pp. 288–298.

Sensitivity of Explosives, VIII: The Effect of Compression of Occluded Gas Bubbles on the Initiation of Liquid Combustibles, by Julius W. Enig, *Navord Rep.* 6093, June 2, 1958, 16 pp.

Similitude in Aerothermochemistry, by Daniel E. Rosner, *Aero. Chem. Res. Labs., Inc., Tech. Pub.* 5, July 1958, 35 pp.

The Analysis of Red Fuming Nitric Acid, I: A Critical Survey, by R. F. Muraca, *Calif. Inst. Tech., Jet Prop. Lab., Progr. Rep.* 20–343, Dec. 1957, 26 pp.

Thermodynamic Properties of Some Boron Compounds, by William H. Evans, Donald D. Wagman and Edward J. Prosen, *Nat. Bur. Standards, Rep.* 4943, Aug. 1956.

The Vapor Pressures of Some Boron Compounds, by William H. Evans, Donald D. Wagman and Edward J. Prosen, *Nat. Bur. Standards, Rep.* 5663, Dec. 1957.

Combustion of Elemental Boron, by *Experiment, Inc., Quarterly Summary Rept.* for Feb. through April 1958, *TM* 1038, May 1958, 7 pp.

An Investigation of the Ignition Temperatures of Solid Metals, by W. C. Reynolds, *Stanford Univ., Dept. Mech. Engng.*, June 1957, 76 pp.

Thermal Stability of Pentaborane in the Range 329° to 419°F, by Glen E. McDonald, *NACA Res. Mem.* E54G16, Dec. 1956, 4 pp., diagrs. (Declassified from Confidential by authority of *NACA Res. Abstr.* 128, 7/28/58.)

Cooperative Test Projects of the Joint Army Navy Air Force Panel on Analytical Chemistry of Solid Propellants, Part I: Introduction to the First Twelve Round Robins and Round Robin I, by R. H. Pierson, *NOTS* 1937, Part I, Feb. 1958, 53 pp.

Dilution of Cryogenic Liquid Rocket Propellants During Pressurized Transfer, S. Greenfield, *Aircr. Engng.*, vol. 30, July 1958, pp. 210–215.

Energy Requirements for the Ignition of Seven Solid Explosives, by G. J. Bryan and C. E. Noonan, *Proc. Roy. Soc., London,* vol. A 246, July 29, 1958, pp. 167–175.

Initiation of Condensed Explosives by Compression of the Surrounding Gas, by J. I. Evans and A. M. Yuill, *Proc. Roy. Soc., London,* vol. A 246, July 29, 1958, pp. 176–179.

Studies on the Oxidation Induced by Ultrasonic Radiation on a Solid System of Lauryl Aldehyde and Potassium Chlorate, by F. A. H. Rice and D. Levine, *Proc. Roy. Soc., London,* vol. A 246, July 29, 1958, pp. 180–188.

Nitromethane, Physical Properties, Thermodynamics, Kinetics of Decomposition, and Utilization as Fuel, by A. Makovky and L. Lenji, *Chem. Rev.*, vol. 58, Aug. 1958, pp. 627–644.

Determination of the O—O Bond Energy in Hydrogen Peroxide by Electron Impact, by L. P. Lindeman and J. C. Guffy, *J. Chem. Phys.*, vol. 29, July 1958, pp. 247–250.

Materials of Construction

Proceedings. High Temperature Materials, Their Strength Potentials and Limitations, *Sagamore Ordnance Materials Research Conference, 4th,* Aug. 21–23, 1957. Co-sponsored by the Ordnance Materials Research Office and the Office of Ordnance Research, Arrangements by Syracuse University Research Institute (*ASTIA AD* 157100), 348 pp.

Elastomers for High Temperature Applications, by E. R. Bartholomew, *NATO, AGARD, Rep.* 178, March-April 1958, 23 pp.

Application of Structural Adhesives in Air Vehicles, by David L. Grimes, *NATO, AGARD, Rep.* 181, March-April 1958, 28 pp.

A Review of the Development of Cermets, by G. C. Deutsch, A. J. Meyer Jr. and G. M. Ault, *NATO, AGARD, Rep.* 185, March-April 1958, 20 pp.

Fatigue and Ageing, by F. Bollenrath, *NATO, AGARD, Rep.* 157, Nov. 1957, 18 pp.

Thermal Stresses in Thin Cylindrical Shells Stiffened by Plane Bulkheads for Arbitrary Temperature Distributions, by D. J. Johns, *Cranfield, Coll. Aeron., Note* 83, July 1958, 22 pp.

Thermal Insulation Ceramic Coatings, by Alan V. Levy, *Inst. Aeron. Sci., Preprint* 857, Oct. 1958, 11 pp.

Ceramic Materials—Properties for Structural Applications, by W. J. Knapp and F. R. Shanley, *Aero/Space Engng.*, vol. 17, Dec. 1958, pp. 34–38.

Relief of Thermal Stresses Through Creep, by H. Poritsky and F. A. Fend, *J. Appl. Mech.* vol. 25, Dec. 1958, pp. 589–597.

Instrumentation, Data Recording, Telemetering

The influence of Modulation on the Recording of Resonance Phenomena, by F. Bruin and D. van Ladesteyn, *Appl. Sci. Res.*, Section B., vol. 7, no. 4, 1958, pp. 270–274.

Determination of the Dynamic Form of Pressure Indicators for Use in a Tube under High Pressure with Shock Waves, by J. Zucrow, *Fusées et Récherche Aéron.*, vol. 3, no. 2, July 1958, pp. 97–102. (In French.)

Current Distribution in Modulated Magnetically Focussed Electron Beams, by M. Chodorow, H. J. Shaw and D. K. Winslow, *J. Appl. Phys.*, vol. 29, Nov. 1958, pp. 1525–1533.

Dynamics of Electron Beams from Magnetically Shielded Guns, by A. Ashkin, *J. Appl. Phys.*, vol. 29, Nov. 1958, pp. 1594–1604.

Measurement of Reflectance and Emissivity of Graphite at Arc Temperature with a Carbon Arc Image Furnace, by M. R. Null and W. W. Lozier, *J. Appl. Phys.*, vol. 29, Nov. 1958, p. 1605.

Properties of a Thermoelectric Cell, by G. M. Grover, D. J. Roehling, E. W. Salmi and R. W. Pidd, *J. Appl. Phys.*, vol. 29, Nov. 1958, pp. 1611–1612.

Disturbance Phenomena in Probe Measurement of Ionized Gases, by Takayoshi Okuda and Kenzo Yamamoto, *J. Phys. Soc., Japan,* vol. 13, Oct. 1958, pp. 1212–1223.

Infrared Pyrometer for Temperature Measurements in Turbine Blades, by J. Crabol and J. Van Kote, *La Récherche Aéron.*, no. 66, Sept.-Oct. 1958, pp. 3–12. (In French.)

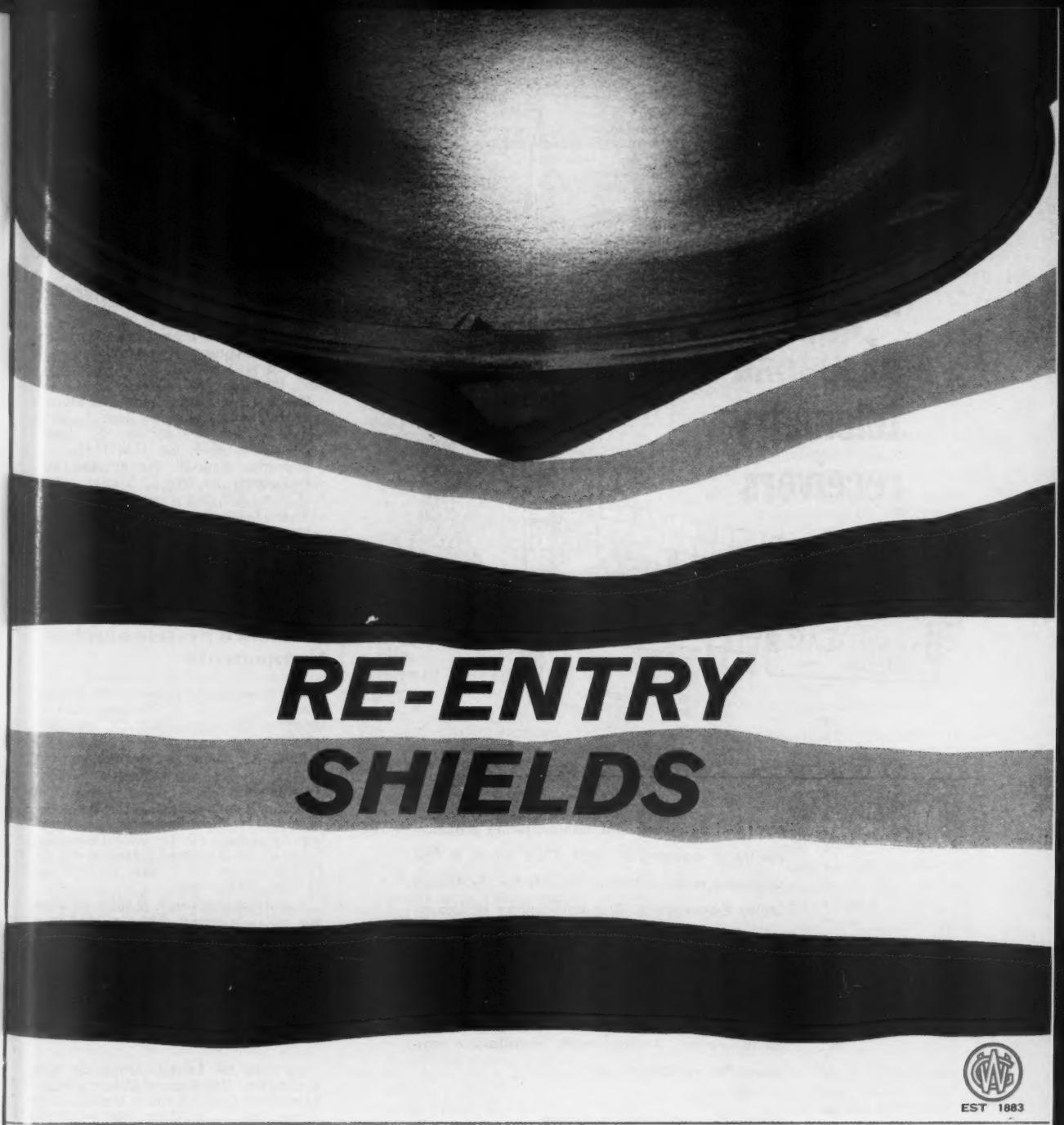

EST 1883

WYMAN-GORDON IS FORGING RE-ENTRY SHIELDS

- Copper in production
- Beryllium in limited production
- Reinforced plastics in development

WYMAN-GORDON

FORGING

ALUMINUM MAGNESIUM STEEL TITANIUM BERYLLIUM MOLYBDENUM COLUMBIUM
AND OTHER UNCOMMON MATERIALS

WORCESTER, MASSACHUSETTS

HARVEY, ILLINOIS
DETROIT, MICHIGAN
GRAFTON, MASSACHUSETTS
FORT WORTH, TEXAS
FRANKLIN PARK, ILLINOIS
LOS ANGELES, CALIFORNIA

Transistorized Relay Amplifier, by R. A. Bruns and J. H. Wilcher, *Calif. Inst. Tech., Jet Prop. Lab., Mem.* 20-170, Sept. 1958, 15 pp.

A Note on the Magnetoresistance Effect of Strain Gauge Wire, by Hideo Takaki and Toshiro Tsuji, *J. Phys. Soc., Japan,* vol. 13, Nov. 1958, p. 1406.

Pressure Gauge for Corrosive Gases in the Micron and Submicron Region, by J. R. Anderson, *Rev. Sci. Instr.,* vol. 29, Dec. 1958, pp. 1073–1078.

Radiation Attenuation Method of Measuring Density of a Two-phase Fluid, by Michael Petrick and Bernet S. Swanson, *Rev. Sci. Instr.,* vol. 29, Dec. 1958, pp. 1079–1085.

Small Oven for High-Temperature Optical Measurements, by D. A. Patterson and H. S. Goulart, *Rev. Sci. Instr.,* vol. 29, Dec. 1958, pp. 1141–1142.

On-off Temperature Control for Electrically Heated Filaments, by Roger E. Little and J. D. McKinley Jr., *Rev. Sci. Instr.,* vol. 29, Dec. 1958, pp. 1143–1144.

Improved Four-Pi Porportional Gas Flow Counter, by Troy C. Martin and O. E. Green, *Rev. Sci. Instr.,* vol. 29, Dec. 1958, p. 1147.

Simulation Techniques in Aeronautics, by J. J. Foody and R. J. A. Paul., *J. Roy. Aeron. Soc.,* vol. 62, Dec. 1958, pp. 878–889.

Guidance Systems and Components

Instrumentation Aspects of Inertial Guidance, by C. S. Draper, *ISA J.* (*Instrum. Soc. Amer.*) vol. 5, Nov. 1958, pp. 54–61.

Radio-Astronomy and Navigation, by C. M. Cade, *J. Roy. Aeron. Soc.,* vol. 62, Nov. 1958, pp. 805–828.

On the Representation of the Trajectory Band and Its Perturbation for Fire-Directing Apparatus, by E. Roth-Desmeules, *Zeitschrift für Angewandte Mathematik und Physik,* vol. 9a, no. 3, Sept. 25, 1958, pp. 235–250. (In German.)

Feasibility and Limits of Infrared Viewing, by T. Schneider, *Zeitschrift für Angewandte Mathematik und Physik,* vol. 9a, no. 3, Sept. 25, 1958, pp. 251–259.

Inertial Navigation, by Ted Newman, *Arma Engng.,* vol. 2, Oct.-Nov. 1958, pp. 8–14.

Aided Inertial Systems, by C. J. Mundo, *Arma. Engng.,* vol. 2, Oct.-Nov. 1958, pp. 15–19.

Formula for Inertial Guidance Gyro Evaluation, "100 Tons of Concrete Plus 2 Seconds of Arc," by Aaron Becker, *Arma Engng.,* vol. 2, Oct.-Nov. 1958, pp. 20–24.

Real-time Airborne Digital Computers, by Gerhard L. Hollander, *ISA J.* (*Instrum. Soc. Amer.*), vol. 5, Dec. 1958, pp. 26–31.

Information Theory Plays Major Role in New Radar Designs, by James P. Holahan, *Space/Aeron.,* vol. 30, Dec. 1958, pp. 138–141, 144–149.

Lear Designs Guidance for Manned Satellite, *Missiles and Rockets.,* vol. 5, Jan. 5, 1959, p. 26.

State of the Art: Inertial Guidance, by W. G. Wing, *Space/Aeron.,* vol. 31, Jan. 1959, pp. 24, 82–87.

State of the Art: Radar, by James Holahan, *Space/Aeron.,* vol. 31, Jan. 1959, pp. 25, 94–96, 98–104.

State of the Art: Infrared, by Raymond H. McFee, *Space/Aeron.,* vol. 31, Jan. 1959, pp. 26, 88–93.

Spiral Antennas Meet Needs of New Vehicles, by Edwin M. Turner, *Space/Aeron.*, vol. 31, Jan. 1959, pp. 56–62.

Far Field Scattering from Bodies of Revolution, by K. M. Siegel, *Appl. Sci. Res.*, Sect. B., vol. 7, no. 4, 1958, pp. 293–328.

Flight Vehicle Design and Testing

Booster Case Design for Hypersonic Vehicles, by Peter E. Grafton and Eugene F. Styer, *Inst. Aeron. Sci., Preprint* 835, July 1958, 24 pp.

Optimum Thrust Direction for Maximum Range, by G. Leitmann, *J. Brit. Interplanet. Soc.*, vol. 16, Sept.-Oct. 1958, pp. 503–507.

Missiles Emerging and Missles Re-entering, by P. Magot-Cuvru, *Fusées et Récherche Aéron.*, vol. 3, no. 2, July 1958, pp. 53–58.

Studies and Tests of a Liquid Propellant Ground-to-ground Missile and a Quasi-rectilinear Trajectory, by C. Belmundo, *Fusées et Récherche Aéron.*, vol. 3, no. 3, July, 1958, pp. 65–68.

Servomechanisms and Controls

D-C Amplifiers for Control Systems, by Larry S. Klivans, *Electronics*, vol. 31, Nov. 21, 1958, pp. 96–98.

Inertial Navigation, Part II, by C. F. O'Donnell, *J. Franklin Inst.*, vol. 266, Nov. 1958, pp. 373–402.

Servo Phase Control Shapes Antenna Pattern, by E. W. Markow, *Electronics*, vol. 32, Jan. 2, 1959, pp. 50–52.

Pneumatic Actuating System for 1000° Operation, by John A. Osterman, *Inst. Aeron. Sci., Preprint* 846, Oct. 1958, 14 pp.

Short Account of the Theories for the Study of Servo Systems Defined by Linear Differential Equations with Constant Coefficients and Influenced by Stochastic Disturbances, by M. Sundstrom and K. Flodin, *Sweden, Roy. Inst. Techn., Dept. Aeron. Engng., TN* 46, 1957, 11 pp.

Relations between Spectral Densities of Inputs and Outputs in Linear Servo Systems with Time Variable Coefficients, by M. Sundstrom, *Sweden, Roy. Inst. Techn., Dept. Aeron. Engng., TN* 45, 1957, 7. pp.

Hypersonic Digital Control Systems, by A. E. Cooper, *Inst. Aeron. Sci., Preprint* 839, July 1958, pp. 32.

On the Use of Spectral Densities in the Study of Servo Circuits Defined by Linear Differential Equations with Time Variable Coefficients and Stochastic Right Member, by M. Sundstrom and K. Flodin, *Sweden, Roy. Inst. Tech., Dept. Aeron. Engng., TN* 44, 1957, 9 pp.

Space Flight

Space Law and Metalaw: Jurisdiction Defined, by Andrew G. Haley, *J. Brit. Interplanet. Soc.*, vol. 16, no. 8, July-Aug. 1958, pp. 472–479.

The Rotation of the First Russian Earth-satellite, by J. H. Thomson, *Phil. Mag.*, vol. 3, no. 32, Aug. 1958, pp. 912–916.

Hearings on H.R. 11881, 85th Congress, 2nd Session, Select Committee on Astronautics and Space Exploration, April 15–May 12, 1958, 1542 pp.

Influence of the Self-rotation of the Central Body on the Motion of Satellites after the Einstein Gravitation Theory, by N. St. Kalitzin, *Il Nuovo Cimento*, vol. 9, no. 3, Aug. 1, 1958, pp. 365–374. (In German.)

Fundamentals of Inertial Guidance and Navigation, by William E. Frye, *J. Astronaut. Sci.*, vol. 5, Spring 1958, pp. 1–4, 10.

Plastic Balloons for Planetary Research, by Malcolm D. Ross, *J. Astronaut. Sci.*, vol. 5, Spring 1958, pp. 5–10.

Space Cabin Design, by Alfred M. Mayo, *J. Astronaut. Sci.*, vol. 5, Spring 1958, pp. 11–14.

A Survey of Propulsion and Space Dynamics, by Douglas B. Cross and Jorgen Jensen, *J. Astronaut. Sci.*, vol. 5, Spring 1958, pp. 15–19, 30.

Basic Sciences Must be Part of Space Team, by L. Eugen Root, *Missiles and Rockets*, vol. 4, Oct. 6, 1958, pp. 31–33.

Departure and Return in Interplanetary Flight, by Karel J. Bossart, *Aero/Space Engng.*, vol. 17, Oct. 1958, pp. 44–52.

The Effect of the Earth's Oblateness on the Orbit of a Near Satellite, by D. G. King-Hele, *Proc. Roy. Soc.*, vol. 247A, no. 1248, Sept. 9, 1958, pp. 49–72.

Atomic Energy

Fusion Chain Reaction—Chain Reaction with Charge Particles, by Michal Gryzinski, *Physical Rev.*, vol. 111, no. 3, Aug. 1, 1958, pp. 900–906.

The Containment of Plasma by the Pinch Discharge, by Sir George Thomson, *Phil. Mag.*, vol. 3, no. 32, Aug. 1958, pp. 886–896.

The Stellarator Concept, by Lyman Spitzer Jr., *Phys. Fluids*, vol. 1, no. 4, July-Aug. 1958, pp. 253–264.

Equilibrium of a Magnetically Confined Plasma in a Toroid, by M. D. Kruskal and R. M. Kulsrud, *Phys. Fluids*, vol. 1, no. 4, July-Aug. 1958, pp. 265–274.

On the Stability of Plasma in Static Equilibrium, by M. D. Kruskal and C. R. Oberman, *Phys. Fluids*, vol. 1, no. 4, July-Aug. 1958, pp. 275–280.

Some Stable Hydromagnetic Equilibria, by J. L. Johnson, C. R. Oberman R. M. Kulsrud and E. A. Frieman, *Phys. Fluids*, vol. 1, no. 4, July-Aug. 1958, pp. 281–296.

On the Ionization and Ohmic Heating of a Helium Plasma, by J. M. Berger, I. B. Bernstein, E. A. Frieman and R. M. Kulsrud, *Phys. Fluids*, vol. 1, no. 4, July-Aug. 1958, pp. 297–300.

Heating of a Confined Plasma by Oscillating Electromagnetic Fields, by J. M. Berger, W. A. Newcomb, J. M. Dawson, E. A. Frieman, R. M. Kulsrud and A. Lenard, *Phys. Fluids*, vol. 1, no. 4, July-Aug. 1958, pp. 301–307.

Generation and Thermalization of Plasma Waves, by Thomas H. Stix, *Phys. Fluids*, vol. 1, no. 4, July-Aug. 1958, pp. 308–317.

On the Theory of Stochastic Processes in Nuclear Reactors, by L. Pal, *Nuovo Cimento, Supplemento*, no. 1, 1958, pp. 25–42. (In English.)

Plasma Loss from Magnetic Bottles, by E. Persico and J. G. Linhart, *Il Nuovo*

Cimento, vol. 8, no. 5, June 1, 1958, pp. 740–753. (In English.)

Dynamic Stability of a Self-pinched Discharge, by H. W. Wyld Jr., *J. Appl. Phys.*, vol. 29, Oct. 1958, pp. 1460–1465.

Research on Power from Fusion and Other Major Activities in the Atomic Energy Programs, *Atomic Energy Commission*, Jan.-June 1958, 410 pp.

Hydromagnetic Instability in a Stellarator, by M. D. Kruskal, J. L. Johnson, M. B. Gottlieb and L. M. Goldman, *Phys. Fluids*, vol. 1, no. 5, Sept.-Oct. 1958, pp. 421–429.

A Programme for Solving the Multigroup Neutron Diffusion Equations in Two Space Dimensions on the Ferranti Mercury Computer, by A. Hassitt, *Gt. Brit., Atomic Energy Res. Estab., AERE T/R* 2487, Feb. 1958, 39 pp.

A High Current Proton Source, by P. C. Thonemann and E. R. Harrison, *Gt. Brit., Atomic Energy Res. Estab., AERE GR/R* 1190, Jan. 1955 (published 1958) 15 pp.

Special Fuel Distribution and Cooling Problems in the Reactors of Nuclear Rockets, by F. Winterberg, *Astronautica Acta*, vol. 4, no. 2, 1958, pp. 138–165. (In German.)

Hydromagnetic Shocks Used in Nuclear Fusion Engine, *Aviation Age*, vol. 30, Aug. 1958, pp. 30–34.

Cleanup of Atomic Hydrogen, by Katherine B. Blodgett, *J. Chem. Phys.*, vol. 29, July 1958, pp. 39–44.

Energy Spectrum of Electrons Emitted from Gases Bombarded by Positive Ions, by David E. Moe and Otto H. Petsch, *Phys. Rev.*, vol. 110, June 15, 1958, pp. 1358–1362.

Neutron Production in Linear Deuterium Pinches, by Oscar A. Anderson, William R. Baker, Stirling A. Colgate, John Ise Jr. and Robert V. Pyle, *Phys. Rev.*, vol. 110, June 15, 1958, pp. 1375–1378.

Instability, Turbulence and Conductivity in Current-carrying Plasma, by O. Buneman, *Phys. Rev. Letters*, vol. 1, no. 1, July 1, 1958, p. 8.

Neutrons of Possible Thermonuclear Origin, by W. C. Elmore, E. M. Little and W. E. Quinn, *Phys. Rev. Letters*, vol. 1, no. 1, July 1, 1958, pp. 32.

R-Matrix Theory of Nuclear Reactions, by A. M. Lane and R. G. Thomas, *Rev. Modern Phys.*, vol. 30, no. 2, Part 1, April 1958, pp. 257–277.

Summary of High-energy Nucleon-nucleon Cross-section Data, by Wilmot N. Hess, *Rev. Modern Phys.*, vol. 30, no. 2, Part 1, April 1958, pp. 368–471.

Electromagnetic Structure of the Neutron, by L. I. Schiff, *Rev. Modern Phys.*, vol. 30, no. 2, Part 1, April 1958, pp. 462–472.

Neutron-electron Interaction, by Leslie L. Foldy, *Rev. Modern Phys.*, vol. 30, no. 2, Part 1, April 1958, pp. 471–481.

Electromagnetic Structure of the Proton and Neutron, by R. Hofstadter, F. Bumiller and M. R. Yearian, *Rev. Modern Phys.*, vol. 30, no. 2, Part 1, April 1958, pp. 482–489.

Direct Cycle Nuclear Turbojet Power Plants, by Eleanor L. Semple and William C. Cooley, *Aero/Space Engng.*, vol. 17, Aug. 1958, pp. 30–36.

Aerophysics, Astrophysics

Hemispherical Distribution of Cosmic Rays at 25° Geomagnetic Latitude, by P. S. Gill and A. N. Mitra, *Il Nuovo Cimento*, vol. 9. no. 3, Aug. 1, 1958, pp. 400–411.

Cosmic Rays in the Earth's Magnetic Field, by P. Rothwell, *Phil. Mag.*, vol. 3, Sept. 1958, pp 961–970.

The Reflexion of Radio Waves from a Stratified Ionosphere Modified by Weak Irregularities, by M. L. V. Pitteway, *Proc. Roy. Soc.*, vol. 246A, no. 1247, Aug. 26, 1958, pp. 556–562.

Sputnik as a Tool for Securing Geodetic Information, by Louis Gold, *J. Franklin Inst.*, vol. 266, no. 2, Aug. 1958, pp. 103–107.

Density and Velocity Distribution of the Interstellar Gas, by H. C. van de Hulst, *Rev. Modern Phys.*, vol 30., no. 3, July 1958, pp. 913–930.

Twenty-one-cm Studies of Some Interstellar Clouds, by R. D. Davies, *Rev. Modern Phys.*, vol. 30, no. 3, July 1958, pp. 931–939.

Validity of the Cloud Model of the Interstellar Medium, by Bertram Donn, *Rev. Modern Phys.*, vol. 30, no. 3, July 1958, pp. 940–942.

On the Formation of Interstellar Gas Clouds, by S. A. Kaplan, *Rev. Modern Phys.*, vol. 30, no. 3, July 1958, pp. 943–951.

Microstructure of the Galactic Magnetic Field, by K. Serkowski, *Rev. Modern Phys.*, vol. 30, no. 3, July 1958, pp. 952–954.

Gross Dynamics of the Interstellar Medium, by E. N. Parker, *Rev. Modern Phys.*, vol 30, no. 3, July 1958, pp. 955–965.

Aerodynamic Dissipation, by H. E. Petschek, *Rev. Modern Phys.*, vol 30, no. 3, July 1958, pp. 966–974.

Magnetohydrodynamic Dissipation, by L. Biermann and A. Schluter, *Rev. Modern Phys.*, vol. 30, no. 3, July 1958, pp. 975–978.

Thermal Inelastic Collision Processes, by M. J. Seaton, *Rev. Modern Phys* , vol. 30, no. 3, July 1958, pp. 979–1008.

On the Cooling of Interstellar Matter, by E. Schatzman, *Rev. Modern Phys.*, vol. 30, no. 3, July 1958, pp. 1009–1011.

On the Condensation of Interstellar Material, by E. Schatzman, *Rev. Modern Phys.*, vol. 30, no. 3, July 1958, pp. 1012–1014.

On the Gravitational Instability of a Medium in Nonuniform Rotation, by N. Bel and E. Schatzman, *Rev. Modern Phys.*, vol. 30, no. 3, July 1958, pp. 1015–1024.

Internal Kinematics of the Planetary Nebulae, by O. C. Wilson, *Rev. Modern Phys.*, vol. 30, no. 3, July 1958, pp. 1025–1032.

Comparison of Gas and Radiation Pressure in the Problems of the Dynamics of Planetary Nebulae, by H. Zanstra, *Rev. Modern Phys.*, vol. 30, no. 3, July 1958, pp. 1030–1033.

Local Density Variations in Planetary Nebulae, by M. J. Seaton, *Rev. Modern Phys.*, vol. 30, no. 3, July 1958, p. 1034.

Internal Motions in the Orion Nebula, by G. Munch, *Rev. Modern Phys.*, vol. 30, no. 3, July 1958, pp. 1035–1041.

Kinematics of the Filaments in the Crab Nebula, by G. Munch, *Rev. Modern Phys.*, vol. 30, no. 3, July 1958, pp. 1042–1046.

On the Nature of the Emission of the Crab Nebula, by I. S. Shklovsky, *Rev. Modern Phys.*, vol 30, no. 3, July 1958, p. 1047.

Cygnus Loop and Some Related Nebulosities, by R. Minkowski, *Rev. Modern Phys.*, vol. 30, no. 3, July 1958, pp. 1048–1052.

Bright Rims in Diffuse Nebulae, by Stuart R. Pottasch, *Rev. Modern Phys.*, vol. 30, no. 3, July 1958, pp. 1053–1057.

On the Stability of Ionization Fronts, by F. D. Kahn, *Rev. Modern Phys.*, vol. 30, no. 3, July 1958, pp. 1058–1061.

On the Propagation and Structure of Ionization Fronts, by F. A. Goldsworthy, *Rev. Modern Phys.*, vol. 30, no. 3, July 1958, pp. 1062–1068.

Collision of Two Highly Ionized Clouds of Gas, by F. D. Kahn, *Rev. Modern Phys.*, vol. 30, no. 3, July 1958, pp. 1069–1072.

Gas-dynamical Effects of Star Formation, by M. P. Savedoff, *Rev. Modern Phys.*, vol. 30, no. 3, July 1958, p. 1073.

Gas Dynamics of Galaxy Collisions, by M. P. Savedoff, *Rev. Modern Phys.*, vol. 30, no. 3, July 1958, pp. 1074–1076.

Examples of Gas Motion and Certain Hypotheses on the Mechanism of Stellar Outbursts, by L. I. Sedov, *Rev. Modern Phys.*, vol. 30, no. 3, July 1958, pp. 1077–1079.

Some Exact Solutions of the Equations of Magnetohydrodynamics when Both Self-attraction and Magnetic Fields Are Present, by G. C. McVittie, *Rev. Modern Phys.*, vol. 30, no. 3, July 1958, pp. 1080–1083.

On the Mathematical Structure of Turbulence, by J. Bass, *Rev. Modern Phys.*, vol. 30, no. 3, July 1958, pp. 1084–1086.

Distortion of a Toroidal Field by Convection, by D. W. Allan and E. C. Bullard, *Rev. Modern. Phys.*, vol. 30, no. 3, July 1958, pp. 1087–1088.

Shock Waves in Magnetogasodynamic Turbulence, by S. A. Kaplan, *Rev. Modern Phys.*, vol. 30, no. 3, July 1958, p. 1089.

Possible Hydromagnetic Simulation of Cosmical Phenomena in the Laboratory, by Winston H. Bostick, *Rev. Modern Phys.*, vol. 30, no. 3, July 1958, pp. 1090–1094.

Russian Technical Articles*

On the Stability of Permanent Rotations of a Body Around a Fixed Point, by V. V. Rumyantsev, *Prikladnaya Matematika i Mekhanika*, vol. 21, no. 3, 1957, pp. 339–346. (In Russian.)

On Bodies of Minimal Resistance in a Supersonic Gas Flow, by M. N. Kogan, *Prikladnaya Matematika i Mekhanika*, vol. 21, no. 2, 1957, pp. 207–212. (In Russian.)

Interaction of a Shock Wave and the Boundary Layer in the Neighborhood of the Leading Edge of a Plane Plate for High Supersonic Velocities and With the Consideration of Radiation, by G. A. Kulonen, *Vestnik Leningradskogo Universiteta, Seriya Matematiki, Mekhaniki i Astronomii*, no. 7 (2), 1958, pp. 172–188. (In Russian.) (Abstract in PB 141037T-1, Office of Technical Services, U. S. Dept. Commerce, $0.50.)

Form of Bodies for Minimum Wave Resistance Studied, by G. I. Kostychev, *Izvestiia Vysshikh Uchebnykh Zabedeniy, Aviatsionnaya Tekhnika*, no. 2, 1958, pp. 9–15. (In Russian.) (Abstract in PB 131891T-9, Office of Technical Services, U. S. Dept. Commerce, p. 97, $2.75 per issue.)

On Motions with Homogeneous Deformations in Magnetic Hydrodynamics, by A. G. Kulikovskiy, *Doklady Akademii Nauk SSSR*, vol. 120, no. 5, June 11, 1958, pp. 984–986. (In Russian.)

On Radiation Cooling of Air. I. General Description of the Phenomenon and the Weak Cooling Wave, by Ya. B. Zel'dovich, A. S. Kompaneyets and Yu. P. Rayzer, *Zhurnal Eksperimental'noy i Teoreticheskoy Fiziki*, vol. 34, no. 5, 1958, pp. 1278–1287. (In Russian.)

The Kinetic Theory of Magnetohydrodynamic Waves, by K. N. Stepanov, *Zhurnal Eksper. i Teoret. Fiziki*, vol. 34, no. 5, 1958, pp. 1292–1301. (In Russian.)

The Effect of Noise Fluctuations on the Accuracy of an Automatic Tracking System With a First Order Astaticism and a Passband Controlled by the Input Signal, by Yu. M. Kazarinov, Yu. A. Kolomenskiy and R. I. Smirnov, *Izvestiia Vysshikh Uchebnykh Zavedeniy-Priborostroyeniye* no. 2, 1958, pp. 3–12. (In Russian.)

Use of Doppler Effect to Determine the Orbital Parameters of Artificial Earth Satellites, by V. A. Kotel'nikov, V. M. Dubrovin, V. A. Morozov, O. N. Rzhiga and A. M. Shakhovskoy, *Radiotekhnikai. Electronika*, no. 7, July 1958, pp. 872–881 (In Russian.)

Silicon Photocells as Solar Energy Converters, by V. S. Vavilov, *Atomnaya Energiya*, vol. 4, June 1958, pp. 571–575. (In Russian.)

The Effective Boundary Conditions in Neutron Diffusion Theory, by G. A. Bat' and D. F. Zaretskiy, *Atomnaya Energiya*, vol. 4, June 1958, pp. 510–519. (In Russian.)

The Energy Spectrum of Neutrons from a Pulsed Source in a Heavy Moderator with Constant Path Length, by M. V. Kawarnovskiy, *Atomnaya Energiya*, vol. 4, June 1958, pp. 539–546. (In Russian.)

Shock Losses in a Divergent Nozzle for Supersonic Flows with Pressure Gradients, by L. P. Volkova and M. Ia. Iudelovich, *Akad. Nauk, SSSR, Izvestiia, Otdel. Tekh. Nauk*, 4, April 1958, pp. 67–72. (In Russian.)

Stability of Shock Waves in Relativistic Hydrodynamics, by V. M. Kontorovich, *Soviet Physics-JETP*, vol. 34 (7), July 1958, pp. 127–132.

Energy Balance in Transition to Turbulent Flow, by B. A. Phidman, *Akad. Nauk SSSR, Izvestiia, Otdelenie Tekh. Nauk*, no. 8, Aug. 1958, pp. 139–142. (In Russian.)

Plane Problems in Magnetohydrodynamics, by G. S. Solitsyn, *Soviet Phys.-JETP*, vol. 34 (7), no. 3, Sept. 1958, pp. 473–476.

On the Theory of Plasma Waves in a Degenerate Electron Liquid, by V. P. Silin, *Soviet Phys-JETP*, vol. 34 (7), no. 3, Sept. 1958, pp. 538–539.

* The editors of Technical Literature Digest are making a systematic search for pertinent Russian articles, both in the original Russian and in translated form. For the balance of 1959, these will appear in a separate section with this heading, mainly to draw the readers' attention to the new listing. After that, they will appear item by item under the proper subject headings.

Index to Advertisers